MULTIFUNCTIONAL POLYMERIC NANOCOMPOSITES FABRICATED BY INCORPORATION OF EXFOLIATED GRAPHENE NANOPLATELETS AND THEIR APPLICATION IN BIPOLAR PLATES FOR POLYMER ELECTROLYTE MEMBRANE FUEL CELLS

By

Xian Jiang

A DISSERTATION

Submitted to
Michigan State University
in partial fulfillment of the requirements
for the degree of

DOCTOR OF PHILSOPHY

Chemical Engineering

2012

ABSTRACT

MULTIFUNCTIONAL POLYMERIC NANOCOMPOSITES FABRICATED BY INCORPORATION OF EXFOLIATED GRAPHENE NANOPLATELETS AND THEIR APPLICATION IN BIPOLAR PLATES FOR POLYMER ELECTROLYTE MEMBRANE FUEL CELLS

By

Xian Jiang

The focus of this research is to investigate the potential of using exfoliated graphene nanoplatelets, GNP, as the multifunctional nano-reinforcement in fabricating polymer/GNP nanocomposites and then explore their prospective applications in bipolar plates for polymer electrolyte membrane (PEM) fuel cells. Firstly, HDPE (high density polyethylene)/GNP nanocomposites were fabricated using the conventional compounding method of melt-extrusion followed by injection molding. The mechanical properties, crystallization behaviors, thermal stability, thermal conductivity, and electrical conductivity of the resulting HDPE/GNP nanocomposites were evaluated as a function of GNP concentration. Results showed that HDPE/GNP nanocomposites exhibit equivalent flexural modulus and strength to HDPE composites filled with other commercial reinforcements but they have superior impact strength. By investigating the crystallization behavior of HDPE/GNP nanocomposites, it was found that GNP is a good nucleating agent at low loading levels and as a result can significantly increase crystallization temperature and crystallinity of HDPE. At high GNP loadings, however, the close proximity of GNP particles retards the crystallization process. The thermal stability and thermal conductivity of HDPE/GNP nanocomposites were significantly enhanced due to the excellent

thermal properties of GNP. Meanwhile, results indicated that the percolation threshold of these nanocomposites prepared by the conventional melt-extrusion and injection molding is relatively high at around 10-15 vol% GNP loading. To enhance the electrical conductivity of HDPE/GNP nanocomposites, two special processing methods named solid state ball milling (SSBM) and solid state shear pulverization (SSSP) were studied. The mechanism by which SSBM and SSSP are capable of producing lower percolation or higher electrical conductivity is to coat the polymer surface by GNP platelets which facilitate the formation of conductive networks during injection molding. However, it was noted that the mechanical and thermal properties of the resulting nanocomposites were compromised at high GNP loadings. A wax coating method was thus applied which is capable of improving both the electrical and mechanical properties in the resulting HDPE/GNP nanocomposites due to a greatly enhanced GNP dispersion. The last but not least, the feasibility of using highly conductive GNP nanocomposites to substitute conventional metallic and graphite bipolar plates was discussed. Polymer/GNP nanocomposites for bipolar plates were made by SSBM and compression molding on account of its good processability and the resulted high electrical conductivity. HDPE/GNP bipolar plates were selected for low-temperature applications, while PPS (polyphenylene sulfide)/GNP bipolar plates were fabricated for a high-temperature usage. Because of the excellent mechanical, structural, thermal and electrical properties of GNP, it is believed that the bipolar plates made from GNP nanocomposites will allow lighter weight of PEM fuel cells with enhanced performance which are particularly suited for automotive applications.

To my wife Chuan Qin
and my parents Fangsheng Jiang & Yanan Pang

ACKNOWLEDGEMENTS

First of all, I would like to express my deepest appreciation to my advisor, Dr. Lawrence T. Drzal, for his advisory and guidance throughout my PhD research and study. Without his persistent support and encouragement, this dissertation would not have been possible. And his enthusiasm and positive attitude have always been a great inspiration for me.

Then I would like to thank my committee members, Dr. Greg Baker, Dr. Krishnamurthy Jayaraman and Dr. Ilsoon Lee for their help and comments on my research. I really learned a lot in the courses offered by them.

I am grateful to every CMSC staff, Mike Rich, Brian Rook, Per Askeland, Ed Drown, Wanjun Liu, Hiroyuki Fukushima, Inhwan Do, Hwan-Man Park, Saswata Bose, Karen Lillis, Inger Weitlauf, and Patricia Miller. Their generous help and assistance enable me to set up and run experiments smoothly.

I also want to thank all my colleagues, Anchita, Huang, Pat, Jinglei, Yan, Dee, Albert, Sanjib and Deb. I really enjoyed staying and working in EB 1105 thanks to the friendly and joyful environment created by them.

The last but not least, I really want to thank my parents for their endless moral and material support during the long years of my education. Especially, I want to express my sincere thanks to my beloved wife Chuan, for her unconditioned love and infinite support during my PhD study. She is always there cheering me up and making my life bright and joyful.

TABLE OF CONTENTS

LIST OF TABLES

LIST OF FIGURES

CHAPTER 1 INTRODUCTION AND LITERATURE REVIEW

1.1 Polymeric Nanocomposites

Recently, polymeric nanocomposites have attracted research interest both in industry and in academia, because they have many useful applications such as power rechargeable batteries, electromagnetic interference (EMI) shielding devices, electronic devices, light emitting diodes (LEDs), gas sensors, super capacitors and photovoltaic cells [1, 2]. Polymeric nanocomposites have become an important alternative to composites filled with conventional fillers [3]. The difference between the conventional fillers and nano-fillers can be explained that nano-reinforcements must have at least one dimension in the nanometer range.

The advantages of using nano-fillers have been summarized in the work by Griffith and Weibull [4, 5]. They both claimed that the smaller the reinforcement, the strong it becomes. According to Griffith's theory, the failure of macroscopic specimens is mainly due to the presence of defects whose size is larger than a critical value. A critical defect size under any given stress conditions can be calculated by this equation:

$$\alpha = \frac{2E\gamma}{\pi\sigma^2} \qquad [1.1]$$

where α is the half of the critical defect length, E is the Young's modulus, γ is the surface tension, and σ is the applied stress. Griffin stated that materials with defects larger than a critical size will fail because of the propagation of cracks, while materials having defects smaller than the critical size are able to reach their intrinsic maximum strength. In this case, composites filled with smaller reinforcements may achieve higher strength because of the smaller defect size that the

fillers may have.

This assumption was further confirmed by Weibull's work in the 1950's. He proposed a statistical model to estimate the probability of fiber failure due to the random distribution of defects in composites. The model was presented as:

$$P_V = 1 - \exp\left[-\left(\frac{\sigma - \sigma_u}{\sigma_0}\right)^m V \right] \tag{1.2}$$

where P_v is the probability of failure, σ is the applied stress, σ_u is the critical stress above which failure would occur in a material, σ_0 is a constant related to material density and the distribution of defects in the material. m is the Weibull constant which is obtained empirically. To simplify this equation, we consider two specimens of the same material but with two different volumes or sizes (V_1 and V_2) and assume that the material has a zero critical stress (σ_u =0). So the stresses at 50% material failure (P_v = 0.5) for these two specimens (σ_1, σ_2) have this relationship:

$$\frac{V_2}{V_1} = \left(\frac{\sigma_1}{\sigma_2}\right)^m \tag{1.3}$$

From this equation, it is easy to conclude that the material having larger size will fail at lower stress, which clearly suggests that smaller materials, especially for nano-fillers, are much better reinforcements than those conventional macro-scale fillers in improving the mechanical strength of composites.

Furthermore, Piggot and Hussain [2, 6] also concluded that nano-fillers are more effective reinforcements than their conventional counterparts and a smaller amount of nanoparticles could result in a larger enhancement in the mechanical, electrical, and thermal properties of the

polymer matrix because of their small size, large aspect ratio, and huge surface area.

1.2 Nano-fillers

Among nanofillers, carbon black is by far mostly used due to its abundance in nature and low price. Carbon black can be found in many applications such as pigment in black ink, as toners in photocopiers and laser printers, as reinforcing additives in automobile tires to enhance tear strength and increase tire life, and also as conductive fillers to impart electrical and thermal conductivity to polymeric composites [7-9]. Carbon black consists mainly of elemental carbon in the form of colloidal particles that are normally fused together into clusters which have an average size of 30-100 nm [10]. Carbon black is basically produced by incomplete thermal decomposition of gaseous or liquid hydrocarbons under controlled processing conditions [7].

Nano-clays, a relatively new kind of nano-filler, were discovered in 1987 and have been intensively explored since then [11-14]. Nano-clays are composed of layered mineral silicates which can be organized into several classes such as montmorillonite, bentonite, kaolinite, hectorite, and halloysite depending on their chemical composition and morphology [15]. Montmorillonite is the most common nano-clay, and has shown promising results in nanocomposites. Montmorillonite exhibits a platelet structure with an average dimension of 1 nm in thickness and 70 to 150 nm in diameter. The platelets closely stack, forming around 10 μm-sized tactoids due to the Van der Waals forces between platelets [12]. In 1990's, a research group at Toyota firstly reported the fabrication of nylon/nano-clays nanocomposites where the individual nano-clays were homogeneously dispersed in the polymer matrix. The results showed

that addition of about 5 wt% nano-clays to nylon-6 increased the tensile modulus by 68%, tensile strength by 42%, heat distortion temperature by 82 °C, and water permeability resistance by 4% [16-18]. Since then, numerous research studies on polymer/nano-clays nanocomposites have appeared in literature which fully cover the design, fabrication, characterization, properties, dispersion issues and the potential applications in the nanocomposites from both an experimental and theoretical prospective. Overall, incorporation of nano-clays into the host polymers could add mechanical strength, fracture resistance, fire resistance, electrical insulation, corrosion stability and thermal stability [19, 20]. However, since nano-clays are electrical and thermal insulators, they can not impart electrical and thermal conductivity to their reinforced nanocomposites.

After nano-clays, carbon nano-tubes (CNTs) were discovered in 1991 by Iijima, who used high resolution transmission electron microscopy to detect their coaxial tube structure [21]. He found that the tube walls of CNTs consist of an extended network of hexagonal rings of carbon atoms rolled up at specific and discrete angles in forming a seamless cylinder. Generally, CNTs are categorized as single-walled nano-tubes (SWNTs) and multi-walled nano-tubes (MWNTs) based on the number of graphene tubes they consist of. SWNTs consist of a single graphene tube with a diameter around 1 nm and a length up to several microns. While MWNTs are composed of an array of SWNTs formed concentrically and separated by 0.35 nm, having a diameter from 2 to 100 nm and a length of tens of microns [22-24]. Because the chemical bonding of CNTs is entirely sp^2 carbon bonds, they provide CNTs with many unique properties. Firstly of all, CNTs are the strongest and stiffest materials discovered so far in terms of tensile strength and Young's

modulus. The Young's modulus is found to be around 1 TPa and the tensile strength was reported as high as 130 GPa [25-27]. Secondly, CNTs are extremely electrically conductive. Due to their one-dimensional nature and sp^2 carbon bonding, charge carriers can travel through nano-tubes exceptionally fast with the carrier mobility as high as 10^5 cm^2/Vs [28]. Furthermore, CNTs can carry an electric current density up to 4×10^9 A/cm^2, which is more than 1,000 times greater than copper and silver [29]. The resulting in-plane electrical conductivity is thus as high as 10^6-10^7 S/cm [30]. Lastly, CNTs are good thermal conductors. A theoretical thermal conductivity value that is up to 6000 W/mK was proposed among several literatures [31-33]. Due to these exceptional mechanical, electrical and thermal properties, CNTs have been extensively explored as the nano-reinforcements in polymers. Many papers have appeared in literature discussing the CNTs-filled polymeric nanocomposites with superb mechanical, electrical and thermal properties for numerous applications [34-37]. However, because of the poor yield, costly fabrication and purifying process, the market price of CNTs is still high, which limits its commercial applications [38].

Carbon nano-fiber, CNF, is another nano-filler having excellent mechanical, thermal, and electrical properties [39, 40]. CNF is also composed of graphene layers. The difference between CNTs and CNF is that CNTs consist graphene layers that are wrapped into perfect cylinders, while graphene layers in CNF are arranged as stacked cones, cups, and planes [41]. Nowadays, CNF can be mass-produced by the method of chemical vapor decomposition (CVD) and the resulting CNF has a diameter around 20-100 nm and a length of hundreds of microns [42]. Due to its excellent properties, CNF is normally served as a substitute for expensive CNTs in certain

applications [43, 44]. However, the price of CNF is still high in the ~ 100 $/pound range [10].

1.3 Exfoliated Graphene Nanoplatelets

To search for an alternative nano-filler which exhibits the superior properties of CNTs but has lower cost and easier fabrication process, graphite based materials are gaining more and more research attention. Polycrystalline graphite is a material that consists of extended networks of sp^2-hybridized carbons in a planar layered structure (graphene), leading to excellent thermal and electrical conductivity within this graphitic basal plate. It is found that exfoliation of these graphite layers and dispersion into polymers offers the potential to bring multifunctionality to the host polymers [45]. Furthermore, research has shown that fully exfoliated graphite nanosheets are as effective in conductivity enhancement as CNTs due to their two-dimensional lattice of sp^2-bond carbon and extremely high aspect ratio [46]. Based on this principal, a new form of graphite based nano-filler, exfoliated graphene nanoplatelets (GNP), has been developed and investigated in the Drzal group for several years [10, 47, 48].

The process of fabricating GNP includes the steps of intercalation, exfoliation and pulverization. First of all, natural graphite was interacted with proton-donor agents and electron acceptors such as sulfuric acid and nitric acid in the interlayer galleries between graphene layers. Then the intercalated graphite was heat-treated in a microwave environment. In this case, the graphite heats rapidly as a result of coupling with the microwave radiation and the entrapped intercalants quickly vaporize. The intercalated graphite particles undergo significant expansion (~500 times) forming worm-like expanded graphite. The morphology of acid intercalated graphite and the

expanded graphite after the microwave treatment is shown in the Figure 1.1. From the image (c), it is clear to see that the distance between graphene layers in expanded graphite has been tremendously increased.

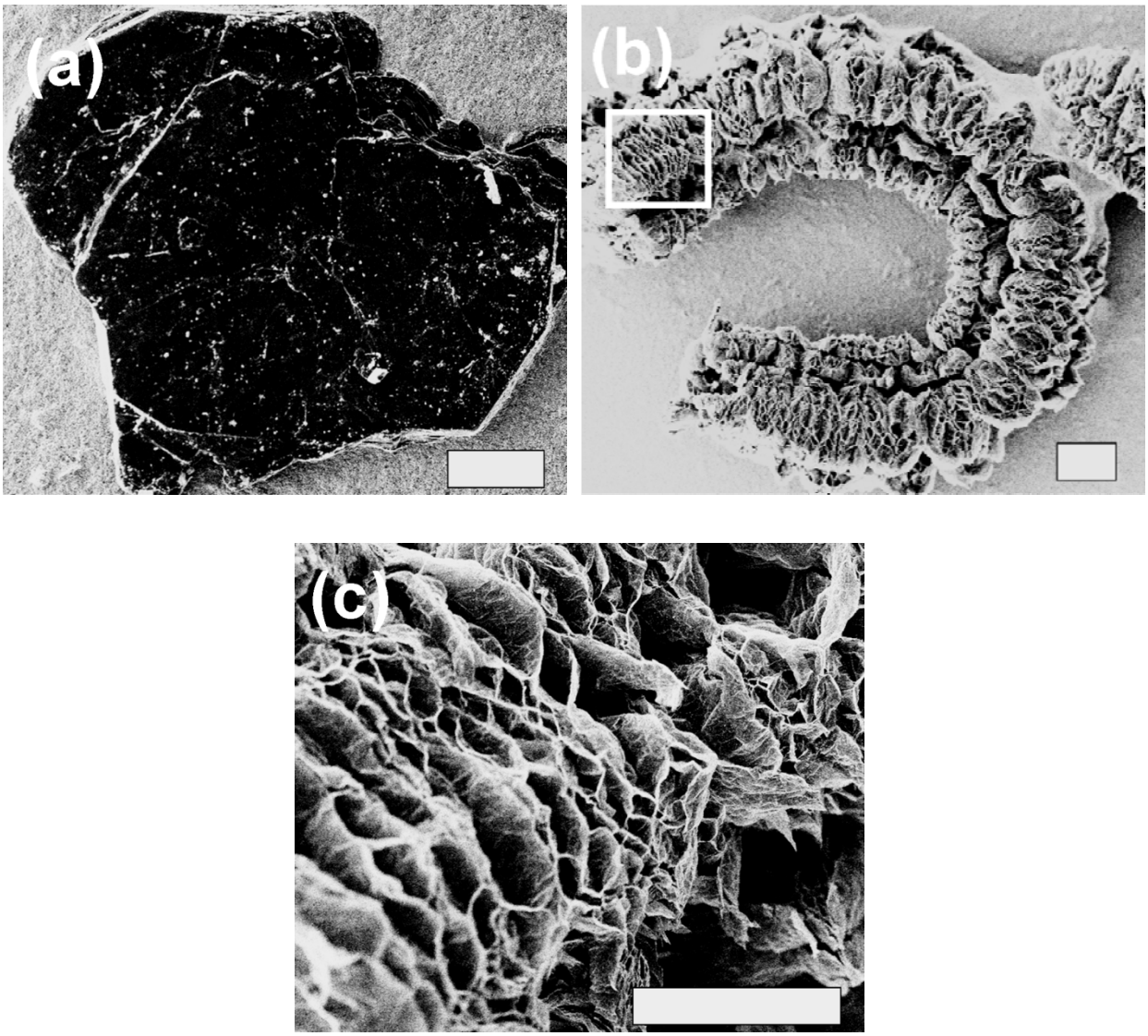

Figure 1.1. The morphology of (a) intercalated graphite (scale bar 100 μm); (b) expanded graphite (scale bar 200 μm); (c) enlarged rectangular area in the image (b) (scale bar 100 μm)

This worm-like expanded graphite is then mechanically pulverized to form the individual graphene nanoplatelets [47]. The platelet diameter of the resulting GNP is controllable by this

fabrication method, which ranges from submicron to 25 μm. And the thickness of GNP is normally within the range of 5-10 nm.

Research work in the Drzal group has shown that this nano-filler is a potential alternative to other nano-reinforcements such as nano-clays and carbon nano-tubes since it combines the low cost and layered structure of nano-clays and the superior thermal and electrical properties of CNTs. And when it is incorporated into a polymer matrix, GNP could simultaneously provide multiple reinforcements in chemical and physical properties [3, 49-57].

1.4 GNP Papers

Recently, reassembly of nano-material into macro-scale structures has become an interesting research topic in order to fully utilize the excellent properties of nano-fillers. CNT paper (Bucky paper) [58-60], CNF paper [61, 62], and reduced graphite oxide (GO) paper [63, 64] have been extensively explored for several years. Reassembly of these nano-fillers into the paper form provides the characteristics of light weight, high mechanical robust and flexibility, excellent thermal and electrical conductivity to the resulting papers, which are thus valuable for many applications such as current collectors, heat dissipaters, lightening protectors, armor plating and filter membranes [65, 66]. Moreover, these nano-filler papers can be used as matting to be embedded into polymeric composites to further enhance their mechanical, thermal and electrical properties. Results showed that the property enhancement by incorporating nano-filler papers is much greater than that from directly mixing the nano-filler with polymers [67]. It is known that nano-reinforcements normally do not disperse well within polymers and they tend to closely

stack with each other in forming agglomerates and aggregates, which constrains the translation of the superb properties of nano-fillers into the resulting nanocomposites. Therefore, the application of nano-filler papers offers a promising method to fully utilize their excellent properties.

The general method of making nano-filler papers involves the use of surfactants, which improves the dispersion of nano-fillers in aqueous solution. These suspensions can then be vacuum filtered to obtain uniform films [68]. Research work in Drzal group has shown that GNP can also be reassembled into a paper form by applying a vacuum filtration method [69]. GNP papers made by this technique are self-standing, robust and have some mechanical flexibility. It was reported that the in-plane electrical conductivity of a GNP paper is over 1000 S/cm and its in-plane thermal conductivity is more than 300 W/mK. In addition, the gas permeability of a GNP paper is extremely low [48].

1.5 GNP as the Conductive Filler in Polymeric Bipolar Plates

One of the GNP's promising applications is to be used as conductive fillers in fabricating polymeric composites for bipolar plates in polymer electrolyte membrane (PEM) fuel cells. PEM fuel cell is a relatively new but fast developing power system which is considered to be one of the most promising power sources for stationary and transportation application in the future due to its high efficiency, high power density, convenient fuel supply, and long life time [70, 71]. Fuel cells produce electrical energy by converting the chemical energy stored in certain fuels like hydrogen, methanol and ethanol through oxidation and reduction reactions [72]. The

configuration of a single fuel cell is schematically shown in the Figure 1.2.

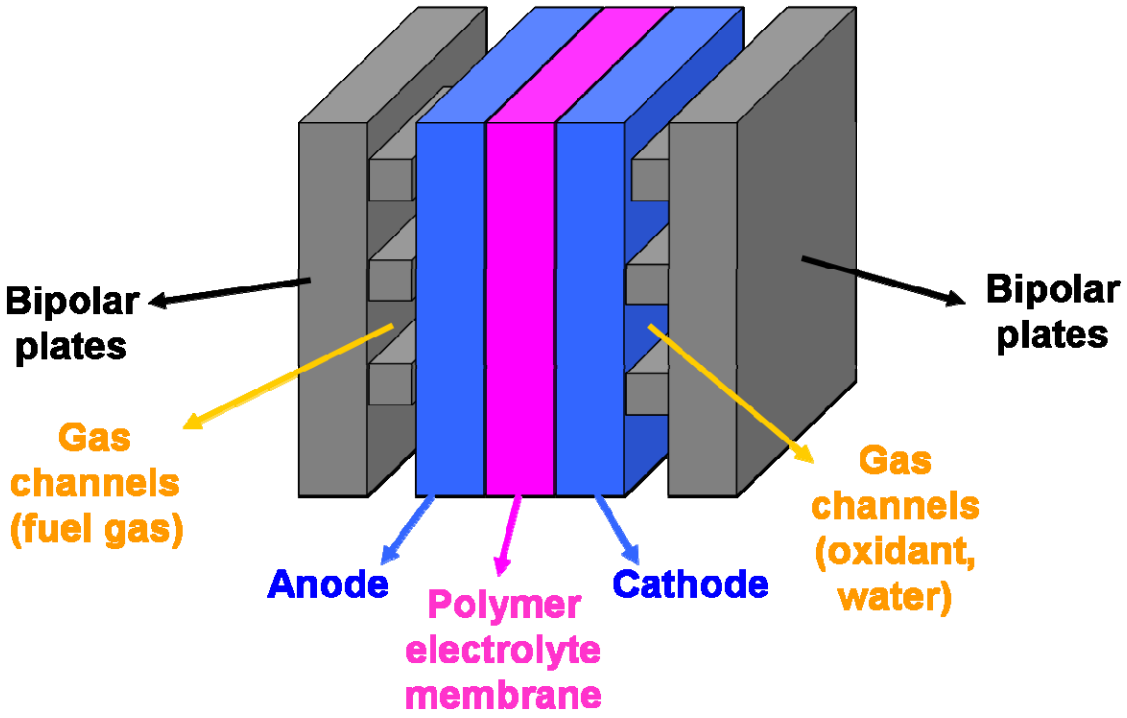

Figure 1.2. The configuration of a single polymer electrolyte membrane fuel cell (For interpretation of the references to color in this and all other figures, the reader is referred to the electronic version of this dissertation)

A key component in the fuel cells is bipolar plates which account for approximately 80% of the fuel cell volume, 70% of the fuel cell weight and as much as 60% of the entire stack cost [73]. The importance of bipolar plates in the fuel cells are fully reflected by these major functions they serve: such as providing a uniform distribution of fuel gas and oxygen within the cell, facilitating water management, conducting electrical current from the anode of one cell to the cathode of the next, enabling heat transfer, and providing adequate mechanical strength to resist the clamping forces for the fuel cell stack assembly [74]. To perform all these functions, bipolar plates must exhibit excellent electrical and thermal conductivity, adequate mechanical strength, good

chemical corrosion resistance, and low gas permeability [75, 76]. The technical targets defined by the U.S. Department of Energy (DOE) for bipolar plated are listed in the Table 1.1.

Table 1.1. U.S. DOE target for bipolar plates [77]

Property	**Value**
Electrical conductivity (in-plane)	>100 S/cm
Thermal conductivity (in-plane)	>10 W/mK
Flexural strength	>25 MPa
Gas permeability	$<2x10^{-6}$ $cm^3cm^{-2}s^{-1}$
Corrosion resistance	<1 μAcm^{-2}

Moreover, light weight, good processability and low manufacturing cost are generally required if bipolar plates are to be widely used in industry [78, 79]. Traditionally, bipolar plates are made from metallic materials and graphite [73, 80]. Metallic materials such as steel and copper have excellent mechanical, thermal and electrical conductivity but their oxidation and chemical corrosion resistance under the fuel cell operation atmosphere are really poor [81]. In this case, additional coatings are required on the surface of these metallic bipolar plates for corrosion protection [82, 83]. However, because the thermal expansion coefficient between the coating layer and the metal plate is different, micro-pores and micro-cracks are easily formed after certain time of fuel operation, which actually deteriorate the protection from the coatings and even cause extra ohmic losses [72]. Bipolar plates made from graphite have the advantages of

high oxidation and chemical corrosion resistance, good electrical and thermal conductivity, and low material cost. But due to its brittleness, it is very difficult to carve gas channels on the surface [84], which makes the manufacturing cost very high and limits the utilization of graphite bipolar plates. These drawbacks of conventional materials have motivated researchers to develop alternative materials for bipolar plates. A conductive polymeric composite is then considered as a promising alternative to both metal and graphite because it has the characteristics of lower cost, higher processability, and lighter weight. Furthermore, gas flow channels can be easily molded into the surfaces of polymeric bipolar plates without a costly secondary machining step [85-87]. However, polymeric composites are associated with the problem of balancing electrical conductivity with their mechanical strength. In order to meet the DOE requirement of electrical conductivity (>100 S/cm) [75], excessive conductive fillers should be incorporated, which substantially reduce the mechanical strength and ductility of the resulting composites [74].

Recently, carbon fiber, carbon black, natural or synthetic graphite, and combinations thereof have been largely explored as the reinforcements to fabricate highly conductive polymeric composites. For these conductive fillers, it is found that their loading should be as high as 70 wt% to achieve an adequate electrical conductivity. At this high filler content, however, the mechanical strength of the resulting composites is usually poor [88], which usually does not satisfy the DOE target. In this case, how to achieve a high electrical conductivity while maintaining good mechanical properties in conductive polymeric composites still remains an important research topic to be explored. And the key issue to solve this problem is to carefully select one or more appropriate conductive fillers that could implement excellent electrical conductivity at relatively low filler

loadings. In this research, GNP was then chosen as the major conductive filler, which is due to its excellent mechanical and structural properties, superior electrical and thermal conductivity, and extremely low gas permeability as discussed above. GNP papers were also considered as valuable supplements to be incorporated into polymeric nanocomposites to further enhance various properties of the resulting bipolar plates.

1.6 Processing of Nanocomposites

It has been well reported that the final properties of nanocomposites are largely depended on the processing methods selected [19, 89, 90]. To fully translate the superb properties of nano-fillers into the resulting nanocomposites, nano-fillers must be well-dispersed in the polymer matrix. However, due to the small size and large surface areas, nano-fillers tend to agglomerate or aggregate and they are difficult to be uniformly distributed. In this case, a processing technique that can achieve a better dispersion of nano-particles would certainly lead to better properties in the resulting nanocomposite. Of course, different nano-fillers also require different processing techniques for an optimum dispersion. A review of processing methods and conditions for fabricating nanocomposites incorporated with different nano-fillers is thus needed.

1.6.1 Processing of Polymer/Nano-clays Nanocomposites

For nano-clays, several fabrication methods have been proposed in literature, the basic ones are:

(1) Solution intercalation method. In this method, a solvent is used to dissolve the polymer and then nano-clays are dispersed in the solution. Once the silicate layers get swollen in the

solution, the polymer chains penetrate and intercalate into the interlayer galleries of nano-clays and displace the solvent within. After evaporation of the solvent, the intercalated structure remains, resulting in polymer/nano-clays nanocomposites [91, 92].

(2) In-situ polymerization method. In this method, nano-clays are first immersed in a liquid monomer or a monomer solution to make the monomer penetrate into the silicate layers. Then the monomer is polymerized inside the interlayer clay galleries and nano-clays also get exfoliated. This technique only applies to a limited category of polymers such as nylon 6, poly(methyl methacrylate, PMMA), epoxy, and phenolic resin [91, 93-95]

(3) Melt intercalation method. In this method, nano-clays are firstly mixed with the polymer in the solid state and then the mixture is heated above the softening point or melting point of the polymer to let the polymer chains penetrate, intercalate, and also exfoliate the silicate layers [91, 96]. Melt intercalation has great advantages over either solution intercalation method or in-situ polymerization. First of all, this method is a solventless and environmentally friendly process. Second, it is suitable to current industrial processing techniques such as melt-extrusion, injection/compression molding, and roll milling. The last but not least, this method allows the use of polymers that are previously not suitable for in-situ polymerization or solution intercalation. Although melt intercalation is a versatile, low cost, and time effectively method to fabricate polymer/nano-clays nanocomposites, it has disadvantages. That is, the dispersion of nano-clays is usually poor due to the insufficient interaction between the polymer matrix and the nano-clays to achieve a high degree of intercalation and exfoliation [91]. A compatibilizer or a dispersing agent is thus needed. The compatibilizer for

nano-clays is normally a functionalized oligomer or polymer whose polar groups will have a strong interaction with nano-clays while its polymer backbone is totally miscible with the polymer matrix where nano-clays are dispersed into. Among all kinds of compatibilizers, maleic anhydride grafted polymers are mostly used due to their high efficiency and easy of synthesis. PE-g-MA, PP-g-MA, PMMA-g-MA, and SEBS-MA (maleic anhydride grafted styrene-ethylene-butylene-styrene block copolymer) [97-99] have all been reported in literature that aim to promote the dispersion of nano-clays in polymers.

1.6.2 Processing of Polymer/Carbon Nano-tubes Nanocomposites

For the processing of CNTs-filled nanocomposites, the same techniques of melt-mixing, solution-mixing and in-situ polymerization can be applied. Results showed that the in-situ polymerization method can achieve a best CNTs dispersion in polymers following by solution-mixing and then melt-mixing [100].

Another approach is to functionalize CNTs that enables a uniform dispersion in different solvents, polymer melts or thermosets. The functionalization of CNTs could be covalent or non-covalent. Covalent functionalization is based on a special treatment of CNTs to obtain functional groups or polymer chains that are compatible with polymers or solvents chemically anchored on the walls. Carboxylic acid and hydroxyl functionalized CNTs [101], hydroxymethyl and vinyl functionalized CNTs [102], aldehyde and amino functionalized CNTs [103] and even polymer grafted CNTs such as CNTs-g-PMMA, CNTs-g-epoxy, CNTs-g-poly(propionylethylenimine-co-ethylenimine) (PPEI-EI), CNTs-g-poly(styrene-co-amino

-methylstyrene) (PSN), CNTs-g-poly(ethylene oxide) (PEO) [104, 105] have all been reported in literature. Non-covalent functionalization of CNTs refers to using certain kinds of dispersing agents that have strong non-covalent binding interactions (π–π stacking, hydrogen bonding and Van der Waals interactions) with CNTs and make them more compatible with solvents or polymers. Polyvinyl pyrrolidone (PVP), polystyrene sulfonate (PSS), and conjugated luminescent polymers [105-107] have been proven as efficient dispersing agents for CNTs. The advantage of the non-covalent modification technique over the covalent one is that it does not disrupt the primary structure of the CNTs, thus retaining their exceptional thermal and electrical properties.

1.6.3 Processing of Polymer/Carbon Nano-fiber Nanocomposites

In case of CNFs, although all the above processing techniques can be applied to fabricate CNFs-filled nanocomposites, melt-mixing is the method commonly used. Due to a well-developed surface modification technique, functionalized CNFs can be well dispersed in the polymer matrix during melt-mixing [39].

1.6.4 Processing of Polymer/Graphene Nanocomposites

The last but not least, the common techniques for processing GNP based nanocomposites will be summarized here. Since GNP exhibit a similar layered structure as nano-clays, the processing methods used for polymer/nano-clays are also applicable for GNP nanocomposites such as solution intercalation, melt intercalation and in-situ polymerization. However, because GNP and

nano-clays are chemically different, some unique processing routs have developed for GNP.

Kalaitzidou [56] proposed a solution coating method which coats the polymer particles by GNP platelets using a liquid phase non-solvent under ultrasonication. Results showed that the coating morphology can be preserved in the resulting GNP nanocomposites, which makes this method more effective at lowering the percolation threshold of nanocomposites than solution mixing method.

Covalent modification of GNP was also investigated recently as an effective processing method to improve the dispersion of GNP in polymers. Miller et al. successfully synthesized epoxy functionalized graphite nanoparticles through the covalently bonding an epoxy monomer to the surface of expanded graphite for their better dispersion in epoxy [108]. Cao et al grafted long alkyl chains to graphene nanosheets through the amidation reaction for their better dispersion in polyolefin [109]. And Ramanathan et al made oxygen and hydroxyl functionalized graphene sheets which are highly compatible with polar polymers [110].

Moreover, various dispersing agents for non-covalent modification of graphene based nano-particles have been proposed. These dispersing agents are mainly aromatic donor and acceptor molecules that are capable of π–π stacking interactions with the surface of graphene [111].

In summary, nanocomposites can be fabricated by various processing techniques. And different compounding methods result in different dispersion status of nano-particles which is important to determine the optimal properties in the resulting nanocomposites. Overall, the techniques of

in-situ polymerization and surface functionalization of nano-particles would lead to better mechanical, thermal and electrical properties in nanocomposites due to a better dispersion and stronger interactions between nano-reinforcements and the polymer matrix. However, although the conventional compounding method of melt-mixing followed by injection molding or compression molding can not achieve a best dispersion of nano-fillers in polymers, it is still considered to be the major processing method used for manufacturing the thermoplastics in industry because of its design flexibility, low cost and labor, short cycle time and minimum scrap loss [112].

1.7 Research Objectives

As discussed above, a novel nano-reinforcement, GNP, exhibits superb structural, electrical and thermal properties. And once incorporated into polymers, it could bring multifunctionality to the resulting nanocomposites which are valuable in many applications, especially in bipolar plates for fuel cells. There are various processing techniques for nanocomposites but it is known that the conventional melt-extrusion and injection/compression molding technique is still the primary choice in industry. So the objectives of this research are (1) determine the mechanical properties, i.e., flexural strength, flexural modulus, and impact strength of polymer/GNP nanocomposites made by melt-extrusion and injection molding and their comparison to the composites reinforced by commercially available fillers such as glass fiber, carbon fiber and carbon black; (2) investigate the crystallization behaviors of a semi-crystalline polymer with the presence of GNP; (3) explore the thermal stability, thermal conductivity, and electrical conductivity of injection

molded polymer/GNP nanocomposites; (4) observe the morphology of polymer/GNP nanocomposites to determine the dispersion and orientation of GNP nanoplatelets under the processing conditions; (5) explore two novel processing techniques of solid state ball milling (SSBM) and solid state shear pulverization (SSSP) to fabricate the resulting polymer/GNP nanocomposites and determine their mechanical, electrical and thermal properties; (6) enhance the dispersion of GNP in polymers by a wax coating method that is suitable for the melt-extrusion and injection molding; (7) evaluate the potential of GNP as the conductive filler in constructing highly conductive polymeric nanocomposites for bipolar plates; (8) making GNP papers to fully utilize the excellent properties of GNP.

REFERENCES

REFERENCES

[1] Vaia RA. Polymer nanocomposites open a new dimension for plastics and composites. AMPTIAC Newsletter. 2003;6(1):17–24.

[2] Hussain F, Hojjati M, Okamoto M, Gorga R. Review article: Polymer-matrix Nanocomposites, Processing, Manufacturing, and Application: An Overview. Journal of Composite Materials. 2006;40(17):1511-75.

[3] Kalaitzidou K, Fukushima H, Drzal LT. Multifunctional polypropylene composites produced by incorporation of exfoliated graphite nanoplatelets. Carbon. 2007;45:1446–52.

[4] Griffith AA. The phenomena of rapture and flaw in solids. Phil Trans R Soc Lond A. 1920;221:163-98

[5] Weibull WJ. A statistical distribution function of wide applicability. Journal of Applied Mechanics. 1951;18:293-7.

[6] Piggott MR. Load Bearing Fibre Composites: Pergamon Press; 1980.

[7] http://en.wikipedia.org/wiki/Carbon_black.

[8] Huang J-C. Carbon black filled conducting polymers and polymer blends. Advances in Polymer Technology. 2002;21(4):299-313.

[9] Stickney PB, Falb RD. Carbon Black-Rubber Interactions and Bound Rubber Rubber Chemistry & Technology 1964;37(5):1299-340.

[10] Kalaitzidou K. Exfoliated Graphite Nanoplatelets as Nanoreinforcement for Multifunctional Polypropylene Nanocomposites [PHD Dissertation]. East Lansing, MI, USA: Michigan State University; 2006.

[11] Pavlidou S, Papaspyrides CD. A review on polymer/ayered silicate nanocomposites. Progress in Polymer Science. 2008;33(12):1119-98.

[12] Uddin F. Clays, Nanoclays, and Montmorillonite Minerals. Metallurgical and Materials Transactions A. 2008;39(12):2804-14.

[13] Sancaktar E, Kuznicki J. Nanocomposite adhesives: Mechanical behavior with nanoclay. International Journal of Adhesion and Adhesives.31(5):286-300.

[14] Swaminathan G, Shivakumar K. Thermomechanical and fracture properties of exfoliated nanoclay nanocomposites. Journal of Reinforced Plastics and Composites.30(3):256-68.

[15] http://www.sigmaaldrich.com.

[16] Kojima Y, Usuki A, Kawasumi M, Okada A, Kurauchi T, Kamigaito O. Synthesis of nylon 6–clay hybrid by montmorillonite intercalated with ϵ-caprolactam. Journal of Polymer Science Part A: Polymer Chemistry. 1993;31(4):983-6.

[17] Yoshitsugu Kojima, Arimitsu Usuki, Masaya Kawasumi, Akane Okada, Yoshiaki Fukushima, Toshio Kurauchi, et al. Mechanical properties of nylon 6-clay hybrid. Journal of Materials Research. 1993;8:1185-9.

[18] Kojima Y, Usuki A, Kawasumi M, Okada A, Kurauchi T, Kamigaito O. One-pot synthesis of nylon 6–clay hybrid. Journal of Polymer Science Part A: Polymer Chemistry. 1993;31(7):1755-8.

[19] Manias E, Touny A, Wu L, Strawhecker K, Lu B, Chung TC. Polypropylene/Montmorillonite Nanocomposites. Review of the Synthetic Routes and Materials Properties. Chemistry of Materials. 2001;13(10):3516-23.

[20] Pavlidou S, Papaspyrides CD. A review on polymer-layered silicate nanocomposites. Progress in Polymer Science. 2008;33(12):1119-98.

[21] Iijima S. Helical microtubules of graphitic carbon. Nature. 1991;354(6348):56-8.

[22] Iijima S, Ichihashi T. Single-shell carbon nanotubes of 1-nm diameter. Nature. 1993;363(6430):603-5.

[23] Bethune DS, Klang CH, de Vries MS, Gorman G, Savoy R, Vazquez J, et al. Cobalt-catalysed growth of carbon nanotubes with single-atomic-layer walls. Nature. 1993;363(6430):605-7.

[24] Chen M, Chen C-M, Chen C-F. Preparation of high yield multi-walled carbon nanotubes by microwave plasma chemical vapor deposition at low temperature. Journal of Materials Science. 2002;37(17):3561-7.

[25] Bellucci S. Carbon nanotubes: physics and applications. physica status solidi (c). 2005;2(1):34-47.

[26] Wong EW, Sheehan PE, Lieber CM. Nanobeam Mechanics: Elasticity, Strength, and Toughness of Nanorods and Nanotubes. Science. 1997;277(5334):1971-5.

[27] Sinnott SB, Andrews R. Carbon Nanotubes: Synthesis, Properties, and Applications. Critical Reviews in Solid State and Material Sciences. 2001;26(3):145-249.

[28] Coleman JN, Khan U, Blau WJ, Gun' ko YK. Small but strong: A review of the mechanical properties of carbon nanotube-polymer composites. Carbon. 2006;44(9):1624-52.

[29] Hong S, Myung S. Nanotube electronics: a flexible approach to mobility. Nature nanotechnology. 2007;2(4):207-8.

[30] http://www.nanocyl.com/CNT-Expertise-Centre/Carbon-Nanotubes.

[31] Hone J, Whitney M, Piskoti C, Zettl A. Thermal conductivity of single-walled carbon nanotubes. Physical Review B. 1999;59(4):R2514-R6.

[32] Yang DJ, Zhang Q, Chen G, Yoon SF, Ahn J, Wang SG, et al. Thermal conductivity of multiwalled carbon nanotubes. Physical Review B. 2002;66(16):165440.

[33] Berber S, Kwon Y, Tomnek D. Unusually High Thermal Conductivity of Carbon Nanotubes. Physical Review Letters. 2000;84(20):4613-6.

[34] Balasubramanian K, Burghard M. Biosensors based on carbon nanotubes ANALYTICAL

AND BIOANALYTICAL CHEMISTRY 2006;385(3):452-68.

[35] Kim IH, Kim JH, KB K. Electrochemical characterization of electrochemically prepared ruthenium oxide/carbon nanotube electrode for supercapacitor application ELECTROCHEMICAL AND SOLID STATE LETTERS. 2005;8(7):A369-A72.

[36] Yao X, Wu H, Wang J, Qu S, Chen G. Carbon nanotube/poly(methyl methacrylate) (CNT/PMMA) composite electrode fabricated by in situ polymerization for microchip capillary electrophoresis Chemistry - A European Journal. 2006;13(3):846 - 53.

[37] Singh KV, Pandey RR, Wang X, Lake R, Ozkan CS, Wang K, et al. Covalent functionalization of single walled carbon nanotubes with peptide nucleic acid: Nanocomponents for molecular level electronics. Carbon. 2006;44(9):1730-9

[38] Kim S, Drzal LT. Comparison of Exfoliated Graphite Nanoplatelets (xGnP) and CNTs for Reinforcement of EVA Nanocomposites Fabricated by Solution Compounding Method and Three Screw rotating Systems Journal of Adhesion Science and Technology. 2009;23:1623–38.

[39] Tibbetts GG, Lake ML, Strong KL, Rice BP. A review of the fabrication and properties of vapor-grown carbon nanofiber/polymer composites. Composites Science and Technology. 2007;67(7-8):1709-18.

[40] Al-Saleh MH, Sundararaj U. A review of vapor grown carbon nanofiber/polymer conductive composites. Carbon. 2009;47(1):2-22.

[41] http://en.wikipedia.org/wiki/Carbon_nanofiber.

[42] Che G, Lakshmi BB, Martin CR, Fisher ER, Ruoff RS. Chemical Vapor Deposition Based Synthesis of Carbon Nanotubes and Nanofibers Using a Template Method. Chemistry of Materials. 1998;10(1):260-7.

[43] Tran PA, Zhang L, Webster TJ. Carbon nanofibers and carbon nanotubes in regenerative medicine. Advanced Drug Delivery Reviews. 2009;61(12):1097-114.

[44] Higgins BA. Carbon Nanofiber-Polymer Composites for Electronic Applications: University of Akron; 2006.

[45] Chung D. Review Graphite. Journal of Materials Science. 2002;37(8):1475-89.

[46] Xie SH, Liu YY, Li JY. Comparison of the effective conductivity between composites reinforced by graphene nanosheets and carbon nanotubes. Applied Physics Letters. 2008;92:243121-3.

[47] Fukushima H. Graphite nanoreinforcements in polymer nanocomposites [PHD Dissertation]. East Lansing, MI, USA: Michigan State University; 2003.

[48] Wu H. Multifunctional Nanocomposite Reinforced by Graphite Nanoplatelets [PHD Dissertation]. East Lansing: Michigan State University; 2011.

[49] Jiang X, Drzal LT. MULTIFUNCTIONAL EXFOLIATED GRAPHITE NANOPLATELETS/HIGH DENSITY POLYETHYLENE NANOCOMPOSITES 41st International SAMPE Technical Conference (ISTC) Wichita, Kansas 2009.

[50] Jiang X, Drzal LT. Multifunctional high density polyethylene nanocomposites produced by incorporation of exfoliated graphite nanoplatelets 1: Morphology and mechanical properties. Polymer Composites. 2010;31(6):1091-8.

[51] Jiang X, Drzal LT. Improving Electrical Conductivity and Mechanical Properties of High Density Polyethylene through Incorporation of Paraffin Wax Coated Exfoliated Graphene Nanoplatelets and Multi-wall Carbon Nano-tubes. Composites Part A: Applied Science and Manufacturing. 2011;42(11):1840-9

[52] Jiang X, Drzal LT. Reduction in Percolation Threshold of Injection Molded High Density Polyethylene/Exfoliated Graphene Nanoplatelets Composites by Solid State Ball Milling and Solid State Shear Pulverization. Journal of Applied Polymer Science 2011; 124(1): 525-535

[53] Jiang X, Drzal LT. Multifunctional high density polyethylene nanocomposites produced by incorporation of exfoliated graphite nanoplatelets 2: crystallization, thermal, and electrical properties. Polymer Composites. 2012, In Press, Accepted Manuscript.

[54] Biswas S, Drzal LT. Multilayered Nanoarchitecture of Graphene Nanosheets and Polypyrrole Nanowires for High Performance Supercapacitor Electrodes. Chemistry of Materials. 2010;22(20):5667-71.

[55] Biswas S, Fukushima H, Drzal LT. Mechanical and electrical property enhancement in exfoliated graphene nanoplatelet/liquid crystalline polymer nanocomposites. Composites Part A: Applied Science and Manufacturing.42(4):371-5.

[56] Kalaitzidou K, Fukushima H, Drzal LT. A new compounding method for exfoliated graphite/polypropylene nanocomposites with enhanced flexural properties and lower percolation threshold. Composites Science and Technology. 2007;67(10):2045-51.

[57] Kalaitzidou K, Fukushima H, Askeland P, Drzal LT. The nucleating effect of exfoliated graphite nanoplatelets and their influence on the crystal structure and electrical conductivity of polypropylene nanocomposites. Journal of Materials Science. 2008;43(8):2895-907.

[58] Endo M, Muramatsu H, Hayashi T, Kim YA, Terrones M, Dresselhaus MS. Nanotechnology: /`Buckypaper/' from coaxial nanotubes. Nature. 2005;433(7025):476-.

[59] Kim YA, Muramatsu H, Hayashi T, Endo M, Terrones M, Dresselhaus MS. Fabrication of High-Purity, Double-Walled Carbon Nanotube Buckypaper. Chemical Vapor Deposition. 2006;12(6):327-30.

[60] Gou J. Single-walled nanotube bucky paper and nanocomposite. Polymer International. 2006;55(11):1283-8.

[61] Yan X, Tai Z, Chen J, Xue Q. Fabrication of carbon nanofiber-polyaniline composite flexible paper for supercapacitor. Nanoscale.3(1):212-6.

[62] Lu H, Liu Y, Gou J, Leng J, Du S. Electroactive shape-memory polymer nanocomposites incorporating carbon nanofiber paper. International Journal of Smart and Nano Materials.1(1):2-12.

[63] Chen H, Müller MB, Gilmore KJ, Wallace GG, Li D. Mechanically Strong, Electrically Conductive, and Biocompatible Graphene Paper. Advanced Materials. 2008;20(18):3557-61.

[64] Compton OC, Dikin DA, Putz KW, Brinson LC, Nguyen ST. Electrically Conductive “Alkylated” Graphene Paper via Chemical Reduction of Amine-Functionalized Graphene Oxide Paper. Advanced Materials.22(8):892-6.

[65] http://www.buckypaper.com/.

[66] Compton OC, Nguyen ST. Graphene Oxide, Highly Reduced Graphene Oxide, and Graphene: Versatile Building Blocks for Carbon-Based Materials. Small.6(6):711-23.

[67] Jiang X, Drzal LT. Exploring the Potential of Exfoliated Graphene Nanoplatelets as the Conductive Filler in Polymeric Nanocomposites for Bipolar Plates (In preparation) 2012.

[68] Vohrer U, Kolaric I, Haque MH, Roth S, Detlaff-Weglikowska U. Carbon nanotube sheets for the use as artificial muscles. Carbon. 2004;42(5-6):1159-64.

[69] Xiang J, Drzal LT. Thermal conductivity of exfoliated graphite nanoplatelet paper. Carbon.49(3):773-8.

[70] Petrach E, Abu-Isa I, Xia W. Synergy Effects of Conductive Fillers on Elastomer Graphite Composite Material for PEM Fuel Cell Bipolar Plates. Journal of Composite Materials. 2010;44(13):1665-76.

[71] Savadogo O. ChemInform Abstract: Emerging Membranes for Electrochemical Systems: (I) Solid Polymer Electrolyte Membranes for Fuel Cell Systems. ChemInform. 1998;29(47):47-66.

[72] Mehta V, Cooper JS. Review and analysis of PEM fuel cell design and manufacturing. Journal of Power Sources. 2003;114(1):32-53.

[73] Davies DP, Adcock PL, Turpin M, Rowen SJ. Bipolar plate materials for solid polymer fuel cells. Journal of Applied Electrochemistry. 2000;30(1):101-5.

[74] Liao S-H, Hung C-H, Ma C-CM, Yen C-Y, Lin Y-F, Weng C-C. Preparation and properties of carbon nanotube-reinforced vinyl ester/nanocomposite bipolar plates for polymer electrolyte membrane fuel cells. Journal of Power Sources. 2008;176(1):175-82.

[75] Cunningham B, Baird DG. The development of economical bipolar plates for fuel cells. Journal of Materials Chemistry. 2006;16(45):4385-8.

[76] Kakati BK, Yamsani VK, Dhathathreyan KS, Sathiyamoorthy D, Verma A. The electrical

conductivity of a composite bipolar plate for fuel cell applications. Carbon. 2009;47(10):2413-8.

[77] http://www1.eere.energy.gov/hydrogenandfuelcells/mypp/pdfs/fuel_cells.pdf.

[78] Borroni-Bird CE. Fuel cell commercialization issues for light-duty vehicle applications. Journal of Power Sources. 1996;61(1-2):33-48.

[79] Cho EA, Jeon US, Ha HY, Hong SA, Oh IH. Characteristics of composite bipolar plates for polymer electrolyte membrane fuel cells. Journal of Power Sources. 2004;125(2):178-82.

[80] Wang H, Turner JA. Reviewing Metallic PEMFC Bipolar Plates. Fuel Cells.10(4):510-9.

[81] Antunes RA, Oliveira MCL, Ett G, Ett V. Corrosion of metal bipolar plates for PEM fuel cells: A review. International Journal of Hydrogen Energy.35(8):3632-47.

[82] Lee Y-M, Lee S-J, Lee C-Y, Lai P-H. Surface Treated SS304 Stainless Steel Bipolar Plates: Its Properties and Single Cell Performance. Journal of Fuel Cell Science and Technology.7(3):031016-6.

[83] Yoshiyuki S. Electrically conductive amorphous carbon coating on metal bipolar plates for PEFC. Surface and Coatings Technology. 2007;202(4-7):1252-5.

[84] Kamarudin SK, Daud WRW, Md.Som A, Takriff MS, Mohammad AW. Technical design and economic evaluation of a PEM fuel cell system. Journal of Power Sources. 2006;157(2):641-9.

[85] Hui C, Liu H-B, Li J-X, Li Y, He Y-D. Characteristics and Preparation of Polymer/Graphite Composite Bipolar Plate for PEM Fuel Cells. Journal of Composite Materials. 2009.

[86] Mathur RB, Dhakate SR, Gupta DK, Dhami TL, Aggarwal RK. Effect of different carbon fillers on the properties of graphite composite bipolar plate. Journal of Materials Processing Technology. 2008;203(1-3):184-92.

[87] Radhakrishnan S, Ramanujam BTS, Adhikari A, Sivaram S. High-temperature, polymer-graphite hybrid composites for bipolar plates: Effect of processing conditions on

electrical properties. Journal of Power Sources. 2007;163(2):702-7.

[88] Antunes RA, de Oliveira MCL, Ett G, Ett V. Carbon materials in composite bipolar plates for polymer electrolyte membrane fuel cells: A review of the main challenges to improve electrical performance. Journal of Power Sources.196(6):2945-61.

[89] Hussain F, Hojjati M, Okamoto M, Gorga RE. Review article: Polymer-matrix Nanocomposites, Processing, Manufacturing, and Application: An Overview. Journal of Composite Materials. 2006;40(17):1511-75.

[90] Jang B, Zhamu A. Processing of nanographene platelets (NGPs) and NGP nanocomposites: a review. Journal of Materials Science. 2008;43(15):5092-101.

[91] Sinha Ray S, Okamoto M. Polymer/layered silicate nanocomposites: a review from preparation to processing. Progress in Polymer Science. 2003;28(11):1539-641.

[92] Aranda P, Ruiz-Hitzky E. Poly(ethylene oxide)-silicate intercalation materials. Chemistry of Materials. 1992;4(6):1395-403.

[93] Yeh J-M, Liou S-J, Lai M-C, Chang Y-W, Huang C-Y, Chen C-P, et al. Comparative studies of the properties of poly(methyl methacrylate)–clay nanocomposite materials prepared by in situ emulsion polymerization and solution dispersion. Journal of Applied Polymer Science. 2004;94(5):1936-46.

[94] Park JH, Jana SC. Mechanism of Exfoliation of Nanoclay Particles in Epoxy-Clay Nanocomposites. Macromolecules. 2003;36(8):2758-68.

[95] Pappas J, Patel K, Nauman EB. Structure and properties of phenolic resin/nanoclay composites synthesized by in situ polymerization. Journal of Applied Polymer Science. 2005;95(5):1169-74.

[96] Deshmane C, Yuan Q, Misra RDK. High strength-toughness combination of melt intercalated nanoclay-reinforced thermoplastic olefins. Materials Science and Engineering: A. 2007;460-461(0):277-87.

[97] Lertwimolnun W, Vergnes B. Influence of compatibilizer and processing conditions on the

dispersion of nanoclay in a polypropylene matrix. Polymer. 2005;46(10):3462-71.

[98] Mohanty S, Nayak SK. Effect of Organo-modified Layered Silicates on the Properties of Poly(Methyl Methacrylate) Nanocomposites. Journal of Thermoplastic Composite Materials. 2010;23(5):623-45.

[99] Mallick S, Kar P, Khatua BB. Morphology and properties of nylon 6 and high density polyethylene blends in presence of nanoclay and PE-g-MA. Journal of Applied Polymer Science.123(3):1801-11.

[100] Viswanathan V, Laha T, Balani K, Agarwal A, Seal S. Challenges and advances in nanocomposite processing techniques. Materials Science and Engineering: R: Reports. 2006;54(5-6):121-285.

[101] Liu J, Rinzler AG, Dai H, Hafner JH, Bradley RK, Boul PJ, et al. Fullerene Pipes. Science. 1998;280(5367):1253-6.

[102] Xie X-L, Mai Y-W, Zhou X-P. Dispersion and alignment of carbon nanotubes in polymer matrix: A review. Materials Science and Engineering: R: Reports. 2005;49(4):89-112.

[103] Chen Q, Dai L, Gao M, Huang S, Mau A. Plasma Activation of Carbon Nanotubes for Chemical Modification. The Journal of Physical Chemistry B. 2000;105(3):618-22.

[104] Mylvaganam K, Zhang LC. Nanotube Functionalization and Polymer Grafting:鈥?An ab Initio Study. The Journal of Physical Chemistry B. 2004;108(39):15009-12.

[105] Peng L. Modifications of carbon nanotubes with polymers. European Polymer Journal. 2005;41(11):2693-703.

[106] O'Connell MJ, Boul P, Ericson LM, Huffman C, Wang Y, Haroz E, et al. Reversible water-solubilization of single-walled carbon nanotubes by polymer wrapping. Chemical Physics Letters. 2001;342(3):265-71.

[107] Star A, Stoddart JF, Steuerman D, Diehl M, Boukai A, Wong EW, et al. Preparation and Properties of Polymer-Wrapped Single-Walled Carbon Nanotubes. Angewandte Chemie International Edition. 2001;40(9):1721-5.

[108] Miller SG, Bauer JL, Maryanski MJ, Heimann PJ, Barlow JP, Gosau J-M, et al. Characterization of epoxy functionalized graphite nanoparticles and the physical properties of epoxy matrix nanocomposites. Composites Science and Technology. 2010;70(7):1120-5.

[109] Cao Y, Feng J, Wu P. Alkyl-functionalized graphene nanosheets with improved lipophilicity. Carbon. 2010;48(5):1683-5.

[110] RamanathanT, Abdala AA, StankovichS, Dikin DA, Herrera Alonso M, Piner RD, et al. Functionalized graphene sheets for polymer nanocomposites. Nat Nano. 2008;3(6):327-31.

[111] Ghosh A, Rao KV, Voggu R, George SJ. Non-covalent functionalization, solubilization of graphene and single-walled carbon nanotubes with aromatic donor and acceptor molecules. Chemical Physics Letters. 2010;488(4):198-201.

[112] Engineers NBoCa. The Complete Technology Book on Plastic Extrusion, Moulding And Mould Designs: Asia Pacific Business Press Inc.; 2006.

CHAPTER 2 MORPHOLOGY AND MECHANICAL PROPERTIES OF HIGH DENSITY POLYETHYLENE NANOCOMPOSITES PRODUCED BY INCORPORATION OF EXFOLIATED GRAPHENE NANOPLATELETS

2.1 Abstract

This chapter investigated the effect of incorporation of exfoliated graphene nanoplatelets, GNP, on the morphology and mechanical properties of high density polyethylene (HDPE). HDPE/GNP nanocomposites were fabricated by the conventional processing method of melt-extrusion and injection molding. Their morphology, flexural strength, modulus, and impact strength were evaluated and compared with HDPE composites filled with some commercial reinforcements such as carbon fibers (CF), carbon black (CB) and glass fibers (GF). Results showed that HDPE/GNP nanocomposites exhibit equivalent flexural strength and modulus to composites reinforced with GF and CB but slightly less than that of HDPE/CF composites at the same filler volume fraction. However, the Izod impact strength of HDPE/GNP nanocomposites was found to be significantly higher.

2.2 Introduction

In recent years polymeric nanocomposites have attracted research interest both in industry and in academia, which become an important alternative to conventional filled polymers or polymer blends [1]. The difference between the conventional fillers and nano-reinforcements can be explained that nano-reinforcements must have at least one dimension in the nanometer range. The advantages of using nano-reinforcements have been summarized in the chapter of

introduction. That is, the smaller the reinforcement is, the strong it becomes. Nano-fillers can thus produce improved mechanical properties without degrading the energy absorption (impact) properties of the composites at the same time as is the case for conventional reinforcements [2]. In addition, nano-particles serve as the stress transfer media that can transfer the stress from the matrix to the reinforcements more efficiently due to the increased surface area and good adhesion at the interface.

High density polyethylene (HDPE) is an engineering thermoplastic that is widely used due to its good physical and mechanical properties, excellent chemical corrosion stability, good gas barrier properties, easy processing and low cost. HDPE can be found in a variety of applications including: food containers, water pipes, gas mains, oil tanks, geo-membranes and so on [3]. HDPE is still increasingly being utilized as an alternative for less environmentally friendly substances. HDPE could be used in more structural applications if its mechanical properties could be improved. Additions of carbon black, glass fibers and even carbon fibers have been used to make HDPE composites that have improved stiffness and strength. Unfortunately the impact properties of these composites are tremendously reduced by addition of these reinforcements [4].

The objectives of this chapter are to: (1) determine the mechanical properties, i.e., impact strength, modulus, and flexural strength of HDPE/GNP nanocomposites; (2) compare the reinforcing effect of GNP to commercially available glass fibers and carbon reinforcements; and (3) observe the morphology of HDPE/GNP nanocomposites to determine the dispersion of the nano-reinforcement.

2.3 Experimental

2.3.1 Materials

In this research, HDPE pellets with the trade name Marlex® HXM 50100 (Density 0.95 g/cm^3, MW~ 230,000) were obtained from Chevron Phillips Chemical Company. GNP nanoplatelets were obtained from XG Science, Inc [5]. There are two kinds of GNP particles used in this study. GNP-1 has the thickness around 5-10 nm and a platelet diameter of 1 μm, while GNP-15 has the same thickness but the diameter is around 15 μm.

Table 2.1. Geometrical and surface characteristics of various fillers

Filler	Length (μm)	Diameter (μm)	Aspect Ratio	Surface Area (m^2/g)	Density (g/cm^3)
GNP-1	<0.01 (platelet thickness)	1	<100	100	2.1
GNP-15	<0.01 (platelet thickness)	15	~1500	40	2.1
PAN CF	175	7.2	~24	16	1.8
GF	51 (mm)	13	~4000	N/A	2.6
CB	0.4–0.5	0.4–0.5	1	1400	1.8

Several commercial reinforcements and fillers were also combined with HDPE to make composites for comparison to the HDPE/GNP nanocomposites. They are: (1) CF-PAN based carbon fiber (PANEX 33 MC Milled Carbon Fibers, Zoltek Co), (2) CB-high structure carbon black (KETJENBLACK EC-600 JD, AkzoNobel Polymer Chemicals LLC), and (3) GF-chopped

glass fiber (StarStran® LCF, Johns Manville Co.). The physical properties of these materials are detailed in Table 2.1.

2.3.2 Processing Methods

The fabrication method used to prepare the HDPE/GNP nanocomposites in this study is melt-extrusion followed by injection molding. Melt-extrusion of HDPE/GNP nanocomposites was carried out in a DSM Micro 15 cc Compounder, (Vertical, co-rotating, twin-screws micro-extruder) operating at 220 °C for 5 minutes at a screw speed of 100 rpm. The composite melt was then transferred to a Daca Micro injector with the T_{barrel}= 220 °C and T_{mold}= 90 °C. The injection pressure applied for the injection molding of flexural coupons was at 0.6 MPa. The melt extrusion and injection molding systems are shown in the Figure 2.1.

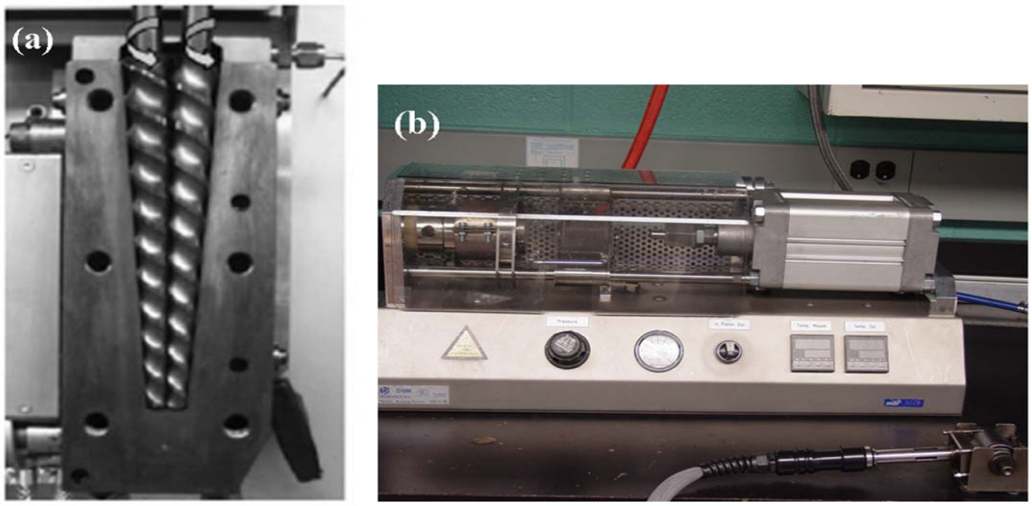

Figure 2.1. (a) A DSM Micro 15cc Compounder, (Vertical, co-rotating, twin-screws microextruder); (b) A Daca Micro injector

2.3.3 Characterization Techniques

Flexural tests were performed with a UTS SFM-20 machine (United Calibration Corp.) at room temperature by following the ASTM D790 standard test method (3-point bending mode). The test was performed at a flexural rate of 0.05 in/min. Impact strength tests (Izod impact type) were performed following the ASTM D256 standard test method. The morphology of the nanocomposites was investigated with the aid of an Environmental Scanning Electron Microscopy (Electroscan 2020). The samples were gold coated to avoid charging and the voltage used was 20 kV

2.4 Results and Discussion

2.4.1 Flexural Properties and Impact Strength of HDPE/GNP Nanocomposites

The flexural strength and modulus of elasticity of HDPE/GNP-1 and HDPE/GNP-15 nanocomposites at the loading levels from 0 to 15 vol% are shown in the Figure 2.2 and Figure 2.3 respectively. The values shown in the figures are the average of five test samples. The flexural strength of both GNP-1 and GNP-15 nanocomposites is increased even at a low GNP loading (1 vol%). As the GNP concentration increases, the flexural strength of HDPE/GNP nanocomposites continues to increase although the reinforcing efficiency of GNP-1 and GNP-15 is different. It is noted that HDPE/GNP-1 nanocomposites always exhibit higher flexural strength than HDPE/GNP-15 counterparts.

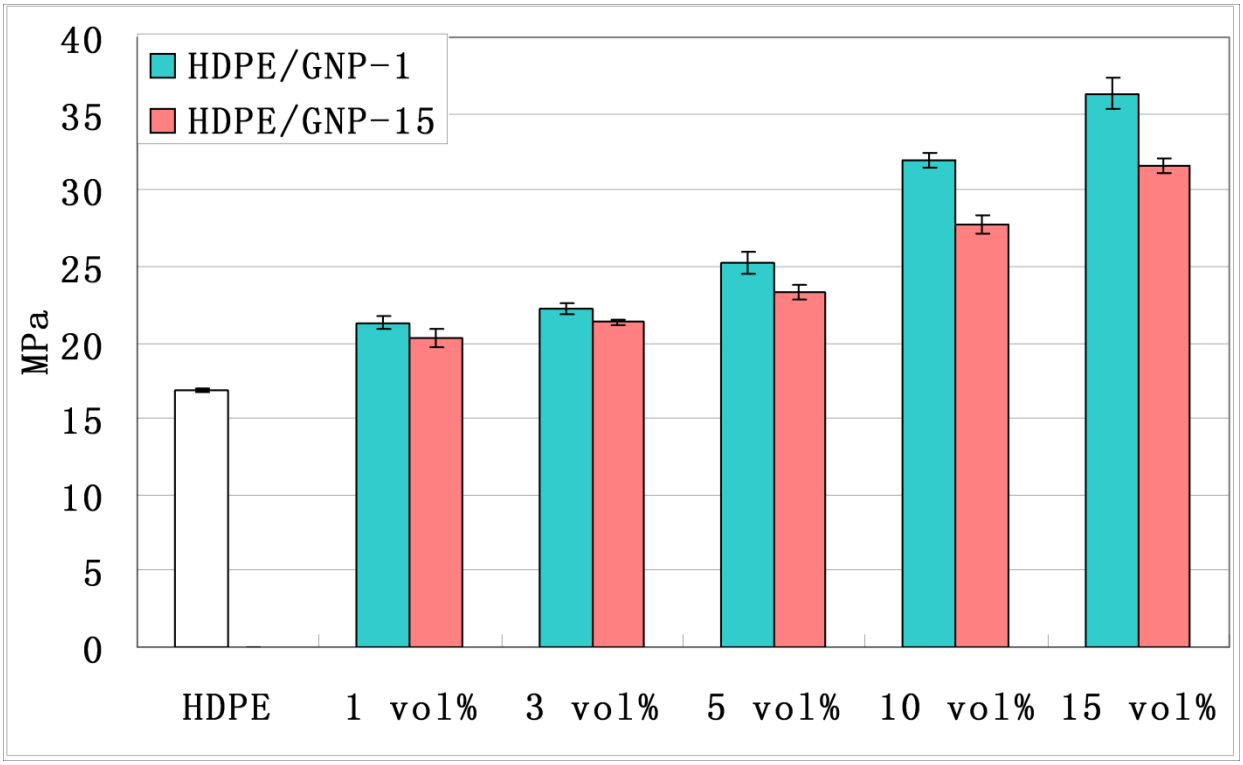

Figure 2.2. Flexural strength of HDPE/GNP nanocomposites

For the modulus of elasticity, both GNP-1 and GNP-15 nanoparticles increase the modulus substantially. And there is no significant difference in flexural modulus between GNP-1 and GNP-15 nanocomposites.

The impact strength of HDPE/GNP nanocomposites up to a loading of 15 vol% is presented in the Figure 2.4. Compared to the neat HDPE, it is noted that HDPE/GNP nanocomposites have lower impact strength and the strength value keeps decreasing as the GNP content increases. Reduced impact strength in GNP nanocomposites suggests that the impact failure mechanism of HDPE has been changed with the presence of GNP. Once again, we can see that HDPE/GNP-1 nanocomposites exhibit higher impact strength at every GNP loading.

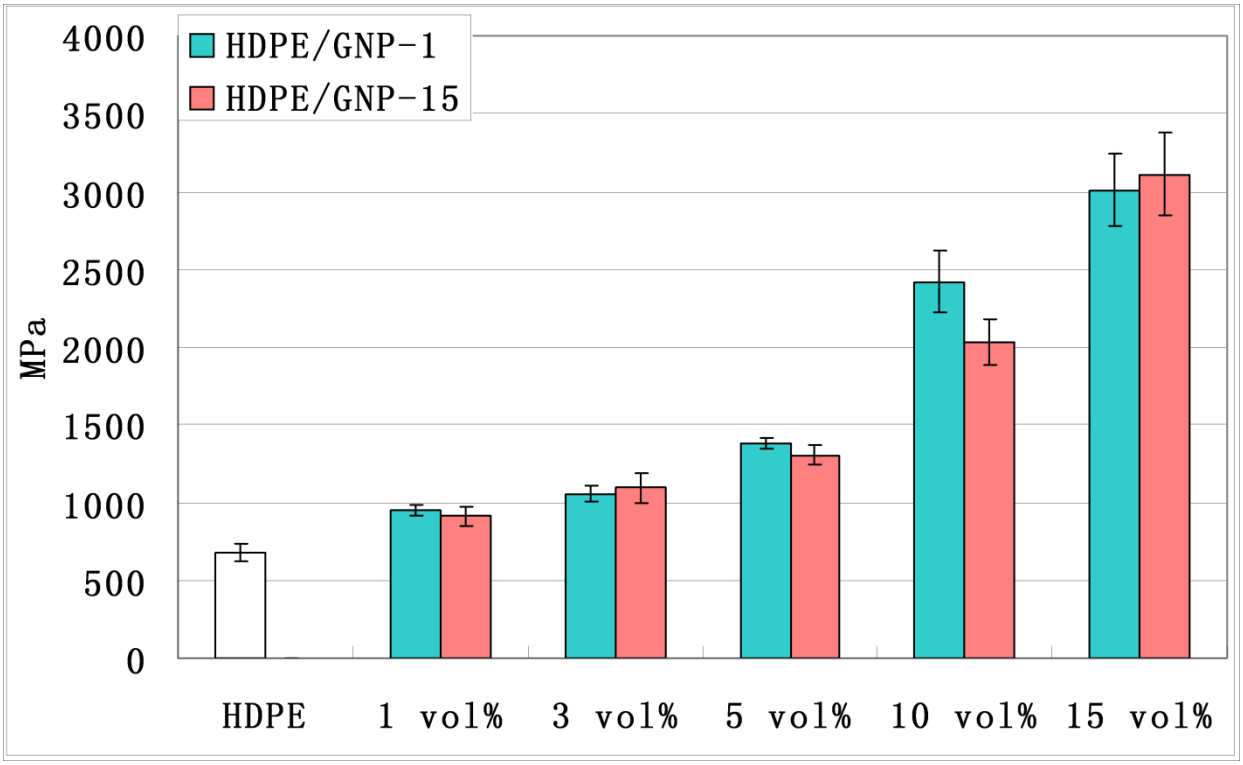

Figure 2.3. Flexural modulus of HDPE/GNP nanocomposites

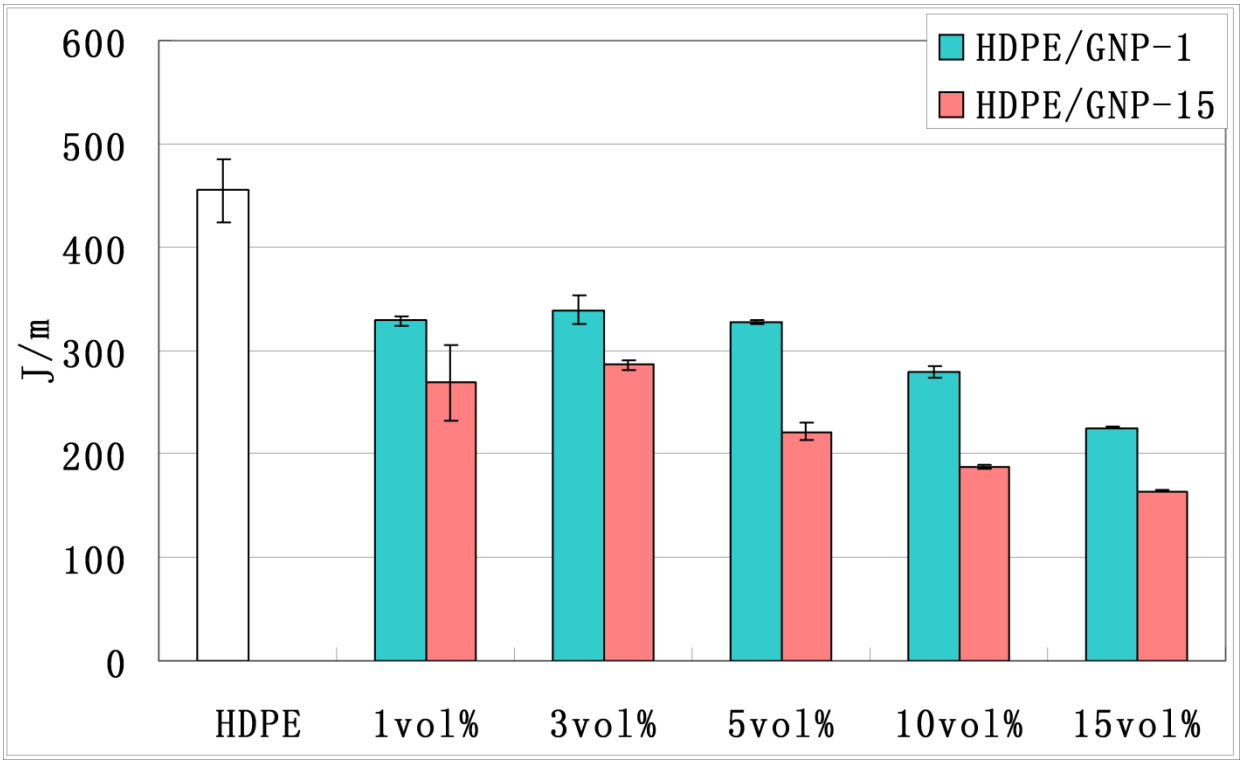

Figure 2.4. Impact strength of HDPE/GNP nanocomposites

The differences in flexural properties and impact strength in HDPE/GNP-1 and HDPE/GNP-15 nanocomposites reflect the difference in the GNP aspect ratio (GNP-1< GNP-15), the difference in the absolute number of reinforcing particles per unit volume (GNP-1> GNP-15) and indicate that dispersion status of GNP-1 and GNP-15 in these nanocomposites may also be different. Better mechanical properties in the GNP-1 nanocomposites also confirm the assumption proposed in the chapter of introduction, that is, the smaller the reinforcement is, the stronger it becomes, since the size of GNP-1 is much smaller than GNP-15.

The dispersion of GNP nanoplatelets in the polymer matrix as well as a qualitative evaluation of how the morphology affects the mechanical properties of the resulting HDPE/GNP nanocomposites is presented below.

2.4.2 Morphology of HDPE/GNP Nanocomposites

The fracture surface of HDPE and HDPE/GNP nanocomposites, obtained by fracture in liquid N_2, are evaluated in the Figure 2.5. Images (a) and (b) illustrate the fracture surface of neat HDPE and the HDPE/GNP-1 nanocomposite at 0.1 vol% GNP loading respectively. From image (a), it is concluded that the fracture surface of neat HDPE is smooth and homogeneous. However, incorporation of only 0.1 vol% GNP-1 significantly alters the surface morphology (image (b)) by increasing surface roughness and surface area.

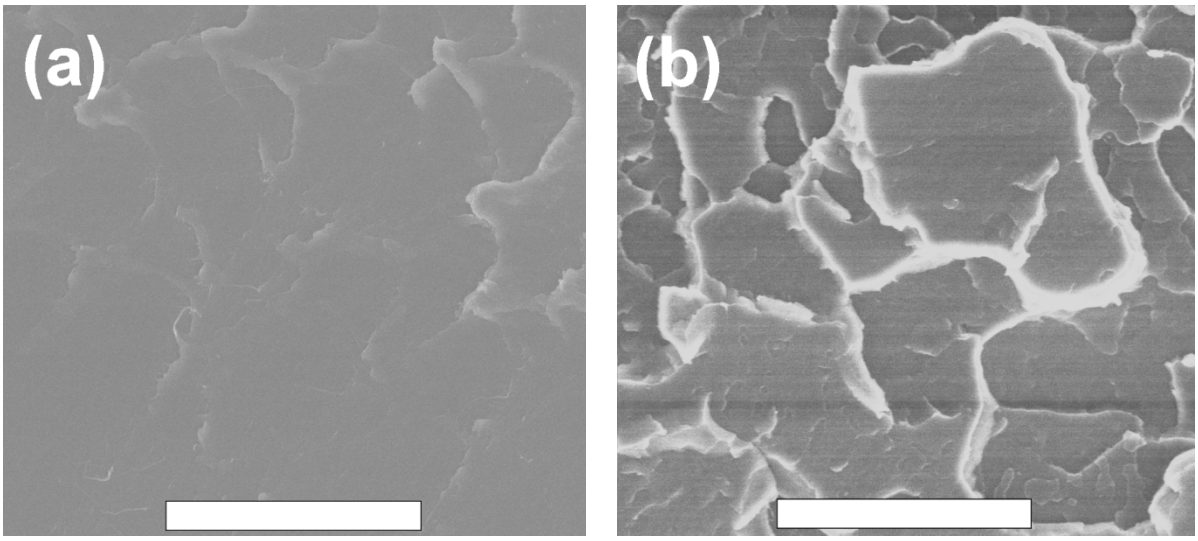

Figure 2.5. ESEM images of the fracture surface of (a) neat HDPE (scale bar 150 μm); (b) HDPE/GNP-1 nanocomposite at 0.1 vol% GNP loading (scale bar 150 μm)

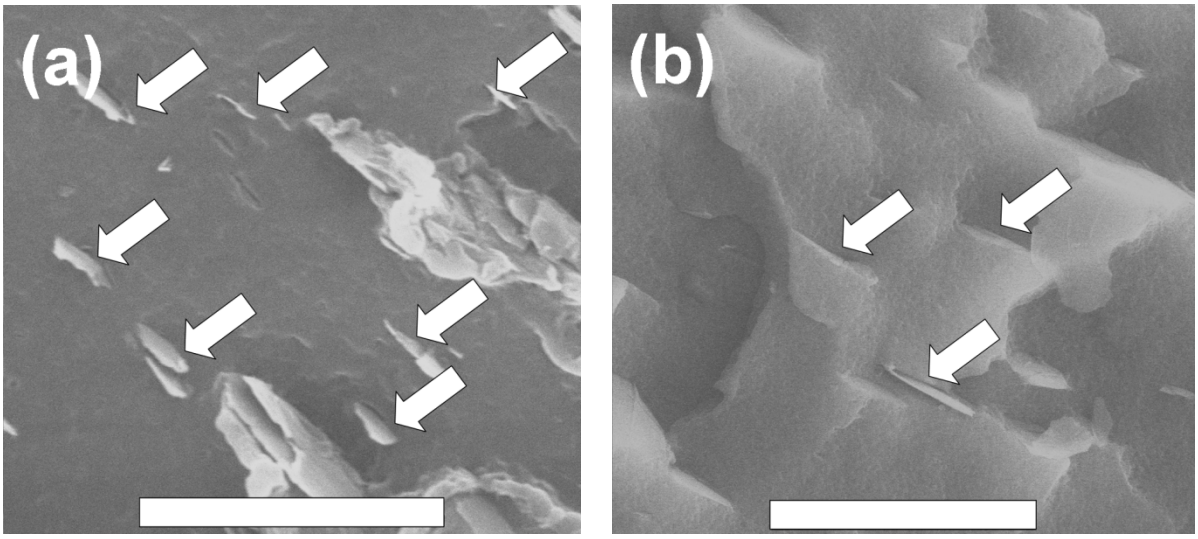

Figure 2.6. Dispersion of GNP nanoparticles (shown by the arrows) in HDPE: (a) 1 vol% GNP-1 (Scale bar 10 μm); (b) 1 vol% GNP-15 (Scale bar 20 μm)

The dispersion of GNP nanoparticles at 1 vol% loading in HDPE can be seen in the Figure 2.6. As shown by the arrows in these images, both GNP-1 and GNP-15 particles are well dispersed in the polymer matrix, which indicates that the DSM melt-extrusion is effective in compounding GNP nano-particles with HDPE at low GNP contents. The edge-on view of GNP nano-platelets shows that both GNP-1 and GNP-15 are embedded into the polymer matrix which also indicates

GNP has a relatively good adhesion with HDPE. Although the volume fractions of GNP-1 and GNP-15 are the same (1 vol%), a larger number of reinforcing particles are detected in the GNP-1 nanocomposite even the image was taken at a higher magnification.

Although both GNP-1 and GNP-15 exhibit platelet morphology [6], it is evident that GNP-15 particles may lose their platelet structure forming folds or rolled-up structure during the processing conditions, resulting the difference in dispersion and reduced effectiveness as a reinforcement. Figure 2.7 (a) and Figure 2.7 (b) are the representatives of these two GNP-15 morphologies. Figure 2.7 (a) shows a folded GNP-15 nanoplatelet and Figure 2.7 (b) indicates a rolled-up structure. However, folding or roll-up is hardly observed in the case of GNP-1. Since the affinity between the non-polar polymer matrix and the non-polar graphene surface should be independent of nano-particle size and the processing conditions are the same for both GNP-1 and GNP-15 nanocomposites, the difference in dispersion is attributable to the larger size of GNP-15 (aspect ratio ~1500), and its higher susceptibility to deform out-of-plane under the melt-extrusion conditions compared to the smaller GNP-1 (aspect ratio <100). Deformed GNP-15 particles are less effective as reinforcements in the polymer matrix since they loss their platelet shape and thus have a smaller aspect ratio during the fabrication of GNP-15 nanocomposites [7]. Meanwhile, based on the fact that at the same volume fraction, the absolute number of GNP-15 particles are a couple of orders of magnitude less than GNP-1, the mechanical properties of HDPE/GNP-15 nanocomposites are therefore not as good as that of HDPE/GNP-1.

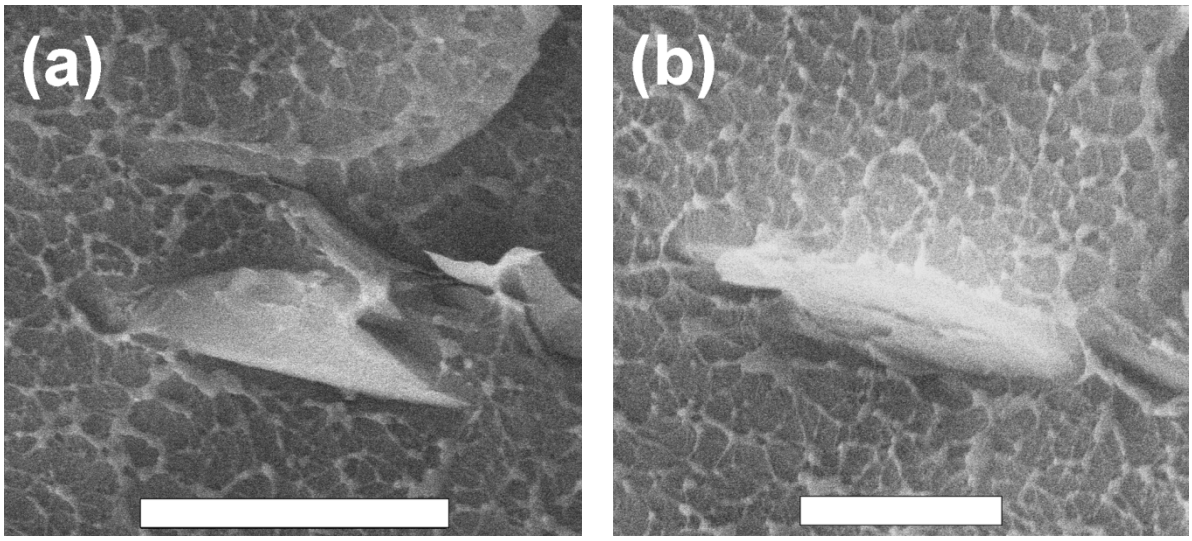

Figure 2.7. (a) a bended GNP-15 nano-particle (scale bar 10 μm) and (b) a rolled-up GNP-15 nano-particle (scale bar 5 μm) in HDPE/GNP-15 nanocomposites at 1 vol% GNP loading

2.4.3 Comparison of GNP to Other Reinforcements in Mechanical Enhancement

The flexural strength and flexural modulus of various HDPE composites incorporated with other fillers and reinforcements up to a filler loading of 15 vol% are presented in the Figure 2.8 and Figure 2.9 respectively. HDPE/CB composites with CB concentration higher than 5 vol% are not included because at the given processing conditions, the viscosity of these composites increases to the level where the extruder could not generate sufficient pressure to extrude the mix properly. For the flexural strength shown in the Figure 2.8, HDPE/CF composites exhibit the highest improvement at all filler loading levels followed by HDPE/GF composites. At the highest loading of 15 vol%, HDPE/CF and HDPE/GF result in ~220% and ~170% improvement in flexural strength compared to the neat HDPE respectively. The great enhancement in the flexural strength for HDPE/CF and HDPE/GF composites is largely due to the high aspect ratio and excellent flexural properties of these fibers [8].

It is noted that HDPE/GNP nanocomposites also exhibit a significant increase in flexural strength. At 15 vol% GNP loading, HDPE/GNP-1 and HDPE/GNP-15 nanocomposites result in ~116% and ~90% improvement in flexural strength respectively, with the GNP-1 nanocomposites being superior to GNP-15 counterparts due to the retention of the platelet morphology during the processing conditions and the much larger number density of GNP-1 nano-particles. At low CB concentrations of up to 5 vol%, HDPE/CB composites have a flexural strength close to those of HDPE/GNP-1.

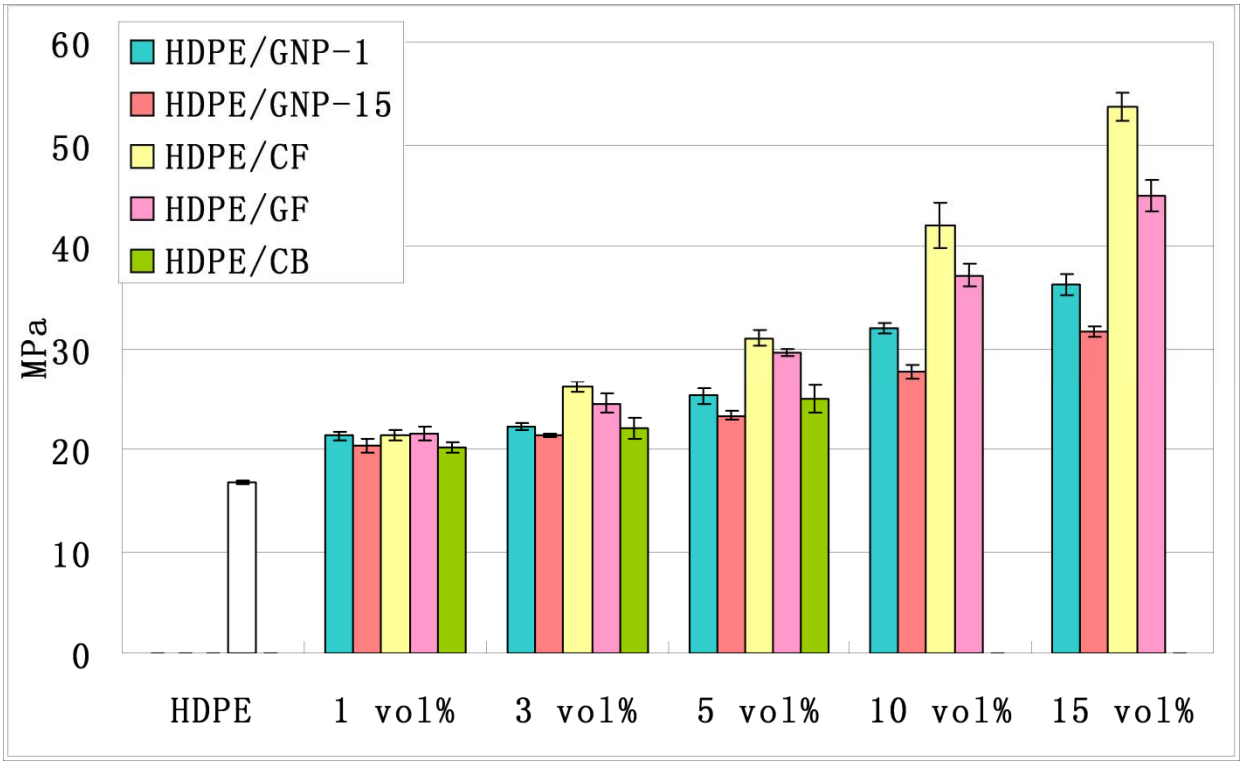

Figure 2.8. Flexural strength of various HDPE composites

For the flexural modulus data presented in the Figure 2.9, again, HDPE/CF composites display the greatest enhancement. HDPE/GNP nanocomposites are competitive to their HDPE/GF and HDPE/CB (up to 5 vol%) counterparts in flexural modulus.

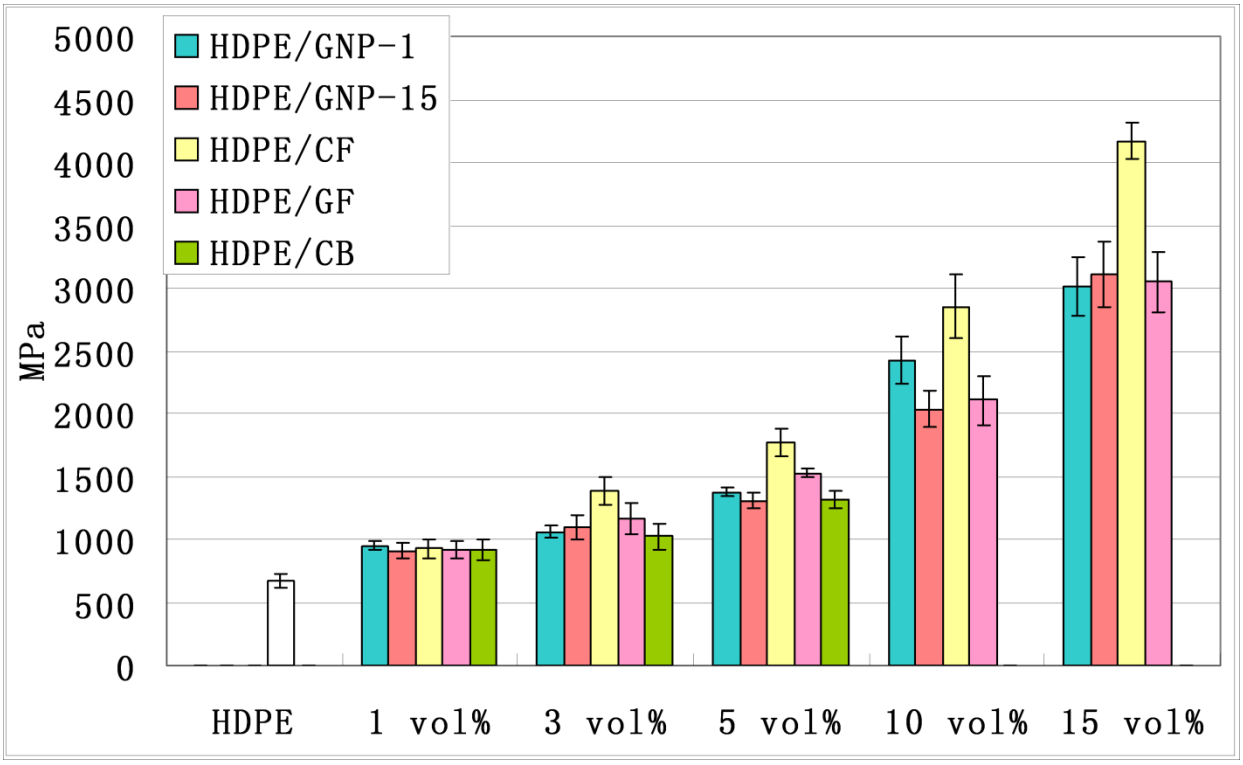

Figure 2.9. Flexural modulus of various HDPE composites

The Izod impact strength of various HDPE composites up to a loading level of 15 vol% is illustrated in the Figure 2.10. A reduction in impact strength is observed in all HDPE composites compared to the neat HDPE sample which normally accompanies incorporation of a rigid filler into a relatively tough polymer [9]. However, HDPE/GNP nanocomposites exhibit the smallest reduction. At reinforcement loadings from 1 vol% to 15 vol%, overall HDPE/GNP-1 nanocomposites have the highest impact strength followed by HDPE/GNP-15 samples and then HDPE/CB composites (up to 5 vol%). HDPE/CF and HDPE/GF show inferior performance compared to the other HDPE composites.

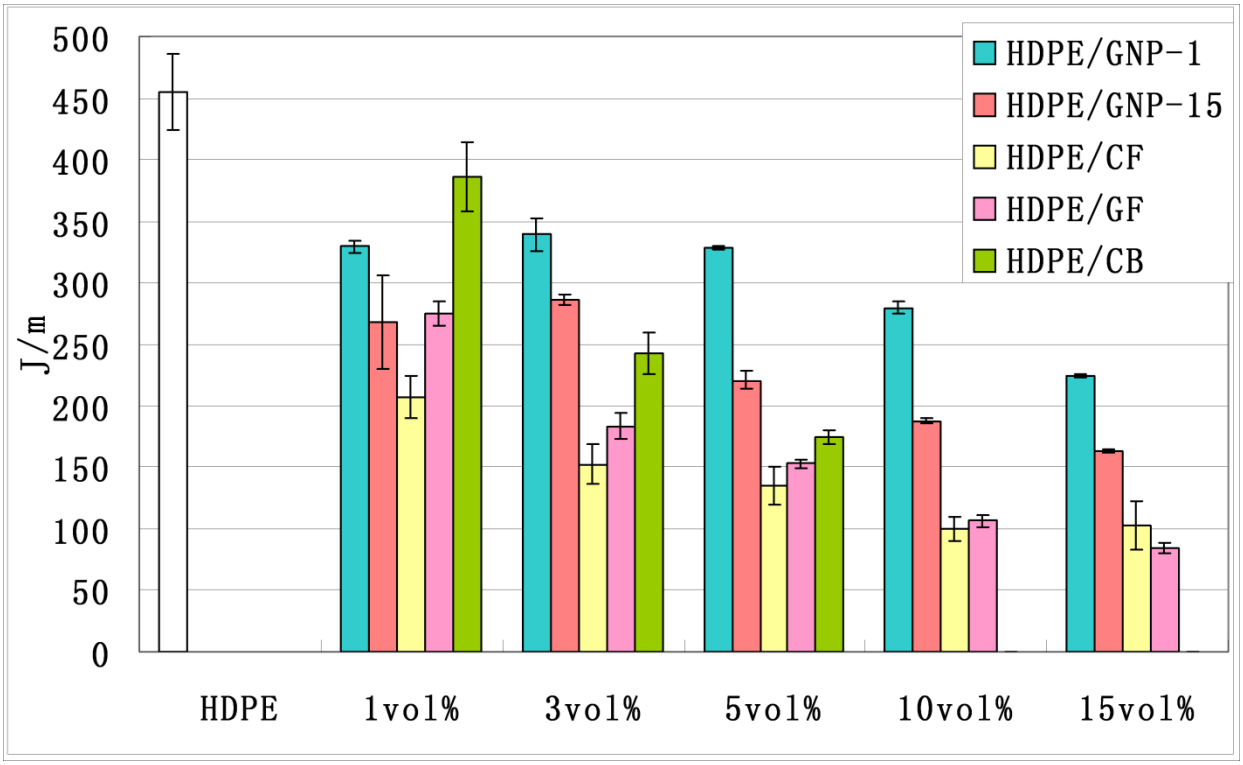

Figure 2.10. Impact strength of various HDPE composites

The difference in impact strength may result from the difference in reinforcements' size and aspect ratio, difference in dispersion situation in the polymer, and the difference in the adhesion between the reinforcements and the polymer matrix. Those differences eventually result in the different energy absorbing mechanisms at the impact fracture surface [10]. The morphology study of the impact fracture surface from various HDPE composites are discussed below.

2.4.4 Morphology of Impact Fracture Surface

To illustrate the difference in impact fracture surface of HDPE composites incorporated with different reinforcements, composite samples at 3 vol% filler loading were taken for the comparison which is shown in the Figure 2.11. Magnifications of these images were kept the

same.

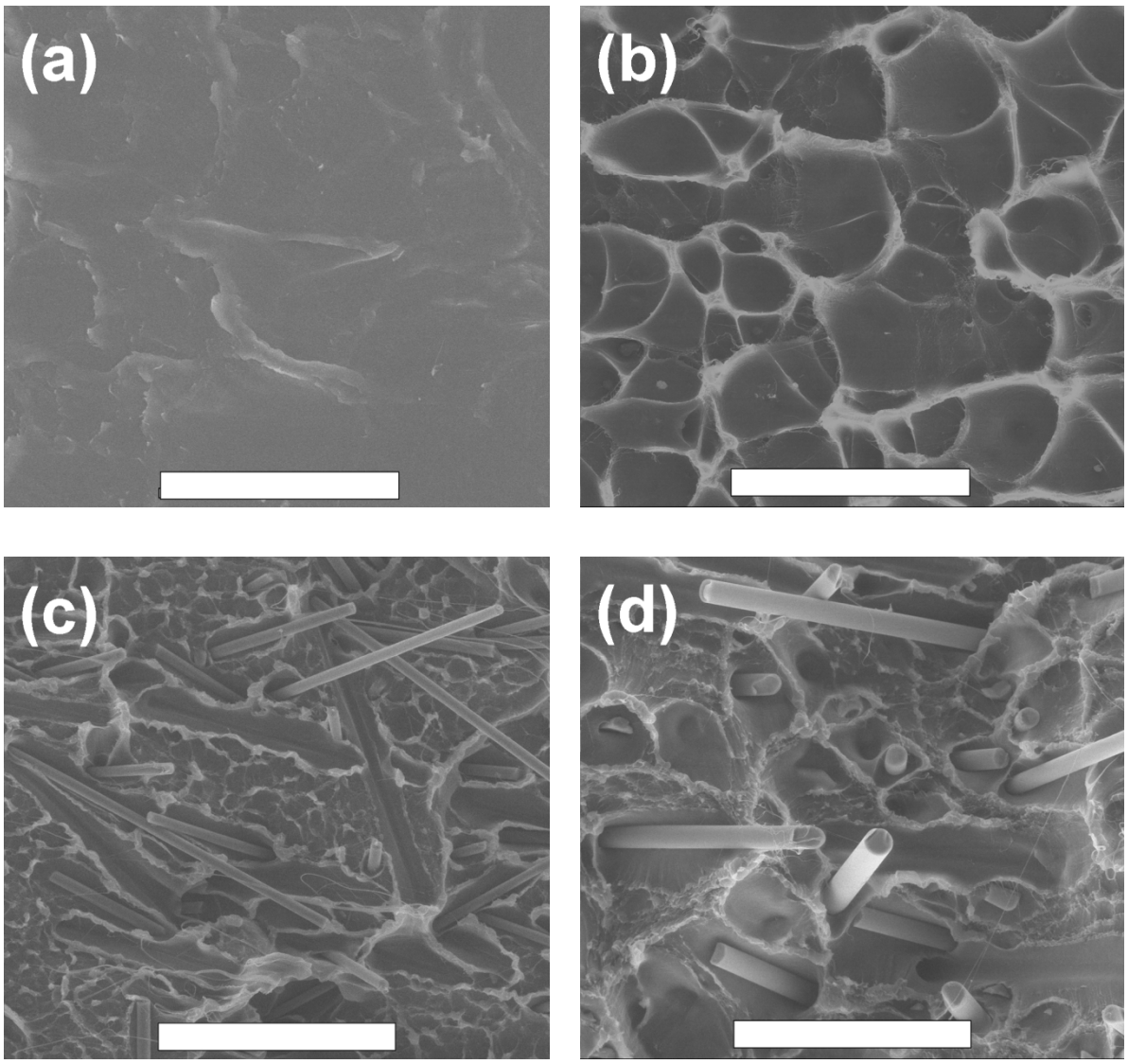

Figure 2.11. Impact fracture surface of various HDPE composites at 3 vol% filler loading: (a) neat HDPE (Scale bar 150 μm); (b) HDPE/CB (Scale bar 150 μm); (c) HDPE/CF (Scale bar 150 μm); (d) HDPE/GF (Scale bar 150 μm); (e) HDPE/GNP-1 (Scale bar 150 μm); (f) HDPE/GNP-15 (Scale bar 200 μm)

Figure 2.11 (cont'd)

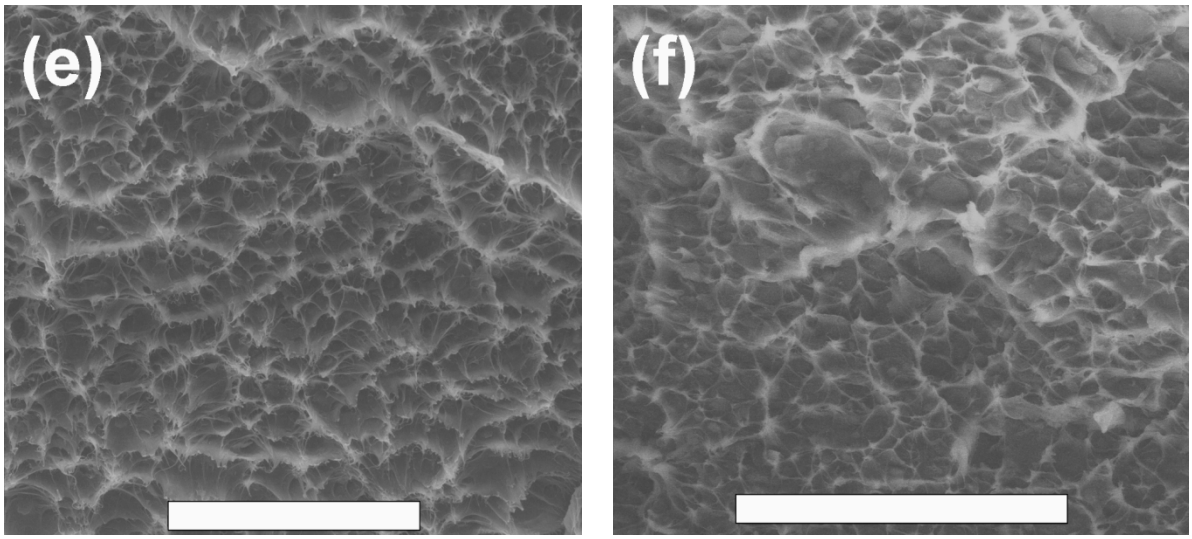

Figure 2.11 (a) is the impact fracture surface of neat HDPE, which is smooth and homogeneous. The impact fracture surface the HDPE/CB composite is shown in the Figure 2.11 (b). It is obvious to detect that the topography of the matrix has been changed which indicates the energy absorbing mechanics was altered by the addition of CB. Figure 2.11 (c) and Figure 2.11 (d) are the fracture surface of HDPE/CF and HDPE/GF composites respectively. The presence of holes, lines and the appearance of fiber 'pull-outs' imply the inadequate adhesion between the CF, GF fibers and the polymer matrix resulting in the minimum impact strength of these HDPE composites. Poor adhesion can also be confirmed by a 'clean' surface on these fibers with little HPDE remaining on the fiber fragments. Figure 2.11 (e) and Figure 2.11 (f) show the impact fracture surface of HDPE/GNP-1 and HDPE/GNP-15 nanocomposites. The fracture surface exhibits 'deformed cellular' morphology. The topography and cellular density clearly show the evidence of increased plastic deformation of the matrix along the matrix-reinforcement interface. To locate the positions of GNP nanoparticles in the 'deformed cellular' structure, ESEM images

at higher magnifications were applied. Figure 2.12 (a) shows the location of GNP-1 nanoparticles and Figure 2.12 (b) depicts the position of GNP-15. Form these images, it is concluded that both GNP-1 and GNP-15 nano-particles are located in the bottom of these 'deformed cells'. Micro polymer fibrils can also be observed around the GNP nanoplatelets. It is noted that formation of these micro polymer fibrils absorbs much deformation energy. However, the GNP surface also appears to be 'clean' and free of HDPE which suggests that the adhesion between HDPE and the surface of GNP is still not so good. In conclusion, increased plastic deformation and formation of micro polymer fibrils at the HDPE-GNP interface is responsible for the relatively higher impact strength of HDPE/GNP nanocomposites. HDPE/GNP-1 samples are superior to HDPE/GNP-15 because of the smaller size coupled with the larger number of reinforcing particles per unit volume and the better dispersion of GNP-1 in the HDPE matrix.

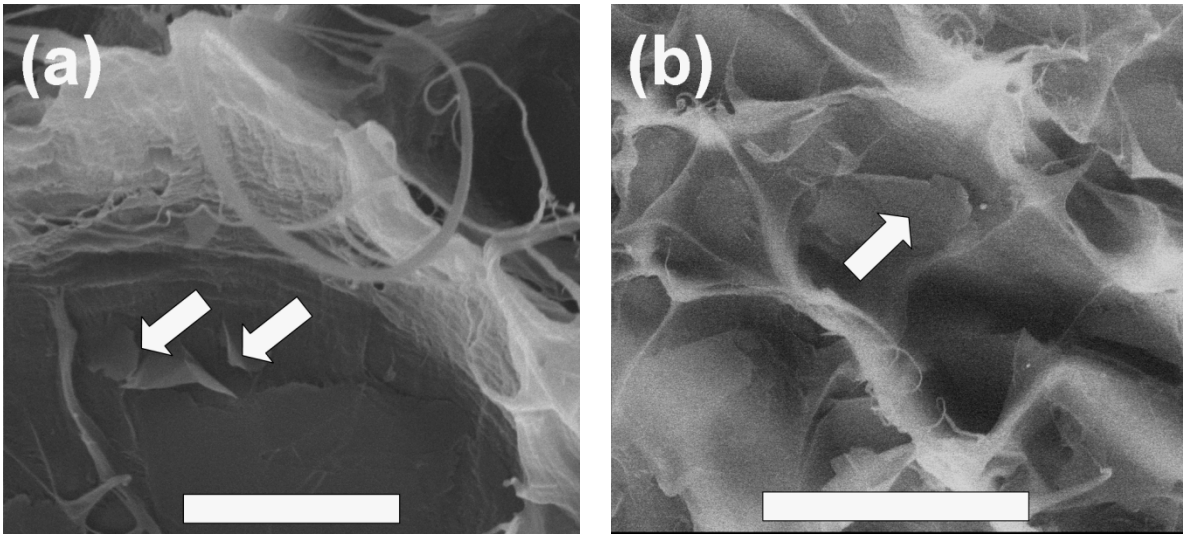

Figure 2.12, The location of GNP nanoparticles in the 'deformed cellular' structure. (a) GNP (Scale bar 5 μm); (b) GNP-15 (Scale bar 20μm)

2.5 Conclusions

Investigation of the mechanical properties (flexural strength, flexural modulus and impact strength) indicates that HDPE/GNP nanocomposites show superior Izod impact properties and competitive stiffness and flexural properties compared to other HDPE composites filled with commercial reinforcements (CF, CB, GF). The superior properties in HDPE/GNP nanocomposites reflect the good compatibility between the nano-reinforcement and the polymer matrix and also the exceptional mechanical properties of GNP as the nano-filler. However, for the two kinds of GNP used in this study, HDPE/GNP-1 nanocomposites always exhibit higher mechanical properties than HDPE/GNP-15 counterparts. The superiority of GNP-1 is attributed to the larger number of reinforcing particles per unit volume, the retention of platelet structure during the processing conditions and the adequate aspect ratio (~ 100), which have been verified by the morphology of their fracture surface.

The investigation of the impact fracture surface of various HDPE composites indicates that GNP nano-particles have a relatively good adhesion with the polymer matrix while the appearance of fiber 'pull-out' in HDPE/CF and HDPE/GF composites reflects the inadequate adhesion between these fibers and HDPE. The difference in adhesion also plays a role in the difference of the mechanical properties. Thus, to obtain the HDPE/GNP nanocomposites with even better mechanical properties, a better mixing/dispersion process and/ or surface treatment of GNP are required in order to improve the dispersion of GNP nanoplatelets in polymers and also improve their compatibility and adhesion.

REFERENCES

REFERENCES

[1] Vaia RA. Polymer nanocomposites open a new dimension for plastics and composites. AMPTIAC Newsletter. 2003;6(1):17–24.

[2] Krishnamoorti R VR. Polymer Nanocomposites Synthesis, Characterization and Modeling. Proc of American Chemical Soc Symp Ser 804. Washington DC2001.

[3] http://en.wikipedia.org/wiki/High-density_polyethylene.

[4] Bigg DM. Mechanical property enhancement of semicrystalline polymers—A review. Polymer Engineering & Science. 1988;28(13):830-41.

[5] http://www.xgsciences.com/.

[6] Fukushima H. Graphite nanoreinforcements in polymer nanocomposites [PHD Thesis]. East Lansing, MI, USA: Michigan State University; 2003.

[7] Kalaitzidou K, Fukushima H, Drzal LT. Mechanical properties and morphological characterization of exfoliated graphite/polypropylene nanocomposites. Composites Part A: Applied Science and Manufacturing. 2007;38(7):1675-82.

[8] Mai K, Li J, Zeng H. Mechanical property and fracture morphology of fiber-reinforced polysulfone plasticized with acetylene-terminated sulfone. Journal of Applied Polymer Science. 1994;52(9):1279-91.

[9] Wakabayashi K, Pierre C, Dikin DA. Polymer-Graphite Nanocomposites: Effective Dispersion and Major Property Enhancement via Solid-State Shear Pulverization. Macromolecules. 2008;41:1905-8.

[10] Kim J-K, Mai Y-W. High strength, high fracture toughness fibre composites with interface control—A review Composites Science and Technology. 1991;41(4):333-78.

CHAPTER 3 CRYSTALLIZATION, THERMAL, AND ELECTRICAL PROPERTIES OF HIGH DENSITY POLYETHYLENE NANOCOMPOSITES PRODUCED BY INCORPORATION OF EXFOLIATED GRAPHENE NANOPLATELETS

3.1 Abstract

This chapter investigated the effect of exfoliated graphene nanoplatelets, GNP, on the crystallization behavior, thermal stability, thermal conductivity, and electrical conductivity of high density polyethylene (HDPE) /GNP nanocomposites. HDPE/GNP nanocomposites were fabricated by the conventional processing method of melt-extrusion followed by injection molding. Results indicated that GNP is a good nucleating agent at low loading levels and as a result can significantly increases crystallization temperature and crystallinity of HDPE. At high GNP loadings, however, the close proximity of GNP particles retards the crystallization process. The thermal stability and thermal conductivity of HDPE/GNP nanocomposites were found to be significantly enhanced as a function of GNP concentration due to the excellent thermal properties of GNP. Meanwhile, results showed that the percolation threshold of these nanocomposites prepared by melt-extrusion and injection molding is relatively high at around 10-15 vol% GNP loading. The high percolation threshold is mainly due to the severe GNP aggregation and preferential platelets alignment during the processing conditions as verified by their morphology.

3.2 Introduction

Thermally and electrically conductive polymeric composites are the materials of high interest because of the potential advantages of these materials in many applications such as for

electromagnetic interference (EMI) shielding devices, power rechargeable batteries, electronic devices, light emitting diodes (LEDs), gas sensors, super capacitors and photovoltaic cells [1-4]. Polymeric composites filled with metallic fillers have been traditionally used because of their excellent thermal and electrical conductivity. But the metal filled composites have the disadvantages such as high density, high susceptibility to oxidation/corrosion and relatively high cost [5]. Currently, carbon black is commonly used as a conductive filler to increase the thermal and electrical conductivity of polymeric composites due to its low cost, low density, high chemical corrosion resistance and the ease of processing into host polymers compared with metallic fillers [6]. However, since carbon black is an amorphous form of carbon having irregular shapes and a disordered structure, the intrinsic electrical conductivity of carbon black is normally low owing to large electron 'hopping' distance between the carbon aggregates. Reports have shown that carbon black filled polymeric composites usually do not have adequate electrical and thermal conductivity as required [7].

To achieve a high thermal and electrical conductivity of polymeric composites but low cost and easy processing, graphite based materials are gaining more and more research attention. Polycrystalline graphite is a material that consists of extended networks of sp^2-hybridized carbons in a planar layered structure (graphene) resulting in the excellent thermal and electrical conductivity within this graphitic basal plane [8]. Exfoliation of these graphite (graphene) layers and dispersion of them into polymers offers the potential to produce multiple conductive pathways in the resulting nanocomposites at low graphite concentrations [9].

As discussed in the introduction chapter, GNP nanoplatelets exhibit excellent thermal and

electrical properties and GNP nanocomposites can also be fabricated with superior thermal and electrical conductivity under appropriate processing conditions [10-14]. However, due to the interaction between the graphene surfaces of GNP and semi-crystalline polymers, the crystallization behavior of the host polymer is altered which can interfere with the electrical and thermal percolation [15, 16]. Therefore, the aim of this research is to (1): determine the crystallization behavior of HDPE/GNP nanocomposites, i.e., the crystallinity and crystallization temperature; (2): investigate the effect of GNP on the thermal properties such as thermal stability and thermal conductivity of HDPE; (3): and investigate how the addition of GNP improves the electrical conductivity of HDPE/GNP nanocomposites.

3.3 Experimental

3.3.1 Materials

In this research, HDPE pellets with the trade name Marlex® HXM 50100 (Density 0.95 g/cm^3, MW~ 230,000) were obtained from Chevron Phillips Chemical Company. GNP-1 and GNP-15 nanoplatelets were obtained from XG Science, Inc.

3.3.2 Processing Methods

The fabrication method used to prepare HDPE/GNP nanocomposites in this study is the same melt-extrusion followed by injection molding as described in the previous chapter. Flexural coupons were made for electrical conductivity measurements and round composite disks (thickness ~1.5 mm, diameter ~25 mm) were injection molded for thermal conductivity test

under the same injection conditions.

3.3.3 Characterization Techniques

The crystallinity and crystallization temperature were measured by using differential scanning calorimetry (DSC 2920, TA Instruments). The samples used were 5–10 mg and non-isothermal crystallization was studied using the following experimental conditions: the sample was heated to 160 °C at a rate of 20 °C/min. The prior thermal history of the sample was erased by maintaining isothermal conditions at 160 °C for 5 minutes. Then the sample was cooled down to 40 °C at a rate of 20 °C/min, reheated at 20 °C/min to 160 °C, and cooled back to 40 °C again. The data of melting enthalpy (ΔH_m) and crystallization peak temperature (T_c) were collected during the second cycle. The degree of crystallization was calculated by the following equation:

$$\chi\% = \frac{1}{1 - wt\%} \frac{\Delta H_m}{\Delta H_m^0} \qquad [3.1]$$

Where χ% is the percent crystallinity of the matrix, wt% is the weight percentage of GNP, and ΔH_m^0 is the theoretical melting enthalpy of the matrix if it is 100% crystalline.

The thermal stability of HDPE/GNP nanocomposites was determined from the thermo-gravimetric analysis (TGA), which was carried out on a TA instrument (TGA 2950) at a heating rate of 20 °C/min under nitrogen from 30 °C to 800 °C. The onset thermal decomposition temperature was determined as the temperature at which there was a 5% HDPE weight loss. Thermal conductivity of HDPE/GNP nanocomposites was measured using Unitherm^{TM} Model

2022 thermal conductivity instrument (contact mode). The through-plane conductivity, i.e., the heat flow was normal to the flow direction induced during injection molding, was evaluated by using the round disks made by DSM melt-extrusion.

To evaluate the in-plane thermal conductivity of HDPE/GNP nanocomposites, the laser flash method (LFA) was applied in this study. Thermal diffusivity (α, m^2/s) (both in-plane and through-plane) of GNP nanocomposites (round disks) was measured by a LFA Nanoflash 447 light flash system. To calculate the thermal conductivity, the bulk density of the samples (ρ, kg/m^3) was obtained by dividing the mass over the volume, and the specific heat capacity (C_p: J/(kg· K)) was measured through the DSC. The thermal conductivity (κ, W/(m·K)) of GNP samples was then calculated by the following equation:

$$\kappa = \alpha \times \rho \times C_p \qquad [3.2]$$

The electrical resistivity of HDPE/GNP nanocomposites was measured both along the flow direction (in-plane resistivity) and through the thickness direction (through-plane resistivity, normal to the flow direction), using impedance spectroscopy by applying a two-probe method at room temperature. Samples with dimensions around 10 x 3.2 x 12.2 mm (Length x Thickness x Width) were cut from the middle portion of flexural coupons. The two surfaces connected to the electrodes were first treated with O_2 plasma (14 minutes, 375 W) in order to remove the top surface layers which are rich in polymer and then conductive silver paste was used to ensure good contact of the sample surface with the electrodes. The resistance of samples was measured and converted to resistivity by taking the sample dimensions into account.

The morphology of the nanocomposites was investigated by a JEOL (model JSM-6400) SEM. The samples were gold coated to avoid charging.

3.4 Results and Discussion

3.4.1 Crystallization Behavior of HDPE/GNP Nanocomposites

Figure 3.1 shows the crystallization temperature of HDPE/GNP nanocomposites. It is seen that incorporation of GNP has a significant effect on the crystallization temperature of HDPE; that is, the crystallization temperature increases as the GNP content increases. A relatively large temperature increase can be detected (around 3 °C) even at a low GNP loading of 1 vol%. The increased crystallization temperature indicates that the presence of GNP particles acts as nucleating agents which facilitate the crystallization process of HDPE [17].

The total percent of crystallinity of HDPE/GNP-1 and HDPE/GNP-15 nanocomposites obtained from the equation [3.1] after the non-isothermal crystallization process is shown in the Figure 3.2. For GNP-1 and GNP-15 nanocomposites, the crystallinity first increases with the GNP content and then drops to an almost constant value. The highest crystallinity of HDPE/GNP-1 and HDPE/GNP-15 nanocomposites both occurs at 3 vol% GNP loading. This interesting phenomenon is believed to be the result of a compromise between the nucleating and retarding effects of GNP on the host polymer during the non-isothermal crystallization [18]. When the GNP content is relatively low, GNP particles exhibit a strong nucleating effect and act as heterogeneous nucleating sites at the GNP-HDPE interfaces, thus increasing the crystallinity of HDPE. When the GNP concentration reaches a high level, the presence of the abundant GNP

particles significantly hinders the diffusion of polymer chains to the growing crystallites. The total percent of crystallinity is therefore reduced.

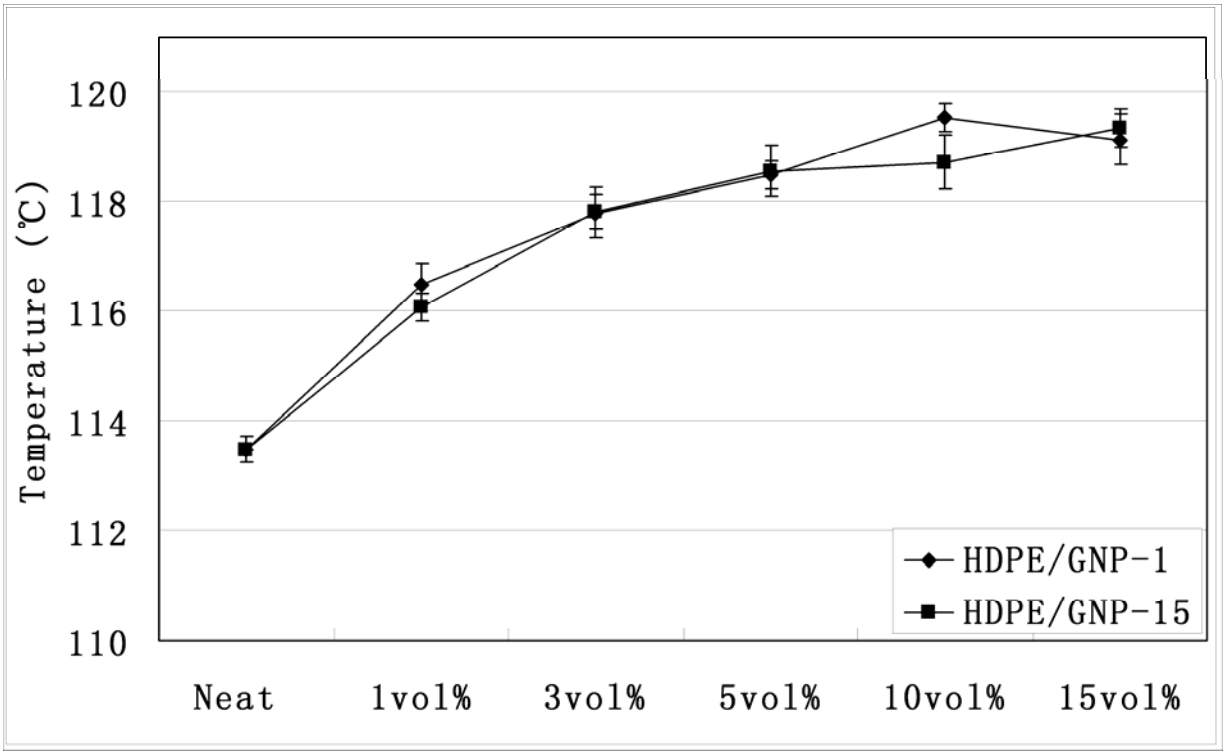

Figure 3.1. Crystallization temperatures of HDPE/GNP nanocomposites

From Figure 3.2, it is also seen that HDPE/GNP-1 nanocomposites always show higher crystallinity than HDPE/GNP-15 counterparts at the same GNP content, which suggests the nucleating efficiency between GNP-1 and GNP-15 is different. The superior nucleating efficiency of GNP-1 is due to the fact that the absolute number of GNP-1 particles is much larger than GNP-15 at the same filler concentration as described in the previous chapter, which provides more nucleating sites to initiate the polymer crystallization.

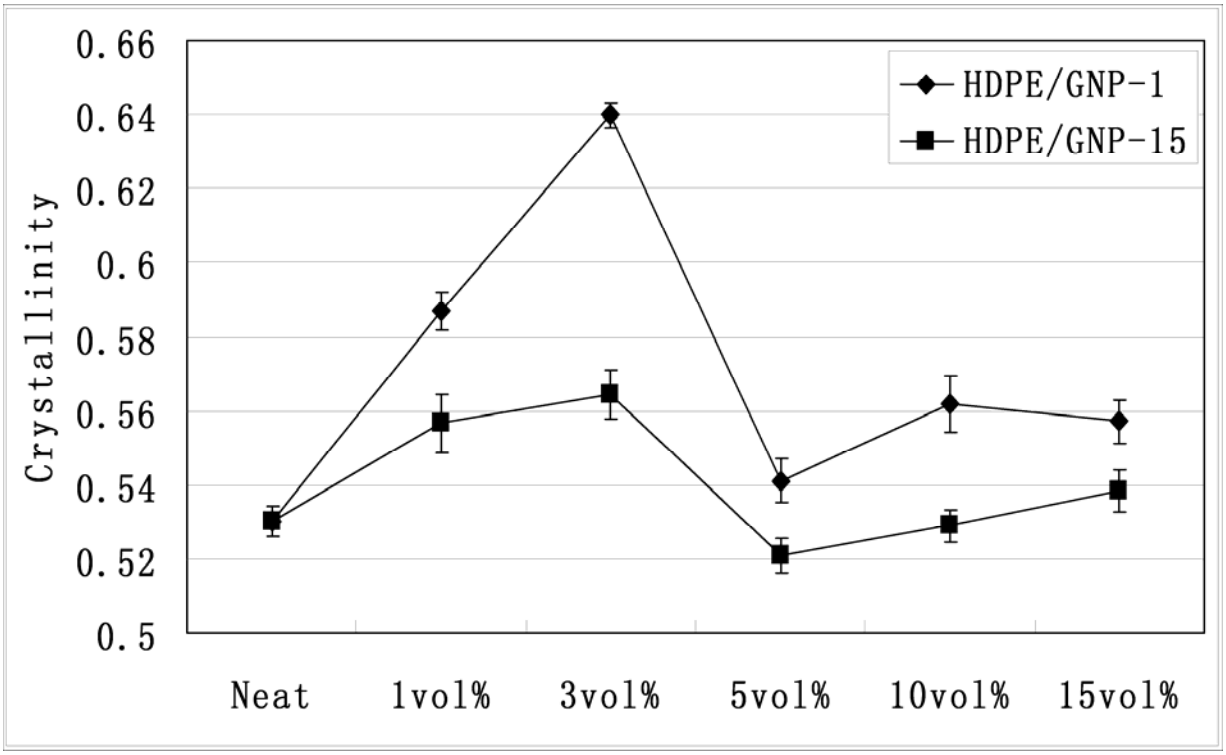

Figure 3.2. Total percent of crystallinity of HDPE/GNP nanocomposites

3.4.2 Thermal Stability of HDPE/GNP Nanocomposites

Figure 3.3 displays the TGA curves of HDPE and HDPE/GNP-1 samples with different GNP-1 loadings carried out in nitrogen. From the thermo-gravimetric curves, it is seen that pure HDPE is thermally stable until around 300 °C and after the onset degradation temperature of 420 °C, the degradation rate of HDPE accelerates. For HDPE/GNP-1 samples, the thermal stability increases to around 400 °C and the onset degradation temperature for 1 vol%, 3 vol%, 5 vol%, 10 vol% and 15 vol% HDPE/GNP-1 nanocomposites increases to 450 °C, 460 °C, 480 °C, 490 °C, 495 °C respectively which are 30 °C, 40 °C, 60 °C, 70 °C, 75 °C higher than neat HDPE. Thus it can be concluded that HDPE/GNP-1 nanocomposites show much better thermal stability than HDPE, which is resulting from the high thermal stability of GNP-1 and the shielding effect of the

nano-reinforcement on the diffusion of combustion gases into and out of the polymer matrix during its thermal decomposition [19].

The TGA curves for HDPE and HDPE/GNP-15 samples are presented in the Figure 3.4. It is concluded that HDPE/GNP-15 nanocomposites also exhibit enhanced thermal stability with the onset thermal degradation temperature increased from 420 °C for neat HDPE to 480 °C for the HDPE/GNP-15 sample at 15 vol% GNP loading.

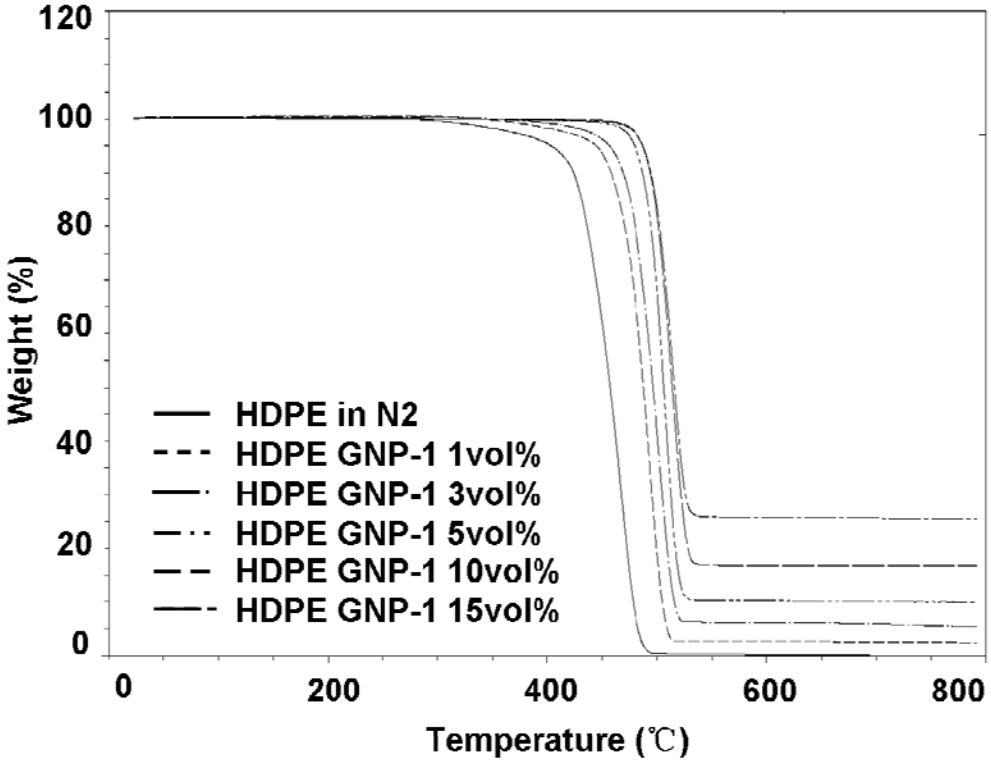

Figure 3.3. TGA curves of HDPE and HDPE/GNP-1 nanocomposites

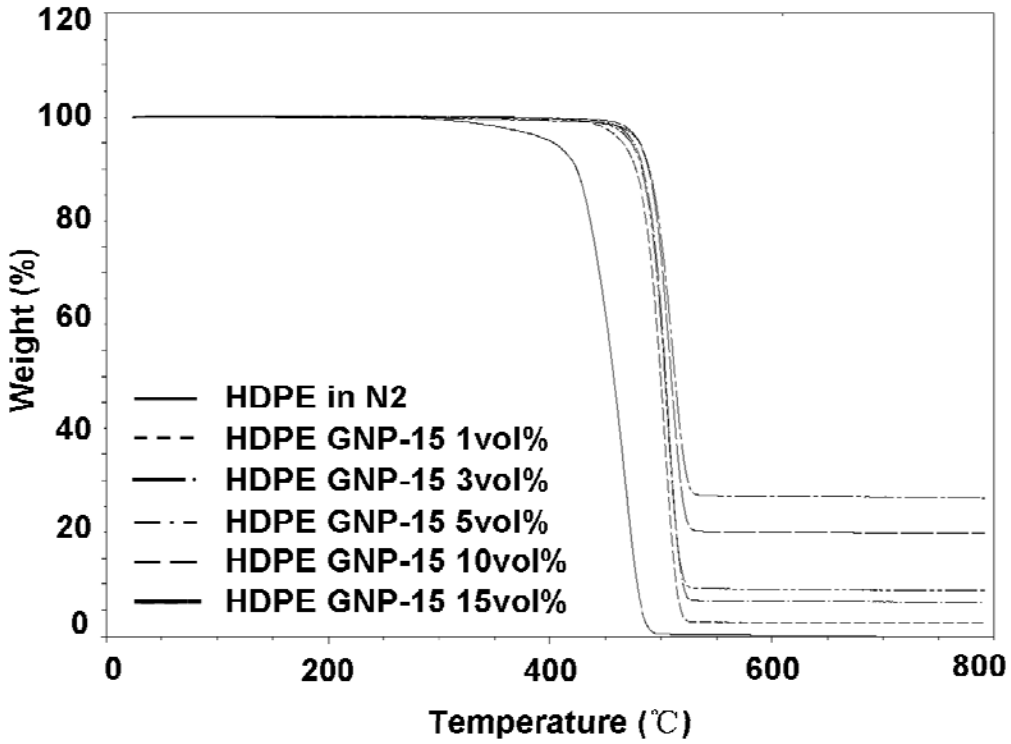

Figure 3.4. TGA curves of HDPE and HDPE/GNP-15 nanocomposites

3.4.3 Thermal Conductivity of HDPE/GNP Nanocomposites

The through-plane thermal conductivity of HDPE/GNP nanocomposites is shown in the Figure 3.5. It is detected that with increasing GNP loadings, the thermal conductivity of GNP-1 and GNP-15 nanocomposites both increases. At relatively low filler contents (from 1 to 5 vol%), the thermal conductivity of HDPE/GNP-15 nanocomposites is almost the same as that of HDPE/GNP-1 samples. However, when the GNP loading is higher than 5 vol%, HDPE/GNP-15 nanocomposites exhibit superior thermal conductivity.

Several models predict the thermal conductivity of composites as a function of filler content. Among them, the Maxwell-Eucken and Bruggeman models are commonly used in literature. Here, I apply these two models to evaluate the thermal conductivity of HDPE/GNP

nanocomposites.

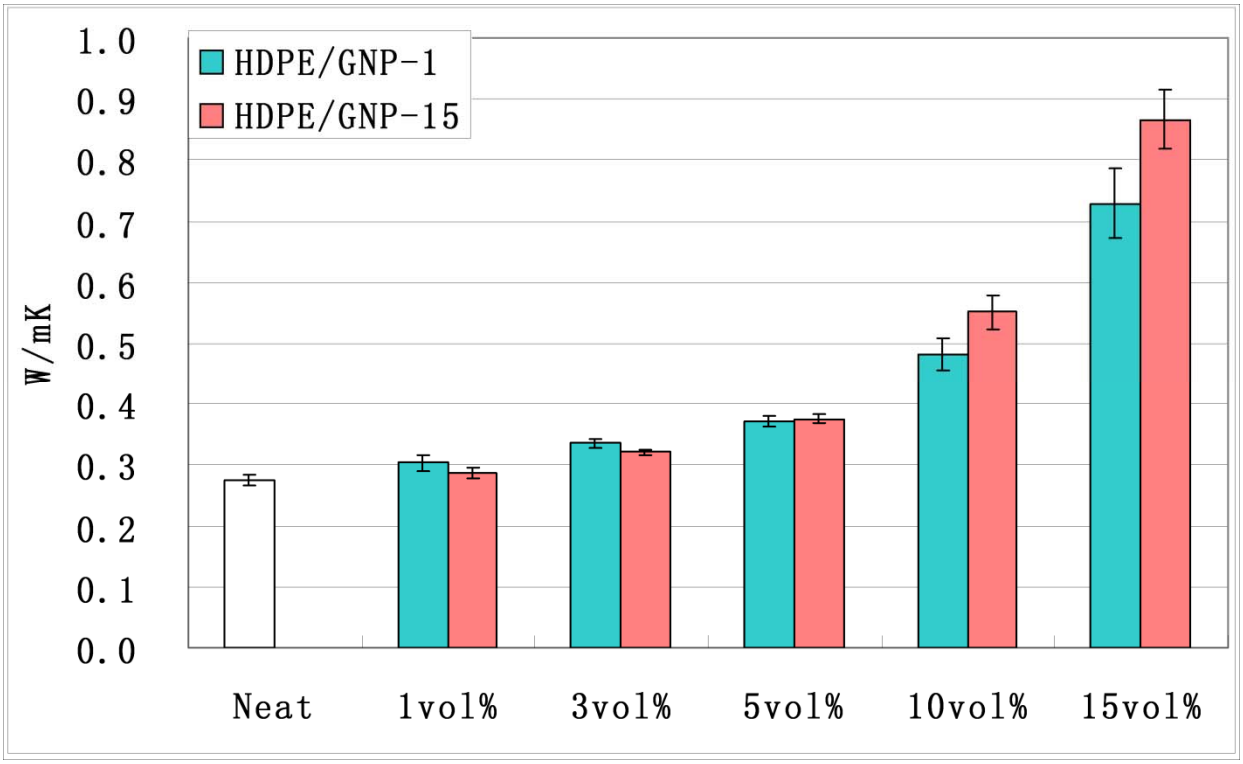

Figure 3.5. Through-plane thermal conductivity of HDPE/GNP nanocomposites by contact mode

Maxwell-Eucken Model:

$$\kappa = \frac{\kappa_p[2\kappa_p + \kappa_f + 2V_f(\kappa_f - \kappa_p)]}{2\kappa_p + \kappa_f - 2V_f(\kappa_f - \kappa_p)} \qquad [3.3]$$

Bruggeman Model:

$$1 - V_f = \frac{(\kappa_f - \kappa)(\kappa_p/\kappa)^{1/3}}{\kappa_f - \kappa_p} \qquad [3.4]$$

where κ, κ_p, κ_f are the thermal conductivity of composites, polymer and filler respectively. And

V_f is the volume fraction of filler.

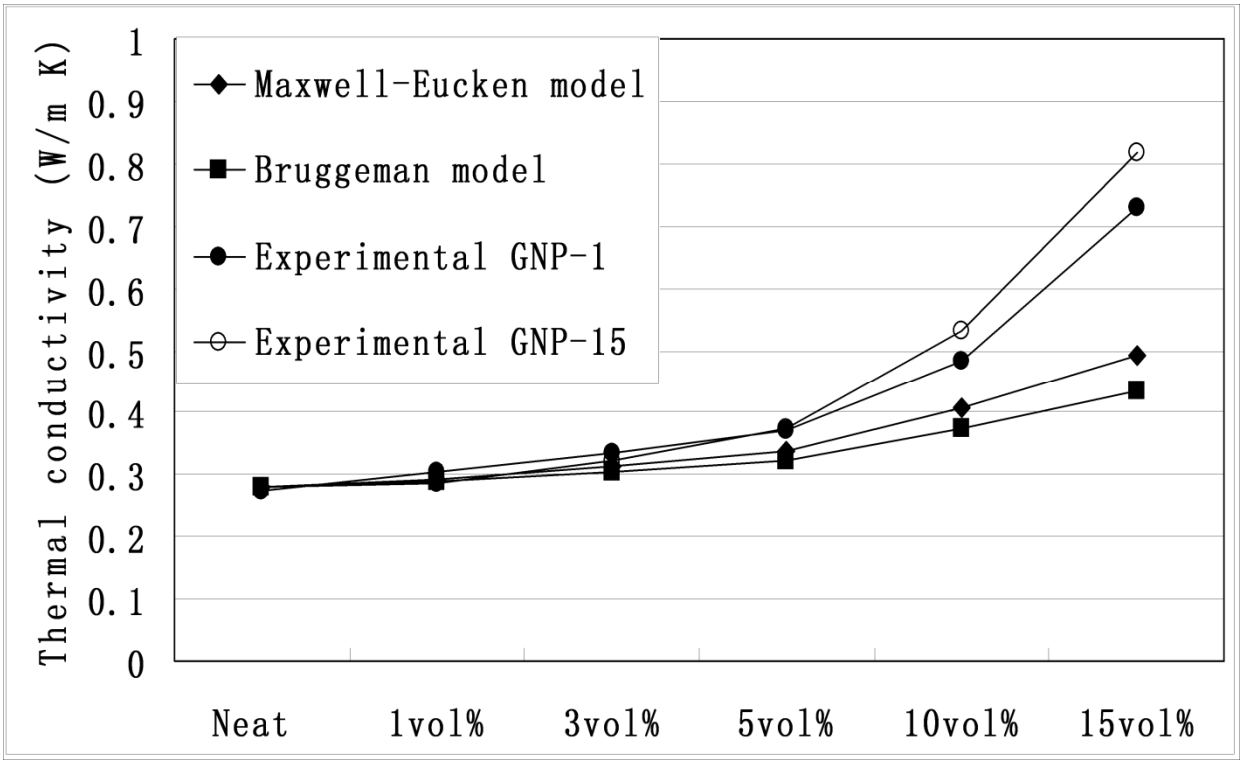

Figure 3.6. Comparison of experimental data with the data predicted by different models for through-plane thermal conductivity of HDPE/GNP nanocomposites

The predicted values for thermal conductivity from both models as well as the experimental data are presented in the Figure 3.6. It is clear from the figure that the experimental data do not agree with Maxwell-Eucken or Bruggeman models well, especially when the GNP loading is over 5 vol%. The experimental data are much higher than those predicted, because both models assume that the shape of filler is spherical and the aspect ratio of filler is not taken into account [19]. Furthermore, the dispersion status and the orientation of the filler in the polymer matrix are not considered in these models as well. However, the dispersion and orientation of fillers in the polymer matrix is believed to be the essential factor affecting the thermal conductivity for the

fillers with high aspect ratio and anisotropic thermal properties [5].

To better investigate the thermal conductivity of HDPE/GNP nanocomposites as a function of GNP loading, the Agari model [20] was applied which considers the effect of aspect ratio by introducing two factors C_1 and C_2:

$$\log \kappa = V_f C_2 \log \kappa_f + (1 - V_f) \log(C_1 \kappa_p) \qquad [3.5]$$

Here again, κ, κ_p, κ_f are the thermal conductivity of composites, polymer and filler respectively. And V_f is the volume fraction of filler. C_1 is the factor relating to the effect on crystallinity and crystal size of polymer. C_2 is the factor relating to the measure of ease for the formation of conductive networks in polymer matrix. According to this model, the larger the value of C_2, the conductive paths will be formed more easily in composites. By fitting the experimental data into the model, C_1 and C_2 for the HDPE/GNP-1 and HDPE/GNP-15 nanocomposites are indicated in the Table 3.1.

Table 3.1. Values of C_1 and C_2 for HDPE/GNP nanocomposites

Materials	C_1	C_2
HDPE/GNP-1	0.991	2.108
HDPE/GNP-15	0.928	2.668

From Table 3.1, the C_1 value of HDPE/GNP-1 nanocomposites is slightly higher than that of HDPE/GNP-15, which indicates GNP-1 have stronger effect on the crystallinity and crystal size of HDPE. This is consistent with the results described in the 3.1 section, that is, HDPE/GNP-1

nanocomposites always show higher crystallinity than HDPE/GNP-15. However, the value of C_2 for HDPE/GNP-15 nanocomposites is much higher, which means that GNP-15 is more capable of forming conductive paths in the resulting nanocomposites. This is because the aspect ratio of GNP-15 (~ 1000) is much larger than that of GNP-1 (~ 100). Thus, GNP-15 nanoplatelets can connect with each other more easily to form conductive paths which lead to lower thermal contact resistance and higher thermal conductivity in HDPE/GNP-15 nanocomposites.

In order to compare the in-plane thermal conductivity of HDPE/GNP nanocomposites with their through-plane conductivity, the LFA method was used and the calculated data from the equation [3.2] is presented in the Figure 3.7. For the through-plane thermal conductivity shown in this figure, it is noted that the absolute values at each GNP loading are different from those in the Figure 3.5 which is due to the different testing mechanisms. However, the overall trend is the same; that is, HDPE/GNP-15 nanocomposites exhibit equivalent through-plane thermal conductivity to HDPE/GNP-1 counterparts at relatively low filler contents (from 1 to 5 vol%). But they have superior thermal conductivity at high GNP loadings. For in-plane thermal conductivity, the same conclusion can be made that HDPE/GNP-15 nanocomposites have much higher in-plane thermal conductivity when the GNP loading is higher than 5 vol%. The superior thermal conductivity in HDPE/GNP-15 nanocomposites is due to the much larger aspect ratio of GNP-15 nanoplatelets and their ease of forming conductive paths as described above.

If we compare the in-plane conductivity with the through-plane conductivity, it is found HDPE/GNP nanocomposites exhibit much higher in-plane thermal conductivity at every GNP loading. For injection molded HDPE/GNP samples, higher in-plane conductivity is resulted from

the preferential GNP alignment during the injection molding process, which will be fully addressed later in the morphology section (3.4.5) and the anisotropic thermal property of GNP as the conductive filler (The in-plane thermal conductivity of GNP platelet is 3000 W/mK, and the through-plane conductivity is only 10 W/mK due to its anisotropic structure [21]).

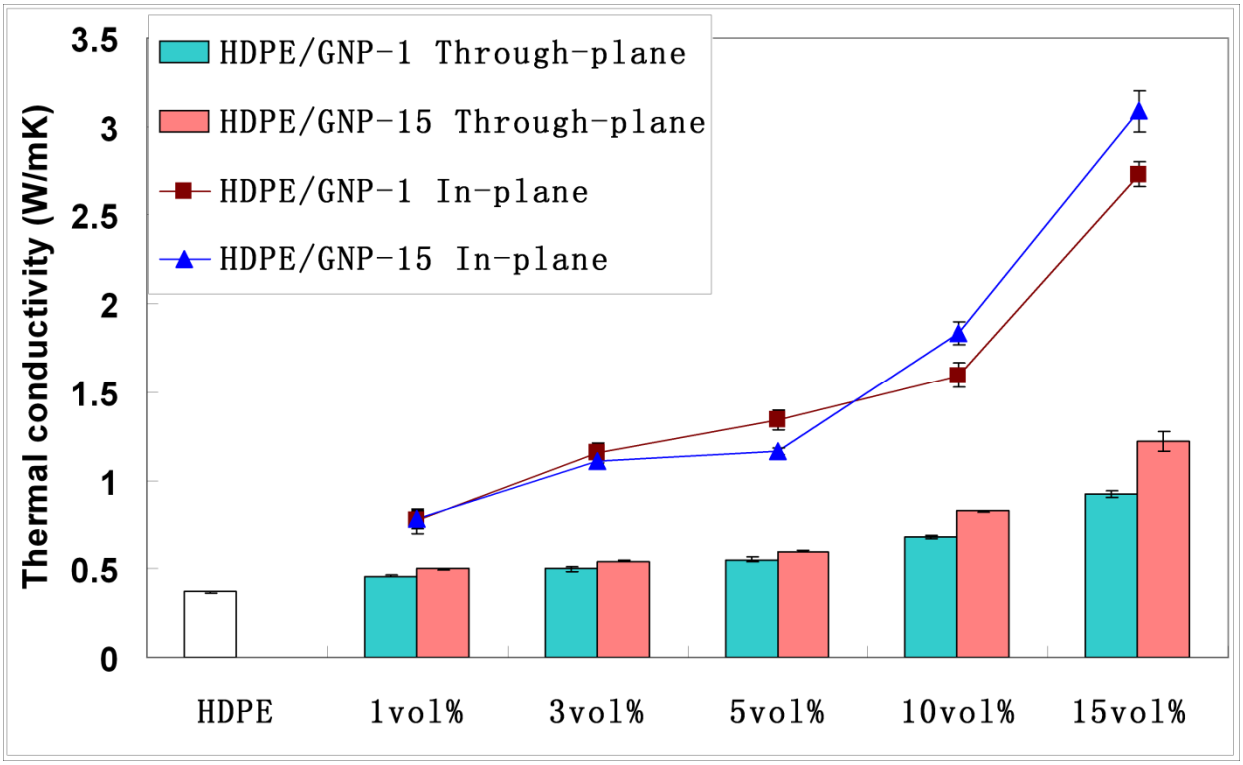

Figure 3.7. In-plane and through-plane thermal conductivity of HDPE/GNP nanocomposites obtained by the LFA method.

3.4.4 Electrical Conductivity of HDPE/GNP Nanocomposites

The in-plane and through-plane electrical resistivity of HDPE/GNP nanocomposites made by melt-extrusion and injection molding are shown in the Figure 3.8. For both in-plane and through-plane resistivity, it is seen that between 10 vol% and 15 vol% GNP content, there is a large decrease in resistivity for HDPE/GNP nanocomposites. This concentration range (10-15

vol%) is thus noted as the percolation threshold for these nanocomposites. The percolation threshold is defined as the concentration where a connected assembly of conductive particles is formed within a polymer matrix. This assembly penetrates throughout the sample in forming conductive paths for electron transportation. At this concentration of the conductive filler, the electrical conductivity of the nanocomposites significantly increase and the nanocomposites become electrical conductive [22].

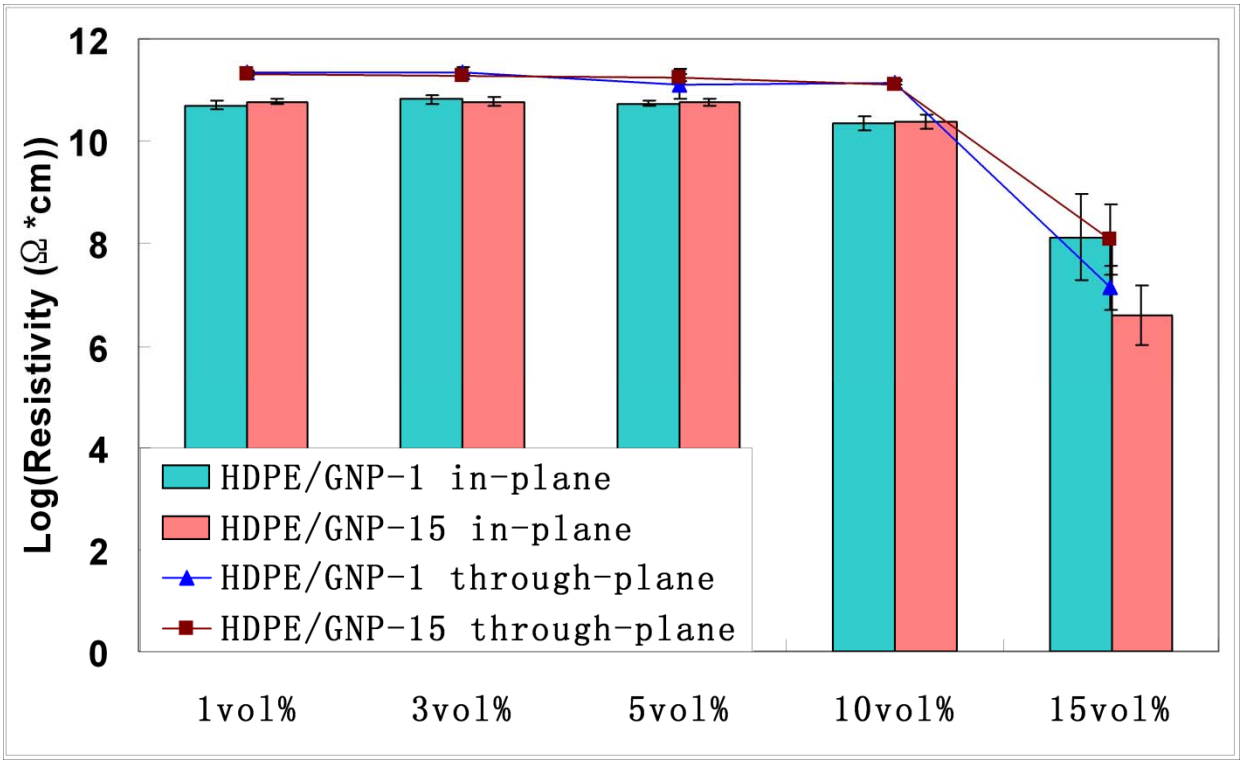

Figure 3.8. In-plane and through-plane electrical resistivity of HDPE/GNP nanocomposites

Interestingly, at 15 vol% GNP (higher than the percolation threshold), HDPE/GNP-15 nanocomposites exhibit a lower in-plane electrical resistivity than HDPE/GNP-1 samples, which means HDPE/GNP-15 nanocomposites are more electrical conductive. However, at this GNP loading, HDPE/GNP-1 samples show a slightly lower through-plane electrical resistivity. By

comparing the in-plane resistivity with the through-plane resistivity, it is concluded that HDPE/GNP-1 and HDPE/GNP-15 nanocomposites (except for the GNP-1 sample at 15 vol% GNP loading) both exhibit lower in-plane resistivity or higher in-plane electrical conductivity, which is due to the platelet structure of GNP particles and the anisotropic property of injection molded composites. During injection molding, GNP platelets are aligned parallel to each other along the material flow direction, and at certain loading levels will they start intersecting with each other to form a conductive path. Because of the platelet morphology, aligned GNP particles are more difficult to get contact with each other through the thickness direction, thus leading to a higher through-plane resistivity or lower electrical conductivity. However, for the 15 vol% HDPE/GNP-1 nanocomposite, it is noted that the in-plane resistivity and the through-plane resistivity are almost the same on the account of their overlapping error bars. This is believed due to the factor that the size of GNP-1 nanoparticles are much smaller, they are more easily to rotate and re-orientate during the processing conditions, which results in more or less isotropic electrical properties at high GNP loadings.

From the literature, it is noted that GNP nanocomposites fabricated by other processing methods such as solution compounding, pre-mixing, solid state ball milling, and solid state shear pulverization tend to have lower percolation threshold or higher electrical conductivity than the samples made by melt-extrusion and injection molding [12, 13]. The high percolation threshold is a result of the GNP aggregation during melt-extrusion and preferential platelets alignment in the injection molding process due to the large aspect ratio and planar shape of GNP, which will be fully explored in the next section.

3.4.5 Morphology of HDPE/GNP Nanocomposites Made by Melt-extrusion and Injection Molding

The morphology of HDPE/GNP-1 and HDPE/GNP-15 nanocomposites fabricated by melt-extrusion and injection molding is presented in the Figure 3.9. The samples at 5 vol% GNP loading were taken as an example. Images (a) and (c) show the injection molded morphology near the mold wall or at the edge, where the shear forces under the injection molding conditions is high. And images (b) and (d) represent the injection molded morphology in the center of the composites, where the shear force is small. From the images of (a) and (c), it is concluded that all the GNP-1 and GNP-15 particles align parallel along the material flow direction and they are totally separated by the polymer matrix. Meanwhile, large GNP aggregates can be observed in these two images, especially in the GNP-15 sample, which is the indication of insufficiency of DSM extrusion to achieve a good GNP separation and dispersion. The presence of these large GNP aggregates drastically reduces the number of GNP platelets available as 'effective' reinforcing particles and significantly decreases the probability of interconnections between GNP platelets in forming electrically conductive pathways. Therefore, the high percolation threshold or low electrical conductivity in HDPE/GNP nanocomposites made by melt-extrusion and injection molding could be attributed to the severe GNP aggregation and preferential GNP alignment during this conventional composite compounding process.

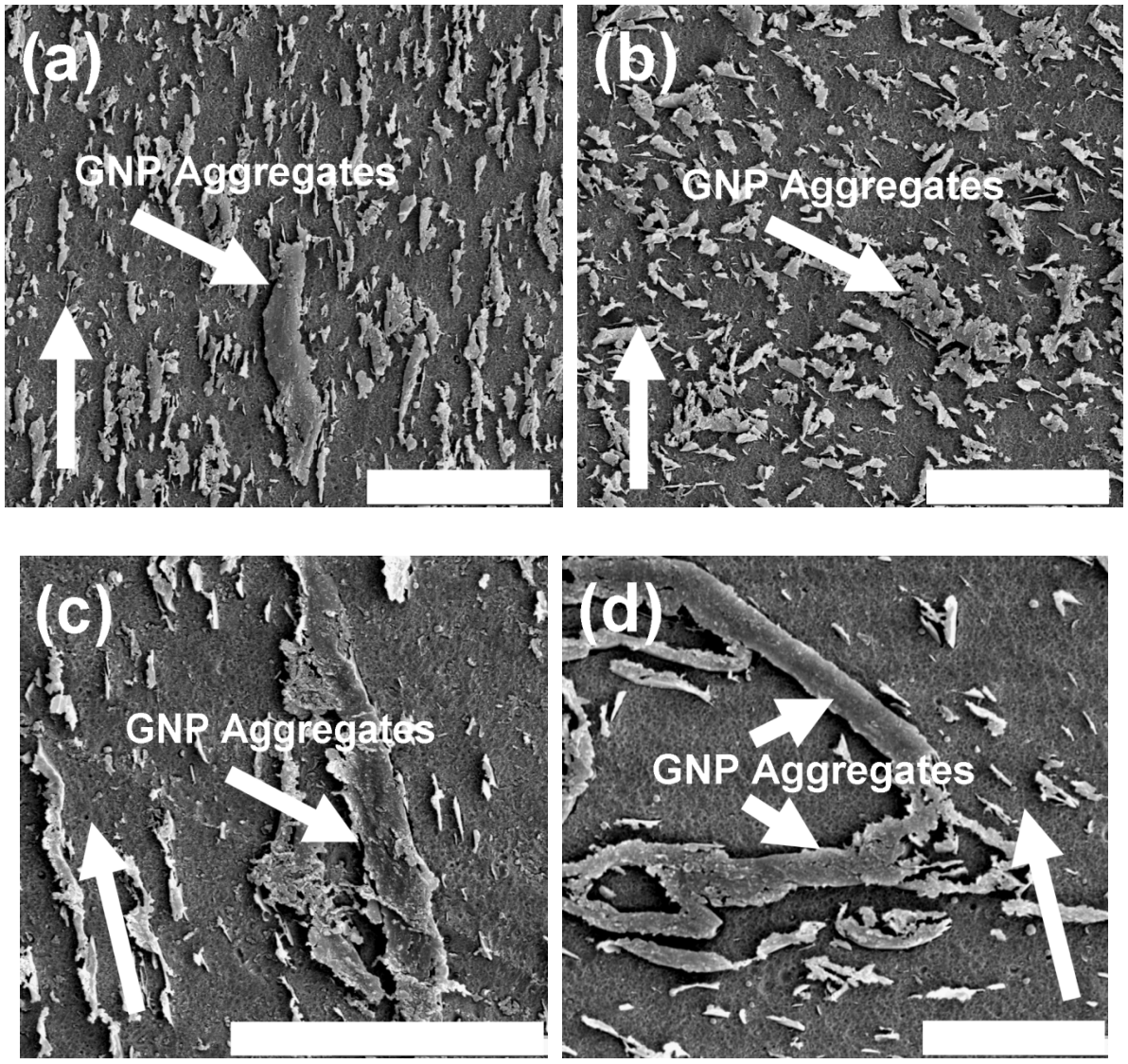

Figure 3.9. Morphology of HDPE/GNP nanocomposites made by melt-extrusion and injection molding. The GNP loading is 5 vol%. (a) GNP-1 sample at the edge (scale bar 10 μm); (b) GNP-1 sample in the center (scale bar 10 μm); (c) GNP-15 sample at the edge (scale bar 20 μm); (d) GNP-15 sample in the center (scale bar 10 μm). The arrow indicates the material flow direction during injection molding.

The aligned structure of GNP platelets in the resulting nanocomposites also leads to much higher in-plane thermal and electrical conductivity as described above. Meanwhile, it is detected that the number density of GNP-1 particles are much larger than that of GNP-15 at the same GNP loading due to their smaller size, which is considered as a major reason of higher flexural

strength, impact strength and crystallinity in the resulting GNP-1 nanocomposites.

Compared with the morphology at the edge, it is seen that GNP platelets in the center of the nanocomposites do not exhibit preferential alignment along the material flow direction. They are randomly oriented because of the minimum shear forces encountered during injection molding. However, large GNP aggregates can also be observed which further confirm the insufficient shear force attainable in the DSM extrusion to break down the GNP aggregates and to achieve a uniform GNP dispersion.

In summary, GNP nanoplatelets tend to align along the material flow direction at the edge of injection molded nanocomposites while they are randomly oriented at the center. The presence of large GNP aggregates constrains the fully translation of superb mechanical, thermal and electrical properties of GNP into the resulting nanocomposites.

3.5 Conclusions

Analysis of the crystallization behavior of HDPE/GNP nanocomposites demonstrates that GNP nanoplatelets are efficient nucleating agents which can significantly increase the crystallization temperature even at low GNP loadings. The total percent crystallinity of HDPE increases with GNP loading until a point is reached where the small separation distance between the GNP particles reduces the crystallinity due to a reduction in the mobility of polymer chains during crystallization.

Due to the excellent thermal properties of GNP nanoplatelets, enhanced thermal stability and thermal conductivity in HDPE were achieved by the addition of GNP. Evaluation of several

thermal conductivity models to predict the thermal conductivity of HDPE/GNP nanocomposites indicates that the Maxwell-Eucken and Bruggeman models do not fit the experimental data well while the Agari model can successfully describe the thermal conductivity of HDPE/GNP nanocomposites.

By comparing the in-plane and through-plane thermal and electrical conductivity, it was found that HDPE/GNP nanocomposites fabricated by the conventional processing method of melt-extrusion and injection molding exhibit anisotropic conductive properties. Much higher in-plane thermal and electrical conductivity is due to the preferential GNP alignment during the injection molding process and the anisotropic properties of GNP. Meanwhile, the percolation threshold of these HDPE/GNP nanocomposites was found to be high, which also results from the GNP orientation and the severe GNP aggregation.

Despite this disadvantage, melt-extrusion and injection molding is still the most popular compounding method for manufacturing the thermoplastics in industry, which offers many advantages including high design flexibility, low cost and labor, short cycle time and minimum scrap loss. In this case, how to enhance the electrical conductivity and/or mechanical properties for the injection molded HDPE/GNP nanocomposites will be the primary research concern for the next two chapters.

REFERENCES

REFERENCES

[1] Chung DDL. Review Graphite Journal of Materials Science. 2002;37:1475-89.

[2] Ding L, Jonforsen M, Roman LS, Andersson MR, Inganäs O. Photovoltaic cells with a conjugated polyelectrolyte. Synthetic Metals. 2000;110(2):133-40.

[3] Heeger AJ. Semiconducting and Metallic Polymers: The Fourth Generation of Polymeric Materials. Journal of Physical Chemistry B. 2001;105:8475-91.

[4] MacDiarmid AG. Nobel Lecture: “Synthetic metals" A novel role for organic polymers. Rev Mod Phys. 2001;73:701 - 12

[5] Lazarenko A, Vovchenko L, Prylutskyy Y, Matzuy L, Ritter U, Scharff P. Mechanism of thermal and electrical conductivity in polymer-nanocarbon composites. Mat-wiss u Werkstofftech. 2009;40:268-72.

[6] Huang J-C. Carbon black filled conducting polymers and polymer blends. Advances in Polymer Technology. 2002;21(4):299-313.

[7] Donnet J-B. Carbon Black, 3rd Edition. New York: Marcel Dekker, Inc.; 1998.

[8] Pavlidou S, Papaspyrides CD. A review on polymer/layered silicate nanocomposites. Progress in Polymer Science. 2008;33(12):1119-98.

[9] Guo-Hua Chen, Da-Jun Wu, Wen-Gui Weng, Bin He, Yan W-l. Preparation of polystyrene-graphite conducting nanocomposites via intercalation polymerization Polymer International. 2001;50:980-5.

[10] Fukushima H, T Drzal L, Rook BP, Rich MJ. Thermal conductivity of exfoliated graphite nanocomposites. Journal of Thermal Analysis and Calorimetry. 2006;85:235-8.

[11] Kalaitzidou K, Fukushima H, Drzal LT. Multifunctional polypropylene composites produced by incorporation of exfoliated graphite nanoplatelets. Carbon. 2007;45:1446–52.

[12] Kalaitzidou K, Fukushima H, Drzal LT. A new compounding method for exfoliated graphite/polypropylene nanocomposites with enhanced flexural properties and lower percolation threshold. Composites Science and Technology. 2007;67(10):2045-51.

[13] Jiang X, Drzal LT. Reduction in Percolation Threshold of Injection Molded High Density Polyethylene/Exfoliated Graphene Nanoplatelets Composites by Solid State Ball Milling and Solid State Shear Pulverization. Journal of Applied Polymer Science 2012;124(1):525-35.

[14] Jiang X, Drzal LT. Improving Electrical Conductivity and Mechanical Properties of High Density Polyethylene through Incorporation of Paraffin Wax Coated Exfoliated Graphene Nanoplatelets and Multi-wall Carbon Nano-tubes. Composites Part A: Applied Science and Manufacturing. 2011;42(11):1840-9

[15] Kalaitzidou K, Fukushima H, Askeland P, Drzal LT. The nucleating effect of exfoliated graphite nanoplatelets and their influence on the crystal structure and electrical conductivity of polypropylene nanocomposites. Journal of Materials Science. 2008;43(8):2895-907.

[16] Miloaga DG, Hosein HAA, Misra M, Drzal LT. Crystallization of poly(3-hydroxybutyrate) by exfoliated graphite nanoplatelets. Journal of Applied Polymer Science. 2007;106(4):2548-58.

[17] PENEVA Y. ML. Non-isothermal and isothermal crystallization of nanocomposites based on functionalized polyethylenes. Polymer Testing. 2006;25:366-76.

[18] Di Maio E, Iannace S, Sorrentino L, Nicolais L. Isothermal crystallization in PCL/clay nanocomposites investigated with thermal and rheometric methods. Polymer 2004;45:8893–900.

[19] Zhou W, Qi S, An Q, Zhao H, Liu N. Thermal conductivity of boron nitride reinforced polyethylene composites. Materials Research Bulletin. 2007;42:1863–73.

[20] Y. Agari AU, S. Nagai. Thermal conductivity of a polymer composite Journal of Applied Polymer Science. 1993;49:1625-34.

[21] Kalaitzidou K. Exfoliated Graphite Nanoplatelets as Nanoreinforcement for Multifunctional Polypropylene Nanocomposites [PHD Dissertation]. East Lansing, MI, USA: Michigan State University; 2006.

[22] I. Krupa, I. Novák, Chodák I. Electrically and thermally conductive polyethylene/graphite composites and their mechanical properties. Synthetic Metals. 2004;145:245–52.

CHAPTER 4 REDUCTION IN PERCOLATION THRESHOLD OF INJECTION MOLDED HIGH DENSITY POLYETHYLENE/EXFOLIATED GRAPHENE NANOPLATELETS COMPOSITES BY SOLID STATE BALL MILLING AND SOLID STATE SHEAR PULVERIZATION

4.1 Abstract

The previous chapter showed that HDPE/GNP nanocomposites fabricated by melt-extrusion and injection molding have a relatively high percolation threshold of 10-15 vol% GNP loading. To lower the percolation threshold of injection molded HDPE/GNP nanocomposites and enhance their electrical conductivity, two special processing methods were investigated: solid state ball milling (SSBM) and solid state shear pulverization (SSSP). Results have confirmed that the percolation threshold of HDPE/GNP nanocomposites was reduced to between 3-5 vol% GNP loading by these two approaches. The mechanism by which SSBM and SSSP are capable of producing lower percolation is to coat the polymer surface with GNP platelets which facilitates the formation of conductive networks during injection molding. However, it was found that HDPE/GNP nanocomposites obtained from these two techniques exhibit lower mechanical and thermal properties at high GNP loadings.

4.2 Introduction

The importance of thermally and electrically conductive polymeric composites and their various applications have been stated in the previous chapter. The advantages in selecting these polymeric composites over traditionally used materials such as metals or ceramics are their low

density, low fabrication cost, high oxidation/chemical corrosion stability, and good barrier properties. Additionally, polymeric composites can be manufactured into complex shapes without expensive secondary processing steps [1]

Among all the conductive fillers, carbon black is by far mostly used due to its abundance in nature and low price. However, composites filled with carbon black generally require large filler concentrations to attain percolation and adequate electrical conductivity as a result of the low aspect ratio of carbon black and the large electron 'hopping' distance between carbon aggregates [2]. The large amount of carbon black added in the composites in order to reach high electrical conductivity results in a polymer melt having extremely high viscosity, making it difficult to process with traditional compounding methods such as melt-extrusion and injection molding [3].

Recently carbon nano-tubes (CNTs) have been intensively explored as the conductive filler in polymers on account of their exceptional mechanical, electrical and thermal properties and potentially low percolation threshold in polymeric nanocomposites [4, 5]. Many papers have appeared in the literature discussing the processing and resulting electrical and/or mechanical properties by fabricating CNTs-filled polymeric nanocomposites for a number of applications [6-10]. However, due to the poor yield, costly fabrication and purifying process, the market price of CNTs is still high today, which limits the commercial applications of CNTs [11, 12].

To achieve a high electrical conductivity in polymeric composites but low cost and easy processing, graphite based materials are gaining more and more research attention [13]. And a new form of graphite based nano-material, exfoliated graphene nanoplatelets, GNP, has been under investigation in the Dr. Drzal group for several years [14, 15]. Research work has shown

that this nano-filler is a potential alternative to other nano-reinforcements such as nano-clays and carbon nano-tubes since it combines the low cost and layered structure of nano-clays and the superior thermal and electrical properties of CNTs. And when it is incorporated into a polymer matrix, GNP could simultaneously provide a multitude of physical and chemical property enhancements [16-21].

The results in the previous chapters have already shown that incorporation of GNP into HDPE could greatly enhance the mechanical and thermal properties by applying the conventional processing technique of melt-extrusion and injection molding. But these nanocomposites have a percolation threshold higher than 10 vol% GNP loading, which is generally much higher than the CNTs-filled nanocomposites made by the similar processing methods [22]. Morphology investigation of HDPE/GNP nanocomposites indicates the high percolation threshold and low electrical conductivity is the result of severe GNP aggregation in melt-extrusion and preferential platelets alignment during injection molding due to the large aspect ratio and planar shape of GNP. Thus, the superb electrical properties of GNP cannot be as yet fully translated into good electrical conductivity of the resulting GNP nanocomposites.

In order to lower the percolation threshold of GNP nanocomposites, several non-traditional processing techniques have been explored such as solution intercalation method in polypropylene/GNP nanocomposites [23], in situ polymerization method in nylon 6/expanded graphite [24] and polyaniline/expanded graphite nanocomposites [25] and polymerization filling technique in polystyrene/exfoliated graphite nanocomposites [26]. These methods have demonstrated that the percolation threshold values were all significantly reduced compared with

the samples made by melt-extrusion. However, since melt-extrusion and injection molding is still the major processing method used for manufacturing the thermoplastics in industry because of its design flexibility, low cost and labor, short cycle time and minimum scrap loss, a method to reduce the percolation threshold in GNP nanocomposites made by melt-extrusion and injection molding remains an area of high interest. The objectives of this chapter is thus to investigate the feasibility of applying two novel processing techniques of solid state ball milling (SSBM) and solid state shear pulverization (SSSP) to lower the percolation threshold and enhance the electrical conductivity of HDPE/GNP nanocomposites. Most importantly, these two methods are suitable for the conventional processing technique of melt-extrusion and injection molding.

4.3 Experimental

4.3.1 Materials

In this research, HDPE pellets with the trade name Marlex® HXM 50100 (Density 0.95 g/cm^3, MW~ 230,000) were obtained from Chevron Phillips Chemical Company. GNP-1 and GNP-15 nanoplatelets were obtained from XG Science, Inc.

4.3.2 Processing Methods

4.3.2.1 Melt Extrusion and Injection Molding

Melt-extrusion of HDPE/GNP nanocomposites was carried out in a DSM mini-extruder system as described in the previous chapters. Flexural coupons were made for mechanical properties and electrical conductivity measurements and round disks (thickness ~1.5 mm, diameter ~25 mm)

were injection molded for thermal conductivity test.

4.3.2.2 Solid State Ball Milling and Injection Molding

The starting material for SSBM is a mixture of GNP and HDPE powder (diameter ~100 μm) which was obtained from the cryogenic milling of as-received HDPE pellets. SSBM process was carried out in a SPEX SamplePrep 8000D Dual Mixer/Mill® system which is shown in the Figure 4.1.

Figure 4.1. SPEX SamplePrep 8000D Dual Mixer/Mill® system and its steel vial set

The mixture of GNP and HDPE powder at selected volume ratios (1 vol%, 3 vol%, 5 vol%, 10 vol% and 15 vol% GNP loading) was added into a stainless steel vial where six steel balls (2 large balls: 1/4 inch in diameter and 4 small balls: 1/8 inch in diameter) were used as the milling medium. SSBM time was kept at 200 minutes which could produce a powder mixture with each polymer particle uniformly coated with GNP platelets. The morphology of HDPE powder after

200 minutes SSBM with and without GNP-15 is presented in the Figure 4.2, which illustrates the uniform GNP coating on HDPE.

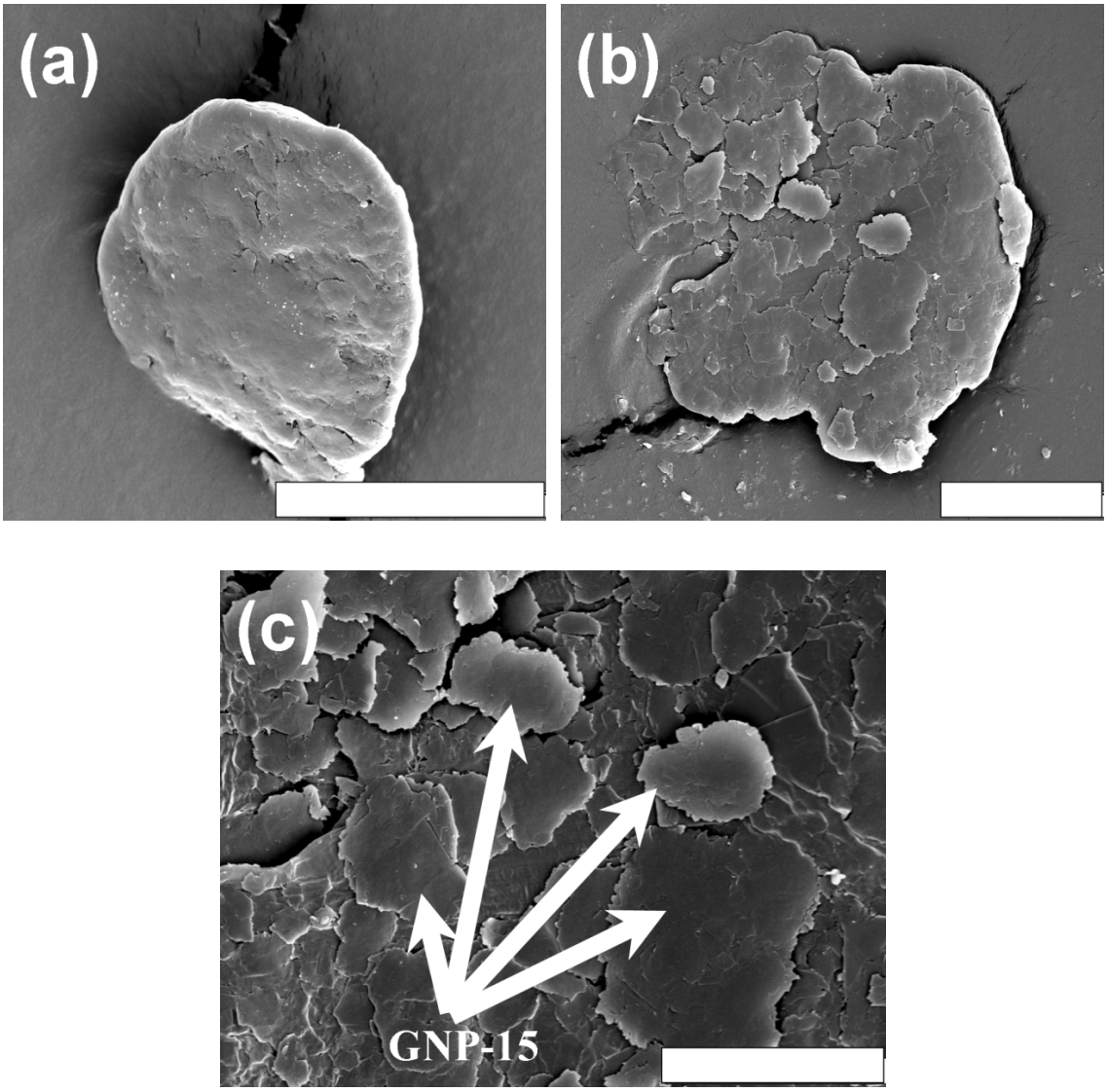

Figure 4.2. (a) SEM images of HDPE powder after 200 minutes SSBM without GNP-15 (scale bar 20 μm); (b) HDPE powder after 200 minutes SSBM with GNP-15 at low magnification (scale bar 20 μm); and (c) image (b) at higher magnification (scale bar 10 μm)

From Figure 4.2 (a), it is noted that the diameter of HDPE particles is reduced from 100 μm to around 20 μm due to the high energy ball milling. And from Figure 4.2 (b), we can see that the HDPE particle is uniformly coated by GNP-15 platelets and the size of most GNP-15 platelets is

also significantly reduced (less than 10 μm) according to the SEM image of higher magnification (Figure 4.2 (c)). The GNP coated HDPE powder mixture was then injection molded to make flexural coupons for mechanical and electrical properties test and round disks for thermal conductivity measurement. The injection molding conditions were kept the same as described in the previous chapter.

4.3.2.3 Solid State Shear Pulverization and Injection Molding

The solid state shear pulverization process (SSSP) was originally devised and explored in the Torkelson Group in Northwestern University as a method for polymer blend compatibilization [27, 28]. Here, I introduce the SSSP technique as a novel strategy to fabricate HDPE/GNP nanocomposites.

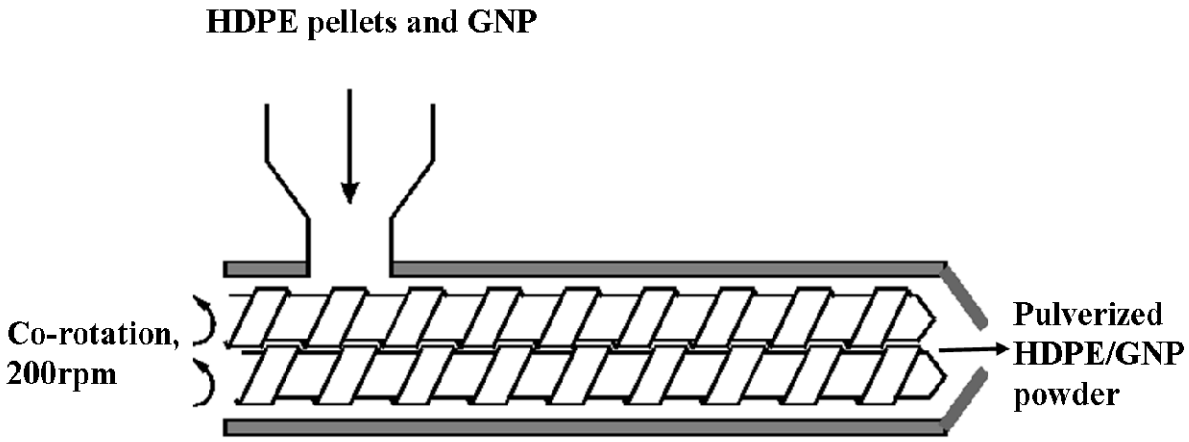

Figure 4.3. A schematic view of the SSSP process

SSSP was conducted within a Leistritz Micro 27 twin extruder (27mm screw diameter, L/D=48, co-rotation). HDPE pellets (as-received) and GNP with selected volume ratios (1 vol%, 3 vol%,

5 vol%, 10 vol% and 15 vol% GNP loadings) were fed at a feed rate of 100 g/hour into the extruder in which they were pulverized to yield a powder mixture output. The screw rpm was 200 and the barrel temperature was kept around 20 °C by the cooling coils surrounding the barrels to ensure that the polymer remained in the solid state. The process of SSSP is schematically shown in the Figure 4.3.

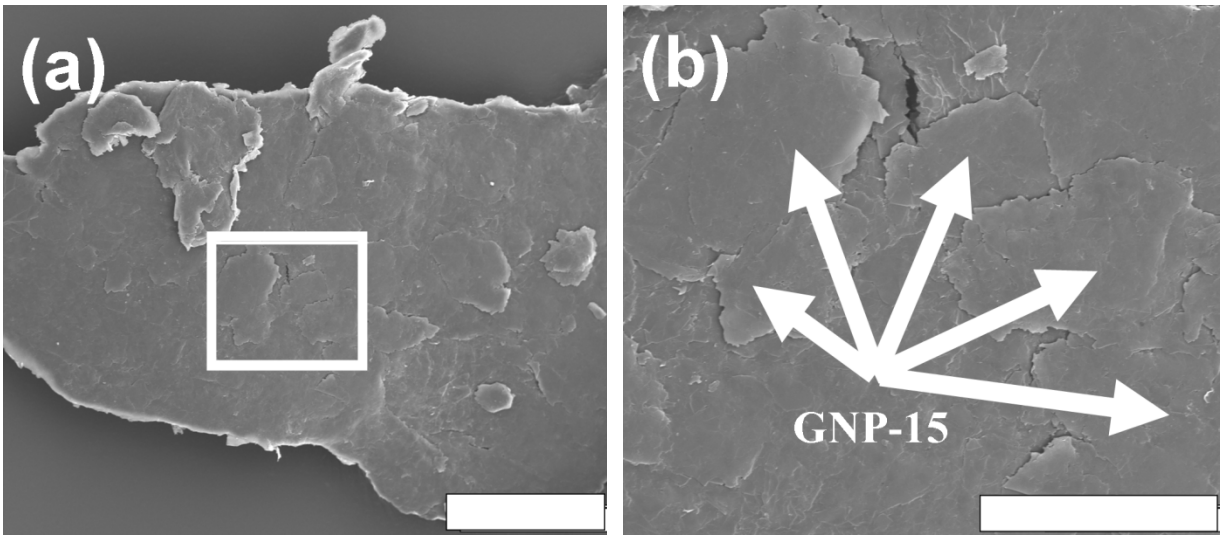

Figure 4.4. SEM images of HDPE pellets after SSSP with GNP-15 nano-particles at (a) low magnification (scale bar 50 μm) (b) high magnification (scale bar 20 μm, enlarged rectangular area in the image (a))

According to the SEM images of Figure 4.4, the SSSP technique also results in a uniform GNP coating on the surface of HDPE. However, the size of HDPE particles after SSSP (>100 μm) is much larger than those processed with SSBM, which is due to the much shorter processing time in SSSP (several minutes vs. 200 minutes). The pulverized HDPE and GNP powder mixture was then injection molded to make flexural coupons for mechanical properties and electrical conductivity test under the same injection conditions as described above.

4.3.3 Characterization Methods

4.3.3.1 Mechanical Property

A UTS SFM-20 machine (United Calibration Corp.) was used to measure the flexural properties. Flexural coupons were tested under 3-point bending mode at a flexural rate of 0.05 in/min following the ASTM D790 standard.

4.3.3.2 Electrical Resistivity

The electrical resistivity of HDPE/GNP nanocomposites was measured both along the flow direction (in-plane resistivity) and through the thickness direction (through-plane resistivity, normal to the flow direction), using impedance spectroscopy by applying a two-probe method at room temperature. Samples with dimensions around 10 x 3.2 x 12.2 mm (Length x Thickness x Width) were cut from the middle portion of flexural bars. The two surfaces connected to the electrodes were first treated with O_2 plasma (14 minutes, 375 W) in order to remove the top surface layers which are rich in polymer and then conductive silver paste was used to ensure good contact of the sample surface with the electrodes. The resistance of samples was measured and converted to resistivity by taking the sample dimensions into account.

4.3.3.3 Thermal Conductivity

Thermal diffusivity (α, m^2/s) (both in-plane and through-plane) of GNP nanocomposites (round disks) was measured by a LFA Nanoflash 447 light flash system. To calculate the thermal

conductivity, the bulk density of the samples (ρ, kg/m^3) was obtained by dividing the mass over the volume, and the specific heat capacity (C_p: J/(kg· K)) was measured through the differential scanning calorimetry (DSC Q2000, TA instrument). The thermal conductivity (κ, W/(m·K)) of GNP samples was then calculated by the following equation: $\kappa = \alpha * \rho * C_p$.

4.3.3.4 Scanning Electron Microscopy (SEM)

The preparation of SEM samples in this study included epoxy mounting, grinding, polishing and etching steps. First, HDPE/GNP specimens for microscopic examination were mounted with epoxy in cylindrical sample holders to maintain a flat surface over the entire grinding area. After the epoxy was fully cured, the samples were then carefully grounded and polished. Plasma etching was applied at the last step to remove the polymer in top surface layers allowing the GNP platelets to stand out. A JEOL (model JSM-6400) SEM with an accelerating voltage of 10 kV and a working distance of 15 mm was then used to collect the SEM images. Samples were also gold coated of a few nanometers in thickness to avoid charging.

4.4 Results and Discussion

4.4.1 Electrical Conductivity of SSBM HDPE/GNP Samples

The in-plane electrical resistivity of HDPE/GNP nanocomposites made by conventional DSM melt-extrusion and injection molding (DSM HDPE/GNP) has been fully discussed in the previous chapter. Results showed that the percolation threshold of these nanocomposites was high at 10-15 vol% GNP loading. The high percolation threshold and low electrical conductivity

is due to severe GNP aggregation in melt-extrusion and preferential platelets alignment during injection molding. To have a better comparison with HDPE/GNP nanocomposites fabricated by SSBM that will be addressed later on, the morphology of DSM HDPE/GNP-1 and HDPE/GNP-15 samples at 5 vol% GNP loading is presented in the Figure 4.5, which clearly shows the large aggregation and preferential orientation of GNP nanoplatelets.

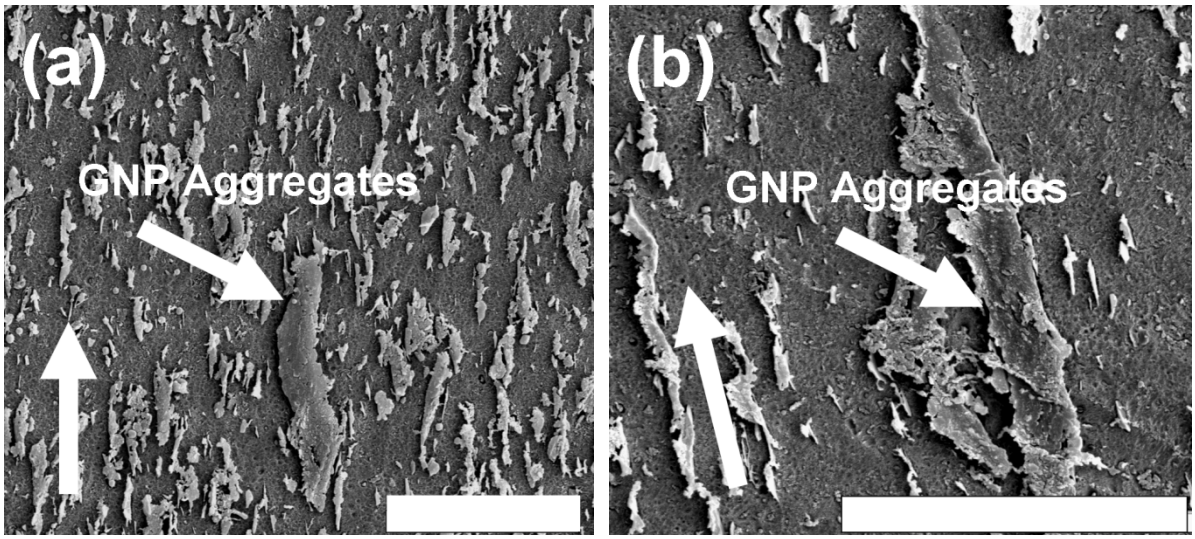

Figure 4.5. Morphology of HDPE/GNP nanocomposites made by melt-extrusion and injection molding. The GNP loading is 5 vol%. The arrows indicate the material flow direction in injection molding. (a) GNP-1 sample (scale bar 10 μm); (b) GNP-15 sample (scale bar 20 μm)

The in-plane electrical resistivity of HDPE/GNP nanocomposites obtained from the SSBM method (SSBM HDPE/GNP) and the comparison with the DSM melt-extrusion samples is presented in the Figure 4.6. As indicated in this figure, SSBM HDPE/GNP nanocomposites have the in-plane percolation threshold of just 3-5 vol% GNP loading compared with the threshold value of 10-15 vol% for the DSM samples. Huge reduction in percolation threshold clearly suggests the formation of conductive networks in the SSBM nanocomposites is better. In addition, the absolute resistivity value of SSBM HDPE/GNP samples from 3 vol% to 15 vol%

GNP loading is found to be dramatically lower which further confirms the substantial improvement in electrical conductivity by the SSBM process.

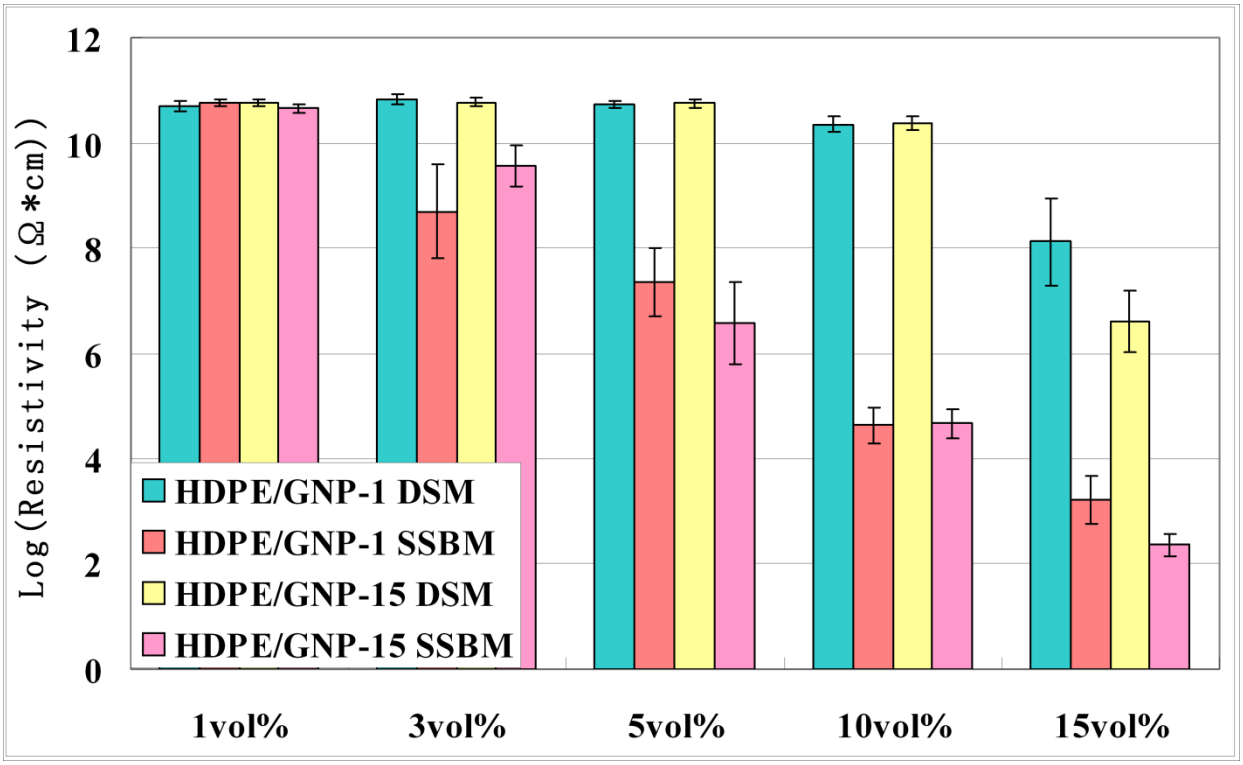

Figure 4.6. In-plane electrical resistivity of SSBM HDPE/GNP nanocomposites and its comparison with DSM HDPE/GNP samples

SEM images of SSBM HDPE/GNP-1 and SSBM HDPE/GNP-15 nanocomposites at 5 vol% GNP loading are presented in the Figure 4.7 and Figure 4.8 respectively. The morphology helps explain why SSBM HDPE/GNP nanocomposites have a lower percolation threshold and higher electrical conductivity.

From Figure 4.5, it is noted that for DSM HDPE/GNP-1 nanocomposites (Figure 4.5 (a)), GNP-1 platelets are relatively homogeneously dispersed in HDPE with preferential alignment along the flow direction. However, for the SSBM sample (Figure 4.7 (a)), it is clear to see that there exist

alternate polymer-rich regions and GNP-rich regions in the polymer matrix. The SEM image with higher magnification (Figure 4.7 (b)) shows that GNP-1 nanoplatelets are all intersecting with each other forming conductive pathways in the GNP-rich regions. It is thus believed that the presence of such conductive pathways throughout the polymer matrix significantly reduces the percolation threshold and increases the electrical conductivity of the resulting SSBM HDPE/GNP-1 nanocomposites.

The formation of this unique morphology by the SSBM process is supposed to be the result of the high-energy ball milling, which produces compression and shear forces to the GNP aggregates to shear them apart and get GNP platelets separated. HDPE powder is thus homogeneously coated by individual GNP platelets. When the GNP coated HDPE powder undergoes the injection molding process, the high-velocity material flow forces HDPE to melt and fuse into one phase (polymer-rich regions), and the GNP platelets originally coated on the surface move along together to re-aggregate, forming another phase (GNP-rich regions or conductive pathways). To verify this assumption, the width of the polymer-rich region is measured to be around 20-30 μm, which is close to the size of HDPE particles after SSBM. This observation proves that HDPE particles are fused together along the flow direction while constrained laterally by the development of GNP-rich regions. The formation of conductive pathways during the SSBM process is then schematically illustrated in the Figure 4.9.

Meanwhile, we can see that the SSBM HDPE/GNP-15 sample also exhibits alternate polymer-rich and GNP-rich regions and GNP platelets are well connected in the GNP-rich regions (Figure 4.8). In this case, it is concluded that the SSBM process substantially improves

the electrical conductivity of HDPE/GNP nanocomposites due to the selective aggregation of GNP platelets at HDPE-GNP interfaces during injection molding, which results in continuous conductive pathways throughout the polymer matrix.

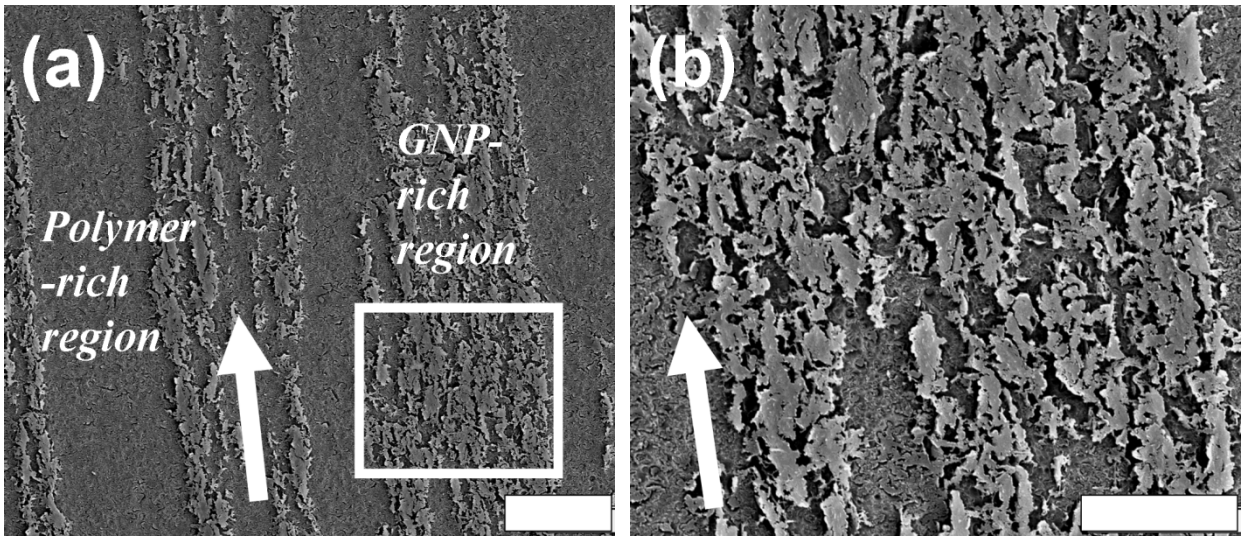

Figure 4.7. SEM images of SSBM HDPE/GNP-1 nanocomposites at 5 vol% GNP loading. (a) low magnification image (scale bar 20 μm); (b) high magnification image (scale bar 10 μm, enlarged rectangular area in the image (a)). Arrows in the images indicate the material flow direction during injection molding

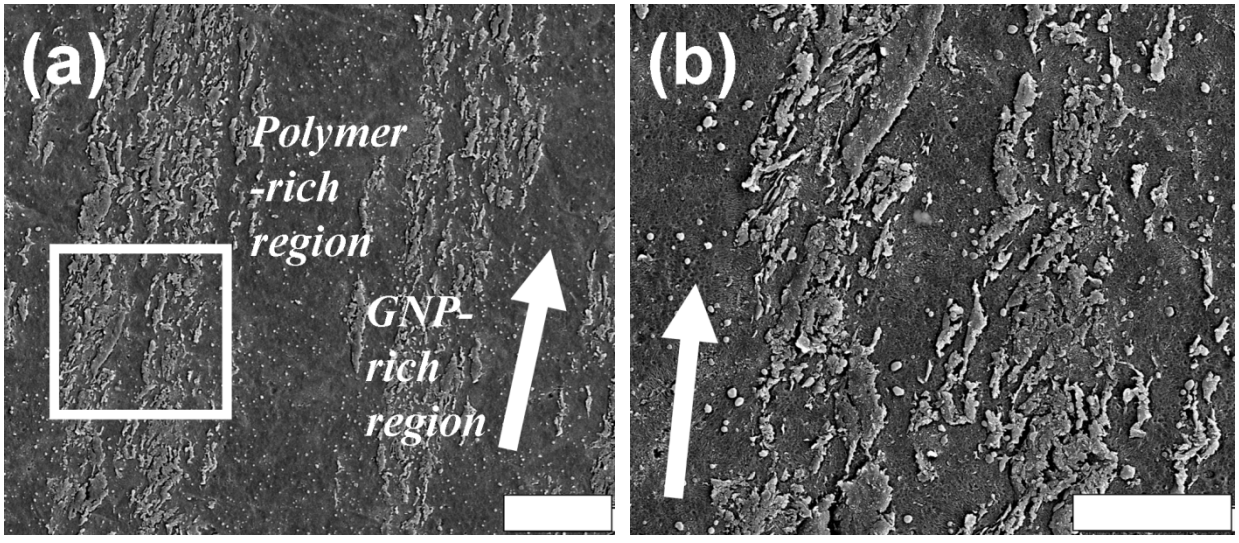

Figure 4.8. SEM images of SSBM HDPE/GNP-15 nanocomposites at 5 vol% GNP loading. (a) low magnification image (scale bar 20 μm); (b) high magnification image (scale bar 10 μm, enlarged rectangular area in the image (a)). Arrows in the images indicate the material flow direction during injection molding

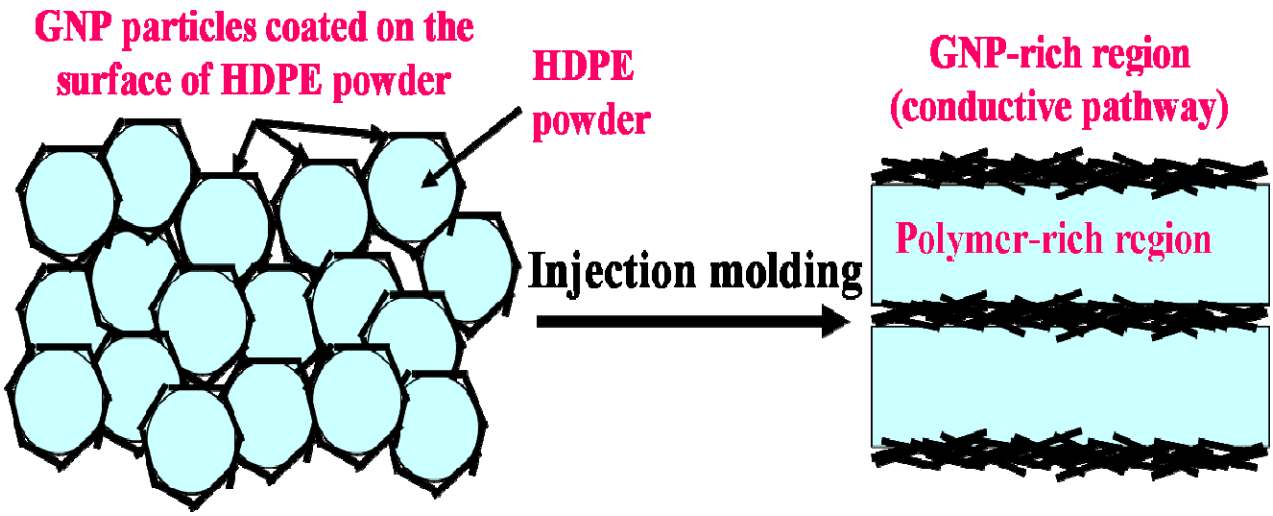

Figure 4.9. Formation of conductive pathways in SSBM HDPE/GNP nanocomposites

4.4.2 Electrical Conductivity of SSSP HDPE/GNP Samples

From the previous section, the advantage of the SSBM process is clear that SSBM could significantly increase the in-plane electrical conductivity of HDPE/GNP nanocomposites. However, SSBM is a discontinuous process and only a small amount of materials can be produced each time which may constrains its potential application in industry. To overcome this deficiency, solid state shear pulverization (SSSP) is introduced here which is capable of producing large amount of materials continuously within a relatively short time. Figure 4.10 compares the in-plane electrical resistivity of HDPE/GNP nanocomposites fabricated by the SSSP process and the samples made from DSM melt-extrusion. From this figure, it is concluded that the in-plane electrical conductivity of SSSP HDPE/GNP nanocomposites is also significantly enhanced and the percolation threshold is reduced to 3-5 vol% GNP loading as well.

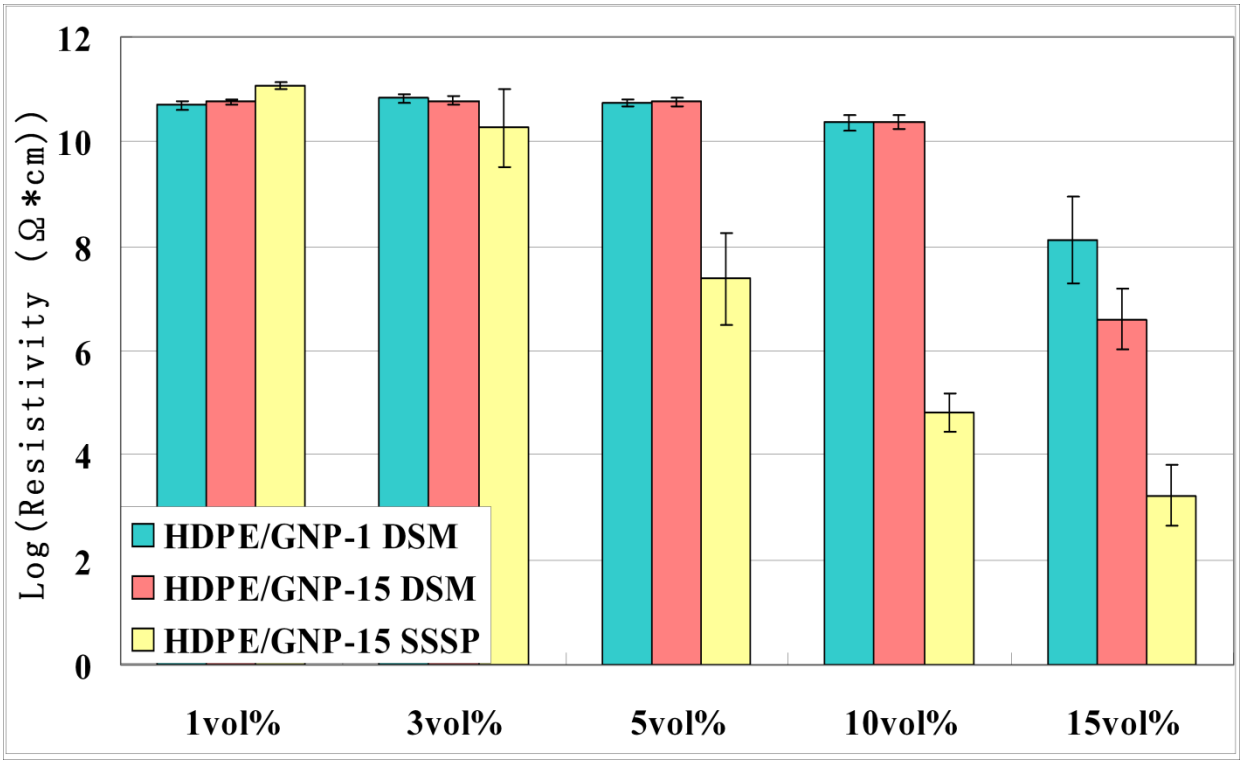

Figure 4.10. In-plane electrical resistivity of SSSP HDPE/GNP-15 nanocomposites and its comparison with DSM HDPE/GNP samples

The morphology of the SSSP HDPE/GNP-15 sample at 5 vol% GNP loading is shown in the Figure 4.11, from which the alternate polymer-rich regions and GNP-rich regions can also be detected. It is noted this morphology appears to be very similar to that of the SSBM samples (Figures 4.7 and 4.8). The mechanism of formation of alternate polymer-rich and GNP-rich regions by the SSSP process is therefore considered to be the same as that of the SSBM method. In the GNP-rich regions, electron pathways are found to be nicely established because of the well-connected GNP aggregates, which greatly improve the electrical conductivity of the resulting nanocomposites.

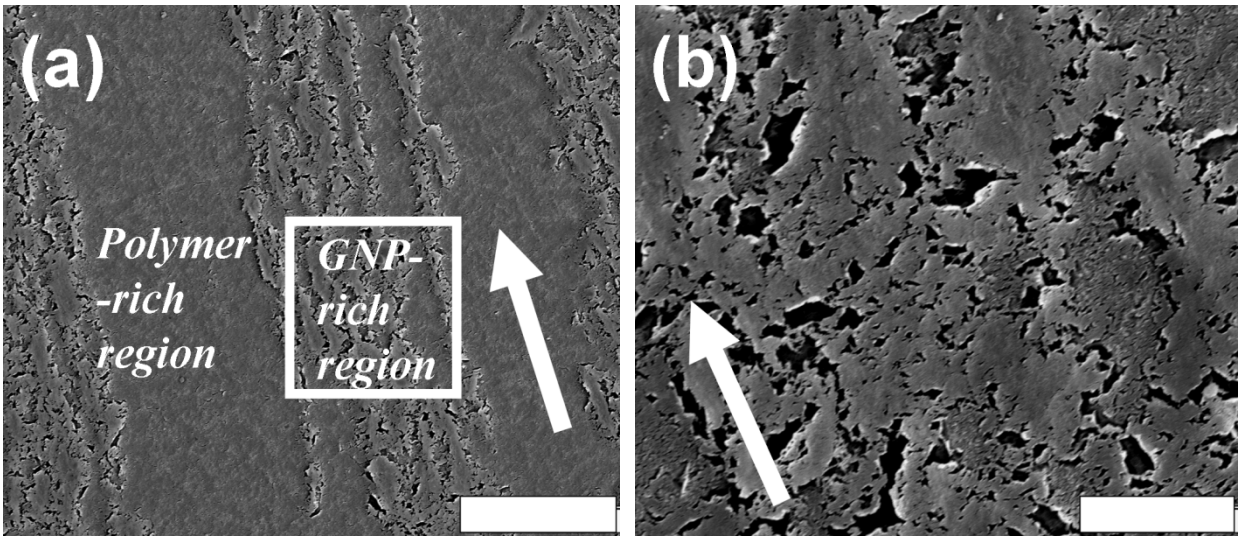

Figure 4.11. SEM images of SSSP HDPE/GNP-15 nanocomposites at 5 vol% GNP loading. (a) low magnification image (scale bar 50 μm); (b) high magnification image (scale bar 10 μm, enlarged rectangular area in the image (a)). Arrows in the images indicate the material flow direction during injection molding

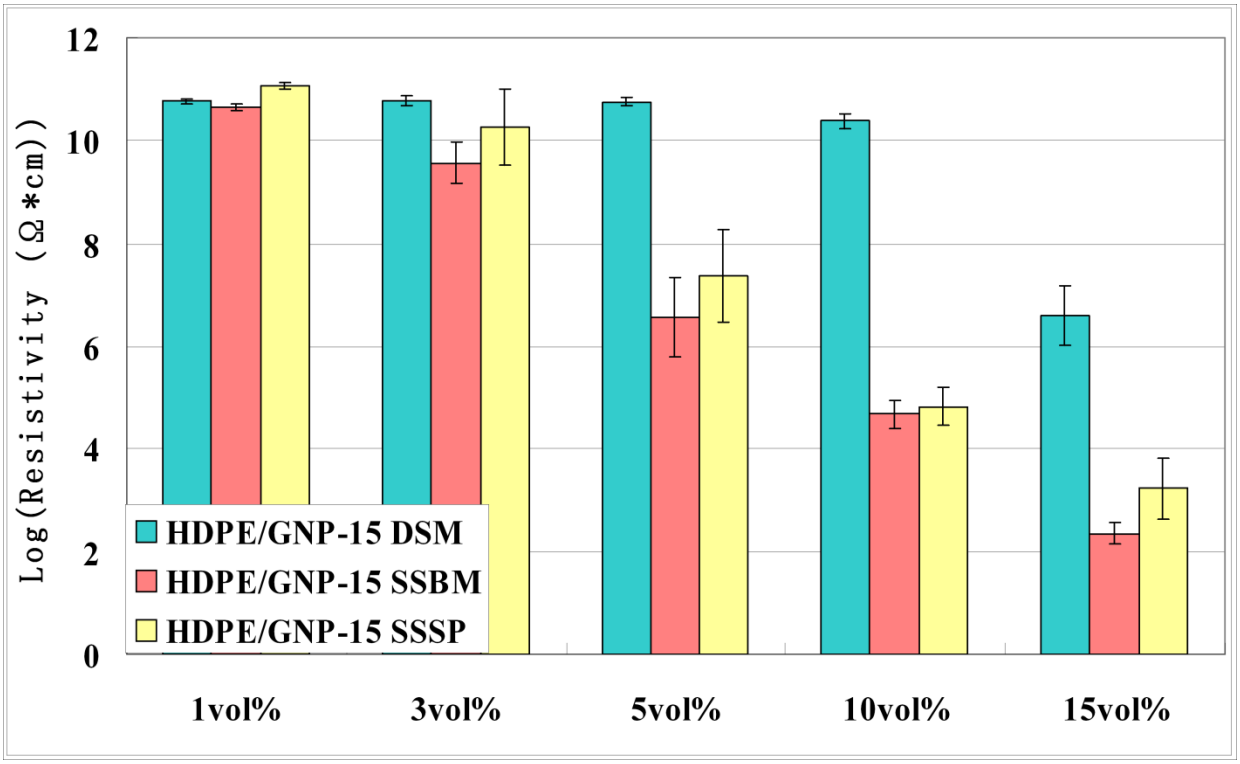

Figure 4.12. In-plane electrical conductivity of 5 vol% HDPE/GNP-15 nanocomposites made by DSM, SSBM and SSSP methods

The comparison between the SSSP and SSBM methods in improving the electrical conductivity in HDPE/GNP-15 nanocomposites is presented in the Figure 4.12. According to this figure, it is observed that SSSP HDPE/GNP nanocomposites exhibit competitive electrical properties to the SSBM samples both in the percolation threshold and the absolute resistivity at most GNP loadings (except for 15 vol% GNP loading). However, due to its capability of continuous mass production and much shorter processing time, the SSSP technique is believed to be more promising for industrial applications

4.4.3 Mechanical Properties of SSBM and SSSP HDPE/GNP Nanocomposites and Comparison with DSM Samples

According to the discussion above, application of the SSBM and SSSP methods is capable of improving the electrical conductivity of injection molded HDPE/GNP nanocomposites. However, nanocomposites are often expected not only to have a good electrical conductivity but also excellent mechanical properties. Bipolar plates in the polymer electrolyte membrane fuel cells and EMI shielding and electrostatic discharge protection materials for aerospace are just two examples [29, 30]. In this case, Figures 4.13 and 4.14 compare the flexural strength and flexural modulus respectively between the SSBM, SSSP HDPE/GNP nanocomposites and their DSM counterparts of which the good mechanical properties have already been demonstrated in the Chapter 2. As a baseline for comparison it is noted that the neat HDPE fabricated by the SSBM and SSSP methods shows higher flexural strength and modulus than the sample made from the DSM melt extrusion. It has been known that high energy ball milling in SSBM and high

pressure shear deformation in SSSP both produce molecular chain scission and breakage [31]. The breakage of polymer chains most often produces free radicals which in turn lead to the cross-linking in the polymer. This cross-linking phenomenon induced by SSBM or SSSP mainly contributes to the enhanced flexural properties in neat HDPE. And for the flexural properties of HDPE/GNP nanocomposites, SSBM and SSSP samples exhibit comparable flexural strength and modulus to the DSM counterparts with GNP loadings up to 5 vol%. At higher GNP loadings, however, SSBM and SSSP HDPE/GNP nanocomposites show inferior flexural properties.

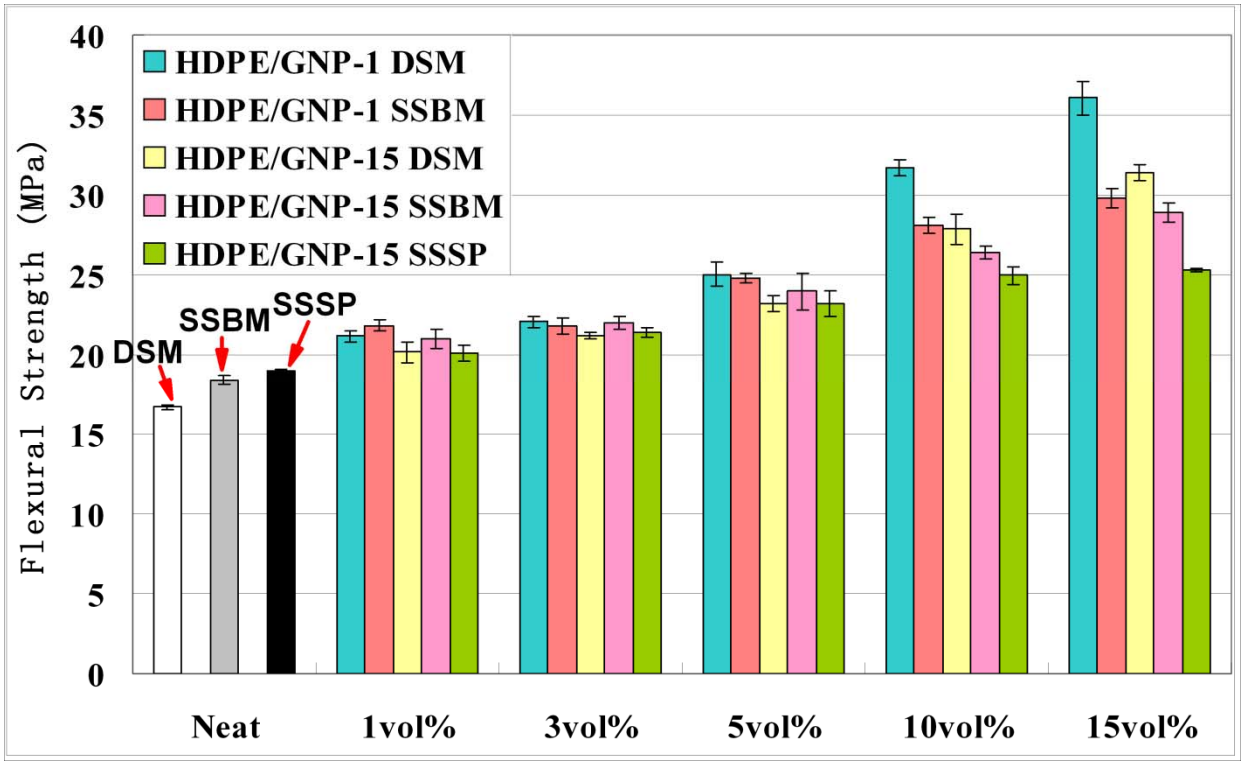

Figure 4.13. Flexural strength of HDPE/GNP nanocomposites made by DSM, SSBM and SSSP methods

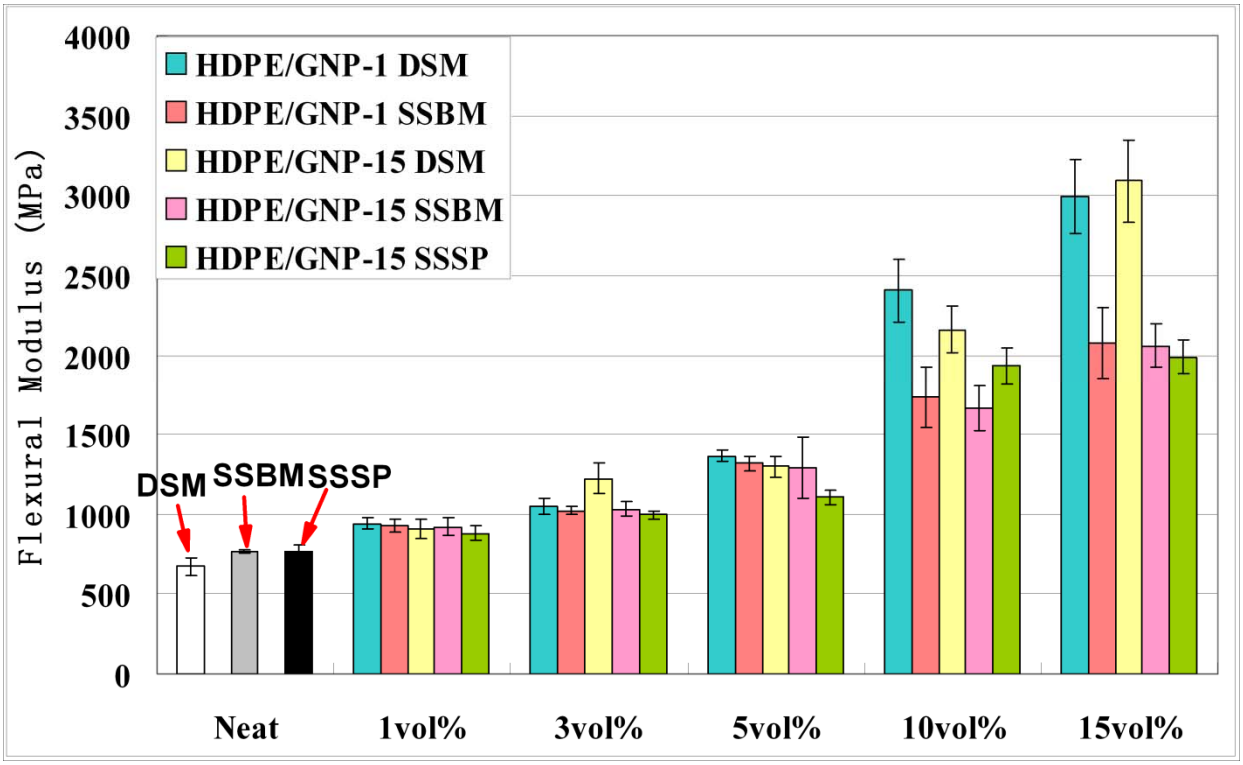

Figure 4.14. Flexural modulus of HDPE/GNP nanocomposites made by DSM, SSBM and SSSP methods

On the basis of morphology analysis for the SSBM and SSSP samples described above, the reduced mechanical properties are mainly due to the poor GNP dispersion in the polymer matrix. GNP platelets in those nanocomposites are not uniformly distributed and the severe GNP aggregation in the GNP-rich regions form stress concentrations similar to those voids and defects in the composites which result in a decrease of flexural strength and modulus.

4.4.4 Thermal Conductivity of SSBM HDPE/GNP Nanocomposites

From the results discussed above, the SSBM and SSSP process could substantially improve the electrical conductivity of HDPE/GNP nanocomposites while reduce their mechanical strength at high GNP loadings. This interesting phenomenon is due to the unique morphology produced by

these two processing techniques, that is, rather than uniformly dispersed in polymer matrix, GNP nanoplatelets are severely aggregated into one continuous phase for the electron transportation. This 'Process-Structure-Property' relationship is also believed to affect the thermal properties of the resulting nanocomposites. The thermal conductivity of HDPE/GNP nanocomposites fabricated by DSM melt-extrusion and SSBM is thus presented in the Figure 4.15 for the comparison. GNP-15 samples were taken for the illustration.

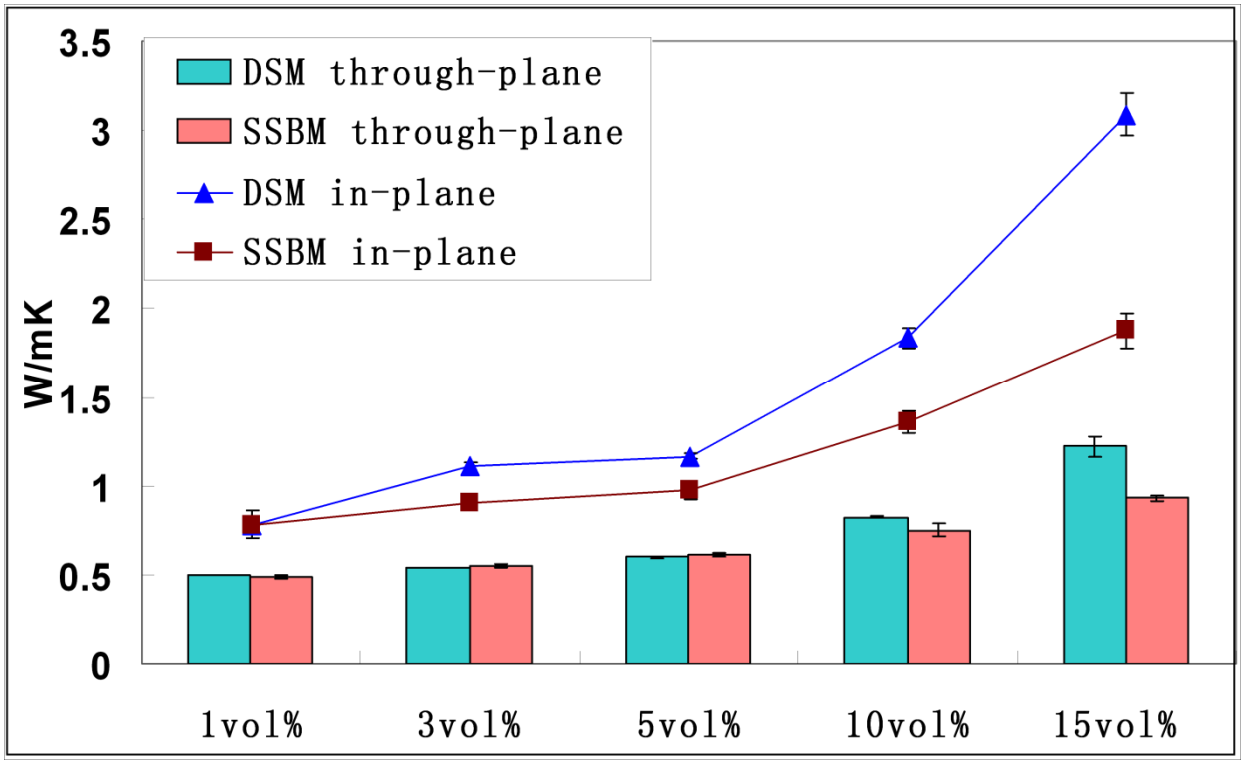

Figure 4.15. Thermal conductivity of SSBM HDPE/GNP-15 nanocomposites and their comparison with DSM counterparts

According to this figure, it is concluded that SSBM HDPE/GNP nanocomposites exhibit inferior in-plane and through-plane thermal conductivity to their DSM counterparts, especially at high GNP loadings (>5 vol%). Reduced thermal conductivity in SSBM samples illustrates the

different mechanism between electron and phonon conduction. For electron transportation, once there is a percolation network throughout the matrix, the composite becomes electrical conductive [32]. However, the phonon conduction in materials is dominated by the scattering effects such as interfacial boundary and defect scattering [33]. Severe GNP aggregation and agglomeration in the SSBM samples significantly reduce the effectiveness of GNP nanoplatelets as the thermal conductors and create lots of defects in scattering the phonons. The thermal conductivity of the resulting SSBM nanocomposites is therefore decreased.

Although the SSSP nanocomposites are not included for the comparison, a reduced thermal conductivity is also expected because of the similar morphology as confirmed by SEM images.

4.5 Conclusions

Although the percolation threshold of HDPE/GNP nanocomposites fabricated by the conventional melt-extrusion and injection molding is high, this study demonstrates that it could be significantly reduced by the SSBM and SSSP techniques before injection molding. GNP platelets were found to be uniformly coated on the surface of HDPE particles after the SSBM or SSSP process as confirmed by SEM images. During injection molding, those GNP platelets on the surface of HDPE tend to selectively aggregate at HDPE-GNP interfaces to form GNP-rich regions (conductive pathways). The electrical conductivity of the resulting nanocomposites is therefore substantially increased by the existence of these well-connected conductive pathways. Meanwhile, the mechanical and thermal properties of SSBM and SSSP HDPE/GNP nanocomposites were investigated. Because of the severe GNP aggregation in the GNP-rich

regions, reduced mechanical strength and thermal conductivity were observed for these nanocomposites at high GNP loadings. The disassociation between the electrical and thermal conductivity also illustrates the different transportation mechanism between electrons and phonons.

The mechanisms by which the SSBM and SSSP methods are capable of enhancing the electrical conductivity of HDPE/GNP nanocomposites appear to be the same. While SSBM is a viable batch method, SSSP is a continuous method that can produce a larger amount of material at a shorter time. These two methods are believed to have wide applicability to all thermoplastics/GNP nanocomposites.

REFERENCES

REFERENCES

[1] G.H. Motlagh, A.N. Hrymak, Thompson MR. Improved Through-Plane Electrical Conductivity in a Carbon-Filled Thermoplastic via Foaming. Polymer Engineering and Science 2008;48(4):687 - 96.

[2] Donnet J-B. Carbon Black, 3rd Edition. New York: Marcel Dekker, Inc.; 1998.

[3] Motlagh GH, Hrymak AN, Thompson MR. Properties of a carbon filled cyclic olefin copolymer. Journal of Polymer Science Part B: Polymer Physics. 2007;45(14):1808-20.

[4] Hermant MC, Klumperman B, Kyrylyuk AV, van der Schoot P, Koning CE. Lowering the percolation threshold of single-walled carbon nanotubes using polystyrene/poly(3,4-ethylenedioxythiophene): poly(styrene sulfonate) blends. Soft Matter. 2009;5:878 - 85.

[5] Andrews R, Weisenberger MC. Carbon nanotube polymer composites. Current Opinion in Solid State and Materials Science. 2004;8(1):31-7.

[6] Balasubramanian K, Burghard M. Biosensors based on carbon nanotubes ANALYTICAL AND BIOANALYTICAL CHEMISTRY 2006;385(3):452-68.

[7] Kim IH, Kim JH, KB K. Electrochemical characterization of electrochemically prepared ruthenium oxide/carbon nanotube electrode for supercapacitor application ELECTROCHEMICAL AND SOLID STATE LETTERS. 2005;8(7):A369-A72.

[8] Singh KV, Pandey RR, Wang X, Lake R, Ozkan CS, Wang K, et al. Covalent functionalization of single walled carbon nanotubes with peptide nucleic acid: Nanocomponents for molecular level electronics. Carbon. 2006;44(9):1730-9

[9] Yao X, Wu H, Wang J, Qu S, Chen G. Carbon nanotube/poly(methyl methacrylate) (CNT/PMMA) composite electrode fabricated by in situ polymerization for microchip capillary electrophoresis Chemistry - A European Journal. 2006;13(3):846 - 53.

[10] Kohler AR, Som C, Helland A, Gottschalk F. Studying the potential release of carbon nanotubes throughout the application life cycle. Journal of Cleaner Production.

2008;16(8-9):927-37.

[11] Kim S, Drzal LT. Comparison of Exfoliated Graphite Nanoplatelets (xGnP) and CNTs for Reinforcement of EVA Nanocomposites Fabricated by Solution Compounding Method and Three Screw rotating Systems Journal of Adhesion Science and Technology. 2009;23:1623–38.

[12] http://www.ptonline.com/articles/carbon-nanotubes-lots-of-potentialif-the-price-is-right.

[13] Celzard A, Krzesinska M, Begin D, Mareche JF, Puricelli S, Furdin G. Preparation, electrical and elastic properties of new anisotropic expanded graphite-based composites. Carbon. 2002;40(4):557-66.

[14] Fukushima H. Graphite nanoreinforcements in polymer nanocomposites [PHD Dissertation]. East Lansing, MI, USA: Michigan State University; 2003.

[15] Kalaitzidou K. Exfoliated Graphite Nanoplatelets as Nanoreinforcement for Multifunctional Polypropylene Nanocomposites [PHD Dissertation]. East Lansing, MI, USA: Michigan State University; 2006.

[16] Biswas S, Drzal LT. Multilayered Nanoarchitecture of Graphene Nanosheets and Polypyrrole Nanowires for High Performance Supercapacitor Electrodes. Chemistry of Materials. 2010;22(20):5667-71.

[17] Biswas S, Fukushima H, Drzal LT. Mechanical and electrical property enhancement in exfoliated graphene nanoplatelet/liquid crystalline polymer nanocomposites. Composites Part A: Applied Science and Manufacturing.42(4):371-5.

[18] Jiang X, Drzal LT. Multifunctional high density polyethylene nanocomposites produced by incorporation of exfoliated graphite nanoplatelets 1: Morphology and mechanical properties. Polymer Composites. 2010;31(6):1091-8.

[19] Jiang X, Drzal LT. Multifunctional high density polyethylene nanocomposites produced by incorporation of exfoliated graphite nanoplatelets 2: crystallization, thermal, and electrical properties. Polymer Composites. 2012; In Press, Accepted Manuscript.

[20] Kalaitzidou K, Fukushima H, Askeland P, Drzal LT. The nucleating effect of exfoliated

graphite nanoplatelets and their influence on the crystal structure and electrical conductivity of polypropylene nanocomposites. J Mater Sci. 2008;43(8):2895-907.

[21] Kalaitzidou K, Fukushima H, Drzal LT. Multifunctional polypropylene composites produced by incorporation of exfoliated graphite nanoplatelets. Carbon. 2007;45:1446–52.

[22] Zhang Q, Rastogi S, Chen D, Lippits D, Lemstra PJ. Low percolation threshold in single-walled carbon nanotube/high density polyethylene composites prepared by melt processing technique. Carbon. 2006;44(4):778-85.

[23] Kalaitzidou K, Fukushima H, Drzal LT. A new compounding method for exfoliated graphite–polypropylene nanocomposites with enhanced flexural properties and lower percolation threshold. Composites Science and Technology. 2007;67:2045–51.

[24] Pan Y-X, Yu Z-Z, Ou Y-C, Hu G-H. A new process of fabricating electrically conducting nylon 6/graphite nanocomposites via intercalation polymerization. Journal of Polymer Science Part B: Polymer Physics. 2000;38(12):1626-33.

[25] Du XS, Xiao M, Meng YZ. Synthesis and characterization of polyaniline/graphite conducting nanocomposites. Journal of Polymer Science Part B: Polymer Physics. 2004;42(10):1972-8.

[26] Xiao P, Xiao M, Gong K. Preparation of exfoliated graphite/polystyrene composite by polymerization-filling technique. Polymer. 2001;42(11):4813-6.

[27] Furgiuele N, Lebovitz AH, Khait K, Torkelson JM. Novel Strategy for Polymer Blend Compatibilization: Solid-State Shear Pulverization. Macromolecules. 1999;33(2):225-8.

[28] Lebovitz AH, Khait K, Torkelson JM. Stabilization of Dispersed Phase to Static Coarsening: Polymer Blend Compatibilization via Solid-State Shear Pulverization. Macromolecules. 2002;35(23):8672-5.

[29] Chung DDL. Electromagnetic interference shielding effectiveness of carbon materials. Carbon. 2001;39:279-85.

[30] Mehta V CJ. Review and analysis of PEM fuel cell design and manufacturing. Journal of

Power Sources. 2003;114:32-53.

[31] Klementina Khait, Carr SH, Mack MH. Solid-state shear pulverization: a new polymer processing and powder technology: Technomic Publishing Company Inc. ; 2001.

[32] Ezquerra TA, Martinez-Salazar J, Baltá Calleja FJ. Percolation threshold of conductive polycarbonate/carbon composites as revealed by electron microscopy. Journal of Materials Science Letters. 1986;5(10):1065-6.

[33] Gojny FH, Wichmann MHG, Fiedler B, Kinloch IA, Bauhofer W, Windle AH, et al. Evaluation and identification of electrical and thermal conduction mechanisms in carbon nanotube/epoxy composites. Polymer. 2006;47(6):2036-45.

CHAPTER 5 IMPROVING ELECTRICAL CONDUCTIVITY AND MECHANICAL PROPERTIES OF HIGH DENSITY POLYETHYLENE THROUGH INCORPORATION OF PARAFFIN WAX COATED EXFOLIATED GRAPHENE NANOPLATELETS AND MULTI-WALLED CARBON NANO-TUBES

5.1 Abstract

HDPE based nanocomposites were reinforced by exfoliated graphene nanoplatelets, GNP, and multi-walled carbon nano-tubes, MWCNT, through melt-extrusion and injection molding in this chapter. To reduce their high percolation threshold and high electrical resistivity, low molecular weight paraffin wax was selected as a coating on the surface of GNP and MWCNT to improve their dispersion in HDPE. Wax coated GNP and MWCNT were fabricated by mixing wax with GNP and MWCNT in hot xylene and followed with the solvent evaporation and vacuum drying. It was found that wax coated GNP and MWCNT are much more efficient than the uncoated ones in improving the electrical conductivity and the flexural properties of the resulting HDPE nanocomposites. Morphology characterization has verified that the dispersion of GNP and MWCNT in the polymer matrix was significantly enhanced by this wax coating method which is responsible for the better electrical and mechanical properties in the resulting nanocomposites.

5.2 Introduction

From the previous discussion, HDPE/GNP nanocomposites fabricated by the conventional processing method of melt-extrusion and injection molding have a relatively high percolation threshold at around 10-15 vol% GNP loading which is due to the severe GNP aggregation during

melt-extrusion and preferential platelets alignment in injection molding as confirmed by their morphology. To reduce the percolation threshold and enhance the electrical conductivity, two novel processing techniques of solid state ball milling (SSBM) and solid state shear pulverization (SSSP) were applied to fabricate the HDPE/GNP nanocomposites. Results showed that the percolation threshold of these nanocomposites was effectively reduced to 3-5 vol% GNP loading and their electrical conductivity was significantly improved. The mechanism of SSBM and SSSP in reducing the percolation threshold is to coat the polymer surface with GNP platelets which induces the selective GNP aggregation at HDPE-GNP interfaces during injection molding [1]. However, their mechanical and thermal properties were found to be compromised with the improvement in electrical conductivity.

If we want to lower the percolation threshold in melt-extruded HDPE/GNP nanocomposites but also enhance or at least maintain their good mechanical and thermal properties, the key factor is getting GNP dispersed uniformly throughout the polymer matrix, which ensures a good connectivity between GNP platelets in forming conductive networks and favors load transfer within the nanocomposites. To enhance the dispersion of GNP in polymers, two major techniques were normally applied in the literature.

The first one is to employ non-traditional processing methods such as solution intercalation method in polypropylene/GNP nanocomposites [2], in situ polymerization method in nylon 6/expanded graphite and polyaniline/expanded graphite nanocomposites [3, 4], and polymerization filling technique in polystyrene/exfoliated graphite nanocomposites [5]. These methods have demonstrated that the dispersion of GNP in these polymer/graphite composites

was all significantly improved which resulted in a reduced percolation threshold and improved mechanical properties compared with the samples made by the conventional melt-extrusion. However, all these methods involve the usage of large amount of solvent, which makes the compounding process more costly and less environmental friendly. Since extrusion and injection molding is still the major processing method used for manufacturing the thermoplastics in industry, a method to reduce the percolation threshold in melt-extruded GNP nanocomposites remains an area of research focus.

The other approach is to covalently modify the surface chemistry of GNP, which is based on a special treatment of GNP platelets to obtain functional groups or polymer chains that are compatible with the polymer matrix chemically anchored on the edge. Recently, epoxy functionalized graphite nanoparticles were successfully synthesized by Sandi G. Miller et al. through the covalently bonding an epoxy monomer to the surface of expanded graphite for their better dispersion in epoxy [6]; Graphene nanosheets grafted with long alkyl chains were produced by Yewen Cao et al. through the amidation reaction for their better dispersion in polyolefin [7]; and oxygen and hydroxyl functionalized graphene sheets were reported by T. Ramanathan et al. through the rapid thermal expansion of completely oxidized graphite oxide for poly(acrylonitrile) and poly(methyl methacrylate) [8]. Results have shown that functionalized GNP affords better interaction with the host polymers compared to the unmodified GNP, thereby imparting superior mechanical, excellent thermal and electrical properties at exceptionally low GNP loadings. However, these methods are relatively complicated due to involving chemical

reactions that always introduce sp^3 bonding and defects to the graphene basal plane which may deteriorate the required mechanical, electrical and thermal properties of GNP platelets.

Therefore, a method that can not only be applicable to the conventional compounding process of melt-extrusion and injection molding, but also maintain the graphene structure and the electronic properties of GNP platelets in their pristine state is still of high research interest to improve the dispersion of GNP in polymers. In this chapter, a wax coating method which is based on the use of a low molecular weight polyethylene (paraffin wax) coating on the surface of GNP to prevent their re-aggregation during melt-extrusion will be developed and evaluated. GNP-15 nanocomposites will be taken for the demonstration. Because of the similar graphene surface structure of multi-walled carbon nano-tubes (MWCNT), it is considered that this method would also be useful to improve the dispersion of MWCNT in the polymer matrix of HDPE.

5.3 Experimental

5.3.1 Materials

In this research, HDPE pellets with the trade name Marlex® HXM 50100 (Density 0.95 g/cm^3, Flow index 10.0 g/10 min, MW~ 230,000) were obtained from Chevron Phillips Chemical Company. Paraffin wax (max C_{30}, Density 0.92 g/cm^3, MW~ 500) with the melting point of 55 °C was purchased from Sigma-Aldrich. GNP nanoplatelets were obtained from XG Science, Inc [9]. The diameter of individual GNP platelet is around 15 μm (GNP-15) and the thickness is less than 10 nm. Multi-walled carbon nano-tubes, MWCNT, were obtained from Bayer Material Science Company with the diameter of individual MWCNT being around 15 nm and the length

between 1 to 10 μm. The physical properties of GNP-15 and MWCNT are detailed in the Table 5.1.

Table 5.1. Geometrical and surface characteristics of GNP-15 and MWCNT

Material	Length (μm)	Diameter (μm)	Aspect Ratio	Surface Area (m^2/g)	Intrinsic Density (g/cm^3)
GNP-15	**<0.01 (platelet thickness)**	**15 (platelet diameter)**	**~1500**	**~40**	**2.1**
MWCNT	**1-10**	**0.015**	**~350**	**~200**	**2.1**

5.3.2 Processing Methods

5.3.2.1 Melt Extrusion and Injection Molding

Melt extrusion of HDPE/GNP and HDPE/MWCNT nanocomposites was carried out in a DSM mini-extruder system as described in the previous chapters. Flexural coupons were made for mechanical properties and electrical conductivity measurements and round disks (thickness ~1.5 mm, diameter ~25 mm) were injection molded for thermal conductivity test.

5.3.2.2 Wax Coating on the Surface of GNP-15 and MWCNT

A uniform coating of paraffin wax on the surface of GNP-15 and MWCNT was achieved by a solution coating method with xylene as the solvent. Wax was first dissolved in xylene at around 60 °C and GNP-15 or MWCNT was added afterwards. Sonication was then applied for 30

minutes at 100 W to initially break down the GNP-15 and MWCNT aggregates and to ensure a uniform wax coating. The resultant mixture was poured into an aluminum pan and left in a hood at room temperature to evaporate the solvent. After xylene was completely evaporated, the wax coated GNP-15 and MWCNT were further dried in a vacuum oven overnight at 30 °C. Four different wax coated GNP-15 samples were prepared having wax to GNP-15 ratios of 5:95, 10:90, 20:80, and 30:70 wt%. Due to a higher surface area of MWCNT, larger wax to MWCNT ratios were applied for the wax coated MWCNT. They were 20:80, 30:70, 40:60, and 50:50 wt% between wax and MWCNT. This procedure of producing wax coated GNP-15 and MWCNT is schematically shown in the Figure 5.1.

Then wax coated GNP-15 and MWCNT were re-dispersed in HDPE by melt-extrusion in the DSM Micro 15cc Compounder with the same processing parameters described before. The actual loading of GNP-15 or MWCNT in the final nanocomposites was kept at 5 vol% in this study. After extrusion, the resulting HDPE/wax coated GNP-15 (HDPE/WaxGNP-15) and HDPE/wax coated MWCNT (HDPE/WaxMWCNT) composite melts were injection molded into flexural coupons for mechanical and electrical properties test and round disks for thermal conductivity measurement. The sample nomenclature for HDPE/WaxGNP-15 and HDPE/WaxMWCNT nanocomposites with different wax to GNP-15 or MWCNT ratios is: 5 vol% HDPE/WaxGNP-15 (20:80wt%) means the actual GNP-15 loading in this nanocomposite is 5 vol% and the weight ratio between wax and GNP-15 is 20:80. 5 vol% HDPE/WaxMWCNT (20:80wt%) presents a nanocomposite with 5 vol% MWCNT loading and a wax to MWCNT weight ratio of 20:80.

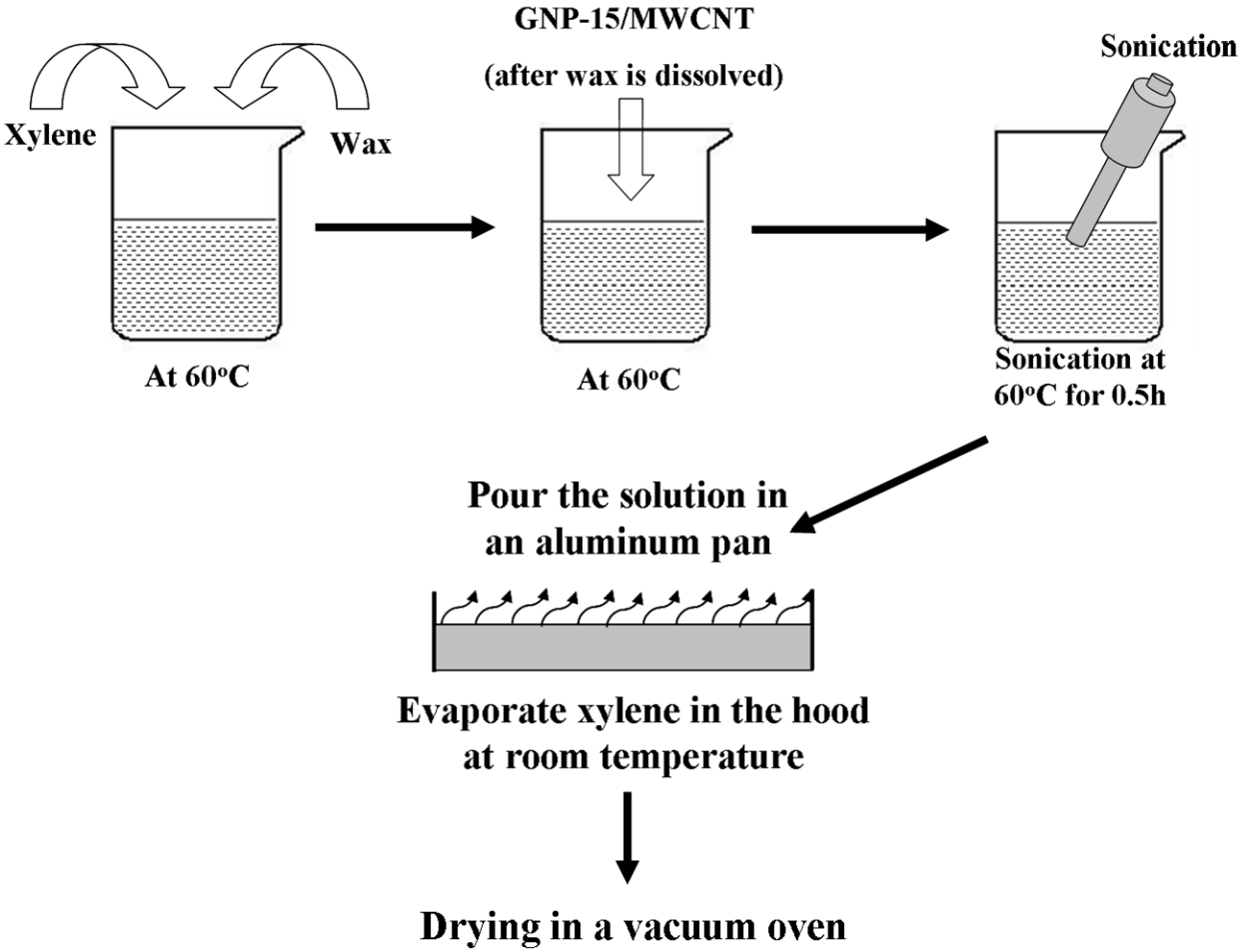

Figure 5.1. The procedure of making wax coated GNP-15 and MWCNT

To exclude any artifact due to the sonication, GNP-15 or MWCNT was added into xylene with the same sonication time of 30 minutes but without the addition of wax. After complete evaporation of xylene, GNP-15 or MWCNT was melt-mixed with HDPE by the same melt-extrusion and injection molding process to obtain the HDPE/GNP-15 (sonic.) and HDPE/MWCNT (sonic.) nanocomposites with GNP-15 or MWCNT loading at 5 vol% as a reference.

5.3.3 Characterization Methods

5.3.3.1 Mechanical Property

A UTS SFM-20 machine (United Calibration Corp.) was used to measure the flexural properties. Flexural coupons were tested under 3-point bending mode at a flexural rate of 0.05 in/min following the ASTM D790 standard.

5.3.3.2 Electrical Resistivity

The electrical resistivity of HDPE/GNP and HDPE/MWCNT nanocomposites was measured both along the flow direction (in-plane resistivity) and through the thickness direction (through-plane resistivity, normal to the flow direction), using impedance spectroscopy by applying a two-probe method at room temperature. Samples with dimensions around 10 x 3.2 x 12.2 mm (Length x Thickness x Width) were cut from the middle portion of flexural bars. The two surfaces connected to the electrodes were first treated with O_2 plasma (14 minutes, 375 W) in order to remove the top surface layers which are rich in polymer and then conductive silver paste was used to ensure good contact of the sample surface with the electrodes. The resistance of samples was measured and converted to resistivity by taking the sample dimensions into account.

5.3.3.3 Thermal Conductivity

Thermal diffusivity (α, m^2/s) (both in-plane and through-plane) of GNP and MWCNT nanocomposites (round disks) was measured by a LFA Nanoflash 447 Light flash system. To

calculate the thermal conductivity, the bulk density of the samples (ρ, kg/m^3) was obtained by dividing the mass over the volume, and the specific heat capacity (C_p: J/(kg· K)) was measured through the differential scanning calorimetry (DSC Q2000, TA instrument). The thermal conductivity (κ, W/(m·K)) of GNP samples was then calculated by the following equation: $\kappa = \alpha * \rho * C_p$.

5.3.3.4 Scanning Electron Microscopy (SEM)

The preparation of SEM samples in this study included epoxy mounting, grinding, polishing and etching steps. First, HDPE/GNP and HDPE/MWCNT specimens for microscopic examination were mounted with epoxy in cylindrical sample holders to maintain a flat surface over the entire grinding area. After the epoxy was fully cured, the samples were then carefully grounded and polished. Plasma etching was applied at the last step to remove the polymer in top surface layers allowing the nano-particles to stand out. A JEOL (model JSM-6400) SEM with an accelerating voltage of 10 kV and a working distance of 15 mm was then used to collect the SEM images. Samples were also gold coated of a few nanometers in thickness to avoid charging.

5.4 Results and Discussion

5.4.1 Electrical Conductivity of HDPE/GNP-15 and HDPE/MWCNT Nanocomposites

The in-plane and through-plane electrical resistivity of HDPE/GNP-15 nanocomposites made by conventional DSM melt-extrusion and injection molding (DSM HDPE/GNP) has been fully discussed in the previous chapter. Results showed that the percolation threshold of these

nanocomposites was quite high at 10-15 vol% GNP loading. The high percolation threshold and low electrical conductivity is due to severe GNP aggregation during melt-extrusion and preferential platelets alignment in injection molding. To have a better comparison with HDPE/WaxGNP-15 nanocomposites that will be addressed later on, the morphology of DSM HDPE/GNP-15 samples at 5 vol% GNP loading is presented in the Figure 5.2, which clearly shows the aggregation and orientation of GNP nanoplatelets. The presence of these large GNP-15 aggregates drastically reduces the number of GNP-15 platelets available as 'effective' reinforcing particles and significantly decreases the probability of interconnections between GNP-15 platelets in forming electrically conductive pathways. As a result, the electrical conductivity of HDPE/GNP nanocomposites made by melt-extrusion and injection molding is low.

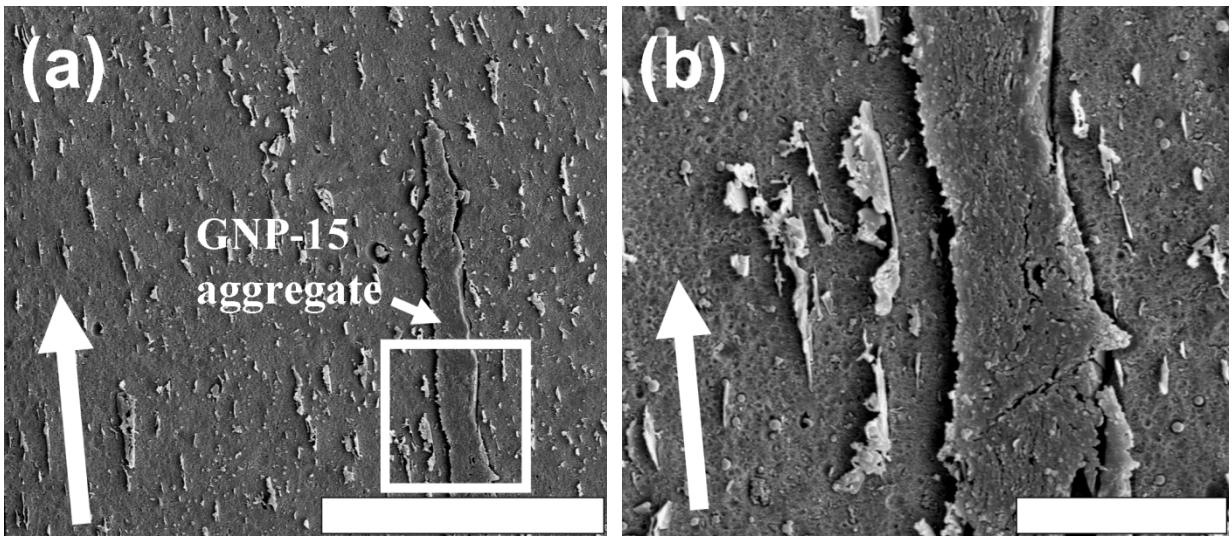

Figure 5.2. SEM images of the HDPE/GNP-15 nanocomposite at 5 vol% GNP loading. The arrow on the left bottom indicates the material flow direction during injection molding. (a) a low magnification image (scale bar 50 μm); (b)enlarged rectangular area in 4(a) (scale bar 10 μm)

The in-plane and through-plane electrical resistivity of melt-extruded HDPE/MWCNT

nanocomposites at various MWCNT loadings are presented in the Figure 5.3. As seen from the figure, the percolation threshold for HDPE/MWCNT nanocomposites is also high and has a value of 5-10 vol% MWCNT loading. Although this percolation threshold is lower than that of the GNP-15 samples, it is still much higher if compared with the CNTs-filled nanocomposites fabricated by other compounding techniques such as solution mixing, gelation/crystallization and high energy ball milling [10-12]. The morphology of the HDPE/MWCNT nanocomposite at 5 vol% MWCNT loading is shown in the Figure 5.4, which helps to explain the cause of the high percolation threshold in melt-extruded HDPE/MWCNT nanocomposites.

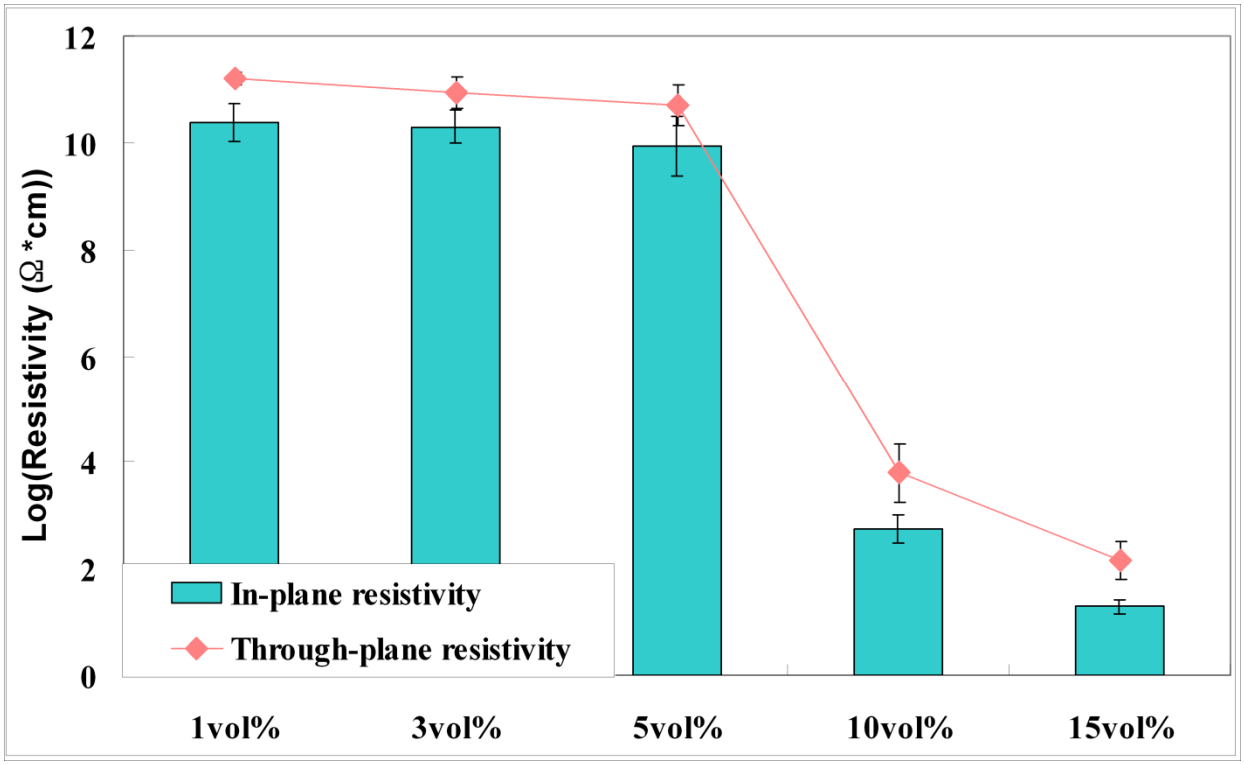

Figure 5.3. In-plane and through-plane electrical resistivity of HDPE/MWCNT nanocomposites at different MWCNT loadings, which are made by the conventional processing method of melt-extrusion and injection molding

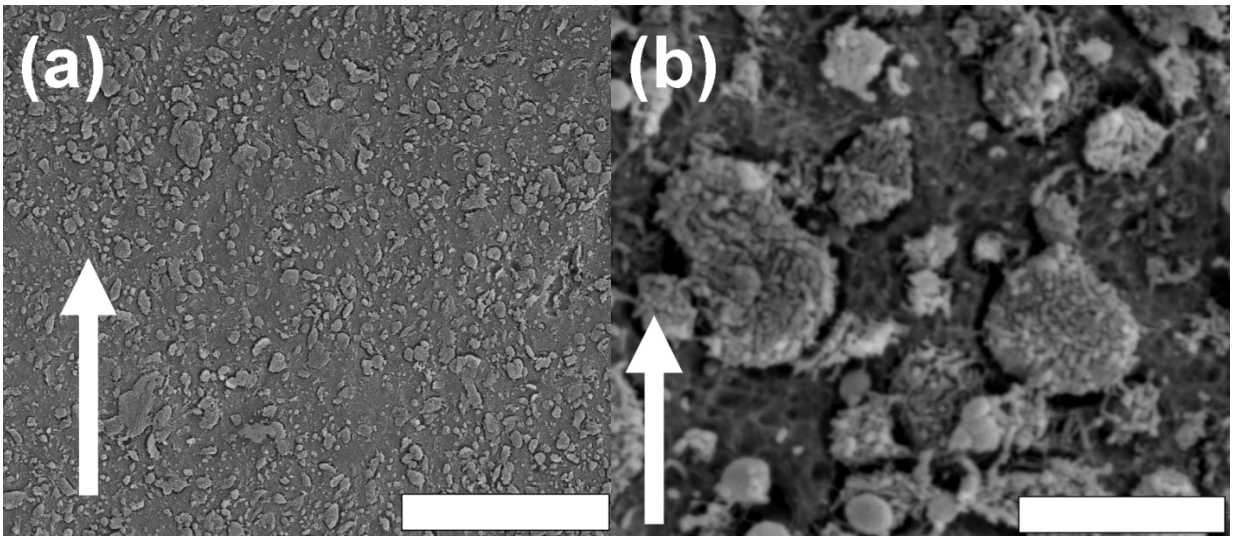

Figure 5.4. SEM images of the HDPE/MWCNT nanocomposite at 5 vol% MWCNT loading. The arrow on the left bottom indicates the material flow direction during injection molding. (a) a low magnification image(scale bar 20 μm); (b) a high magnification image (scale bar 2 μm)

According to the Figure 5.4 (a), numerous MWCNT aggregates are detected and they are totally isolated from each other. It seems that these MWCNT aggregates do not exhibit obvious alignment along the material flow direction which is different from GNP-15 platelets. And from the Figure 5.4 (b), the size of the aggregates is found to be 1-2 μm and the individual nano-tubes are packed tightly within the agglomerates. The interconnections between MWCNT aggregates are thus poor which lead to the low electrical conductivity and the high percolation threshold in the resulting MWCNT nanocomposites. Severe MWCNT aggregation in the polymer matrix comes from the inability of individual MWCNT particles to be highly separated and dispersed which is due to the high melt viscosity and the lack of adequate shear forces during the DSM melt-extrusion. Combined with the results of the GNP-15 samples, it is concluded that nano-fillers such as GNP and MWCNT are likely to aggregate under the melt processing conditions since the affinity between nano-fillers is much larger than that between the nano-filler

and the polymer matrix. So how to get rid of these big aggregates is the key issue to improve the dispersion of nano-fillers and to achieve a lower percolation threshold in the resulting nanocomposites. The following sections will investigate a special method of coating the surface of GNP and MWCNT with wax, which is capable of preventing the aggregation of these nano-fillers under the processing conditions.

5.4.2 Electrical Conductivity of HDPE/WaxGNP-15 and HDPE/WaxMWCNT Nanocomposites

The in-plane and through-plane electrical resistivity of HDPE/WaxGNP-15 nanocomposites at 5 vol% GNP loading is displayed in the Figure 5.5. Interestingly, with the presence of wax coated on the surface of GNP, the previous non-conductive 5 vol% HDPE/GNP-15 nanocomposite (control sample) becomes electrical conductive along the material flow direction. And the in-plane resistivity is continuously decreased as the wax content increases. A more than 5 orders of magnitude decrease in resistivity is seen from the control sample to the 5 vol% HDPE/WaxGNP-15 (30:70wt%) nanocomposite, suggesting that the electrical conductivity of HDPE/WaxGNP-15 nanocomposites is significantly enhanced. Therefore, the percolation threshold of melt-extruded HDPE/GNP-15 nanocomposites is reduced from the previous 10-15 vol% GNP loading to less than 5 vol%. However, the through-plane electrical resistivity of these nanocomposites remains high and it is unaffected by the addition of wax.

Meanwhile, if we compare the resistivity value of the sonicated sample (5 vol% HDPE/GNP-15 (sonic.)) with the control sample, no significant difference in resistivity is observed. This implies

that the application of sonication alone without the use of wax is insufficient to improve the electrical conductivity of the resulting nanocomposites.

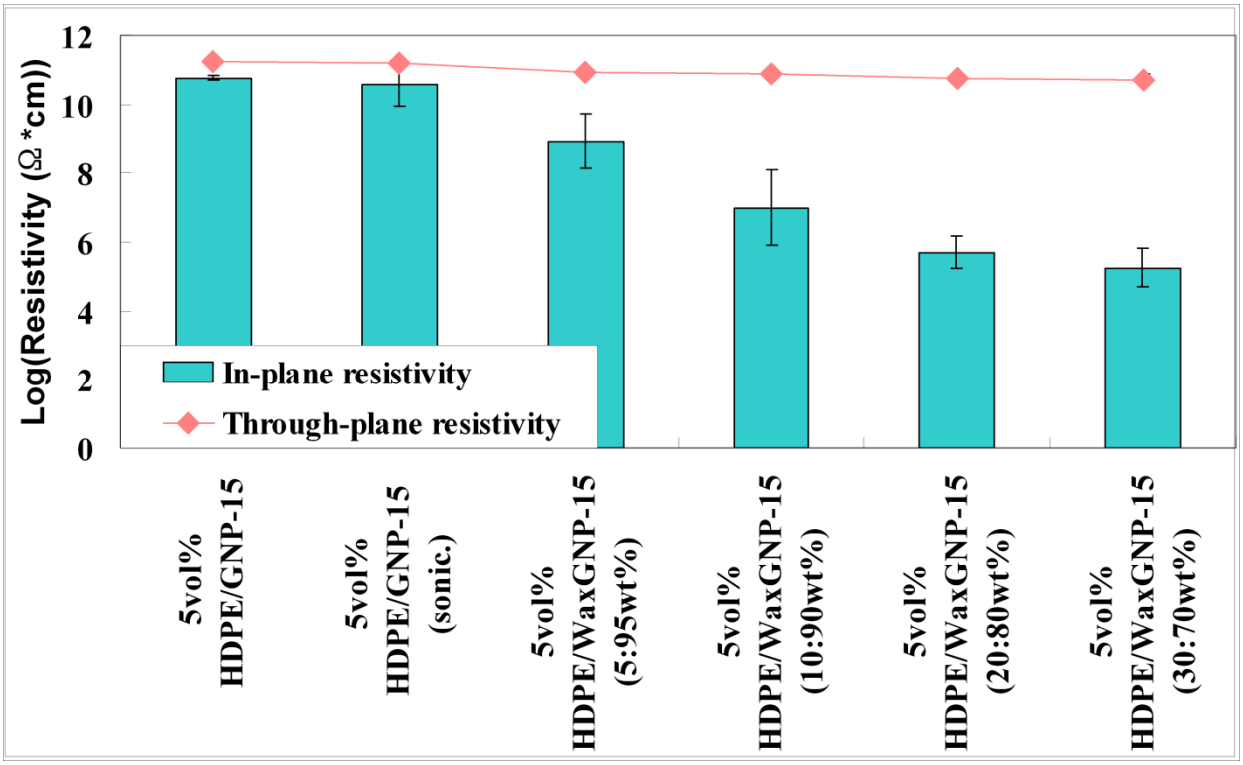

Figure 5.5. In-plane and through-plane electrical resistivity of HDPE/WaxGNP-15 nanocomposites at 5 vol% GNP loading

Figure 5.6 illustrates the in-plane and the through-plane electrical resistivity of HDPE/WaxMWCNT nanocomposites at 5 vol% MWCNT loading. Again, it is seen that the in-plane resistivity is dramatically reduced as the wax to MWCNT ratio increases. From the control sample to the 5 vol% HDPE/WaxMWCNT (50:50wt%) nanocomposite, the resistivity value drops by almost 7 orders of magnitude which clearly demonstrates the huge improvement in the electrical conductivity. In contrast to the results of the GNP-15 samples, the through-plane electrical resistivity is also found to be significantly reduced as the amount of wax coating

increases, showing the efficiency of this wax coating method in improving the electrical conductivity of HDPE/MWCNT nanocomposites. In the same time, it is found that the sonicated sample (5 vol% HDPE/MWCNT (sonic.)) does not exhibit any enhancement in conductivity either which further confirms the insufficiency of using sonication alone.

The SEM images display the unique morphology of these samples and explain why the electrical conductivity of both HDPE/GNP-15 and HDPE/MWCNT nanocomposites is greatly improved by the wax coating method.

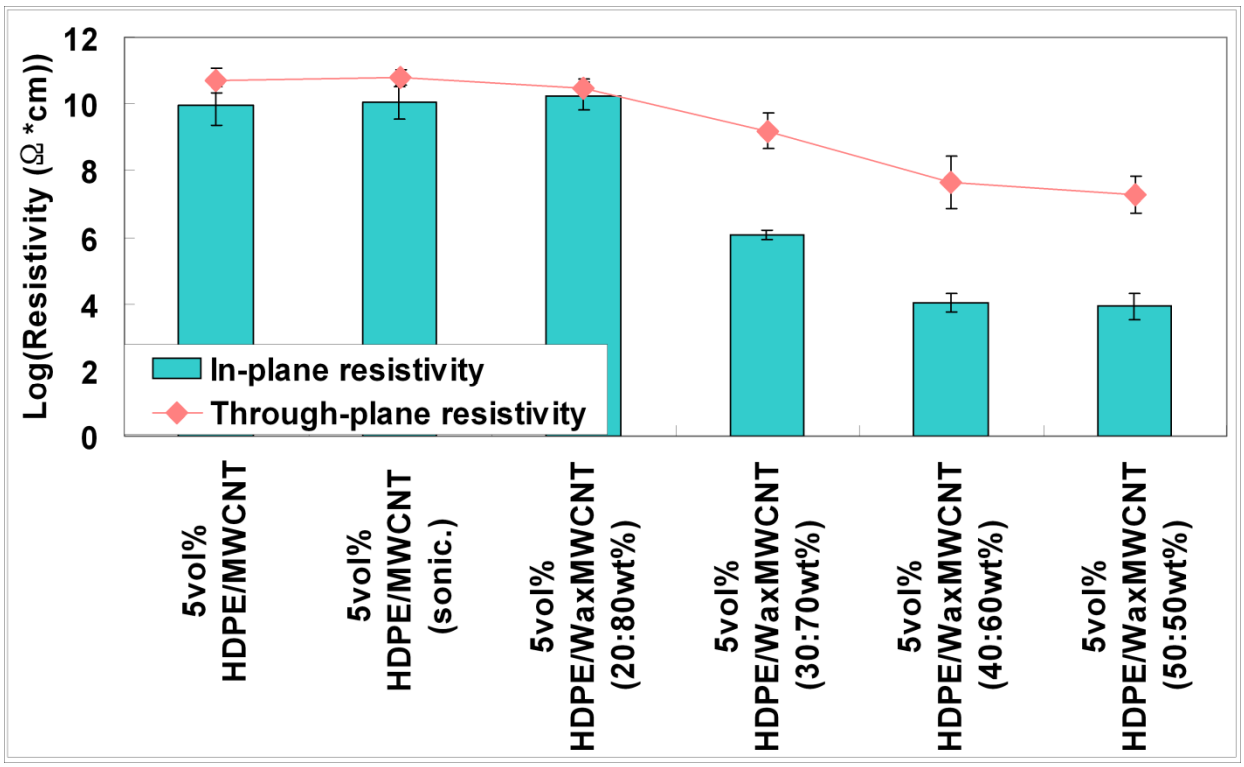

Figure 5.6. In-plane and through-plane electrical resistivity of HDPE/WaxMWCNT nanocomposites at 5 vol% MWCNT loading

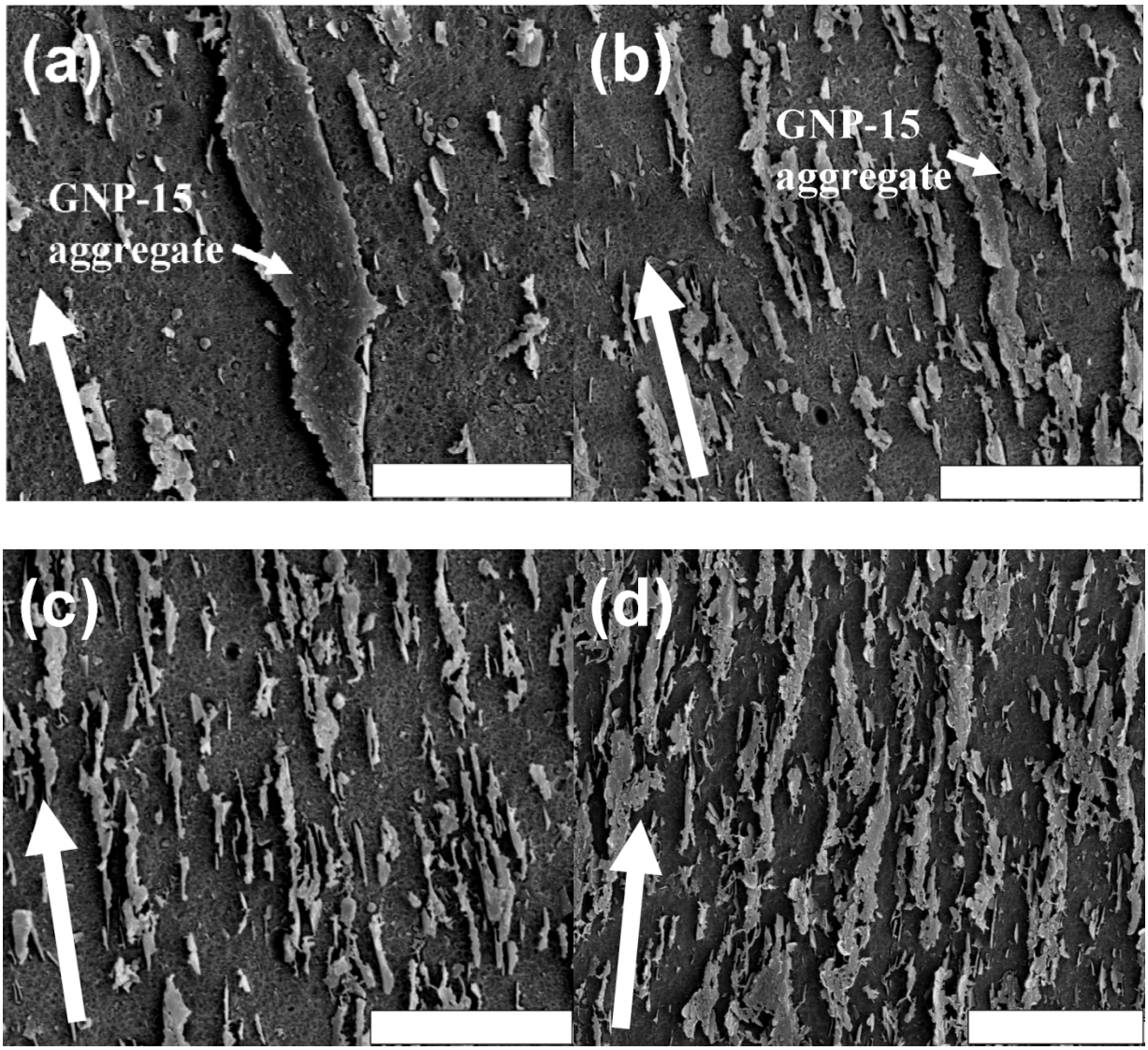

Figure 5.7. Morphology of various HDPE/WaxGNP-15 nanocomposites at 5 vol% GNP loading: (a) sonicated HDPE/GNP-15 (scale bar 10 μm); (b) HDPE/WaxGNP-15 (10:90wt%) (scale bar 10 μm); (c) HDPE/WaxGNP-15 (20:80wt%) (scale bar 10 μm); (d) HDPE/WaxGNP-15 (30:70wt%) (scale bar 10 μm). The arrow on the left bottom indicates the material flow direction during injection molding

The morphology of 5 vol% HDPE/WaxGNP-15 nanocomposites with different wax to GNP-15 ratios as well as the sonicated sample is presented in the Figure 5.8. As discussed in the previous section, GNP-15 platelets in the control sample are aligned along the material flow direction and large GNP-15 aggregates are present (Figure 5.2). From the Figure 5.8 (a), which is the

morphology of the sonicated sample, a similar morphology can be seen, that is, there exhibit preferential GNP-15 alignment and large GNP-15 aggregates. This similarity in morphology between the sonicated sample and the control sample suggests that sonication alone without wax is not sufficient to improve the dispersion of GNP-15 in HDPE. Although the technique of sonication is proved as an efficient method to break down the agglomerates or aggregates of nano-particles in solution [13], once incorporated in polymers, these nano-particles which were initially separated would like to be re-aggregated again during the melt processing conditions.

Figures 5.7 (b) to 5.7 (d) compare the morphology of 5 vol% HDPE/WaxGNP-15 nanocomposites with increasing wax content. It is clear to see that the number density of GNP-15 platelets is increasing as the wax content increases and big GNP-15 aggregates can no longer be detected. The disappearance of GNP aggregates as well as the increased GNP number density indicates that the re-aggregation of GNP-15 platelets is indeed prevented by the addition of a proper amount of wax coating on the surface. In this case, individual GNP-15 platelets can be dispersed uniformly in the polymer matrix. Meanwhile, the presence of well dispersed GNP-15 platelets significantly improves their interconnections in forming conductive pathways along the material flow direction, which is mainly responsible for the enhanced in-plane electrical conductivity of HDPE/WaxGNP-15 nanocomposites.

Figure 5.9 shows the morphology of various 5 vol% HDPE/WaxGNP-15 nanocomposites at a lower magnification, which further illustrates the disappearance of GNP aggregates and the increased GNP number density as the content of wax increases.

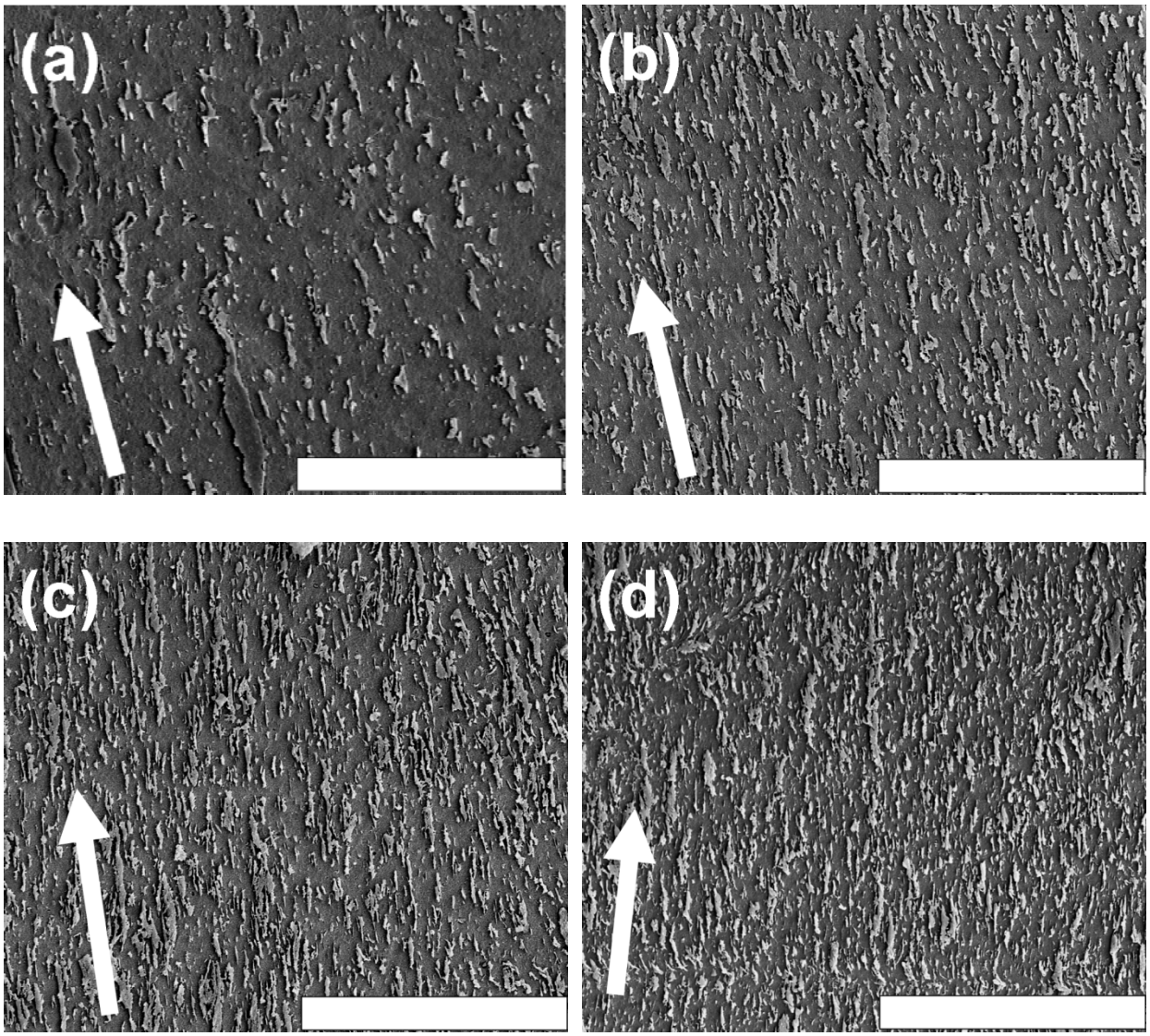

Figure 5.8. Morphology of various 5 vol% HDPE/WaxGNP-15 nanocomposites at a lower magnification: (a) sonicated HDPE/GNP-15 (scale bar 50 μm); (b) HDPE/WaxGNP-15 (10:90wt%) (scale bar 50 μm); (c) HDPE/WaxGNP-15 (20:80wt%) (scale bar 50 μm); (d) HDPE/WaxGNP-15 (30:70wt%) (scale bar 50 μm). The arrow on the left bottom indicates the material flow direction during injection molding

Figure 5.9 gives the morphology of the 5 vol% HDPE/MWCNT (sonic.) sample and 5 vol% HDPE/WaxMWCNT nanocomposites with different wax to MWCNT ratios. According to the Figure 5.9 (a), tightly-packed MWCNT aggregates are found in the sonicated samples which are very similar to those in the HDPE/MWCNT control sample (Figure 5.4).

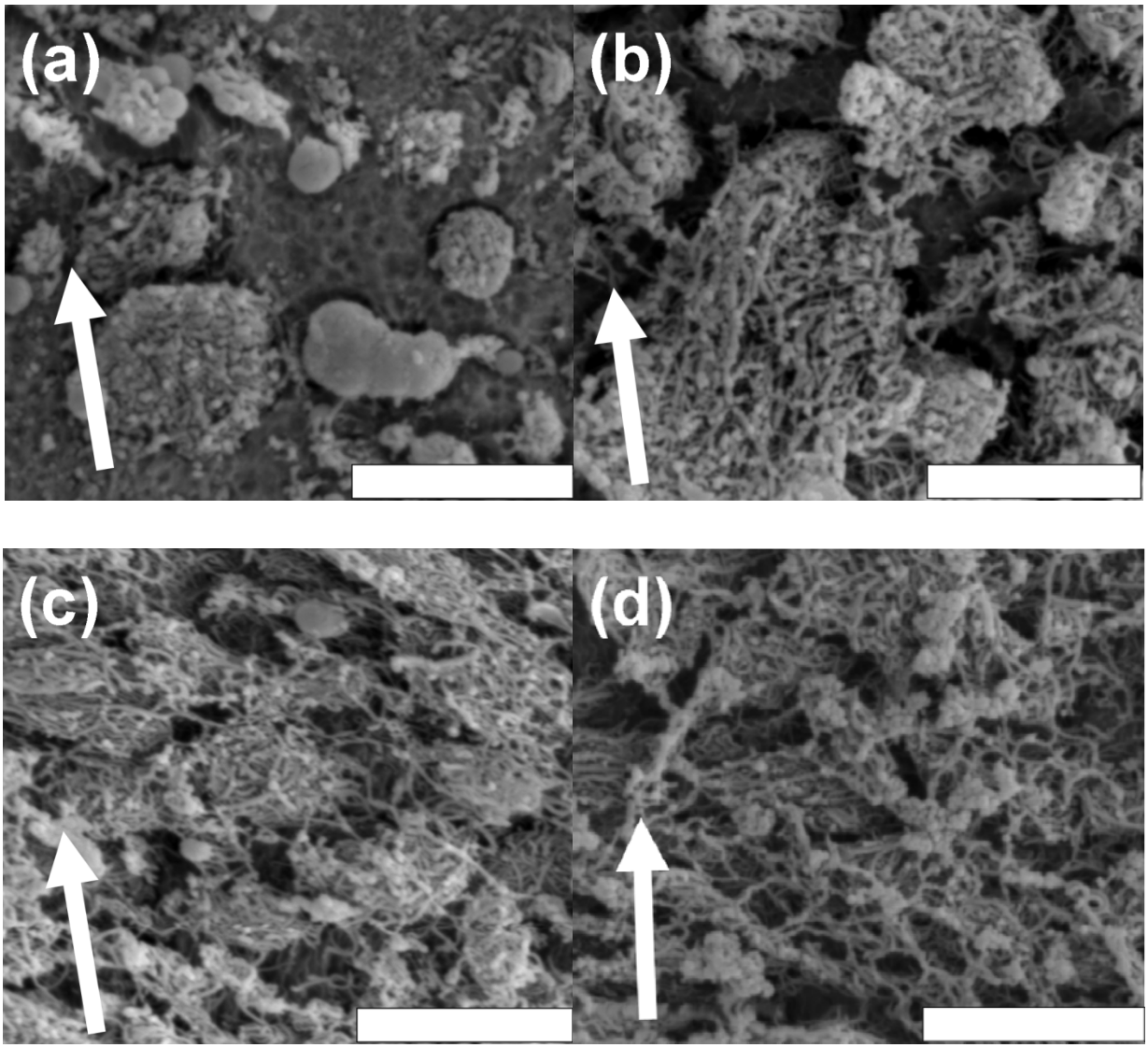

Figure 5.9. Morphology of various HDPE/MWCNT nanocomposites at 5 vol% MWCNT loading: (a) sonicated HDPE/MWCNT (scale bar 2 μm); (b) HDPE/WaxMWCNT (20:80wt%) (scale bar 2 μm); (c) HDPE/WaxMWCNT (30:70wt%) (scale bar 2 μm); (d) HDPE/WaxMWCNT (40:60wt%) (scale bar 2 μm). The arrow on the left bottom indicates the material flow direction during injection molding

Images 5.9 (b) to 5.9 (d) illustrate the morphology of HDPE/WaxMWCNT nanocomposites with increasing wax to MWCNT ratios. As the wax content increases, the MWCNT aggregates are getting expanded and the individual MWCNT is becoming more dissociated from each other. Besides, a large number of nano-tubes are seen to be extending out from the aggregates and they

are interleaving with each other forming well-connected conductive networks as seen in the images of 5.9 (c) and 5.9 (d). The presence of these MWCNT conductive networks greatly facilitates the transportation of electrons in all directions. Therefore, both the in-plane and the through-plane electrical conductivity of HDPE/WaxMWCNT nanocomposites are tremendously enhanced as a result of the greatly improved MWCNT dispersion in the polymer matrix. The substantially improved MWCNT dispersion in HDPE as the wax content increases can be further confirmed by the SEM images at a lower magnification, which are shown in the Figure 5.10.

In summary, the application of the wax coating method can both improve the dispersion of GNP and MWCNT substantially in HDPE which gives rise to the enhanced electrical conductivity of the resulting HDPE/WaxGNP-15 and HDPE/WaxMWCNT nanocomposites. The mechanism of the wax coating method is based on two factors. The first is the use of ultrasonication, which initially reduces the aggregates of nano-particles to a large extent. The second factor relies on the wax coating. With the help of the ultrasonication, wax is uniformly coated on the surface of GNP-15 and MWCNT, which consequently prevents their re-aggregation during the processing conditions based on a steric repulsion force between the wax coated nano-particles. Individual GNP-15 and MWCNT can thus be uniformly dispersed within the polymer matrix in forming conductive networks. In addition, the presence of the low molecular weight paraffin wax, which has a lower viscosity than the HDPE matrix, may also facilitate the movement of nano-particles in forming the percolated network [14].

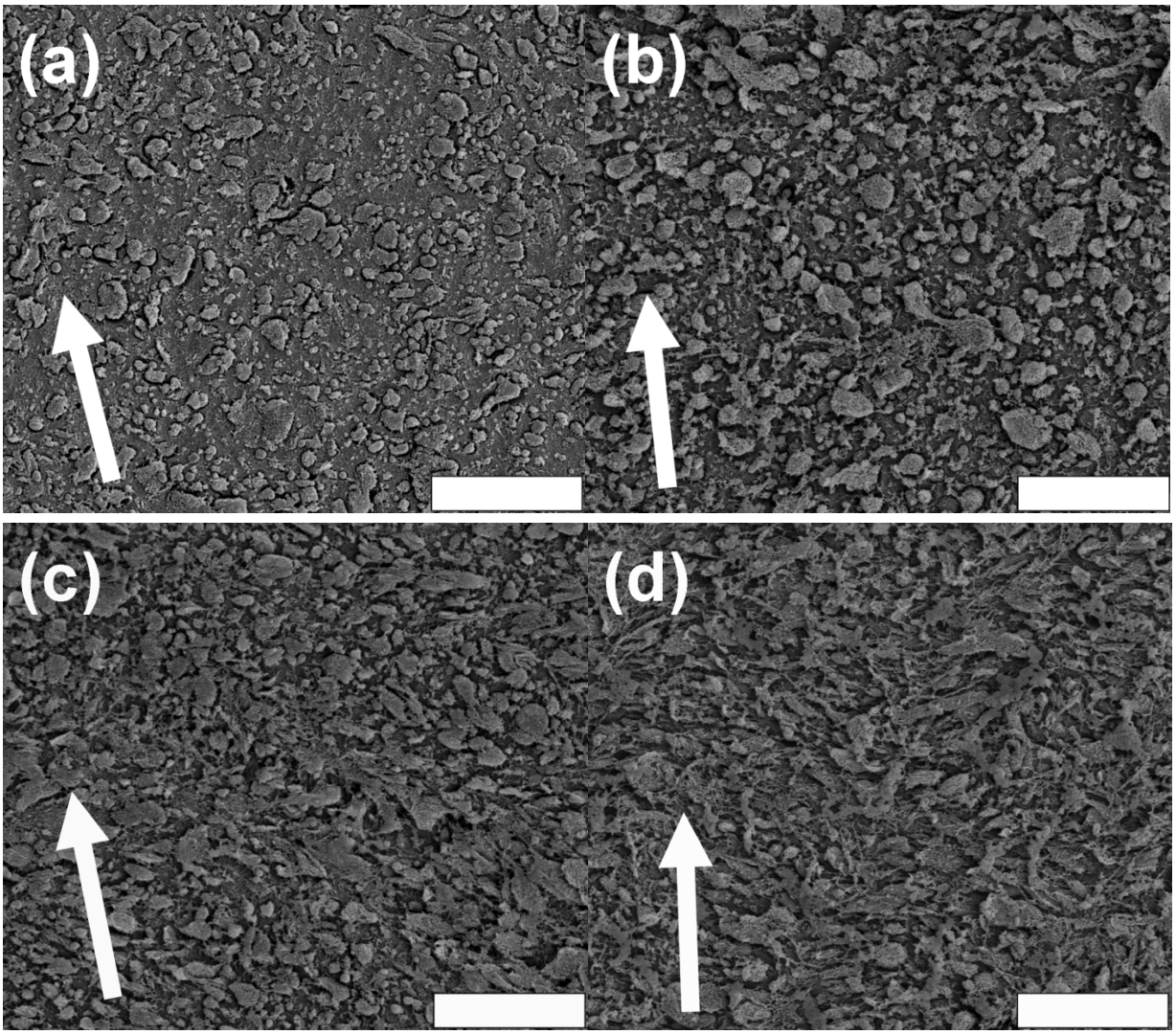

Figure 5.10. Morphology of various 5 vol% HDPE/MWCNT nanocomposites at a lower magnification: (a) sonicated HDPE/MWCNT (scale bar 10 μm); (b) HDPE/WaxMWCNT (20:80wt%) (scale bar 10 μm); (c) HDPE/WaxMWCNT (30:70wt%) (scale bar 10 μm); (d) HDPE/WaxMWCNT (40:60wt%) (scale bar 10 μm). The arrow on the left bottom indicates the material flow direction during injection molding

5.4.3 Mechanical Properties of HDPE/WaxGNP-15 and HDPE/WaxMWCNT Nanocomposites

From the results presented in the previous section, the advantages of using the wax coating method to lower the percolation threshold and to increase the electrical conductivity of

HDPE/GNP-15 and HDPE/MWCNT nanocomposites are clearly illustrated. However, the presence of the low molecular weight paraffin wax may be detrimental to the mechanical properties of HDPE nanocomposites.

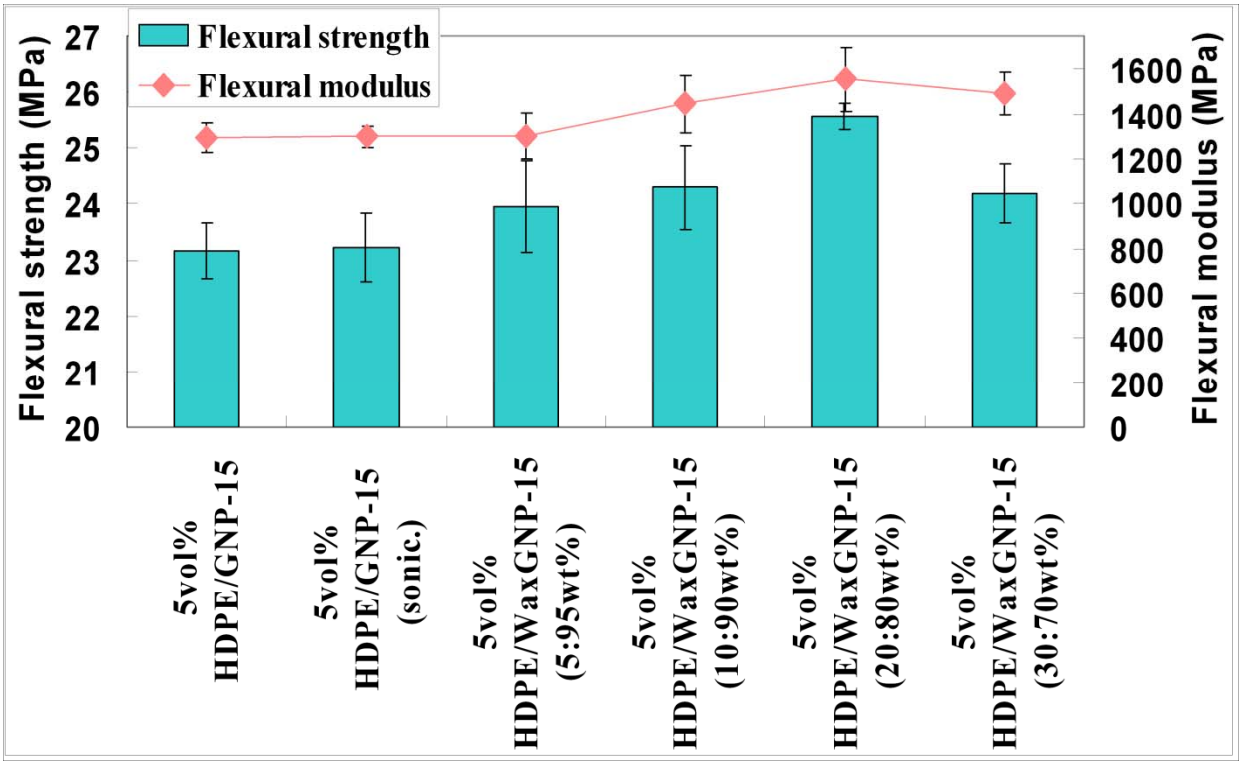

Figure 5.11. Flexural strength and flexural modulus of various HDPE/WaxGNP-15 nanocomposites at 5 vol% GNP loading

Figure 5.11 illustrates the flexural strength and the flexural modulus of various HDPE/WaxGNP-15 nanocomposites at 5 vol% GNP loading. It is found that both the flexural strength and the flexural modulus are first improved as the wax content increases then the trend reverses. The largest enhancement in the flexural properties occurs at the 5 vol% HDPE/WaxGNP-15 (20:80wt%) nanocomposite, of which the flexural strength is increased by 12% and the flexural modulus is improved by 20%. Higher flexural strength and modulus is

another indication of an improved GNP dispersion in HDPE [15].

To explain the reduced mechanical property in the 5 vol% HDPE/WaxGNP-15 (30:70wt%) nanocomposite, the mechanical properties of HDPE/Wax polymer blends were investigated. Figure 5.12 presents the flexural strength and the flexural modulus of HDPE/Wax polymer blends with various wax contents. The wax loading of 0.62 wt%, 1.35 wt%, 2.91 wt%, 5.0 wt%, 6.96 wt% and 10.46 wt% in the HDPE/Wax polymer blends corresponds to the wax content in the samples of 5 vol% HDPE/WaxGNP-15 (5:95wt%), 5 vol% HDPE/WaxGNP-15 (10:90wt%), 5 vol% HDPE/WaxGNP-15 (20:80wt%) and 5 vol% HDPE/WaxMWCNT (20:80wt%), 5 vol% HDPE/WaxGNP-15 (30:70wt%) and 5 vol% HDPE/WaxMWCNT (30:70wt%), 5 vol% HDPE/ WaxMWCNT (40:60wt%), and 5 vol% HDPE/ WaxMWCNT (50:50wt%) respectively.

As seen from the Figure 5.12, the flexural properties of HDPE are not affected by the addition of paraffin wax until the loading of wax reaches 5 wt%. This is due to the compatibility between HDPE and wax as confirmed in the literature [16]. In this case, no phase separation occurs between HDPE and wax which is otherwise the major reason for the reduction of mechanical properties in the polymer blends with two immiscible components [17]. However, after the wax concentration is higher than 5 wt%, both the flexural strength and the flexural modulus are noticeably reduced which is owing to a considerably increased fraction of low molecular weight polyethylene in the HDPE/Wax polymer blends.

Based on this result, we can conclude that there are two factors controlling the mechanical properties of HDPE/WaxGNP-15 nanocomposites. Improved GNP dispersion tends to increase the mechanical properties while the addition of paraffin wax, if it exceeds a certain amount, will

impair the mechanical strength. For the HDPE/WaxGNP-15 samples with the wax to GNP ratios from 5:95 wt% to 20:80 wt%, the wax contents in these nanocomposites are all below 5 wt%. In this case, the enhanced flexural properties are mainly due to an improved GNP dispersion in these samples. While for the HDPE/WaxGNP-15 (30:70wt%) sample, of which the wax content is 5 wt%, the reduction in the flexural strength and modulus is largely caused by the addition of too much low molecular weight paraffin wax.

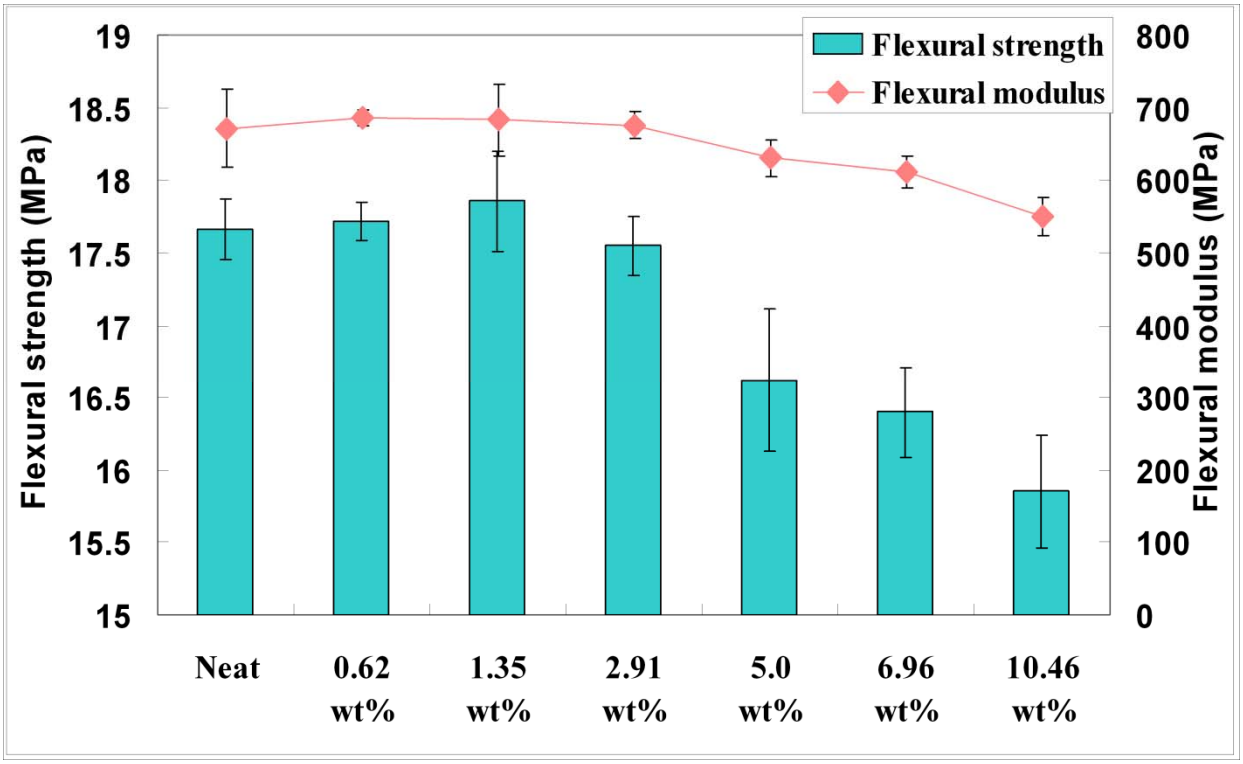

Figure 5.12. Flexural strength and flexural modulus of HDPE/Wax polymer blends

Figure 5.13 displays the flexural strength and the flexural modulus of HDPE/WaxMWCNT nanocomposites at 5 vol% MWCNT loading. It is noted that the flexural strength of these nanocomposites is not influenced much by the addition of wax and there is only a slight increase in the flexural modulus. The same reasoning can be applied to explain this phenomenon. Greatly

improved MWCNT dispersion in HDPE is likely to boost the mechanical strength as verified by the morphology. However, since the wax content in most of the HDPE/WaxMWCNT samples is higher than 5 wt%, too much wax added in the composites compromises the positive effect of the enhanced MWCNT dispersion on the mechanical properties. So the flexural strength appears to be unchanged. Although the mechanical properties of HDPE/WaxMWCNT nanocomposites are not benefited much from the wax coating method, huge improvement in the electrical conductivity still shows the advantage of this technique in enhancing the dispersion of MWCNT in HDPE.

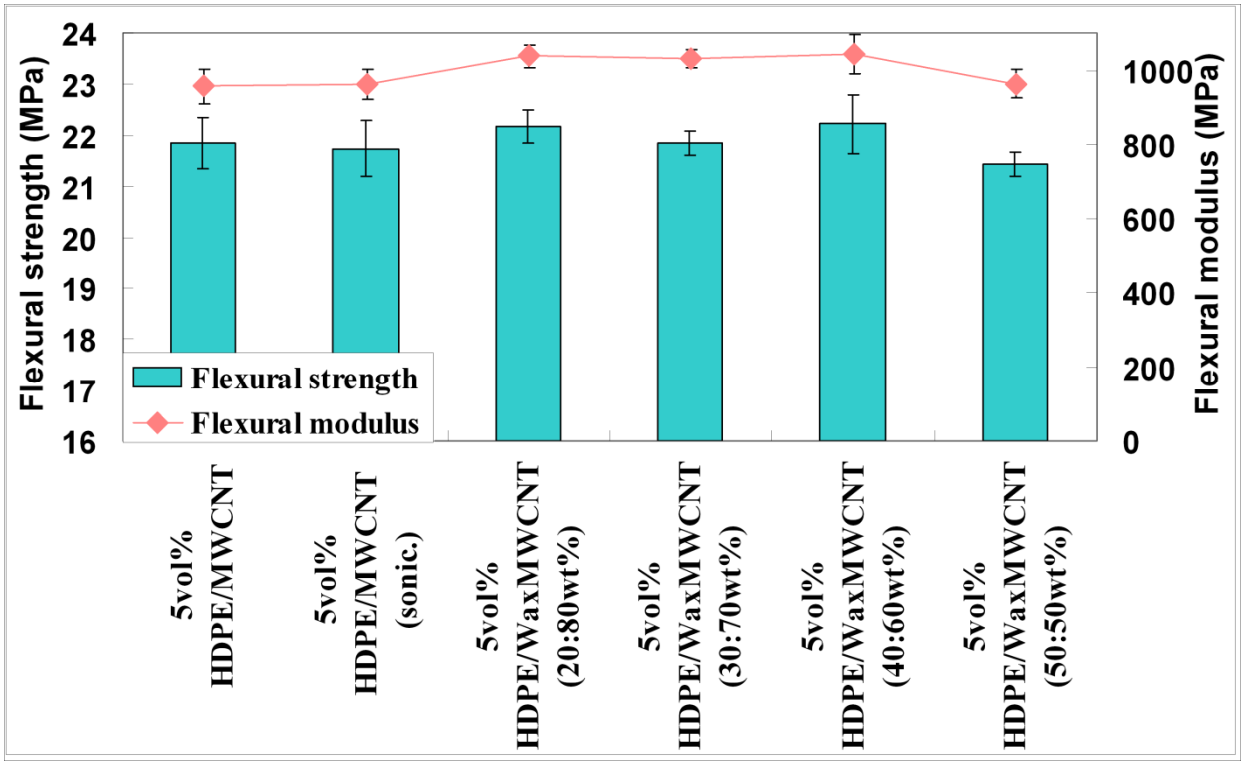

Figure 5.13. Flexural strength and flexural modulus of various HDPE/WaxMWCNT nanocomposites at 5 vol% MWCNT loading

5.4.4 Thermal Conductivity of HDPE/WaxGNP-15 and HDPE/WaxMWCNT Nanocomposites

Based on the discussion above, the wax coating method is capable of enhancing electrical and mechanical properties of HDPE/WaxGNP-15 and HDPE/WaxMWCNT nanocomposites due to a significantly improved GNP and MWCNT dispersion in HDPE. Improved nano-filler distribution is also believed to have a great effect on the thermal conductivity of the resulting nanocomposites [18]. In this case, in-plane and through-plane thermal conductivity of various HDPE/WaxGNP-15 and HDPE/WaxMWCNT nanocomposites at 5 vol% GNP or MWCNT loading is presented in the Figure 5.14 and Figure 5.15 respectively for the demonstration.

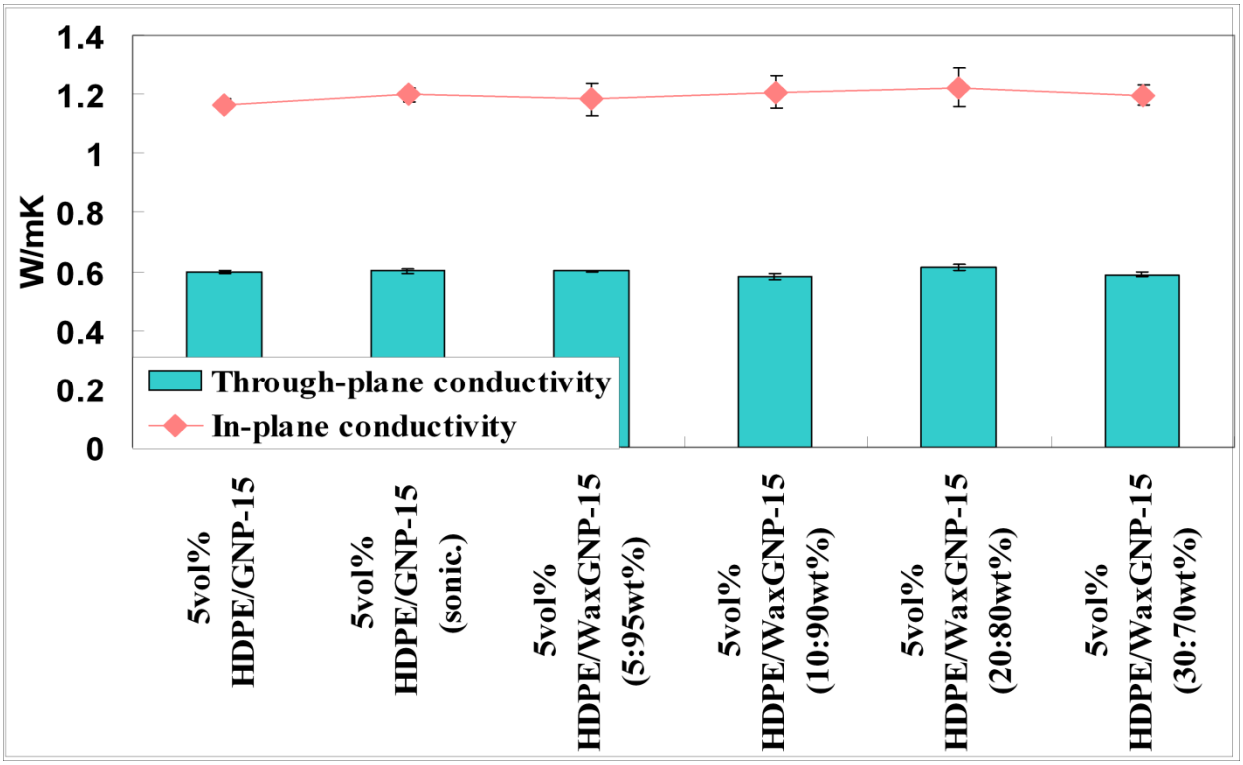

Figure 5.14. In-plane and through-plane thermal conductivity of various HDPE/WaxGNP-15 nanocomposites at 5 vol% GNP loading

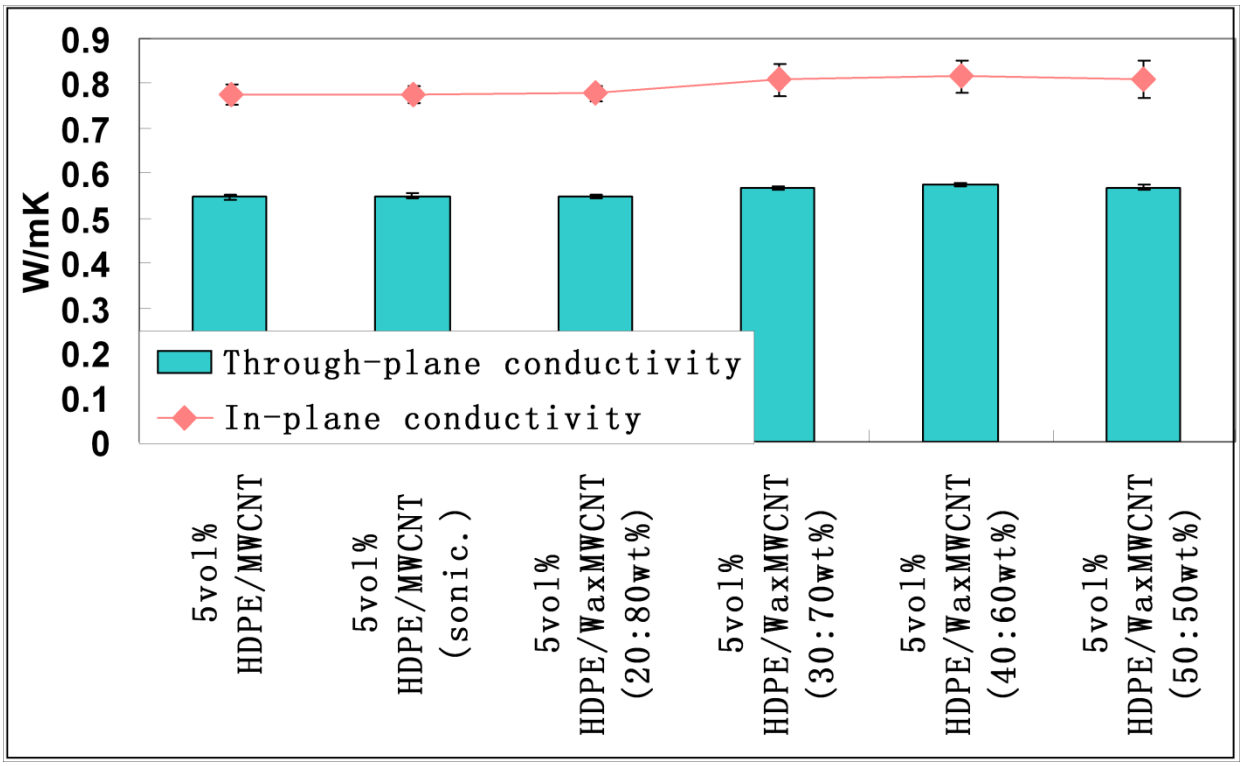

Figure 5.15. In-plane and through-plane thermal conductivity of various HDPE/WaxMWCNT nanocomposites at 5 vol% MWCNT loading

From these two figures, it is concluded that the wax coating method does not improve the thermal conductivity of the resulting HDPE/WaxGNP-15 and HDPE/WaxMWCNT nanocomposites, which implies that the thermal conductivity is not as sensitive to the improved nano-filler dispersion as that to the electrical and mechanical properties. Based on the discussion in the previous chapter, the thermal conductivity is mainly determined by the phonon scattering at the interface between the nano-fillers and the polymer matrix [19]. In this case, there is a compromise effect for the enhanced nano-filler dispersion on the thermal conductivity. On one hand, enhanced dispersion improves the effectiveness of nano-fillers as thermal conductors. On the other hand, it also increases the interfacial area between the nano-fillers and the polymer matrix, which leads to more phonon scattering at the interface. The resulting thermal

conductivity is thus appeared to be unaffected by the wax coating method. In order to improve the thermal conductivity, how to increase the interfacial bonding between the nano-fillers and the polymer matrix seems to be a more effective method, which will facilitate the phonon transport at the interface, thereby reducing the interfacial thermal resistance [20].

5.5 Conclusions

This study has investigated the effect of using the wax coating method in improving the electrical conductivity of HDPE nanocomposites filled with two cutting-edge nano-particles: GNP and MWCNT. It is shown that the high percolation threshold in the melt-extruded HDPE/GNP-15 and HDPE/MWCNT nanocomposites could be substantially reduced through the addition of a proper amount of wax coating on the surface of these nano-particles, which significantly improves their dispersion in HDPE and subsequently facilitates the formation of percolated networks throughout the polymer matrix. The mechanism of wax coating in improving the dispersion of nano-fillers in HDPE is to prevent their re-aggregation during processing conditions based on a steric repulsion force between the wax coated nano-particles. Meanwhile, the flexural properties of the resulting HDPE/GNP-15 and HDPE/MWCNT nanocomposites were found to be considerably increased or at least maintained regardless of the presence of low molecular weight paraffin wax. These improvements are the results of an improved GNP and MWCNT dispersion in HDPE and also from the total miscibility between HDPE and wax. However, the thermal conductivity of the resulting nanocomposite was unaffected by this wax coating method, which is due to a different phonon transportation mechanism in nanocomposites.

REFERENCES

REFERENCES

[1] Jiang X, Drzal LT. Reduction in percolation threshold of injection molded High Density Polyethylene/Exfoliated Graphene Nanoplatelets composites by Solid State Ball Milling and Solid State Shear Pulverization. Journal of Applied Polymer Science 2012;124(1):525-35.

[2] Kalaitzidou K, Fukushima H, Drzal LT. A new compounding method for exfoliated graphite-polypropylene nanocomposites with enhanced flexural properties and lower percolation threshold. Composites Science and Technology. 2007;67(10):2045-51.

[3] Du XS, Xiao M, Meng YZ. Synthesis and characterization of polyaniline/graphite conducting nanocomposites. Journal of Polymer Science Part B: Polymer Physics. 2004;42(10):1972-8.

[4] Pan Y-X, Yu Z-Z, Ou Y-C, Hu G-H. A new process of fabricating electrically conducting nylon 6/graphite nanocomposites via intercalation polymerization. Journal of Polymer Science Part B: Polymer Physics. 2000;38(12):1626-33.

[5] Xiao P, Xiao M, Gong K. Preparation of exfoliated graphite/polystyrene composite by polymerization-filling technique. Polymer 2001;42:4813-6.

[6] Miller SG, Bauer JL, Maryanski MJ, Heimann PJ, Barlow JP, Gosau J-M, et al. Characterization of epoxy functionalized graphite nanoparticles and the physical properties of epoxy matrix nanocomposites. Composites Science and Technology. 2010;70(7):1120-5.

[7] Cao Y, Feng J, Wu P. Alkyl-functionalized graphene nanosheets with improved lipophilicity. Carbon. 2010;48(5):1683-5.

[8] RamanathanT, Abdala AA, StankovichS, Dikin DA, Herrera Alonso M, Piner RD, et al. Functionalized graphene sheets for polymer nanocomposites. Nat Nano. 2008;3(6):327-31.

[9] GNP is an exfoliated graphene nanoplatelet material obtained from XG Sciences, Inc., East Lansing, MI (www.xgsciences.com).

[10] Jeon K, Lumata L, Tokumoto T, Steven E, Brooks J, Alamo RG. Low electrical conductivity threshold and crystalline morphology of single-walled carbon nanotubes /high density polyethylene nanocomposites characterized by SEM, Raman spectroscopy and AFM. Polymer.

2007;48(16):4751-64.

[11] Gorrasi G, Sarno M, Di Bartolomeo A, Sannino D, Ciambelli P, Vittoria V. Incorporation of carbon nanotubes into polyethylene by high energy ball milling: Morphology and physical properties. Journal of Polymer Science Part B: Polymer Physics. 2007;45(5):597-606.

[12] Du JH, Bai J, Cheng HM. The present status and key problems of carbon nanotube based polymer composites. Express Polym Lett. 2007;1(5):253-73.

[13] Bang JH, Suslick KS. Applications of Ultrasound to the Synthesis of Nanostructured Materials. Advanced Materials. 2010;22(10):1039-59.

[14] Kim S, Drzal L. Comparison of Exfoliated Graphite Nanoplatelets (xGnP) and CNTs for Reinforcement of EVA Nanocomposites Fabricated by Solution Compounding Method and Three Screw Rotating Systems. Journal of Adhesion Science and Technology. 2009;23:1623-38.

[15] Kashiwagi T, Fagan J, Douglas JF, Yamamoto K, Heckert AN, Leigh SD, et al. Relationship between dispersion metric and properties of PMMA/SWNT nanocomposites. Polymer. 2007;48(16):4855-66.

[16] Hato MJ, Luyt AS. Thermal fractionation and properties of different polyethylene/wax blends. Journal of Applied Polymer Science. 2007;104(4):2225-36.

[17] Gregor R, ccaron, Vojko M, Ivan S. Compatibilization of polypropylene/polystyrene blends with poly(styrene--butadiene--styrene) block copolymer. Applied Polymer Science. 1998;69(13):2625-39.

[18] Wang S, Liang R, Wang B, Zhang C. Dispersion and thermal conductivity of carbon nanotube composites. Carbon. 2009;47(1):53-7.

[19] Gojny FH, Wichmann MHG, Fiedler B, Kinloch IA, Bauhofer W, Windle AH, et al. Evaluation and identification of electrical and thermal conduction mechanisms in carbon nanotube/epoxy composites. Polymer. 2006;47(6):2036-45.

[20] Yu W, Choi SUS. The Role of Interfacial Layers in the Enhanced Thermal Conductivity of Nanofluids: A Renovated Maxwell Model. Journal of Nanoparticle Research. 2003;5(1):167-71.

CHAPTER 6 SYNTHESIS OF BIPOLAR PLATES FOR FUEL CELLS BASED ON EXFOLIATED GRAPHENE NANOPLATELETS FILLED POLYMERIC NANOCOMPOSITES

6.1 Abstract

The objective of this chapter is to investigate the potential of using exfoliated graphene nanoplatelets (GNP) as the conductive filler to construct highly conductive polymeric nanocomposites to substitute for conventional metallic and graphite bipolar plates in the polymer electrolyte membrane (PEM) fuel cells. High density polyethylene (HDPE) and polyphenylene sulfide (PPS) were selected as the polymer matrix and solid state ball milling (SSBM) followed by compression molding was applied to fabricate the GNP nanocomposites. Results showed that HDPE/GNP and PPS/GNP nanocomposites made by this processing method exhibit excellent flexural properties and low gas permeability with GNP loadings up to 60wt%, which successfully meet the DOE requirements for bipolar plates. However, it was found that using GNP alone as a single conductive filler is insufficient to achieve the required electrical conductivity (>100 S/cm). Combining GNP with a minor second conductive filler such as carbon black (CB) and carbon nano-tubes (CNT) could substantially enhance the electrical conductivity of the resulting nanocomposites. At the same time, the processing time of SSBM was considered as a crucial parameter in optimizing the various properties of the final nanocomposites. It is believed that the bipolar plates made from HDPE/GNP and PPS/GNP nanocomposites will allow lighter weight of PEM fuel cells with enhanced performance which are particularly suited for automotive applications.

6.2 Introduction

The importance of bipolar plates in the fuel cells has been discussed in the introduction chapter. In short, bipolar plates perform these major functions during fuel cell operation, including connecting and separating the individual fuel cells in series to form a fuel cell stack with required voltage, aiding uniform distribution of fuel gas and oxygen in fuel cells, conducting current from one cell to another, facilitating water management within the cells, and supporting thin membranes and electrodes from the clamping forces [1]. The technical targets defined by the United States Department of Energy (DOE) require bipolar plates must exhibit excellent electrical conductivity (>100 S/cm), good thermal conductivity (>10 W/mK), adequate mechanical strength (flexural strength>25 MPa), good chemical corrosion resistance (<1 μAcm^{-2}), and low gas permeability (<$2x10^{-6}$ $cm^3cm^{-2}s^{-1}$) [2-4]. Moreover, good processability and low manufacturing cost are highly desirable if bipolar plates are to be widely used in the automotive industry [5, 6]. Metal and graphite are the materials conventionally used for fabricating bipolar plates due to their excellent electrical and thermal properties. But the drawbacks such as low chemical corrosion resistance or poor mechanical properties confine their real applications in industry [6-9]. Polymeric composites filled with conductive fillers have now gained more and more research attention which show the advantages such as lower cost, higher processability, and lighter in weight over the metallic and graphite bipolar plates [10-12]. The key research concern associated with the polymeric bipolar plates now is to find one or more appropriate conductive fillers that could implement excellent electrical and thermal properties at

relatively low filler loadings to ensure a good mechanical strength [13].

In this chapter, exfoliated graphene nanoplatelets, GNP, was chosen as the major conductive filler in fabricating polymeric nanocomposites for bipolar plates due to its excellent mechanical and structural properties, superior electrical and thermal conductivity, and extremely low gas permeability as shown in the research work in the Dr. Drzal group [14-17]. CB and CNT were considered as minor conductive fillers to attain a positive synergistic effect with GNP. HDPE was selected as the polymer matrix for low temperature applications due to its good physical and mechanical properties, excellent chemical stability, low gas barrier property, easy processability and low cost [18]. And PPS was chosen for high temperature usage on the account of its superior chemical corrosion resistance, good mechanical properties, excellent dimensional stability, and high-temperature resistance [19]. And the compounding method to fabricate HDPE/GNP and PPS/GNP nanocomposites was solid state ball milling (SSBM) followed by compression molding. The reason of selecting this compounding method is because of its capability of achieving a high electrical conductivity in GNP nanocomposites as described in a previous study [20]. In the SSBM process, it is found that polymer particles are uniformly coated by GNP platelets which facilitate the formation of conductive pathways during the following injection molding or compression molding steps. The electrical conductivity of the resulting nanocomposites is thus excellent. It is believed that GNP based nanocomposites made from this compounding technique may offer the potential to satisfy the DOE targets for electrical and thermal conductivity while maintaining the GNP content at relatively low levels (≤60 wt%) to ensure a good mechanical strength.

6.3 Experimental

6.3.1 Materials

In this research, HDPE pellets with the trade name Marlex® HXM 50100 (Density 0.95 g/cm^3) were obtained from Chevron Phillips Chemical Company. PPS powder with the trade name Fortron® 0205 (Powder size: 300-400 μm, Density: 1.35 g/cm^3) was obtained from Ticona. GNP nanoplatelets with the diameter around 25 μm (GNP-25) and thickness around 5-10 nm were from XG Science, Inc [21]. Multi-walled carbon nano-tubes, MWCNT, were obtained from Bayer Material Science Company with the diameter of individual MWCNT being around 15 nm and the length between 1 to 10 μm. 'High Structure' carbon black (CB, KETJENBLACK EC-600 JD, aggregate size: 30-100 nm), was from AkzoNobel Polymer Chemicals LLC.

6.3.2 Processing Method: Solid State Ball Milling (SSBM) and Compression Molding

The details of the SSBM process have been described in the chapter 4. In this chapter, HDPE powder (~ 100 μm diameter) was obtained from the cryogenic milling of as-received HDPE pellets. And the PPS powder (300-400 μm) was the as-received material. Six weight ratios between the polymers and GNP-25 were selected. They are 10 wt%, 20 wt%, 30 wt%, 40 wt%, 50 wt%, and 60 wt%. The SSBM time was first kept at 200 minutes and then the time was adjusted accordingly to optimize the various properties of GNP nanocomposites which will be discussed later. Based on a previous study, SSBM could produce a polymer and GNP powder mixture with polymer particles uniformly coated by GNP platelets. The size of polymer particles

and GNP platelets was significantly reduced after SSBM. It was found that the size of GNP-25 was down to less than 5 μm after 200 minutes ball milling. Then the powder mixture was compression molded into flexural coupons for mechanical properties and electrical conductivity test, round disks for thermal conductivity analysis, and thin films (thickness: ~100 μm) for gas/oxygen permeability measurement. The molding temperature for HDPE/GNP nanocomposites was kept at 200 °C. For PPS/GNP nanocomposites, a lower compression molding temperature of 300 °C was selected to fabricate PPS nanocomposites with less than 40 wt% filler loading for a better processability and a higher temperature of 325 °C was chosen for the nanocomposites containing 40 wt% or higher conductive filler to achieve a better PPS wetting and infiltration. The molding pressure was kept at 25 MPa for all the GNP nanocomposites.

6.3.3 Experimental Characterization

A UTS SFM-20 machine (United Calibration Corp.) was used to measure the flexural properties. Flexural coupons were tested under 3-point bending mode at a flexural rate of 0.05 in/min by following the ASTM D790 standard.

Electrical conductivity measurements were taken on the flexural coupons by a four point method. The set-up of the four-point measurement is schematically shown in the Figure 6.1. For this technique, a current source forces a constant current through the sample bar, which is measured by a separate ammeter. And a voltmeter simultaneously measures the voltage produced across the inner part of the flexural coupon.

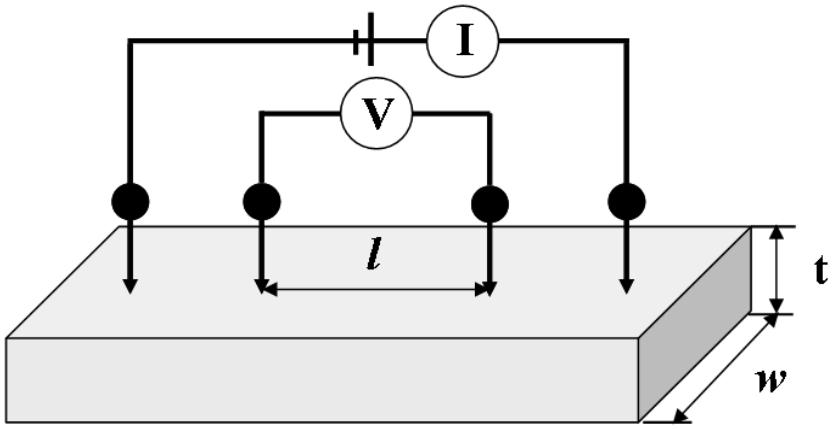

Figure 6.1. A four-point technique for measuring the electrical conductivity of GNP nanocomposites

The four-point electrical conductivity is then calculated as:

$$\rho = \frac{Vwt}{Il}$$

$$S = 1/\rho$$

Equation 6.1

Where: ρ = Electrical resistivity of the sample (Ω*cm)

S = Electrical conductivity of the sample (S/cm)

V = Voltage measured by the voltmeter (Volts)

I = Current measured by the ammeter (Amperes)

w = The width of the sample (cm)

t = The thickness of the sample (cm)

l = The distance between the two points where the voltmeter measures the voltage (cm)

Thermal conductivity (W/mK) (both in-plane and through-plane) of GNP nanocomposites (round

disks) was measured by a LFA Nanoflash 447 Light flash system as described in the previous chapters.

The gas/O_2 permeability of GNP nanocomposite films was measured based on ASTM D3985 standard by using a MOCON® Ox-Tran 2/20 instrument at room temperature. The testing pressure was set as 0.21 MPa and the thickness of the composite films was kept at 0.1 mm.

The dispersion of GNP in the polymer matrix was observed with an environmental scanning electron microscopy (ESEM Carl Zeiss EVO) at an accelerating voltage of 15 kV. The preparation of SEM samples in this study included epoxy mounting, grinding, polishing and etching steps. First, nanocomposite specimens were mounted with epoxy in cylindrical sample holders to maintain a flat surface over the entire grinding and polishing area. After the epoxy was fully cured, samples were carefully ground and polished. O_2 plasma etching (35 minutes, 375 W) was then applied at the last step to remove the polymer in top surface allowing the GNP platelets to stand out under SEM observation.

6.4 Results and Discussion

6.4.1 Various Properties of HDPE/GNP Nanocomposites Made by SSBM and Compression Molding

The flexural properties of HDPE/GNP nanocomposites fabricated by SSBM and compression molding are presented in the Figure 6.2. From this figure, it is noted that both the flexural strength and the flexural modulus exhibit a monotonic increase with the increasing GNP loading up to 50 wt%. At 20 wt% GNP loading, the flexural strength of the nanocomposite is around 28

MPa, which has exceeded the DOE target (>25 MPa) for bipolar plates. The highest flexural strength (~ 50 MPa) occurs at the sample of 50 wt% GNP loading, which is almost twice as much as the DOE target. For the HDPE/GNP sample at 60 wt%, a decrease in flexural strength is observed, which indicates the insufficient amount of HDPE to wet all the GNP platelets. However, the flexural strength remains at a high value of 45 MPa.

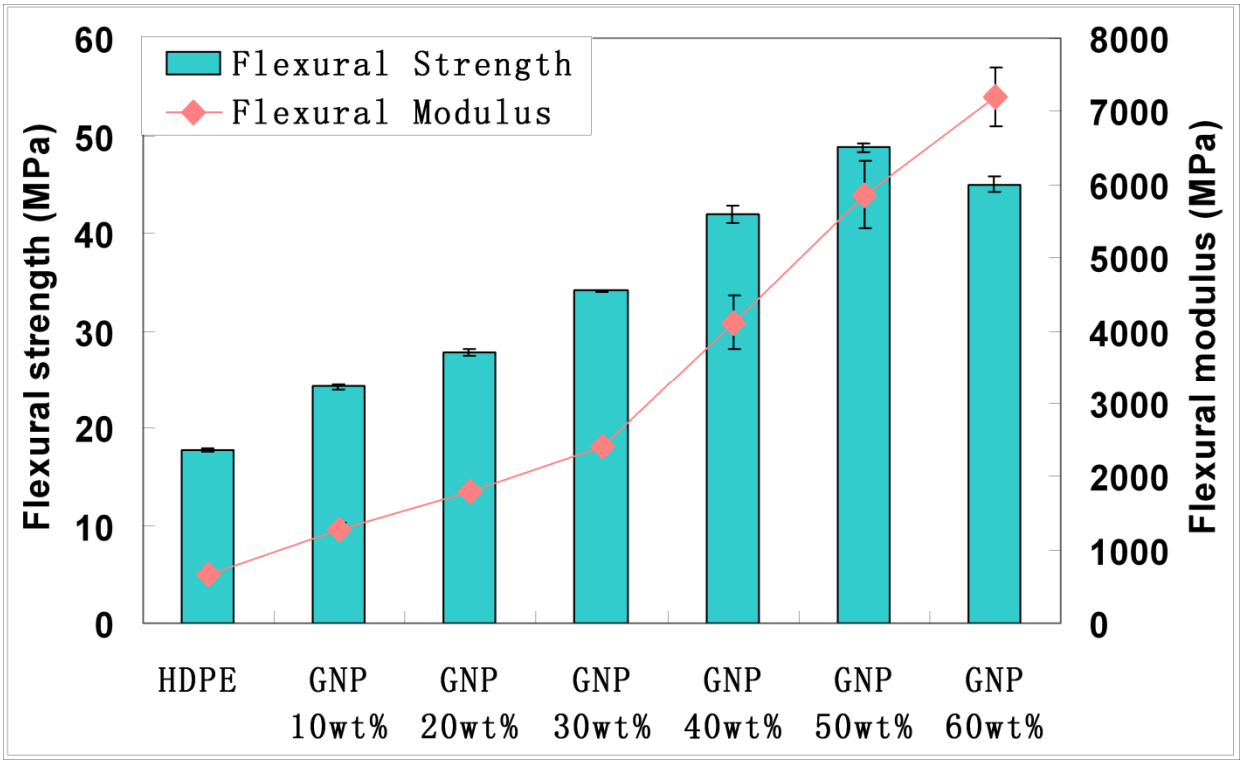

Figure 6.2. Flexural properties of HDPE/GNP nanocomposites made by SSBM and compression molding

The gas permeability of these nanocomposite films as a function of GNP loading is shown in the Figure 6.3. It is seen that the gas permeability keeps decreasing with the increasing GNP content, which is due to the excellent gas barrier properties of GNP platelets [17]. And if compared with the DOE target for the gas permeability, it is found that even the neat HDPE film could

successfully satisfy the requirement. And the permeability value of the HDPE/GNP nanocomposite with 60 wt% GNP content is around two orders of magnitude lower than the DOE target, which suggests that HDPE/GNP nanocomposites fabricated by the method of SSBM and compression mold can totally meet the permeability request for bipolar plates.

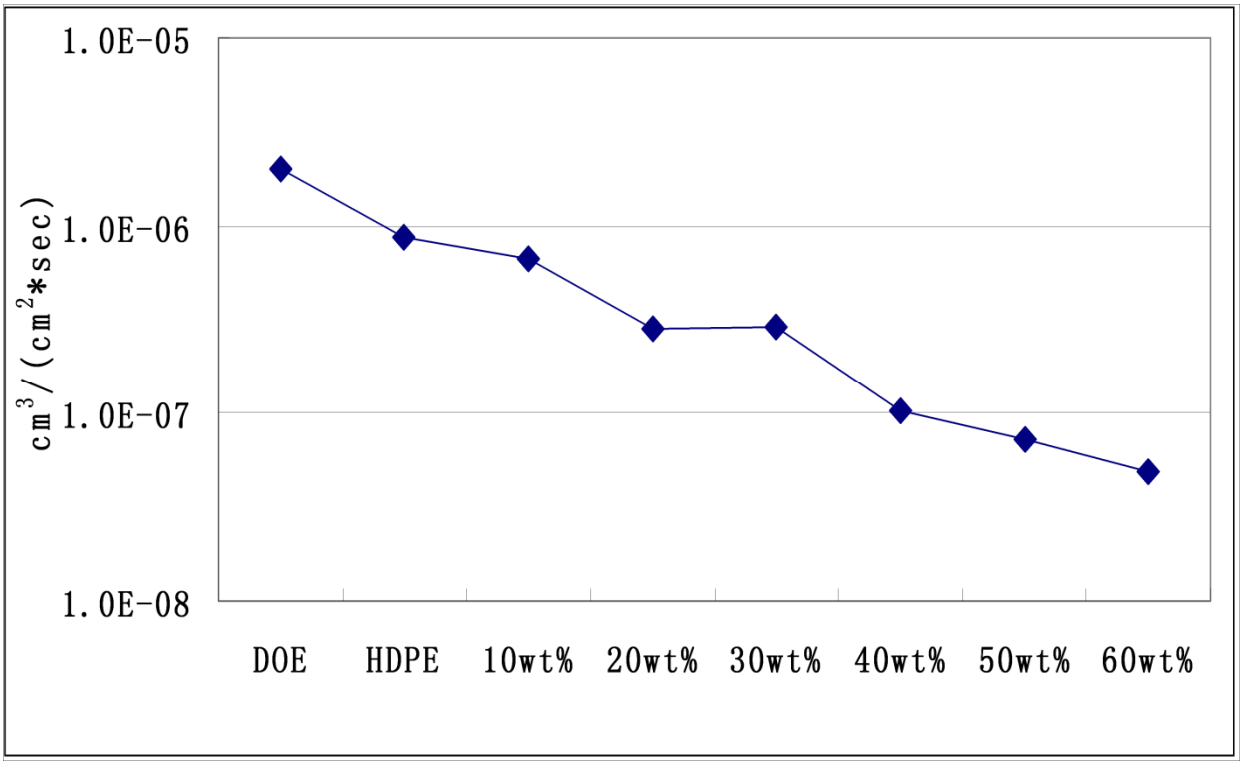

Figure 6.3. The gas permeability of HDPE/GNP nanocomposites made by SSBM and compression molding

Figure 6.4 then displays the in-plane electrical conductivity of these nanocomposites. Unfortunately, it is seen that the electrical conductivity does not meet the DOE target (>100 S/cm) even at the GNP loading of 60 wt%, which implies that using GNP alone as the single conductive filler may not be sufficient to provide enough electrical conductive paths for a desired electrical conductivity.

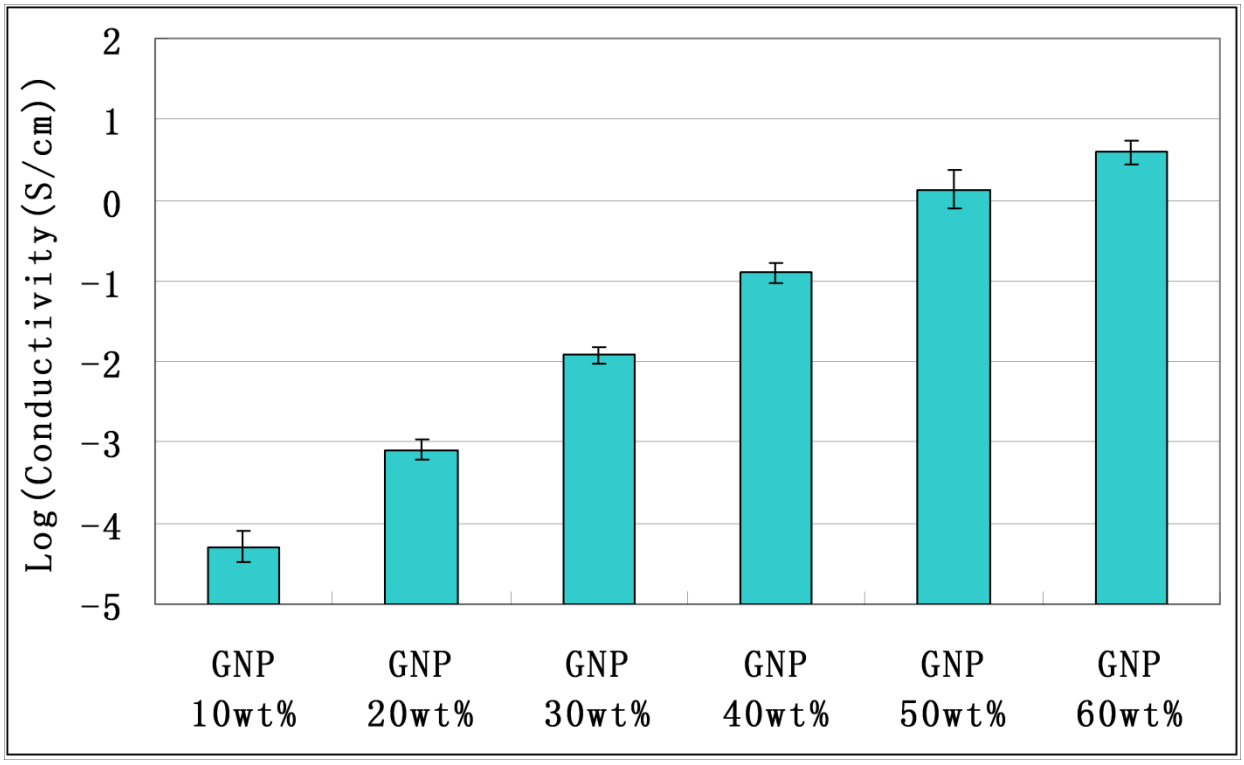

Figure 6.4. In-plane electrical conductivity of HDPE/GNP nanocomposites made by SSBM and compression molding

The morphology of these GNP nanocomposites (Figure 6.5) helps to explain why HDPE/GNP nanocomposites exhibit excellent mechanical and gas barrier properties but unsatisfactory electrical conductivity.

As seen from these ESEM images, the GNP density in the polymer matrix significantly increases with the increasing GNP content. At 60 wt% GNP loading, a good coverage of GNP platelets throughout the composite is observed. Increased GNP density greatly contributes to the enhanced mechanical, electrical and gas barrier properties of the resulting GNP nanocomposites. However, there are numerous micro-pores and micro-gaps between GNP nanoplatelets that are clearly detected in the sample at 60 wt% GNP loading. It is thus believed that the presence of these

micro-pores and micro-gaps dramatically inhibits the interconnections between GNP platelets and reduces the electron transportation pathways within the polymer matrix, which is the main reason for the unsatisfied electrical conductivity. Therefore, how to fill up these pores and voids will be considered in the next section to improve the electrical conductivity of the HDPE/GNP nanocomposites.

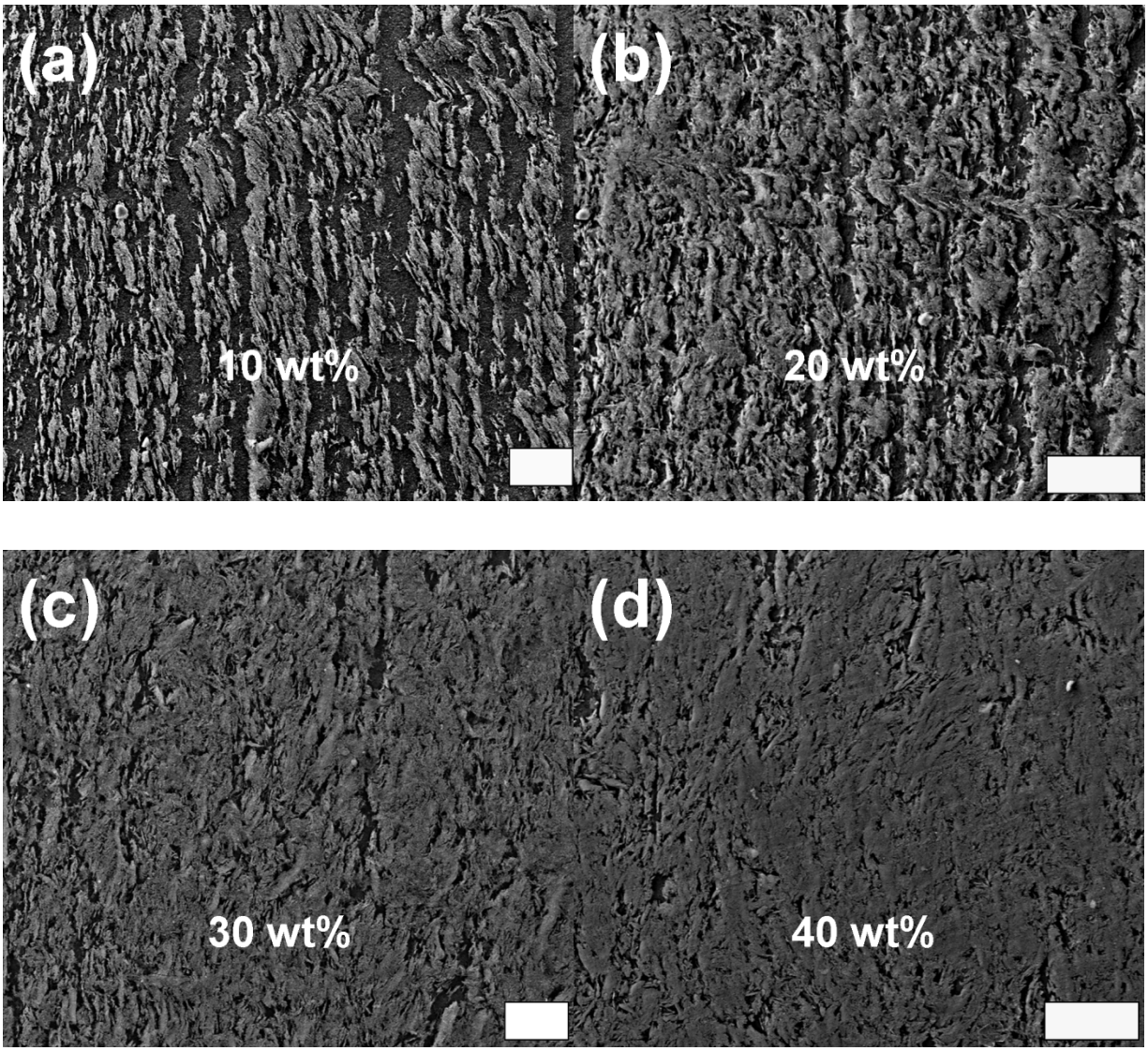

Figure 6.5. Morphology of HDPE/GNP nanocomposites made by SSBM and compression molding at various GNP loadings

Figure 6.5 (cont'd)

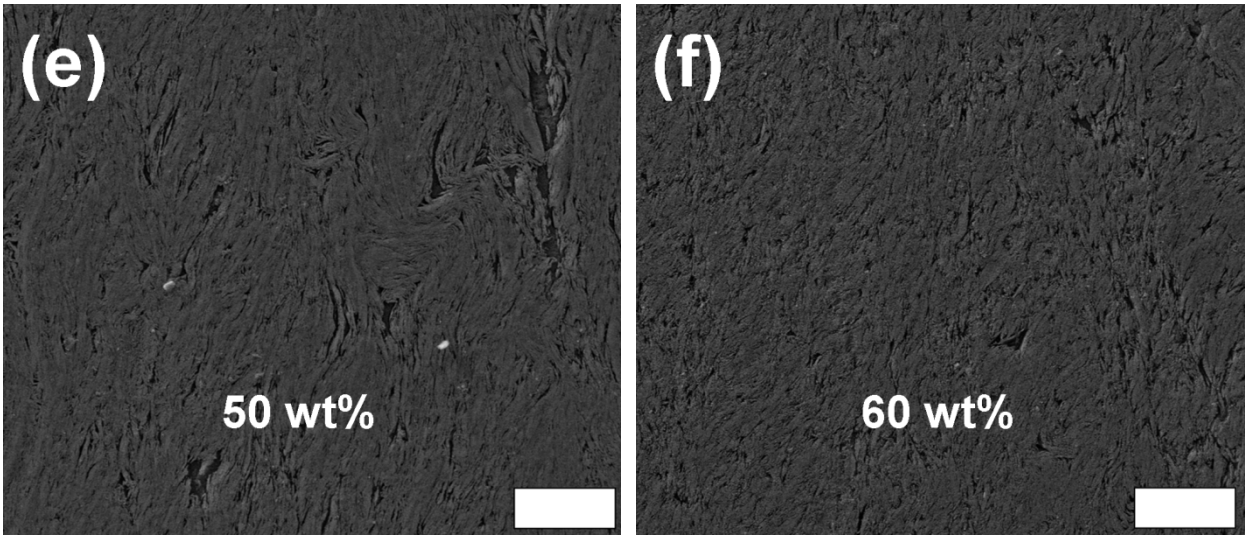

6.4.2 Synergistic Effect of Adding Second Conductive Filler

As discussed in the previous section, HDPE/GNP nanocomposites obtained from SSBM and compression molding exhibit good mechanical and gas barrier properties but inadequate electrical conductivity. In order to enhance the electrical conductivity to meet the DOE requirement for bipolar plates, combining GNP with a second conductive filler of different geometry was considered for a synergistic effect. In this study, MWCNT and CB were applied for this purpose. The hybridized HDPE/GNP nanocomposites with MWCNT or CB were also fabricated by the same SSBM and compression molding process as described in the experimental section. The total filler loading was kept at 60 wt% and the weight ratio between GNP and MWCNT or CB was changing from 50:10 to 30:30 wt%. The electrical and mechanical properties of these hybridized nanocomposites are shown in the Figure 6.6 and Figure 6.7 respectively.

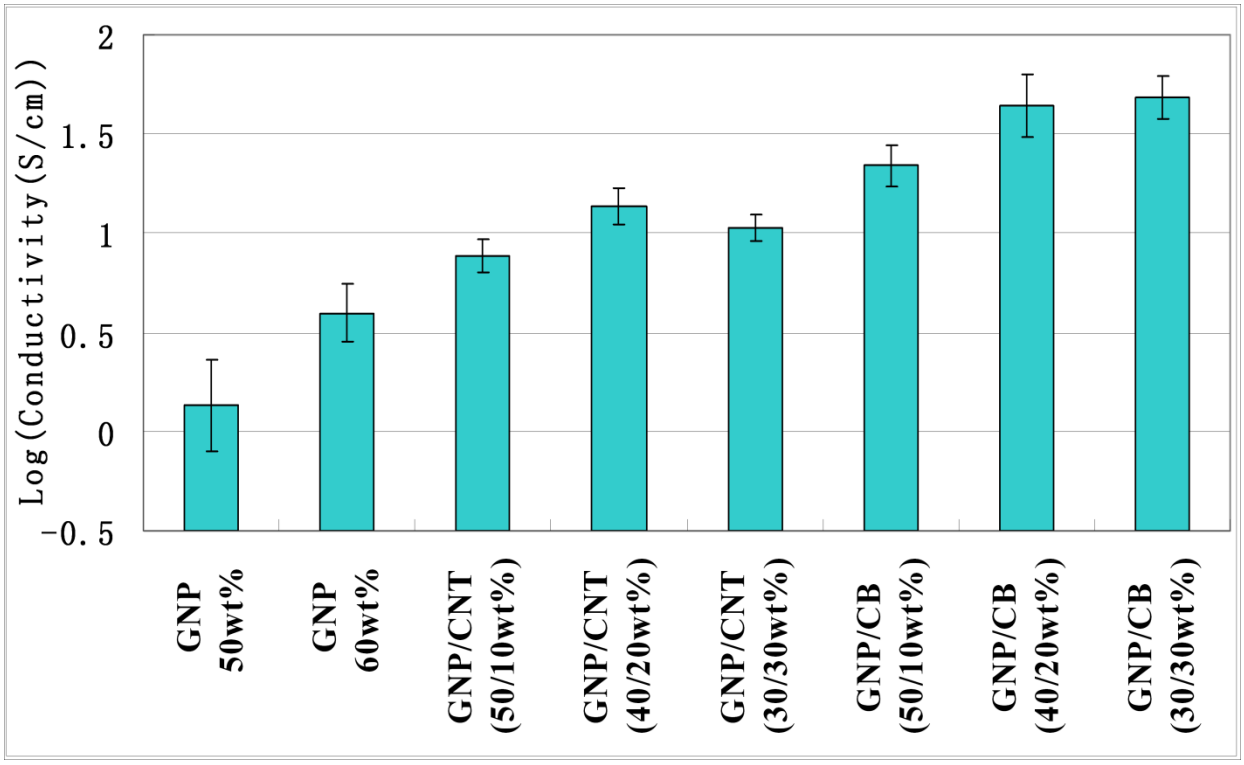

Figure 6.6. Electrical conductivity of hybridized HDPE/GNP nanocomposites with MWCNT and CB

From the results of the electrical conductivity measurement (Figure 6.6), it is seen that a sharp increase in electrical conductivity is observed when 10 wt% of GNP is substituted with CB. As the CB content further increases, the electrical conductivity goes to a maximum of 48 S/cm at around 40:20 (2:1) GNP to CB ratio, which is more than 5 times higher than that of the control sample (HDPE/GNP 60 wt%). Significantly increased electrical conductivity proves the positive synergistic effect between GNP platelets and CB particles in enhancing electron transportation throughout out the composites, which is believed due to the fact that the size of CB aggregates (~ 30 nm) is small, so they can fill up the micro-gaps and micro-pores between GNP platelets, providing additional electron pathways. And for the GNP/MWCNT hybridized nanocomposites,

an increased electrical conductivity is also detected and the highest electrical conductivity occurs at 40:20 (2:1) GNP to CNT ratio. However, the enhancement is much smaller than the GNP/CB hybridized samples. Based on a previous study, MWCNT tends to agglomerate in HDPE matrix without special surface treatment [22], which may explain the lower improvement in the electrical conductivity of GNP/MWCNT hybridized nanocomposites

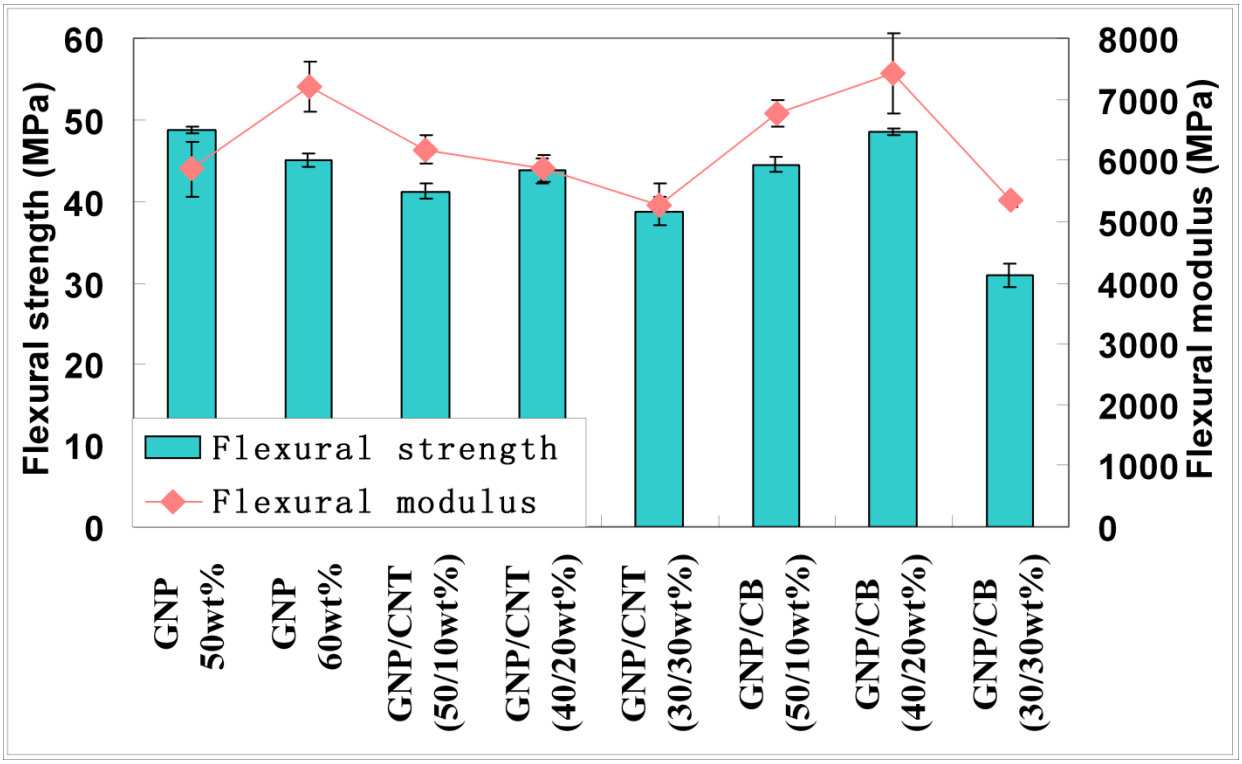

Figure 6.7. Flexural properties of hybridized HDPE/GNP nanocomposites with MWCNT and CB

And based on the results of flexural properties displayed in the Figure 6.7, it is concluded that combination of GNP platelets with MWCNT actually lowers the flexural strength and flexural modulus while GNP/CB hybridized samples exhibit even higher flexural properties than the control sample (HDPE/GNP 60 wt%) if the GNP/CB weight ratio is not lower than 2:1.

Therefore, it is concluded that GNP/CB hybridized nanocomposite offers better enhancements in

electrical and mechanical properties. For the sample with 40:20 (2:1) GNP to CB weight ratio, the electrical conductivity is increased by more than one order of magnitude and the flexural strength and modulus are enhanced by 8% and 4% respectively.

6.4.3 Synergistic Effect in the Combination of Small and Large GNP Platelets

From the results shown above, it is concluded that combination of GNP with CB could substantially increase the electrical conductivity of the resulting nanocomposites. However, the best conductivity (~ 48 S/cm) got so far still does not meet the DOE target. In this case, the GNP size effect was taken into consideration. Based on a previous research, it is known that smaller GNP platelets provide better enhancements in mechanical properties while larger ones contribute to a lower percolation threshold or a higher electrical conductivity [23]. Combination of smaller GNP platelets with larger ones was then investigated for a positive synergistic effect. Importantly, the size of GNP platelets can be easily controlled by the SSBM time. Take the composition of HDPE/CB/GNP(s)/GNP(l) (40:20:20:20wt%) for example, GNP (s) stands for the small GNP particles which are SSBM processed with HDPE and CB for a total of 200 minutes. The final diameter of this GNP is less than 5 μm as described in the experimental section. GNP (l) represents larger GNP platelets which are SSBM processed only for 30 minutes. Their final size is maintained at around 15-20 μm. Particularly, this portion of GNP is added when the mixture of HDPE, CB and GNP (s) is ball milled for 170 minutes.

The synergistic effect of combining small GNP platelets with larger ones on the electrical, thermal, and mechanical properties is shown in the Figure 6.8, Figure 6.9, and Figure 6.10

respectively.

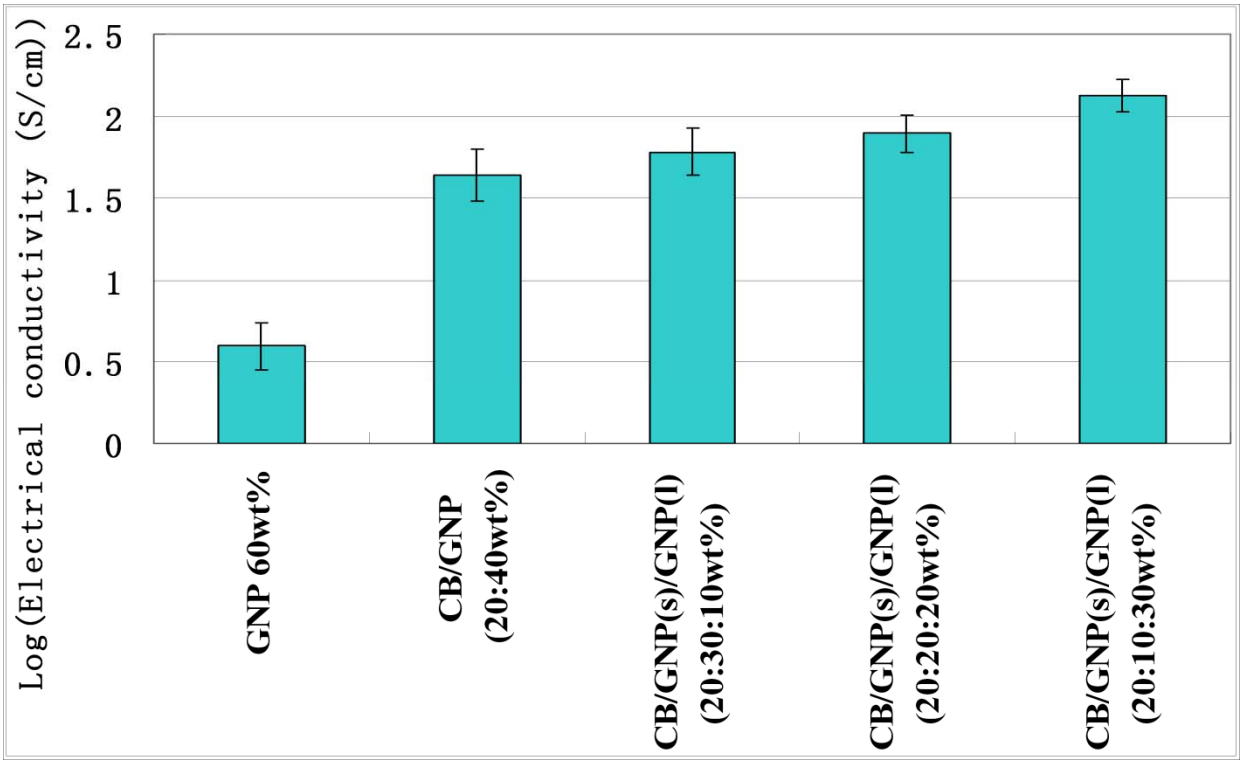

Figure 6.8. Synergistic effects on electrical conductivity of combining small GNP platelets with large ones (HDPE nanocomposites)

From the Figure 6.8 and Figure 6.9, it is clearly seen that both the electrical conductivity and the thermal conductivity are tremendously increased with the increasing fraction of large GNP platelets (GNP (l)). At the sample composition of HDPE/CB/GNP(s)/GNP(l) (40:20:10:30wt%), where the total filler loading is still kept at 60 wt%, the in-plane electrical conductivity reaches 132 S/cm and the in-plane thermal conductivity is 10.4 W/mK. Both of them have already exceeded the DOE target. Higher electrical and thermal conductivity in the nanocomposites with large GNP platelets can be attributed to the fact that the aspect ratio of large GNP platelets is much higher, which makes them intersect with each other much easier in forming conductive

networks in the polymer matrix. And based on the results of the flexural properties displayed in the Figure 6.10, the flexural strength drops a little as expected in the nanocomposite with 30 wt% large GNP platelets, but it remains as high as 38 MPa, which is 53% higher than the DOE target (>25 MPa). Therefore, we may conclude that by properly controlling the amount of large GNP platelets added, all the properties shown in the resulting nanocomposite can successfully meet the DOE requirements for bipolar plates.

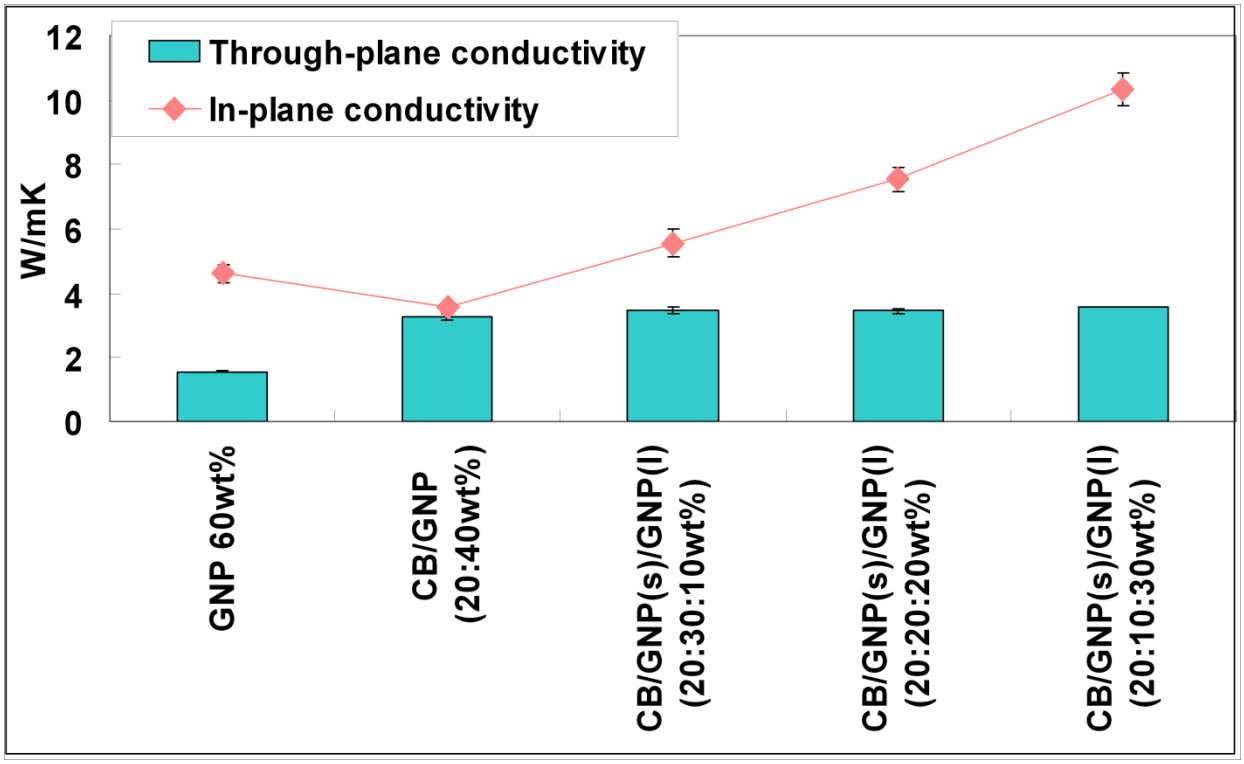

Figure 6.9. Synergistic effects on thermal conductivity of combining small GNP platelets with large ones (HDPE nanocomposites)

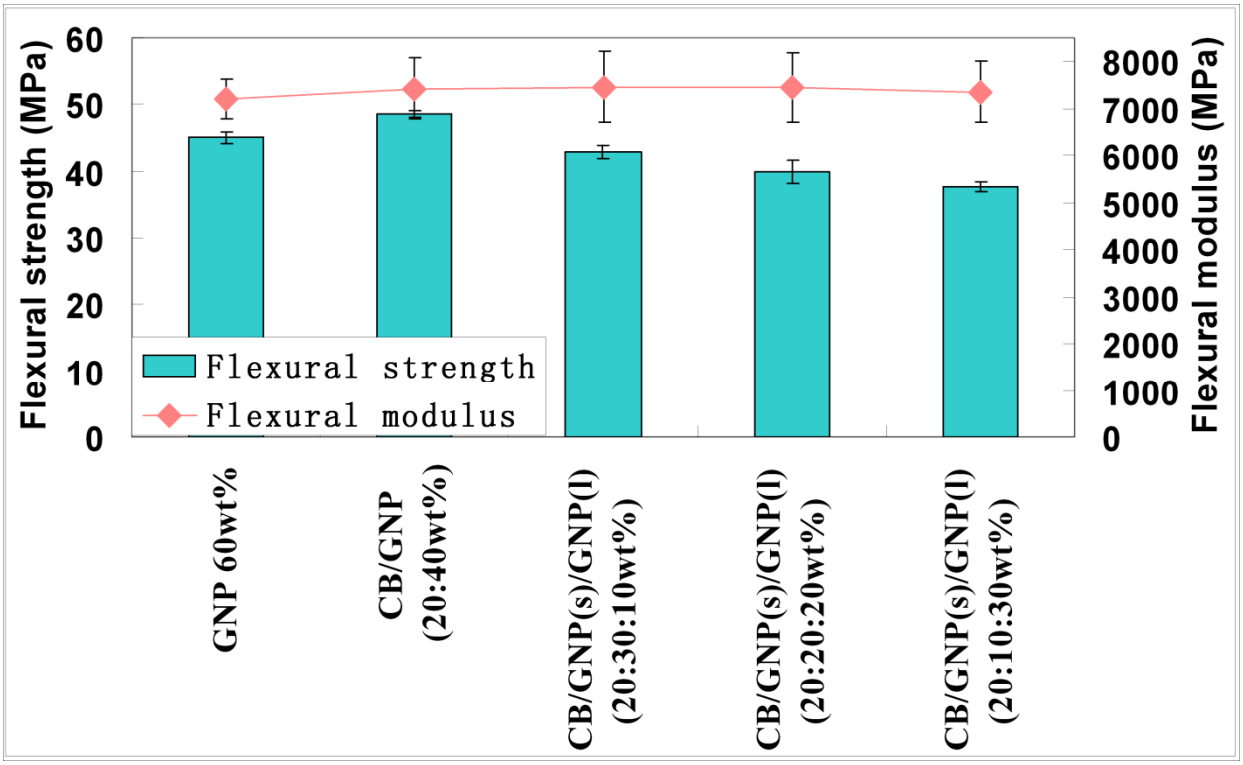

Figure 6.10. Synergistic effects on flexural properties of combining small GNP platelets with large ones (HDPE nanocomposites)

5.4.1 Properties of PPS/GNP Nanocomposites as Bipolar Plates

The various properties of HDPE nanocomposites made by SSBM and compression molding have been characterized above. It is concluded that the synergistic effects between GNP, CB and GNP platelets of different sizes allow the optimization of processing characteristics to fabricate highly electrical and thermal conductive nanocomposites that can satisfy the DOE targets for bipolar plates. However, the thermal stability of HDPE/GNP nanocomposites was found to be up to only 100 °C due to the low melting temperature of HDPE (~130 °C), which constrains their application in high-temperature fuel cells. It has been well reported that higher operating temperature in fuel cells leads to higher powder density and higher fuel efficiency [24], a

polymeric nanocomposite that can resist high temperature is thus highly desired. PPS, a high-performance thermoplastic which exhibits thermal stability up to 220 °C, was then considered as the polymer matrix to fabricate PPS/GNP nanocomposites.

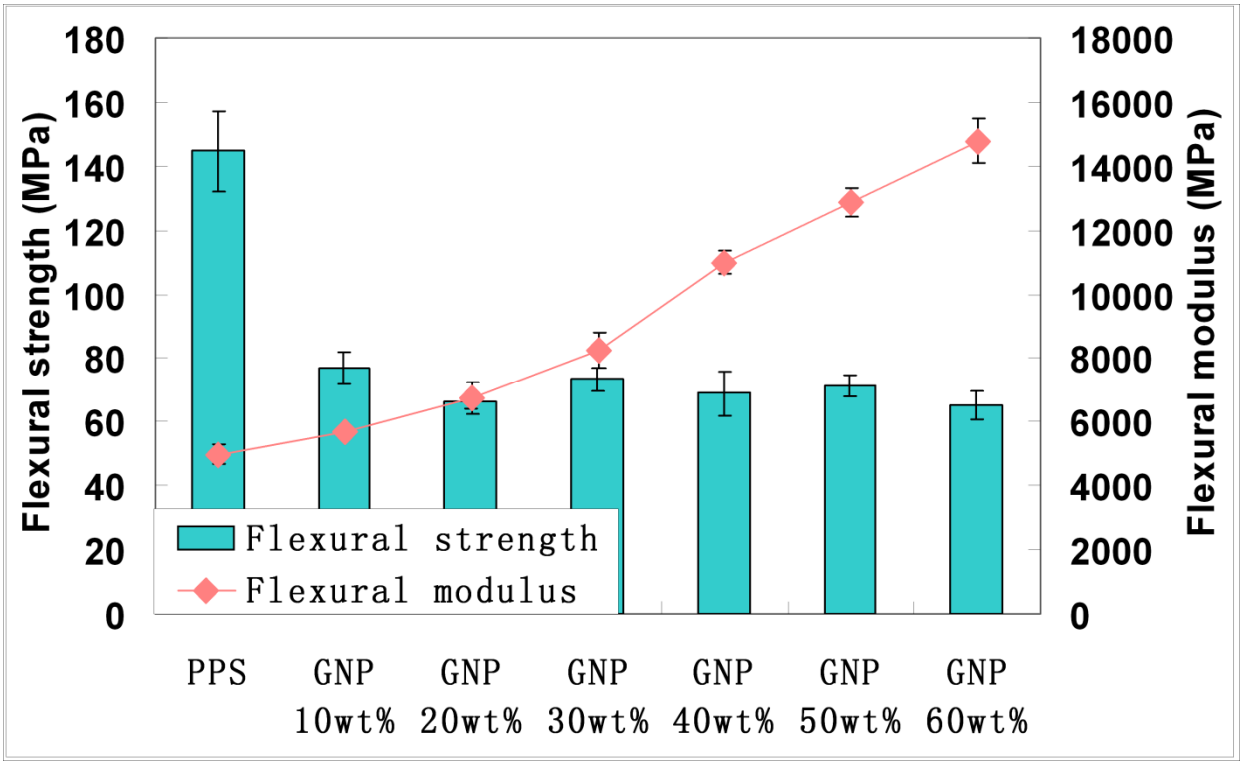

Figure 6.11. Flexural properties of PPS/GNP nanocomposites made by SSBM and compression molding

Figure 6.11 shows the flexural properties of PPS/GNP nanocomposites made by SSBM and compression molding. From this figure, it is noted that the modulus of these nanocomposites exhibits a monotonic increase with the increasing GNP content. At 60 wt% GNP loading, the modulus is enhanced by almost 200% compared to that of neat PPS. Meanwhile, the flexural strength of these PPS/GNP nanocomposites is found to be much lower than the neat PPS but it is not affected much by the increase of GNP content. Especially at 60 wt% GNP loading, the

flexural strength of the nanocomposite is still as high as 66 MPa, which is more than twice as much as the DOE requirement for bipolar plates (>25 MPa). To have a better understanding for the flexural behavior of these nanocomposites, their strain values at break during the mechanical testing are presented in the Figure 6.12.

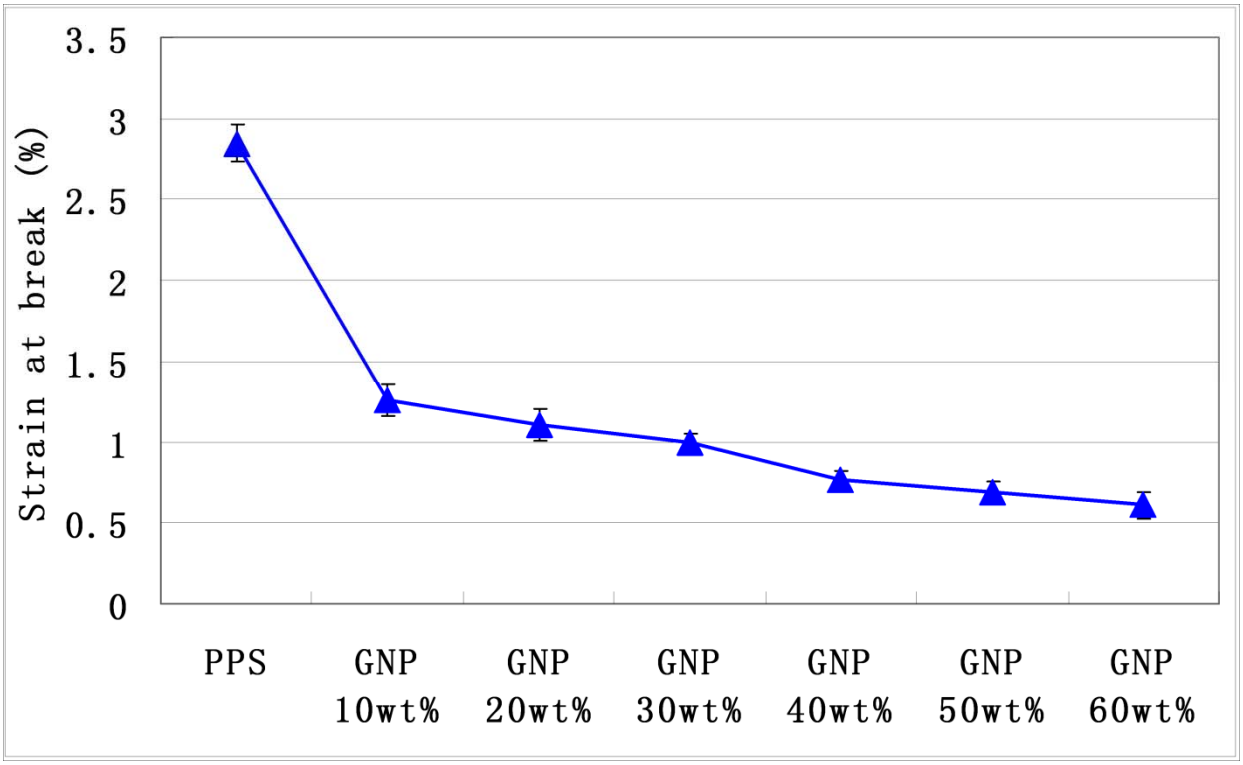

Figure 6.12. Strain at break of PPS/GNP nanocomposites made by SSBM and compression molding

According to this figure, huge decrease in strain at break is observed between the neat PPS and the PPS/GNP sample with 10 wt% GNP, which implies that incorporation of GNP platelets makes PPS much more brittle and less ductile. As the GNP content increases, the strain value at break decreases gradually while the flexural modulus of these nanocomposites increases significantly as shown in the Figure 6.11. In consequence, the flexural strength stays slightly

unchanged.

Figure 6.13 describes the gas permeability of PPS/GNP nanocomposites up to 60 wt% GNP loading. It is seen that the gas permeability firstly drops tremendously from the neat PPS to the nanocomposite with 40 wt% GNP loading and then it falls into a plateau. Again, if compared with the DOE target for the gas permeability, we can see that all the PPS/GNP nanocomposites can successfully meet the requirement.

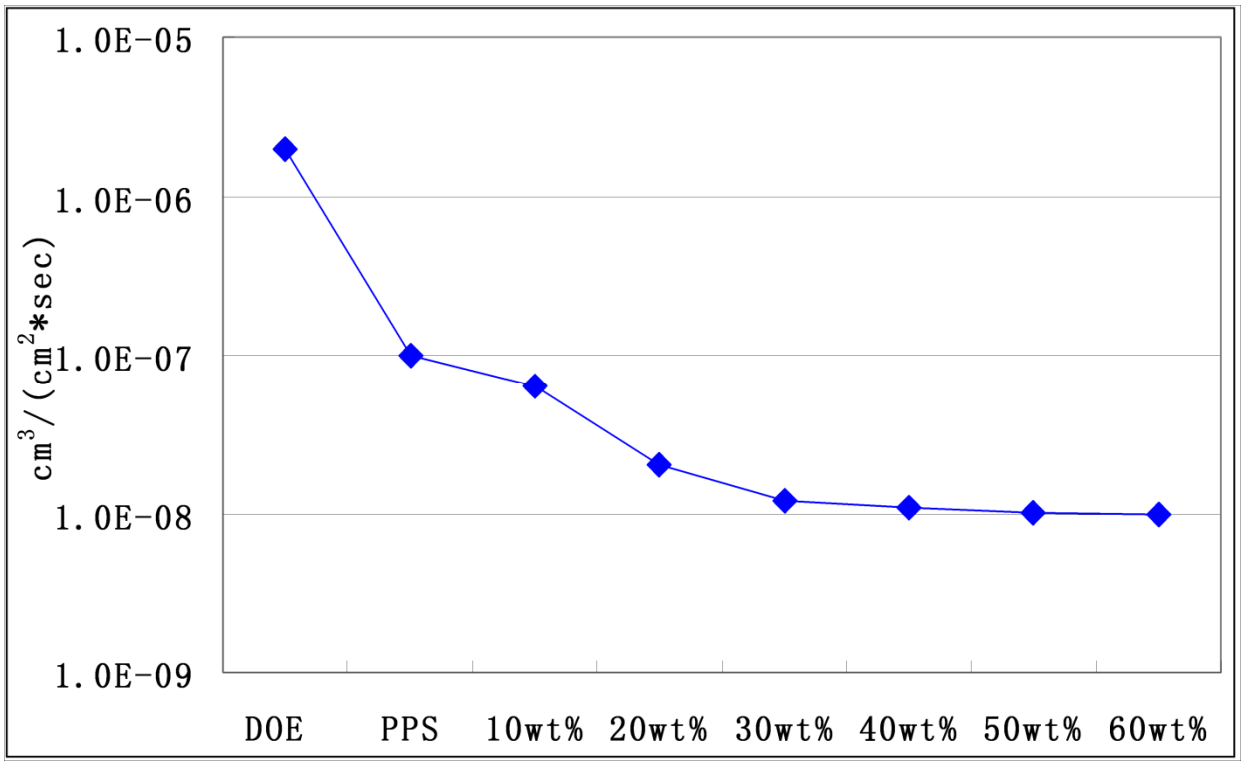

Figure 6.13. The gas permeability of PPS/GNP nanocomposites made by SSBM and compression molding

The in-plane electrical conductivity of these nanocomposites is then displayed in the Figure 6.14. It is seen that although the electrical conductivity exhibits a dramatic increase with the increasing GNP content, it is still falling short of the DOE target (>100 S/cm) even at 60 wt% GNP loading.

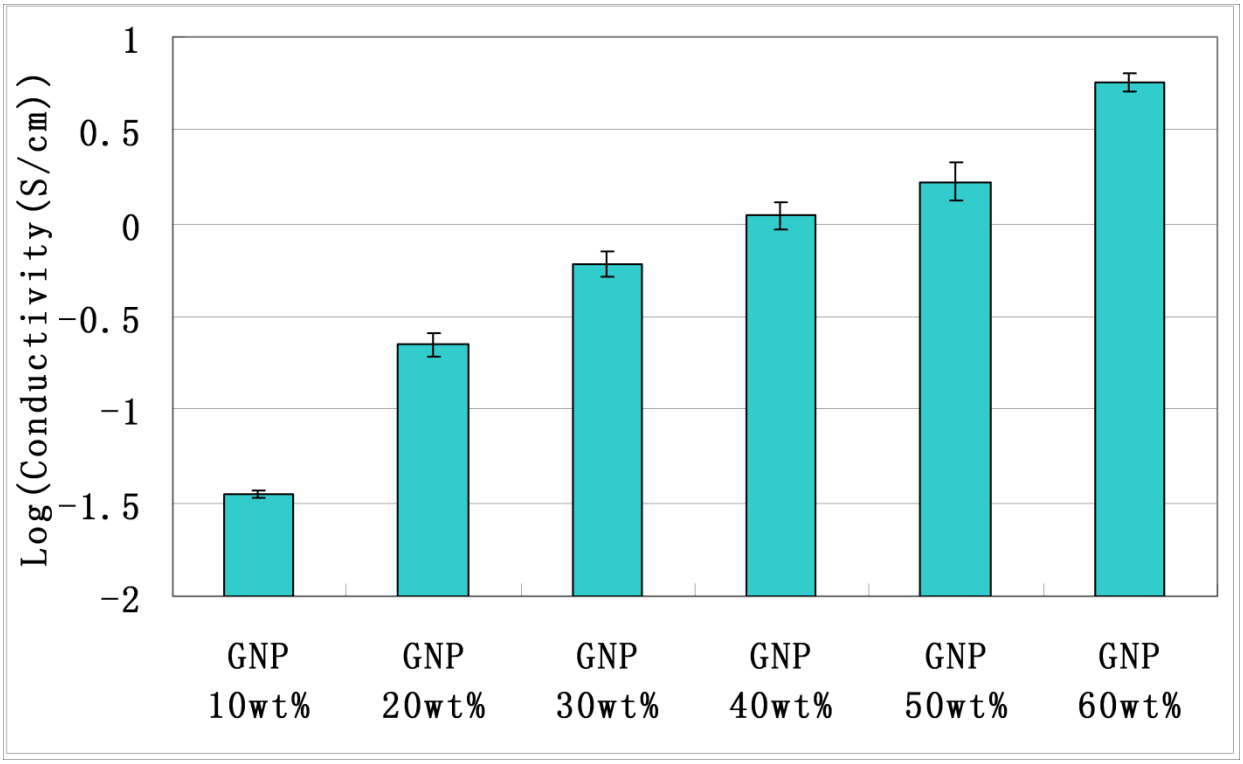

Figure 6.14. In-plane electrical conductivity of PPS/GNP nanocomposites made by SSBM and compression molding

Based on the discussion in the previous sections, binary blends of GNP with CB could lead to better electrical and mechanical properties in the resulting nanocomposites. Hybridized PPS/CB/GNP nanocomposites were thus fabricated and their electrical conductivity and flexural properties are shown in the Figure 6.15 and Figure 6.16 respectively. The total filler loading was kept at 60 wt%.

As seen from the electrical measurement in the Figure 6.15, improved electrical conductivity is also observed due to a positive synergistic effect between GNP and CB. The highest conductivity also occurs at the composition where the weight ratio between GNP and CB is 2:1. However, if this weight ratio is below 2:1, a reduction in conductivity is detected, which is based on the fact

that the intrinsic electrical conductivity of CB is much lower than that of GNP [25]. The presence of too much CB disrupts the formation of GNP conductive networks which subsequently lowers the overall electrical conductivity of the resulting nanocomposites.

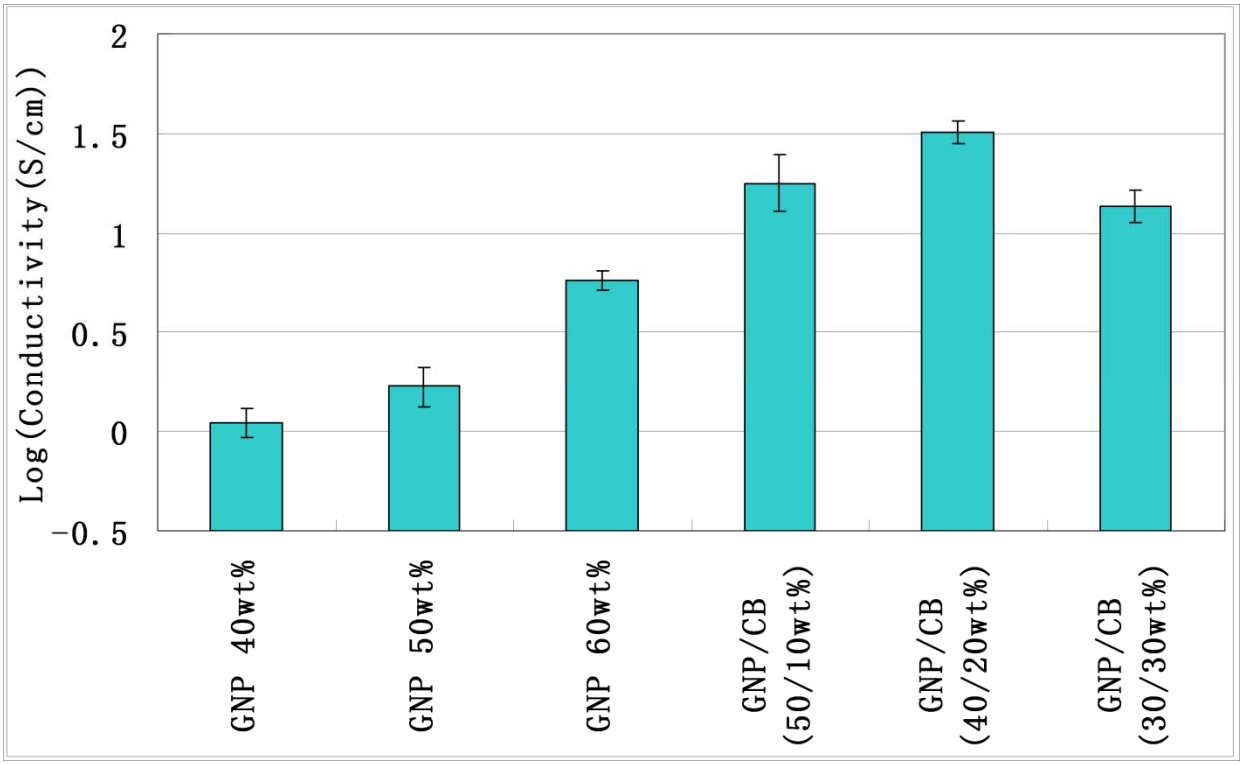

Figure 6.15. In-plane electrical conductivity of PPS/CB/GNP hybrid nanocomposites made by SSBM and compression molding

Figure 6.16 describes the flexural properties of these hybridized nanocomposites. It is noted that both flexural strength and flexural modulus are not affected much by the addition of CB if the weight ratio between GNP and CB is not lower than 2:1. Huge decrease in the flexural properties is then observed for the PPS/CB/GNP hybrid nanocomposite with 30 wt% CB. Reduction in the flexural properties for this hybridized sample is also believed due to the disruption of GNP network formation by the excess of CB, which fundamentally changes the fracture behavior of

the nanocomposite.

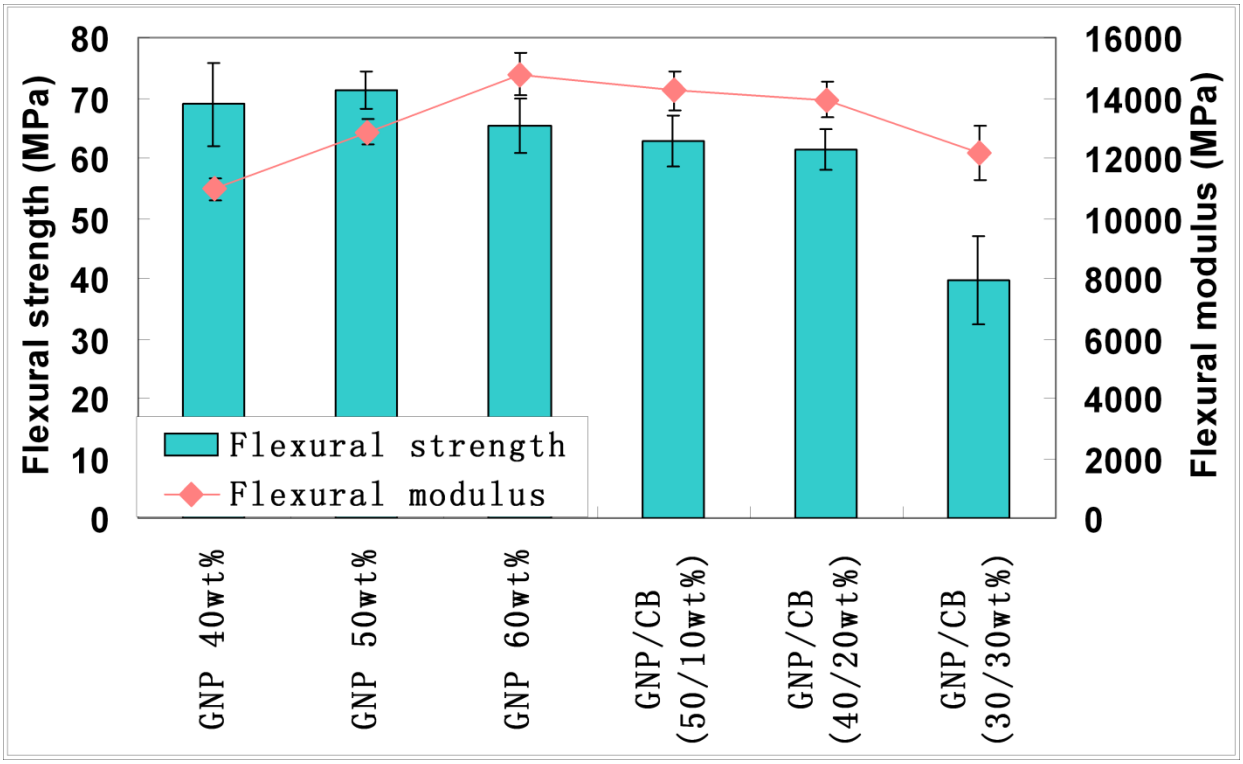

Figure 6.16. Flexural properties of PPS/CB/GNP hybrid nanocomposites made by SSBM and compression molding

In order to further enhance the electrical and thermal properties of PPS/GNP nanocomposites to meet the DOE targets for bipolar plates. Combination of large GNP platelets with small ones was also considered for a synergistic effect as described in HDPE/GNP nanocomposites. The electrical, thermal, and mechanical properties of the resulting PPS/CB/GNP(s)/GNP(l) nanocomposites are displayed in the Figure 6.17, Figure 6.18, and Figure 6.19 respectively, which once again illustrate the positive synergistic effect between small and large GNP nano-particles.

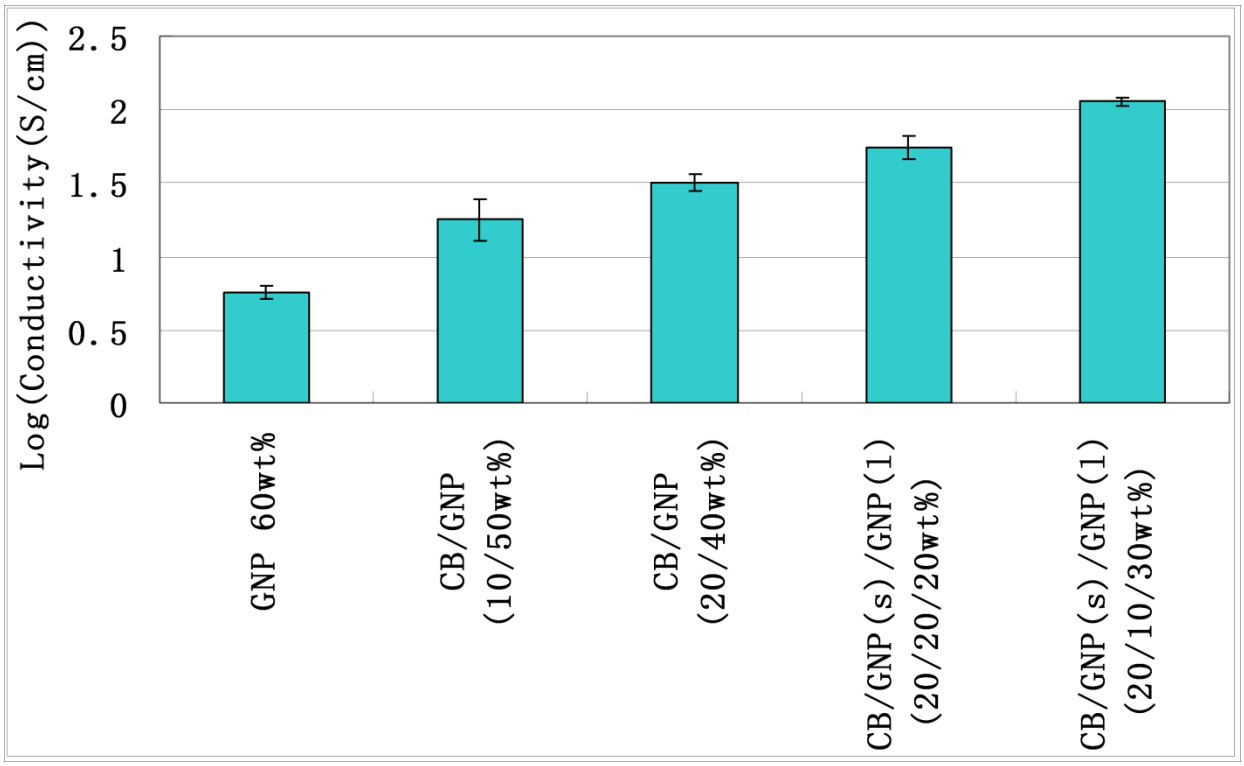

Figure 6.17. In-plane electrical conductivity of various PPS/CB/GNP hybridized nanocomposites

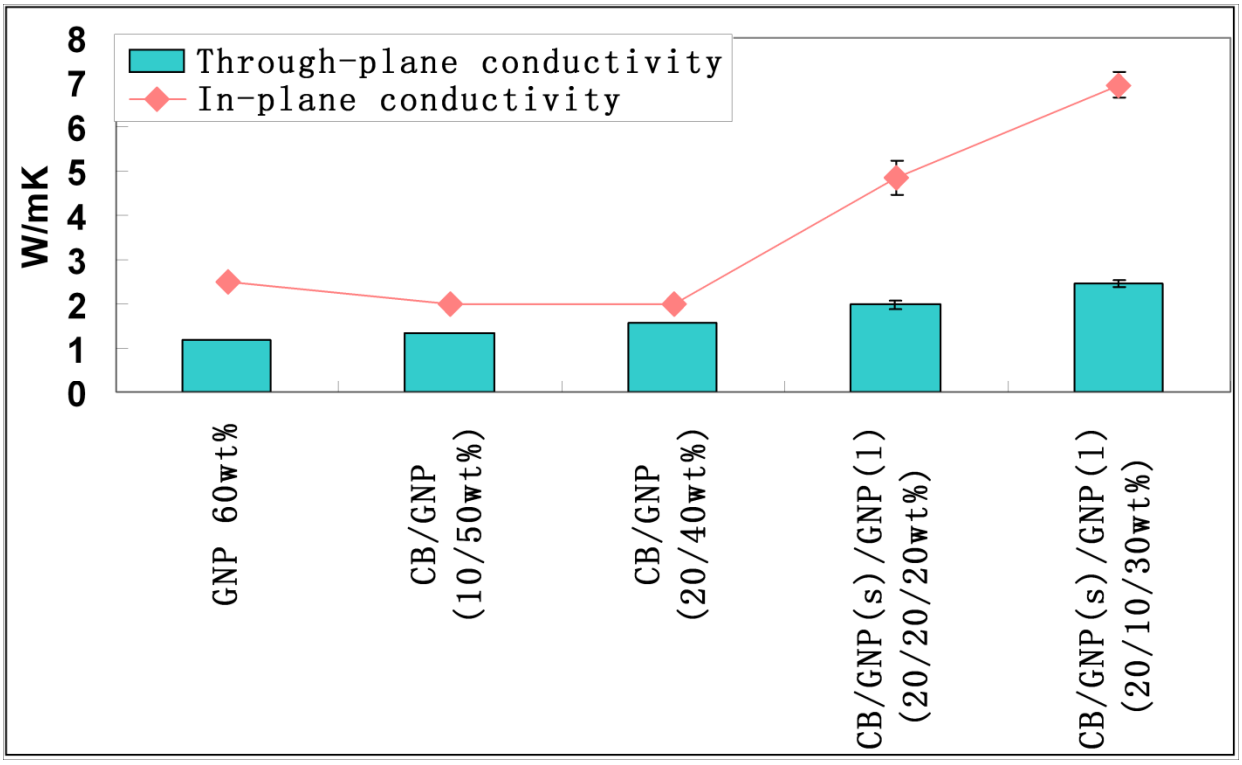

Figure 6.18. Thermal conductivity of various PPS/CB/GNP hybridized nanocomposites

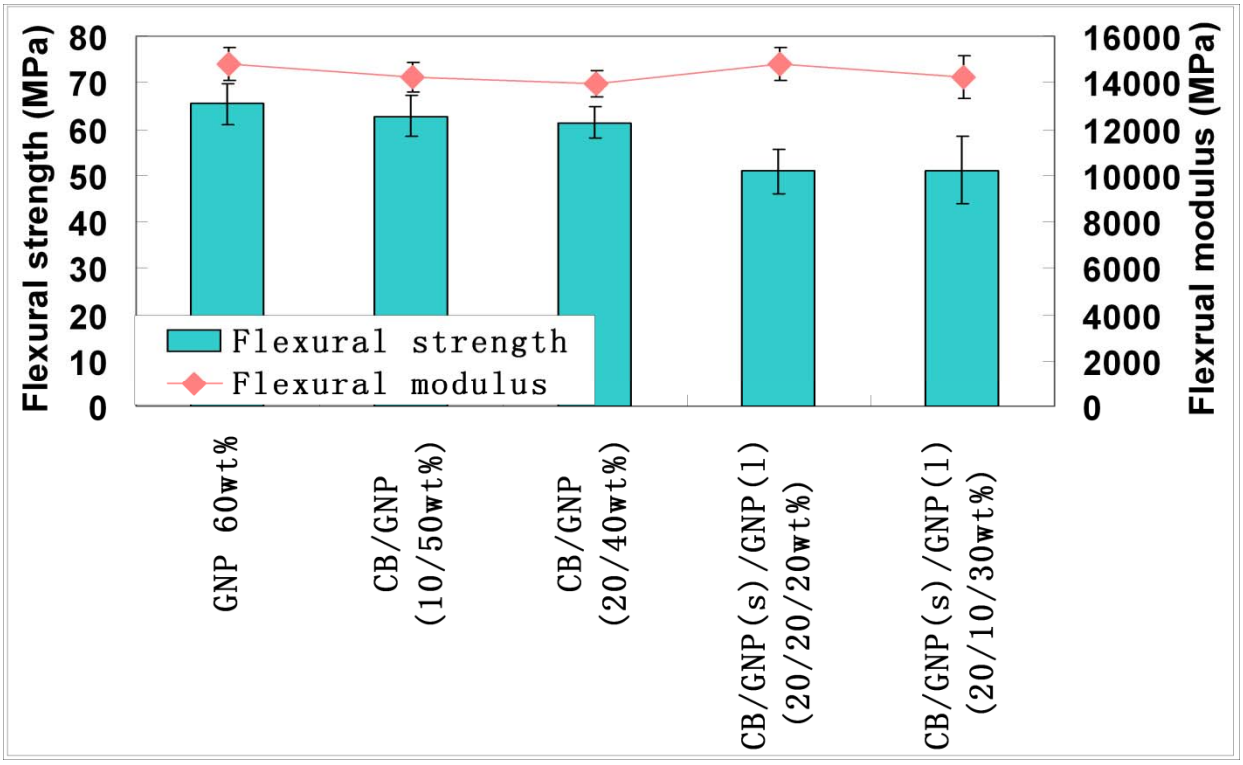

Figure 6.19. Flexural properties of various PPS/CB/GNP hybridized nanocomposites

From these figures, it is concluded that the highest electrical conductivity (~ 114 S/cm) occurs at the hybrid nanocomposite with 30 wt% large GNP platelets, which has satisfied the DOE target. The flexural strength of this sample is found to be 50 MPa which is also twice as much as the DOE target (>25 MPa). However, the best in-plane thermal conductivity got so far (~ 7 W/mK) falls short of the DOE requirement (>10 W/mK).

6.4.4 Properties Comparison between PPS and HDPE Nanocomposites for Bipolar Plates

Previous sections have thoroughly described the potentials of HDPE and PPS nanocomposites as bipolar plates for fuel cells. This section will carry out a property comparison between these two kinds of GNP nanocomposites. First of all, the gas permeability of HDPE and PPS

nanocomposites is presented in the Figure 6.20.

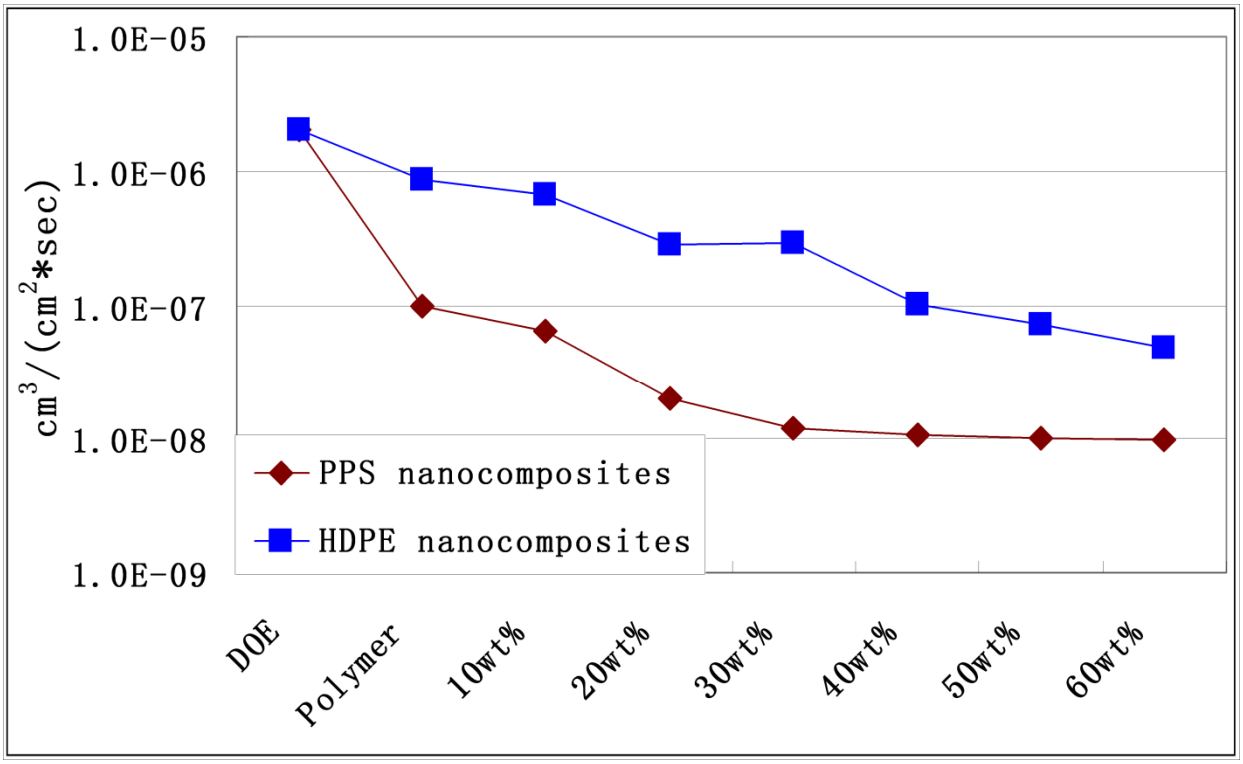

Figure 6.20. Gas permeability of HDPE and PPS nanocomposites at various GNP loadings

From this figure, it is concluded that both HDPE/GNP and PPS/GNP nanocomposites have met the DOE target for gas permeability. And PPS samples exhibit even lower gas permeability than HDPE counterparts which is largely due to the better gas barrier properties of PPS as the polymer matrix.

The flexural properties of HDPE and PPS nanocomposites at various filler compositions are listed in the Table 6.1. It is noted that PPS nanocomposites show superior flexural strength and flexural modulus than HDPE samples at every filler composition. Better flexural properties of PPS nanocomposites at relatively low filler loadings (<50 wt%) are believed due to the superb mechanical properties of PPS as the polymer matrix and its higher affinity to GNP nanoplatelets

on the account of its molecular structure (consisting of benzene rings), GNP can thus be better dispersed in PPS. At high filler loadings (>50 wt%), however, because of the low viscosity at the processing conditions [26], PPS is capable of infiltrating and wetting GNP and CB nano-particles more effectively. The adhesion between the polymer matrix and the nano-fillers is thus good, leading to a better mechanical strength in PPS/GNP nanocomposites.

Table 6.1. Flexural properties of HDPE and PPS nanocomposites

Sample Composition	Flexural Strength PPS (MPa)	Flexural Strength HDPE (MPa)	Flexural Modulus PPS (MPa)	Flexural Modulus HDPE (MPa)
Neat Polymer	144.6	17.7	4972.6	670.8
GNP 10wt%	76.8	24.2	5697.5	1284.3
GNP 20wt%	66.6	27.8	6745.3	1796.1
GNP 30wt%	73.3	34.1	8252.1	2412.2
GNP 40wt%	69.0	42.0	10979.8	4115.6
GNP 50wt%	71.2	48.8	12859.9	5856.8
GNP 60wt%	65.3	45.0	14783.7	7199.3
CB/GNP (10/50wt%)	62.8	44.5	14235.0	6762.9
CB/GNP (20/40wt%)	61.4	48.6	13737.7	7416.5
CB/GNP(s)/GNP(l) (20/20/20wt%)	50.9	39.9	14812.1	7458.5
CB/GNP(s)/GNP(l) (20/10/30wt%)	51.1	37.7	14244.7	7358.2

Table 6.2 describes the in-plane electrical conductivity of various HDPE and PPS

nanocomposites, from which an interesting phenomenon is found. That is, at low filler loadings (≤50 wt%), PPS nanocomposites have a higher electrical conductivity while the result is opposite when the filler loading is higher than 50 wt%. Higher conductivity in PPS nanocomposites at low filler loadings is resulted from a better GNP dispersion as described above. At high filler contents, however, because PPS can better wet GNP and CB, the direct contact between conductive fillers are thus prevented, which leads to an increased interfacial resistance and a reduced electrical conductivity.

Table 6.2. In-plane electrical conductivity of HDPE and PPS nanocomposites

Sample Composition	Electrical Conductivity PPS (S/cm)	Electrical Conductivity HDPE (S/cm)
GNP 10wt%	0.04	5.05E-05
GNP 20wt%	0.22	8.01E-04
GNP 30wt%	0.60	0.01
GNP 40wt%	1.10	0.13
GNP 50wt%	1.68	1.36
GNP 60wt%	5.75	3.97
CB/GNP (10/50wt%)	17.82	22.00
CB/GNP (20/40wt%)	31.86	43.99
CB/GNP(s)/GNP(l) (20/20/20wt%)	54.67	78.40
CB/GNP(s)/GNP(l) (20/10/30wt%)	113.83	132.81

Table 6.3. Thermal conductivity of HDPE and PPS nanocomposites

Sample Composition	Through-plane Thermal Conductivity PPS (W/mK)	Through-plane Thermal Conductivity HDPE (W/mK)	In-plane Thermal Conductivity PPS (W/mK)	In-plane Thermal Conductivity HDPE (W/mK)
Neat Polymer	0.21	0.35	0.25	0.36
GNP 10wt%	0.41	0.61	0.60	0.98
GNP 20wt%	0.52	0.75	0.97	1.36
GNP 30wt%	0.64	0.93	1.16	1.88
GNP 40wt%	0.83	1.10	1.58	2.51
GNP 50wt%	1.04	1.24	1.88	2.80
GNP 60wt%	1.20	1.58	2.48	4.64
CB/GNP (10/50wt%)	1.34	2.23	1.99	2.94
CB/GNP (20/40wt%)	1.58	3.28	2.00	3.58
CB/GNP(s)/GNP(l) (20/20/20wt%)	1.99	3.47	4.86	7.55
CB/GNP(s)/GNP(l) (20/10/30wt%)	2.47	3.57	6.94	10.34

Table 6.3 then gives the in-plane and through-plane thermal conductivity of HDPE and PPS nanocomposites at various filler compositions. We can see that HDPE nanocomposites exhibit significantly higher in-plane and through-plane thermal conductivity at every filler composition. Especially at the filler composition of CB/GNP(s)/GNP(l) (20:10:30wt%), the PPS sample does not meet the DOE target for in-plane thermal conductivity.

Table 6.4. Density, heat capacity and thermal diffusivity of HDPE and PPS nanocomposites

Sample Composition	Density PPS (g/cm^3)	Density HDPE (g/cm^3)	Heat Capacity PPS (J/gK)	Heat Capacity HDPE (J/gK)	Thermal diffusivity PPS (mm^2/s)	Thermal diffusivity HDPE (mm^2/s)
Neat Polymer	1.35	0.96	1.06	2.30	0.18	0.17
GNP 10wt%	1.40	1.01	1.03	2.14	0.42	0.45
GNP 20wt%	1.45	1.07	0.99	1.99	0.67	0.64
GNP 30wt%	1.51	1.14	0.96	1.83	0.80	0.90
GNP 40wt%	1.58	1.22	0.93	1.67	1.08	1.23
GNP 50wt%	1.64	1.31	0.90	1.52	1.28	1.41
GNP 60wt%	1.72	1.41	0.86	1.36	1.68	2.41
CB/GNP (10/50wt%)	1.71	1.41	0.85	1.37	1.34	1.53
CB/GNP (20/40wt%)	1.70	1.40	0.87	1.37	1.35	1.86
CB/GNP(s)/GNP(l) (20/20/20wt%)	1.69	1.40	0.85	1.37	3.28	3.93
CB/GNP(s)/GNP(l) (20/10/30wt%)	1.70	1.40	0.85	1.37	4.69	5.38

To explain why PPS nanocomposites have inferior thermal conductivity, the density, specific heat capacity, and thermal diffusivity of these nanocomposites are illustrated in the Table 6.4. It is known that the thermal conductivity of a composite is based on the multiplication of these three parameters. According to the results of thermal diffusivity measurements (in-plane thermal diffusivity is taken for the comparison), PPS nanocomposites show a competitive thermal

diffusivity to HDPE counterparts at relatively low filler loadings. At high filler loadings, however, PPS nanocomposites have a much lower thermal diffusivity. This observation is very similar to the results of electrical conductivity. The same reasoning can also be applied, that is, better PPS wetting on conductive fillers results in a higher interfacial resistance, which leads to a lower thermal diffusivity. Meanwhile, the density of PPS nanocomposites is found to be larger than the HDPE samples, but their heat capacity values are significantly lower due to the low heat capacity of PPS as the polymer matrix. All these factors contribute to an inferior thermal conductivity in the resulting PPS nanocomposites.

6.4.5 Formability of HDPE and PPS Nanocomposites for Bipolar Plates

The bipolar plate has many fine flow channels on both sides for the flow of oxygen and hydrogen during fuel cell operation. The formability of these channels thus becomes one of the key requirements for bipolar plates. To test the formability of gas channels on the surface of HDPE and PPS nanocomposites, a stainless steel mold with flow patterns were firstly designed and made as shown in the Figure 6.21. The channels width is from 0.5 mm to 1.5 mm and the depth is from 0.5 mm to 1 mm. These dimensions are within the ranges that are normally selected in literature for the gas channels on bipolar plates [27-29]. Then these channel patterns were transferred to the surface of HDPE and PPS nanocomposites by applying a hot press between the mold and a plain composite plate fabricated by SSBM and compression molding as described before.

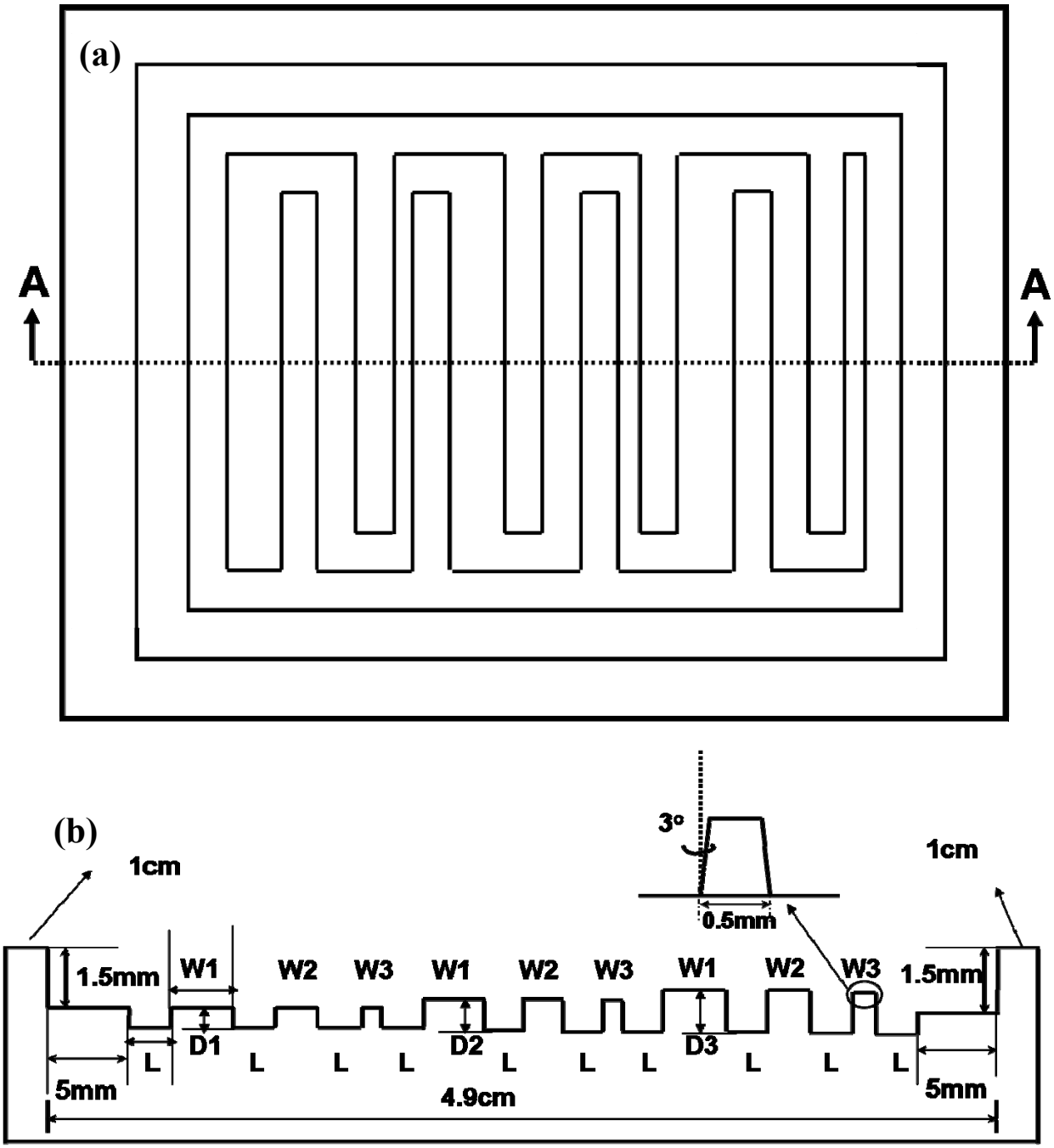

L (Land width): 3mm

W (Groove width): W1,1.5mm; W2, 1mm; W3, 0.5mm

D (Groove depth): D1, 0.5mm; D2, 0.75mm; D3, 1mm

Figure 6.21. Bipolar plates mold design (a) Top-view; (b) Cross-section view (A-A)

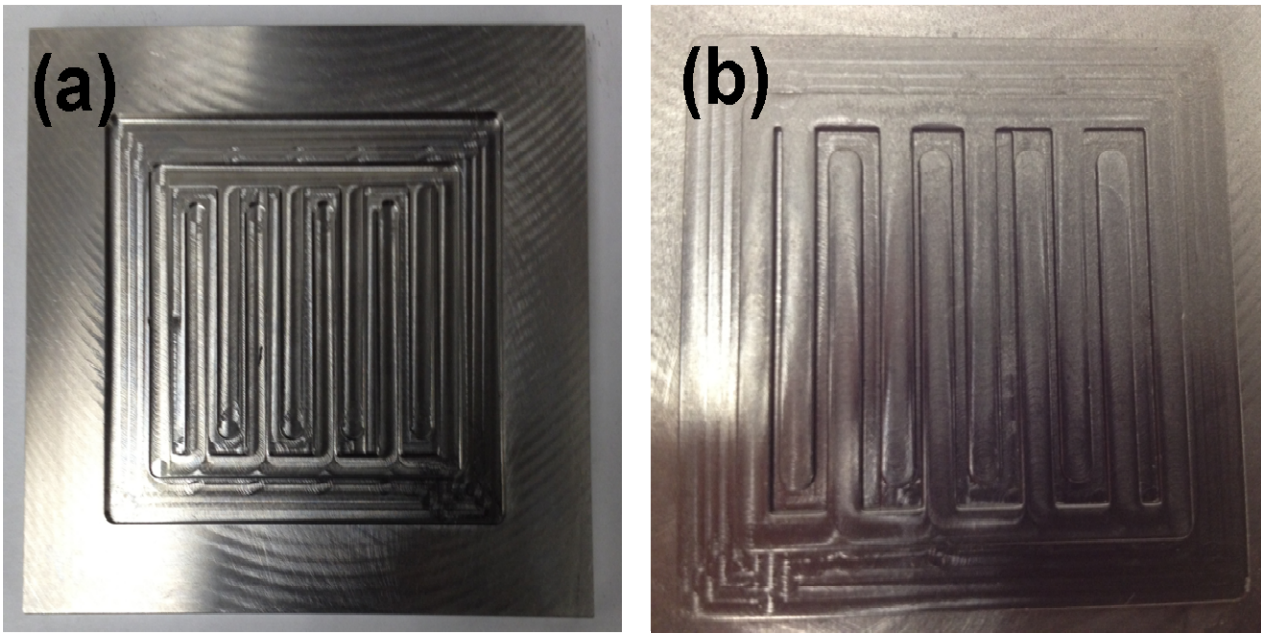

Figure 6.22. Bipolar plates mold (a) and the PPS bipolar plates (b)

Figure 6.22 shows the stainless steel mold and a PPS bipolar plate made from the hot press between the mold and a plain PPS composite plate. Here we can see that the gas channel patterns were successfully transferred to the surface of the PPS nanocomposite. A Keyence optical microscope which could generate 3-D images was then applied to measure the dimension accuracy of gas channels on the PPS and HDPE bipolar plates. Figure 6.23 shows a 3-D image of a gas channel pattern from the stainless steel mold, from which we can obtain the channel width and channel depth. The nomenclature for the gas channels with different width and depth is: channel C1010 means that the width of the channel is 1 mm and depth is 1 mm. And channel C15075 has the channel width of 1.5 mm and depth of 0.75 mm. Table 6.5 then displays the channel width and depth values from the mold, HDPE bipolar plate, and PPS bipolar plate measured by the Keyence optical microscope.

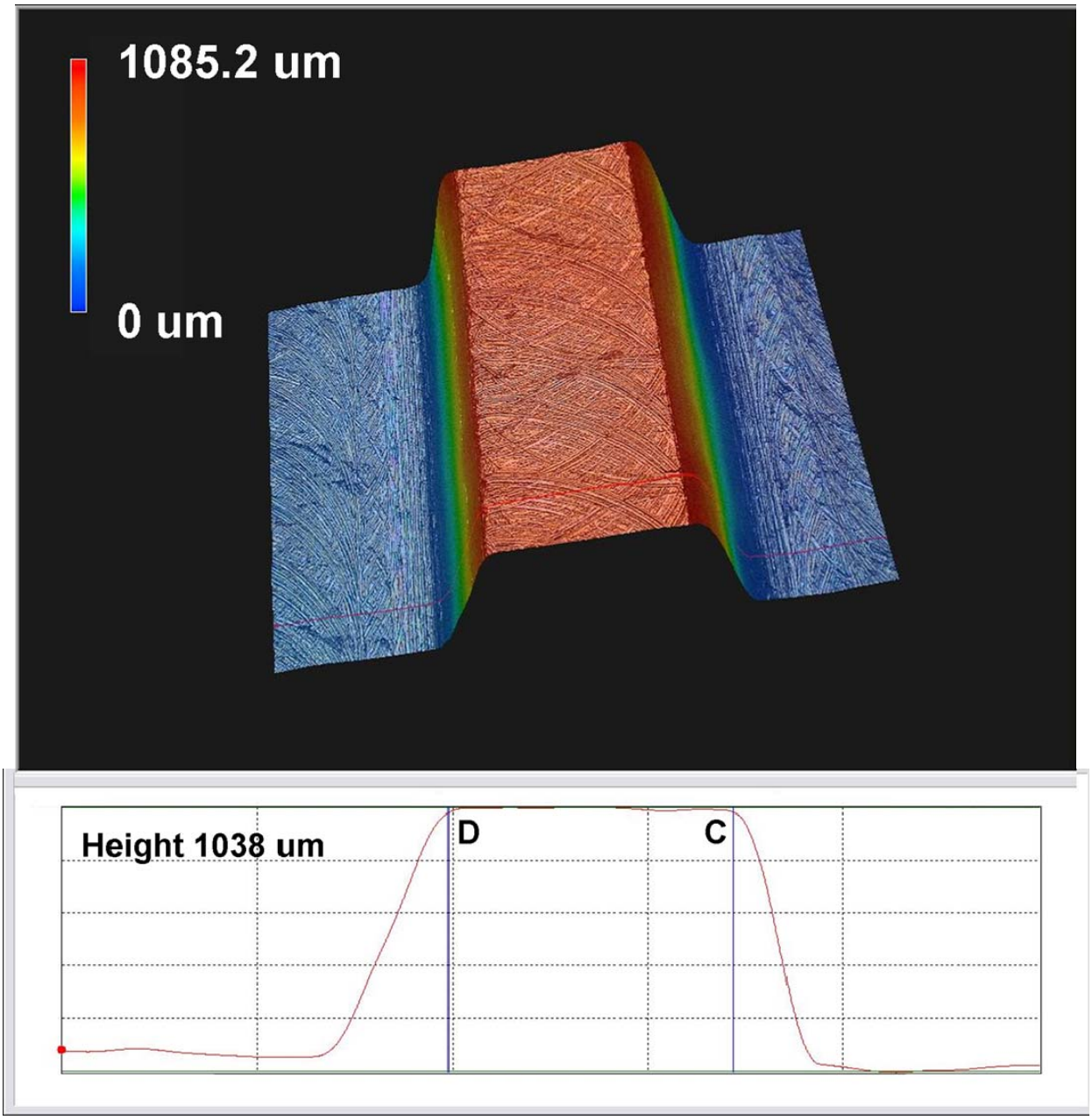

Figure 6.23. A 3-D image of gas channel on the stainless steel mold generated by Keyence optical microscope.

To have a better comparison, all the width values from the mold, HDPE bipolar plate, and PPS bipolar plate are shown in the Figure 6.24. First of all, it is seen that the width values of the gas channels on the mold do not exactly match those in the mold design, which is caused by the tooling errors during the machining of the mold. However, we do see that the gas channels on the

HDPE and PPS bipolar plates match those on the mold very well. Meanwhile, Figure 6.25 gives the depth values from the mold, HDPE and PPS bipolar plates. Once again, it is detected that the depth values from the polymeric bipolar plates are very close to those on the stainless steel mold. Therefore, we can conclude that the formability of gas channels on the surface of HDPE and PPS nanocomposites is very good, which further confirms their feasible applications in bipolar plates.

Table 6.5. Gas Channel width and depths on mold, HDPE and PPS bipolar plates

	Mold (μm)	HDPE Bipolar Plate (μm)	PPS Bipolar Plate (μm)
0505 width	445.7	443.4	440.9
depth	526.7	500.8	507.2
05075 width	324.5	333.9	324.1
depth	796.5	742.5	752.8
0510 width	333.6	332.6	324.6
depth	1043.9	974.9	969.7
1005 width	946.4	953.3	934.4
depth	544.5	498.6	519.7
10075 width	831.2	829.2	821.5
depth	785.8	760.9	769.0
1010 width	859.8	857.1	858.8
depth	1041.3	967.5	1015.2
1505 width	1500.4	1494.0	1492.5
depth	487.3	463.7	478.1
15075 width	1359.0	1367.4	1356.9
depth	776.1	764.1	770.1
1510 width	1409.3	1389.3	1393.1
depth	1044.8	1013.6	1021.1

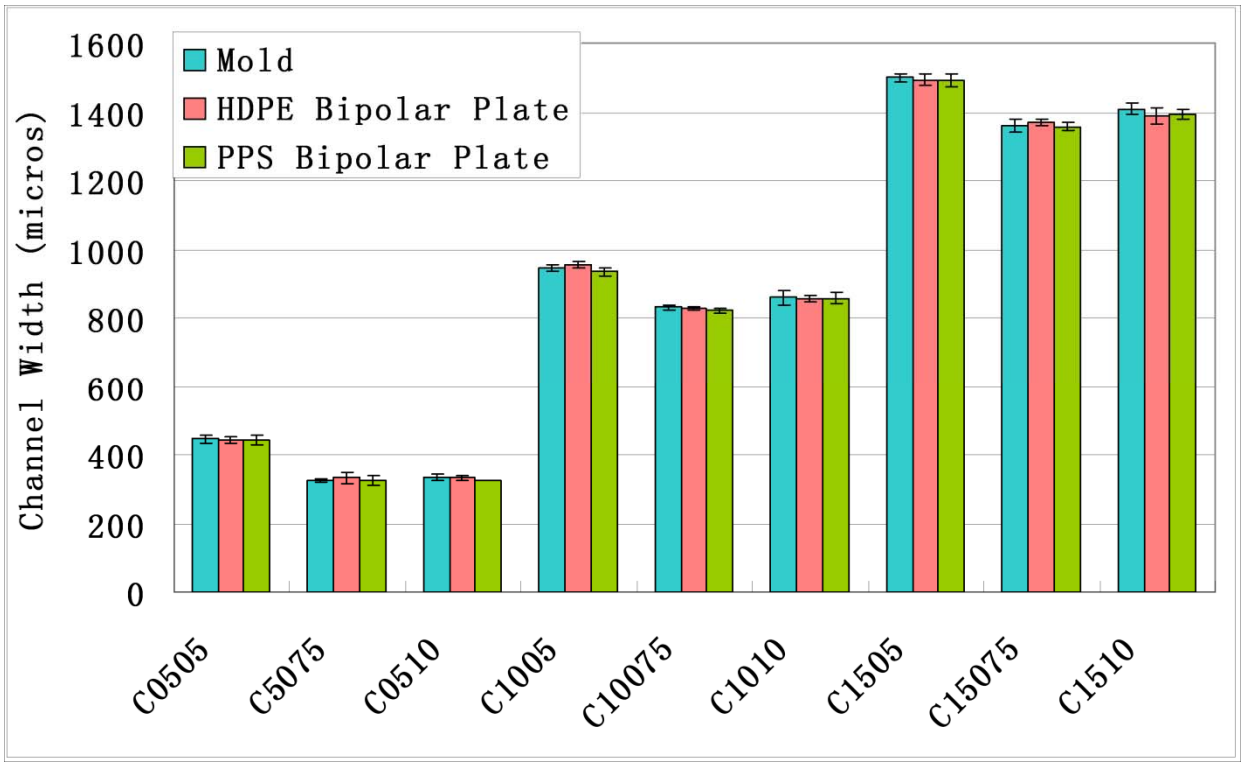

Figure 6.24. Width of gas channels from the mold, HDPE and PPS bipolar plates

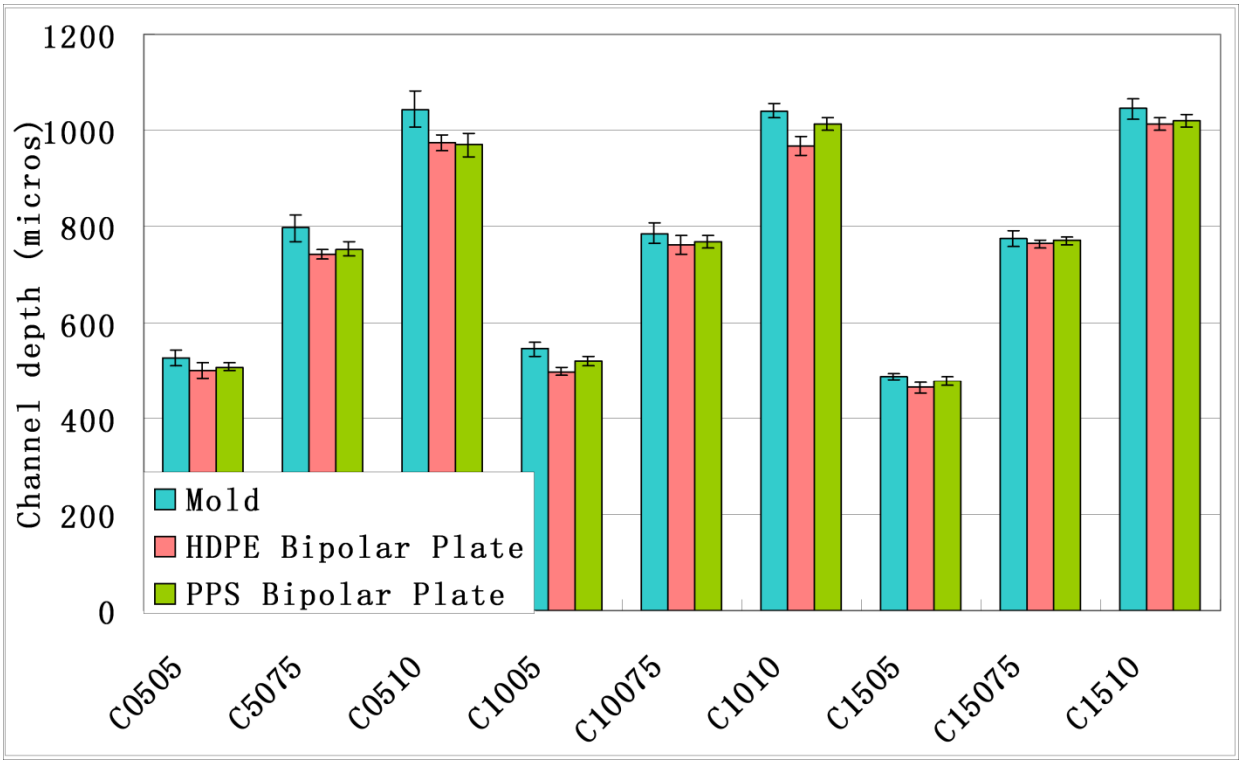

Figure 6.25. Depth of gas channels from the mold, HDPE and PPS bipolar plates

6.5 Conclusions

This study has explored the potential of utilizing HDPE/GNP and PPS/GNP nanocomposites as novel polymeric bipolar plates in fuel cells. GNP nanocomposites were fabricated by SSBM and compression molding in this study and the effectiveness of GNP platelets in enhancing the mechanical properties and lowering the gas permeability of the nanocomposites was investigated. It was found that HDPE/GNP and PPS/GNP nanocomposites at 60 wt% GNP loading exhibit good flexural strength and excellent gas barrier properties that can successfully meet the DOE target for bipolar plates.

Synergistic effects between GNP and other conductive fillers such as MWCNT and CB to increase the electrical conductivity was also discussed. It was found that the binary blends of GNP with CB result in better enhancement in electrical and mechanical properties. Meanwhile, the combination of small GNP platelets with larger ones was discovered to be another positive synergistic effect in determining the various properties of the resulting nanocomposites. These synergistic effects have offered us a useful insight into the processing of polymeric bipolar plates with tailored properties to meet the stringent requirements.

Furthermore, the formability of gas channels on the surface of HDPE and PPS nanocomposites was also proved to be excellent, which suggests that these HDPE and PPS nanocomposites can successfully meet all the DOE targets for bipolar plates.

REFERENCES

REFERENCES

[1] Hermann A, Chaudhuri T, Spagnol P. Bipolar plates for PEM fuel cells: A review. International Journal of Hydrogen Energy. 2005;30(12):1297-302.

[2] Cunningham B, Baird DG. The development of economical bipolar plates for fuel cells. Journal of Materials Chemistry. 2006;16(45):4385-8.

[3] Kakati BK, Yamsani VK, Dhathathreyan KS, Sathiyamoorthy D, Verma A. The electrical conductivity of a composite bipolar plate for fuel cell applications. Carbon. 2009;47(10):2413-8.

[4] Dhakate SR, Sharma S, Borah M, Mathur RB, Dhami TL. Expanded graphite-based electrically conductive composites as bipolar plate for PEM fuel cell. International Journal of Hydrogen Energy. 2008;33(23):7146-52.

[5] Borroni-Bird CE. Fuel cell commercialization issues for light-duty vehicle applications. Journal of Power Sources. 1996;61(1-2):33-48.

[6] Cho EA, Jeon US, Ha HY, Hong SA, Oh IH. Characteristics of composite bipolar plates for polymer electrolyte membrane fuel cells. Journal of Power Sources. 2004;125(2):178-82.

[7] Mighri F, Huneault MA, Champagne MF. Electrically conductive thermoplastic blends for injection and compression molding of bipolar plates in the fuel cell application. Polymer Engineering & Science. 2004;44(9):1755-65.

[8] Wind J, et.al. Metallic bipolar plates for PEM fuel cells. Journal of Power Sources. 2002;105(2):256-60.

[9] Brandon NP, Skinner S, Steele BCH. Recent Advances in Materials for Fuel Cells Annual Review of Materials Research. 2003;33:183-213.

[10] Dweiri R, Sahari J. Electrical properties of carbon-based polypropylene composites for bipolar plates in polymer electrolyte membrane fuel cell (PEMFC). Journal of Power Sources. 2007;171(2):424-32.

[11] Lee JH, Jang YK, Hong CE, Kim NH, Li P, Lee HK. Effect of carbon fillers on properties

of polymer composite bipolar plates of fuel cells. Journal of Power Sources. 2009;193(2):523-9.

[12] Liao S-H, Yen C-Y, Weng C-C, Lin Y-F, Ma C-CM, Yang C-H, et al. Preparation and properties of carbon nanotube/polypropylene nanocomposite bipolar plates for polymer electrolyte membrane fuel cells. Journal of Power Sources. 2008;185(2):1225-32.

[13] Antunes RA, de Oliveira MCL, Ett G, Ett V. Carbon materials in composite bipolar plates for polymer electrolyte membrane fuel cells: A review of the main challenges to improve electrical performance. Journal of Power Sources. 2010;196(6):2945-61.

[14] Biswas S, Fukushima H, Drzal LT. Mechanical and electrical property enhancement in exfoliated graphene nanoplatelet/liquid crystalline polymer nanocomposites. Composites Part A: Applied Science and Manufacturing. 2010;42(4):371-5.

[15] Fukushima H, Drzal L, Rook B, Rich M. Thermal conductivity of exfoliated graphite nanocomposites. Journal of Thermal Analysis and Calorimetry. 2006;85(1):235-8.

[16] Fukushima H, Drzal LT. A carbon nanotube alternative: Graphite nanoplatelets as reinforcements for polymers. ANTEC-Society of Plastics Engineers2003. p. 2230–4.

[17] Kalaitzidou K, Fukushima H, Drzal LT. Multifunctional polypropylene composites produced by incorporation of exfoliated graphite nanoplatelets. Carbon. 2007;45:1446–52.

[18] http://en.wikipedia.org/wiki/High-density_polyethylene.

[19] Xia L-g, Li A-j, Wang W-q, Yin Q, Lin H, Zhao Y-b. Effects of resin content and preparing conditions on the properties of polyphenylene sulfide resin/graphite composite for bipolar plate. Journal of Power Sources. 2008;178(1):363-7.

[20] Jiang X, Drzal LT. Reduction in Percolation Threshold of Injection Molded High Density Polyethylene/Exfoliated Graphene Nanoplatelets Composites by Solid State Ball Milling and Solid State Shear Pulverization. Journal of Applied Polymer Science 2012;124(1):525-35.

[21] GNP is an exfoliated graphene nanoplatelet material obtained from XG Sciences, Inc., East Lansing, MI (www.xgsciences.com).

[22] Jiang X, Drzal LT. Improving Electrical Conductivity and Mechanical Properties of High Density Polyethylene through Incorporation of Paraffin Wax Coated Exfoliated Graphene Nanoplatelets and Multi-wall Carbon Nano-tubes. Composites Part A: Applied Science and Manufacturing. 2011;42(11):1840-9

[23] Jiang X, Drzal LT. Multifunctional high density polyethylene nanocomposites produced by incorporation of exfoliated graphite nanoplatelets 2: crystallization, thermal, and electrical properties. Polymer Composites. 2012; In Press, Accepted Manuscript.

[24] Yang C, Srinivasan S, Arico AS, Creti P, Baglio V, Antonucci V. Composite Nafion/Zirconium Phosphate Membranes for Direct Methanol Fuel Cell Operation at High Temperature. Electrochemical and Solid-State Letters. 2001;4(4):A31-A4.

[25] Dhakate SR, Sharma S, Borah M, Mathur RB, Dhami TL. Development and Characterization of Expanded Graphite-Based Nanocomposite as Bipolar Plate for Polymer Electrolyte Membrane Fuel Cells (PEMFCs). Energy & Fuels. 2008;22(5):3329-34.

[26] http://www.blackwellplastics.com/PPS.html.

[27] Blunk RHJ, Lisi DJ, Yoo Y-E, Tucker CL. Enhanced conductivity of fuel cell plates through controlled fiber orientation. AIChE Journal. 2003;49(1):18-29.

[28] Kim M, Yu HN, Lim JW, Lee DG. Bipolar plates made of plain weave carbon/epoxy composite for proton exchange membrane fuel cell. International Journal of Hydrogen Energy. 2012;37(5):4300-8.

[29] Li X, Sabir I. Review of bipolar plates in PEM fuel cells: Flow-field designs. International Journal of Hydrogen Energy. 2005;30(4):359-71.

CHAPTER 7 INCORPORATION OF POLYMERS INTO EXFOLIATED GRAPHENE NANOPLATELETS PAPERS

7.1 Abstract

A binder-free, self-standing and robust paper consisting of exfoliated graphene nanoplatelets (GNP) can be fabricated by the method of vacuum assisted self-assembly. It was found that the electrical conductivity of a GNP paper is more than 1000 S/cm and the thermal conductivity is over 300 W/mK. GNP papers are thus considered as useful components to be embedded into polymeric GNP nanocomposites to enhance their electrical and thermal properties. To ensure a good adhesion between a GNP paper and a polymeric nanocomposite, the GNP paper should be firstly saturated with the host polymer before it is embedded into the composite. Two techniques named solution incorporation and co-filtration were applied for this purpose. Results showed that even with around 50 wt% polymer content, the GNP paper composite still exhibits excellent electrical and thermal conductivity due to the highly continuous GNP networks formed in the paper-making process. It was also noted that once this kind of GNP paper is embedded into a polymeric nanocomposite, the mechanical, electrical, thermal, and gas barrier properties can be significantly improved.

7.2 Introduction

Graphene and graphene based nano-particles such as GNP have gained more and more research attention due to their superb mechanical strength (~1 TPa in Young's modulus, ~130 GPa in

flexural strength [1-3]), exceptional electrical and thermal properties (>10^6 S/cm in electrical conductivity [4, 5] and >5000 W/mK in thermal conductivity [6, 7]), and extremely low gas permeability due to the platelet structure [8, 9]. One way of utilizing the excellent properties of GNP nanoplatelets is to add them into a polymer matrix. However, based on the previous study, it is concluded that achieving a uniform and homogenous dispersion of GNP in a polymer matrix is normally very difficult [10-14]. The full translation of exceptional properties of GNP into the resulting nanocomposites is thus constrained. For example, the highest electrical conductivity obtained so far for HDPE/GNP nanocomposites at 60 wt% GNP loading is only around 130 S/cm and their thermal conductivity is just close to 11 W/mK, which are much lower than the intrinsic electrical and thermal properties of GNP nanoplatelets.

To fully use the excellent electrical and thermal properties of conductive nano-fillers, a large continuous phase is normally required for a percolated network [12, 14]. A good approach to realize this is to reassemble the nano-filler into a paper structure first, and then incorporate polymers into the resulting nano-filler paper. CNT paper (Bucky paper) [15-17], CNF paper [18, 19], and reduced graphite oxide (GO) paper [20, 21] have been extensively explored for several years. Reassembly of these nano-fillers into a paper form has the advantages of light weight, high mechanical robustness and flexibility, and exceptional thermal and electrical conductivity which make these nano-filler papers valuable for many applications such as current collectors, heat dissipaters, lightening protectors, armor plating and filter membranes [22, 23]. The general method of making nano-filler papers involves the use of surfactants, which improves the dispersion of nano-fillers in aqueous solutions. The nano-filler suspensions can then be

membrane filtered to obtain uniform films [24].

Research work in Drzal group has shown that GNP can also be reassembled into a paper form by applying a vacuum filtration method [25]. The details of this paper-making process will be fully discussed later. Two methods were applied in this study to impregnate a polymer into the pores of a GNP paper. The first one is the solution incorporation method that a GNP paper is immersed into a polymer solution for the penetration of polymer chains into the pores. The second one is the co-filtration technique where the polymer powders are dispersed in water with GNP nanoplatelets and then filtrated together to form polymer incorporated GNP papers. Although these two methods can both effectively impregnate a polymer into GNP papers, the co-filtration method has several advantages such as: it is a solventless and environmentally friendly method; it can control the amount of polymer impregnated into a GNP paper; and it is suitable to any thermoplastics, especially for those polymers there is no ordinary solvent to dissolve them. Polyphenylene sulfide (PPS) is just an example.

7.3 Experimental

7.3.1 Materials

In this research, HDPE pellets with the trade name Marlex® HXM 50100 (Density 0.95 g/cm^3) were obtained from Chevron Phillips Chemical Company. PPS powder with the trade name Fortron® 0205 (Density: 1.35 g/cm^3) was obtained from Ticona. The average size of as-received PPS powder is around 300-400 μm and then these PPS powders were ball milled for 10 hours to reduce the powder size to around 20-30 μm. The morphology of as-received PPS powder and the

powder after ball milling is shown in the Figure 7.1. GNP nanoplatelets with the diameter around 15 μm (GNP-15) and thickness around 5-10 nm were received from XG Science, Inc. Polyethylenimine (branched, PEI) from Sigma-Aldrich was used to help the dispersion of PPS and GNP in water. Meanwhile, xylene was used as the solvent to dissolve HDPE at 110 °C.

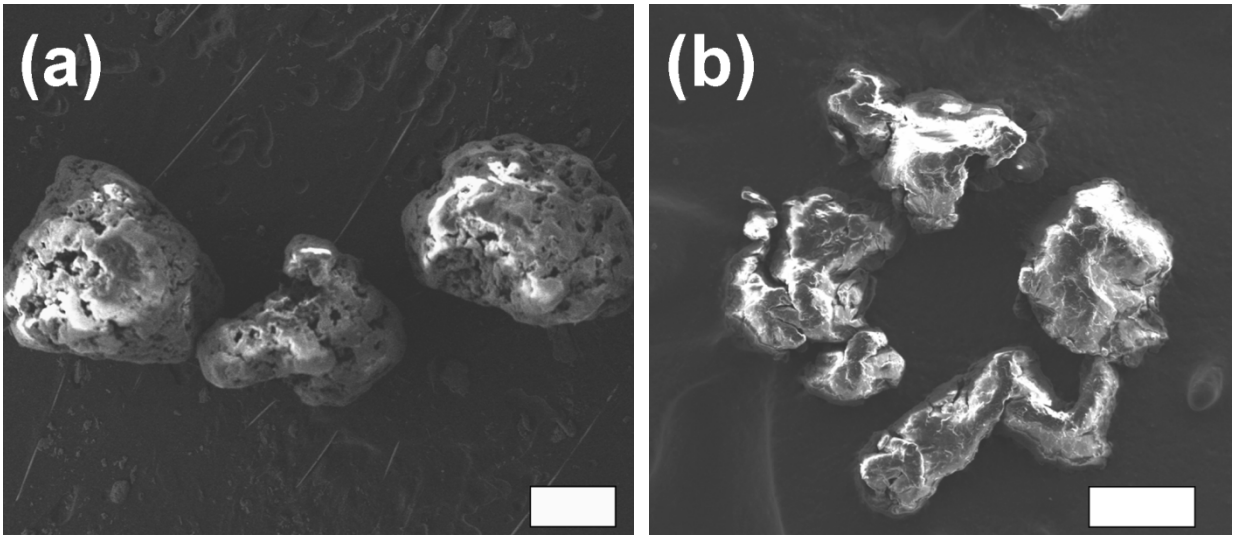

Figure 7.1. The morphology of (a) as-received PPS powder (scale bar 300 μm) and (b) the PPS powder after 10 hours ball milling (scale bar 30 μm)

7.3.2 Experimental Characterization

In this chapter, a UTS SFM-20 machine (United Calibration Corp.) was used to measure the flexural properties. Flexural coupons were tested under 3-point bending mode at a flexural rate of 0.05 in/min by following the ASTM D790 standard.

Thermo-gravimetric analysis (TGA) was carried out on a TA instrument (TGA Q500) at a heating rate of 15 °C/min in air from 30 °C to 800 °C.

Electrical conductivity measurements were taken on the flexural coupons by a four point method as described in the previous chapter. Thermal conductivity was still obtained by the LFA

Nanoflash 447 light flash system. The environmental scanning electron microscopy (ESEM Carl Zeiss EVO) was applied to collect SEM images. The same SEM sample preparation method was used which includes the steps of epoxy mounting, grinding, polishing and plasma etching.

7.4 Results and Discussion

7.4.1 Fabrication of a GNP Paper

GNP-15 nanoplatelets were dispersed in water with the help of PEI. The weight ratio between GNP-15, PEI and water is 1:1:1000. Ultra-sonication at 100 W was applied for 3 minutes to break down GNP aggregates and to ensure a better GNP dispersion. Then the GNP suspension was stirred for 24 hours before it was filtrated with a glass micro-fiber filter paper (~ 1 μm pore size, Whatman) under vacuum. This GNP filtration procedure is schematically shown in the Figure 7.2

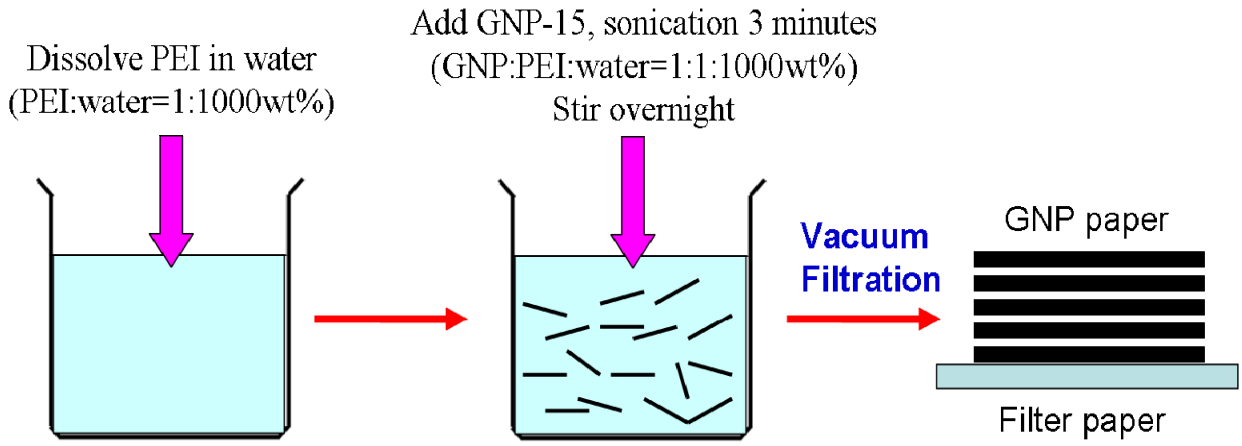

Figure 7.2. The procedure of making a GNP paper

The filtered GNP with the filter paper was dried at 100 °C overnight to remove any residual

moisture. Due to the hydrophobicity of GNP nanoplatelets, it was very easy to peel the GNP layer off from the hydrophilic glass fiber filter paper. Then the GNP paper was further annealed at 340 °C for 1 hour to get rid of the remaining PEI [26]. The GNP paper made from this method is self-standing, robust, and has some mechanical flexibility. The cross-section morphology of a GNP paper is presented in the Figure 7.3. From the image (a), it is seen that GNP platelets exhibit very good alignment, which gives the mechanical strength to the GNP paper. Image (b) reveals the porous structure of the GNP paper, which offers the opportunity for the impregnation of polymers into these pores.

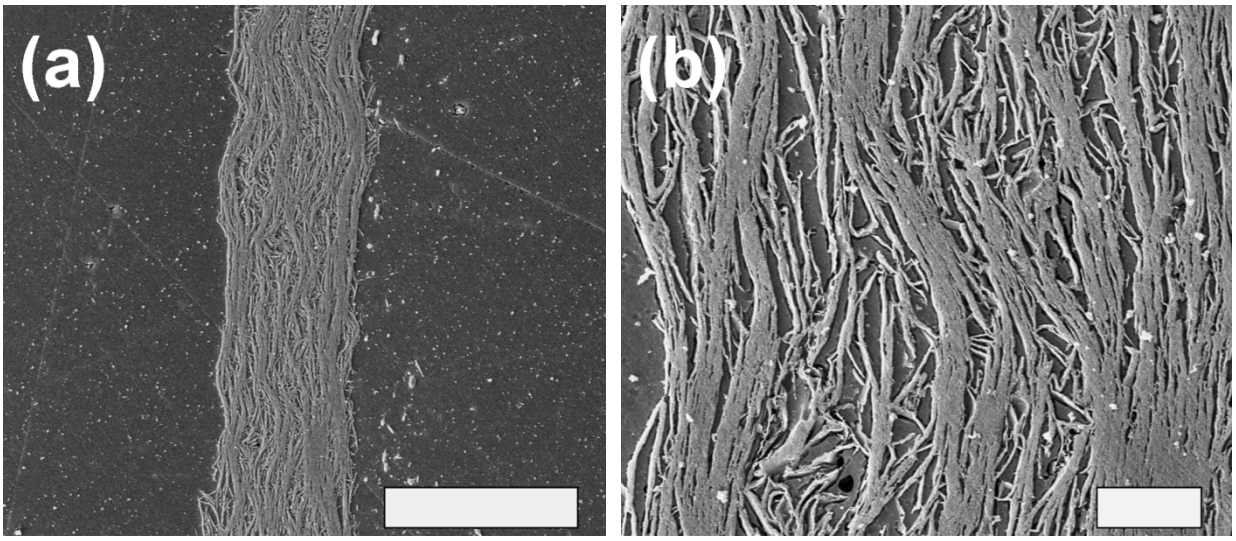

Figure 7.3. SEM images show the cross-section morphology of a GNP paper made by the vacuum filtration method (a) scale bar 100 μm; (b) scale bar 10 μm

To eliminate the effect of porosity and to obtain better conductive properties, the GNP paper can also be mechanically compressed under room temperature. Figure 7.4 then displays the cross-section morphology of a pressed GNP paper by applying about 20 MPa pressure. From these two images, it is concluded that the alignment of GNP is further improved and the most of

the pores have disappeared by the cold compression. Furthermore, GNP nanoplatelets are more closely packed and they have a good contact with each other. The electrical conductivity of this kind of GNP paper is thus as high as 1300 S/cm and its thermal conductivity is over 300 W/mK.

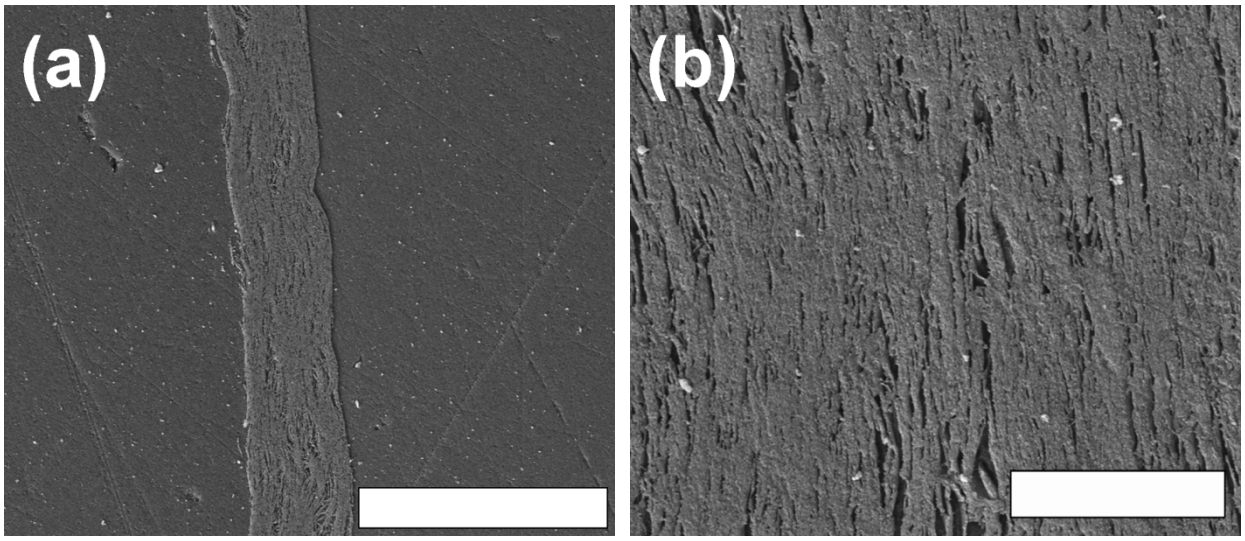

Figure 7.4. SEM images show the cross-section morphology of a GNP paper after compression (a) scale bar 100 μm; (b) scale bar 10 μm

7.4.2 Impregnation of Polymer into GNP Papers by Solution Incorporation

To demonstrate this technique, HDPE was selected as the polymer and xylene was used as the solvent to dissolve HDPE at 110 °C. The concentration of HDPE/xylene solution was prepared at 0.2 g/ml. An as-made and un-pressed GNP paper was then soaked in the solution for 1 hour and then died under room temperature to evaporate the solvent. The soaked GNP paper can be further hot pressed at 200 °C and 10 MPa pressure resulting in a compact and void free HDPE impregnated GNP paper. This solution incorporation method is schematically shown in the Figure 7.5. And Figure 7.6 illustrates the cross-section morphology of a HDPE impregnated GNP paper. The amount of HDPE in the GNP paper can be calculated by the weight change

before and after impregnation and it is found that the loading of HDPE is around 20-30 wt%. However, the amount of the polymer impregnated can not be concisely controlled.

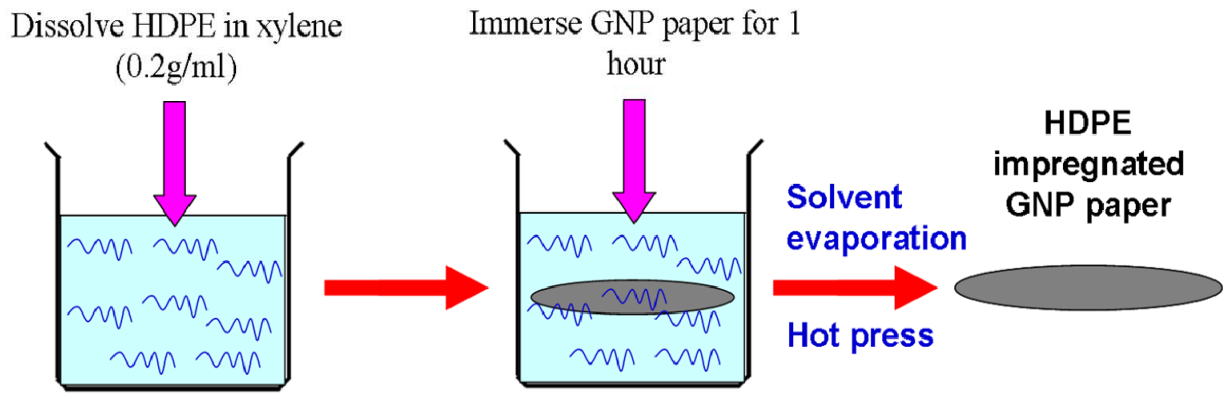

Figure 7.5. The procedure of impregnating polymer into GNP papers by a solution incorporation method.

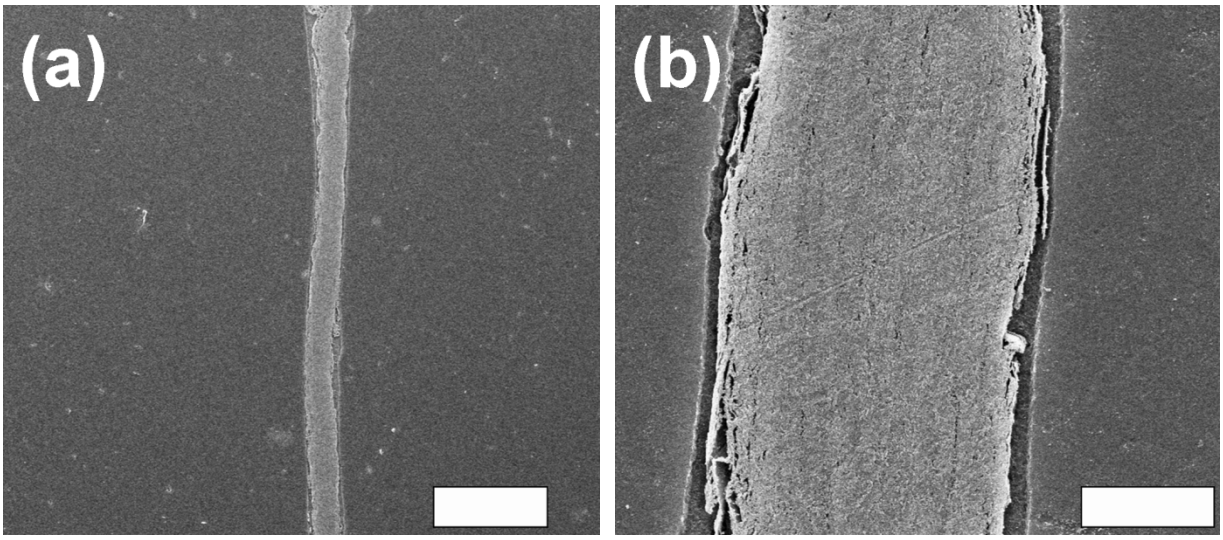

Figure 7.6. SEM images show the cross-section morphology of a HDPE impregnated GNP paper, HDPE content: 30 wt% (a) scale bar 100 μm; (b) scale bar 10 μm

From these two SEM images, it is concluded that the structure of the HDPE impregnated GNP paper is compact. No big pores and voids can be detected and the alignment of GNP nanoplatelets is good. The electrical conductivity of this GNP paper is thus as high as 650-750 S/cm even with the presence of 30 wt% polymer. This value is found to be much higher than a

polymeric composite filled with 70 wt% graphite or expanded graphite in literature [27-30]. The superb electrical conductivity of the HDPE impregnated GNP paper is mainly due to the continuous conductive networks present in the paper which are pre-formed in the GNP paper-making process. Meanwhile, the thermal conductivity of this GNP paper is found be around 180 W/mK.

7.4.3 Impregnation of Polymer into GNP Papers by Co-filtration

As discussed above, the solution incorporation method is good to impregnate a thermoset or a thermoplastic matrix (if an appropriate solvent can be found) into a GNP paper. However, there are some thermoplastics that there is no common solvent to dissolve them. PPS is just an example. Here I present a novel co-filtration technique that is capable of impregnating PPS into GNP papers without the use of any other solvent rather than water. What is more, this technique can concisely control the amount of polymer added to the GNP papers. Take the fabrication of PPS/GNP paper with 50 wt% PPS content for example. First of all, ball milled PPS powder (diameter around 30 μm, shown in the Figure 7.1) was dispersed into the PEI/water solution. The weight ratio between PPS, PEI and water is 1:2:1000. Sonication at 100 W was then applied for 5 minuets to break down any powder aggregates and also to achieve a better PPS dispersion. Then GNP-15 was added into the suspension, another 3 minuets sonication (100 W) was used under the constant stirring. The weight ratio between all the components is kept as 1:1:2:1000 (GNP: PPS: PEI: water), which makes the PPS content in the resulting PPS impregnated GNP paper to be 50 wt%. The suspension was kept stirring for 24 hours before the same vacuum filtration was

applied to filter the GNP with PPS. The resulting GNP paper containing PPS powder was dried at 100 °C overnight to remove any residual moisture and then the GNP layer was peeled off from the filter paper. It was found that this kind of GNP paper is still self-standing and mechanically robust. The cross-section morphology of the GNP paper is shown in the Figure 7.7, from which we can clearly see that PPS powders are embedded in the paper.

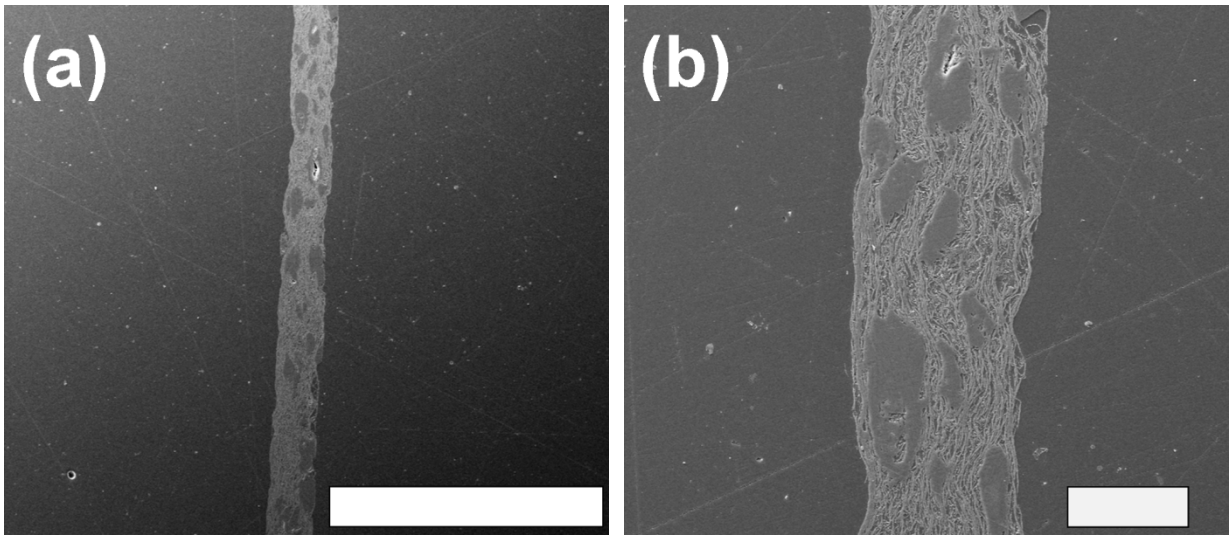

Figure 7.7. SEM images show the cross-section morphology of a PPS powder impregnated GNP paper, PPS content: 50 wt% (a) scale bar 1 mm; (b) scale bar 100 μm

To fully melt these trapped PPS powders for a better connection and adhesion between GNP platelets and PPS, the GNP paper with PPS powders was firstly annealed at 340 °C in furnace to get rid of excessive PEI and then hot pressed at 325 °C for 5 minutes under 10 MPa pressure. The cross-section morphology of a hot pressed GNP paper with PPS is then displayed in the Figure 7.8.

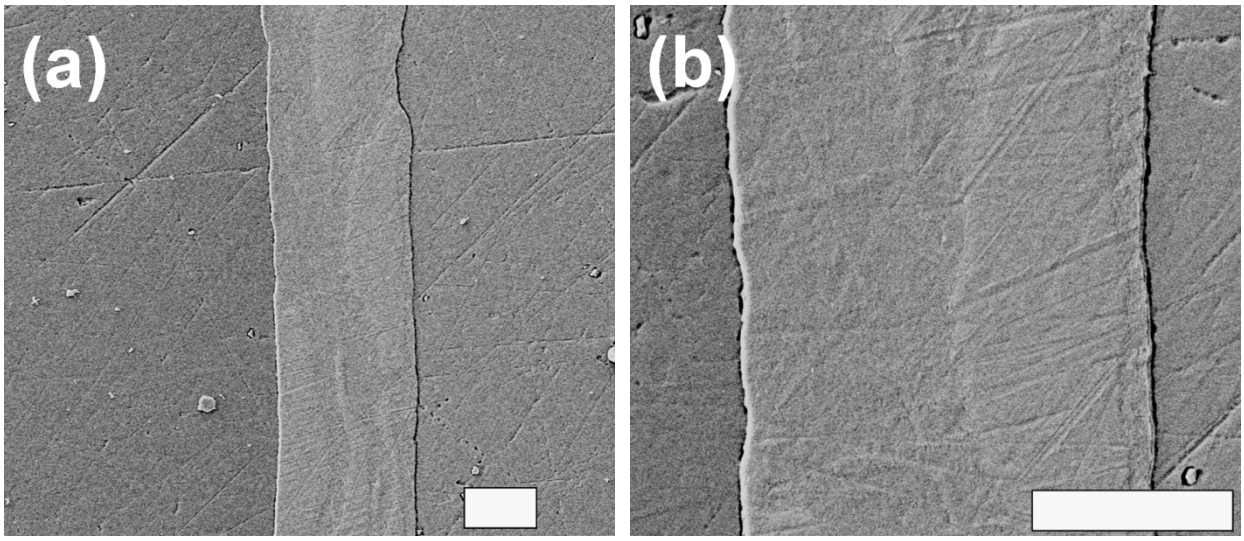

Figure 7.8. SEM images show the cross-section morphology of a PPS impregnated GNP paper after hot compression, PPS content: 50 wt% (a) scale bar 30 μm; (b) scale bar 30 μm

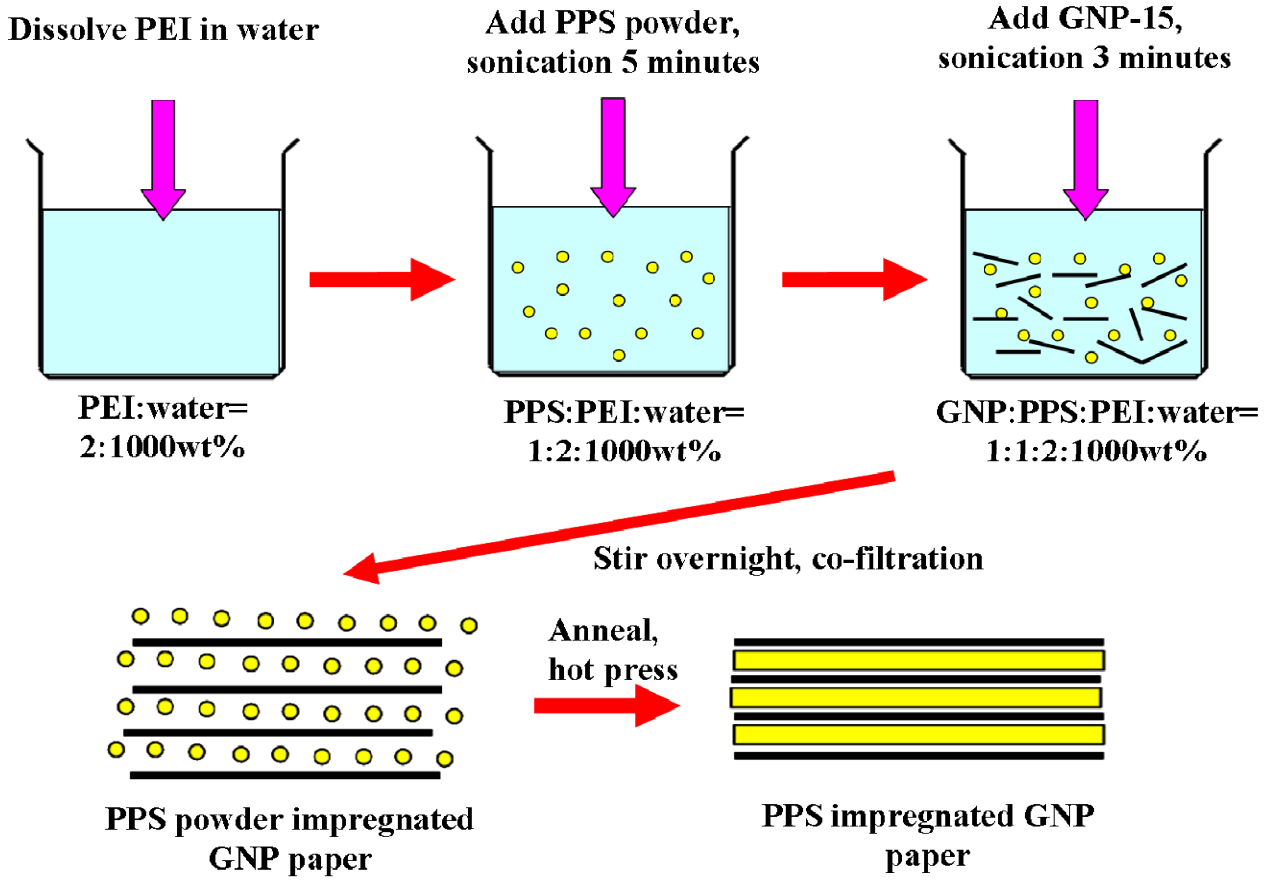

Figure 7.9. The procedure of applying a co-filtration technique to fabricate a PPS impregnated GNP paper

According to the Figure 7.7, it is seen that the GNP paper are fully wetted and covered by the polymer and no platelet morphology can be detected, which suggests the adhesion between PPS and GNP is excellent. Although this GNP paper was plasma treated for 40 minutes, PPS was not etched out, showing the toughness of this polymer. The procedure of fabricating PPS impregnated GNP paper through the co-filtration method is schematically illustrated in the Figure 7.9.

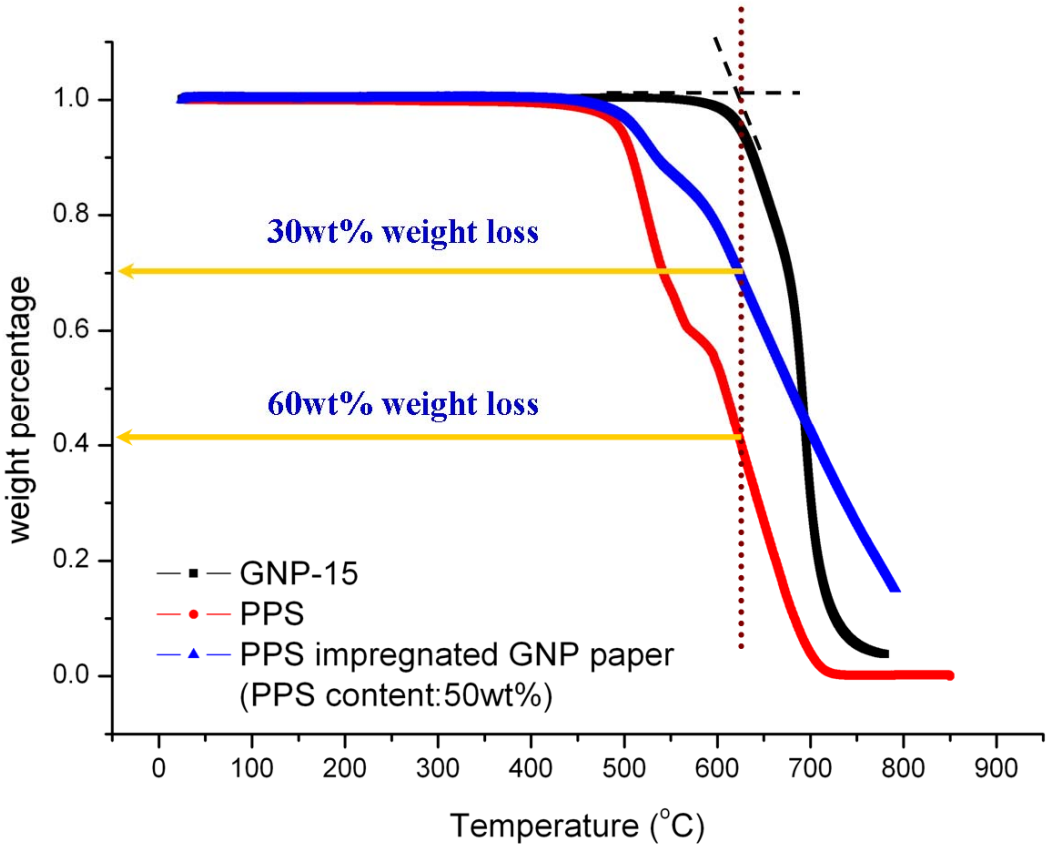

Figure 7.10. TGA curves of neat PPS, neat GNP-15, and PPS impregnated GNP paper (PPS content: 50 wt%)

To verify the exact amount of PPS in the GNP paper, TGA was carried out from 30 to 800 °C in air at a heating rate of 15 °C/min. Figure 7.10 shows the TGA curves for neat PPS, neat GNP-15,

and a PPS impregnated GNP paper (PPS content: 50 wt%). From this figure, we can see that PPS is not fully decomposed at the onset thermal decomposition temperature of GNP (~ 620 °C) and there is still 40 wt% PPS remaining. At this temperature, it is detected that the weight loss in the PPS impregnated GNP paper is around 30 wt%. So the actual content of PPS in the GNP paper is 30 wt%/(1-40 wt%)= 50 wt%, which is the exact amount added during the co-filtration process. Therefore, we can conclude that the co-filtration method is capable of concisely controlling the amount of polymer incorporated into the GNP papers, which is one of its advantages over the solution incorporation method. Furthermore, the electrical conductivity of this GNP paper with 50 wt% PPS is still as high as 700 S/cm and its thermal conductivity is around 110 W/mK.

7.4.4 Embedding Polymer Impregnated GNP Papers into GNP Nanocomposites

As discussed above, polymer impregnated GNP papers can be fabricated either by a solution incorporation method or a co-filtration method. And the resulting GNP papers exhibit excellent electrical and thermal properties. In this case, these polymer impregnated GNP papers can be used as good components in GNP nanocomposites to enhance their electrical and thermal conductivity. Take PPS/GNP nanocomposites for example, the embedding of a PPS impregnated GNP paper into PPS/GNP nanocomposites can be realized by a compression molding method which is schematically displayed in the Figure 7.11. Here PPS/CB/GNP(s)/GNP(l) (40:20:10:30wt%) powder mixture made by SSBM is used as the host nanocomposite. Of course, the number of the GNP paper embedded could be one, two, and more as required.

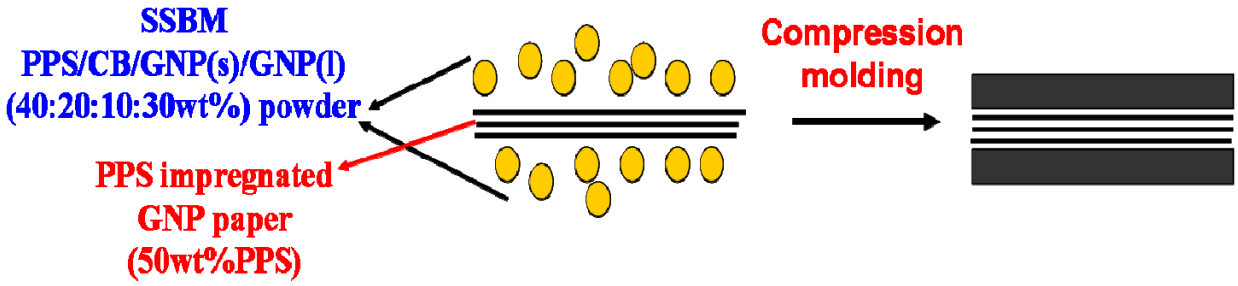

Figure 7.11. The procedure of embedding a PPS impregnated GNP paper into a PPS/CB/GNP hybridized nanocomposite

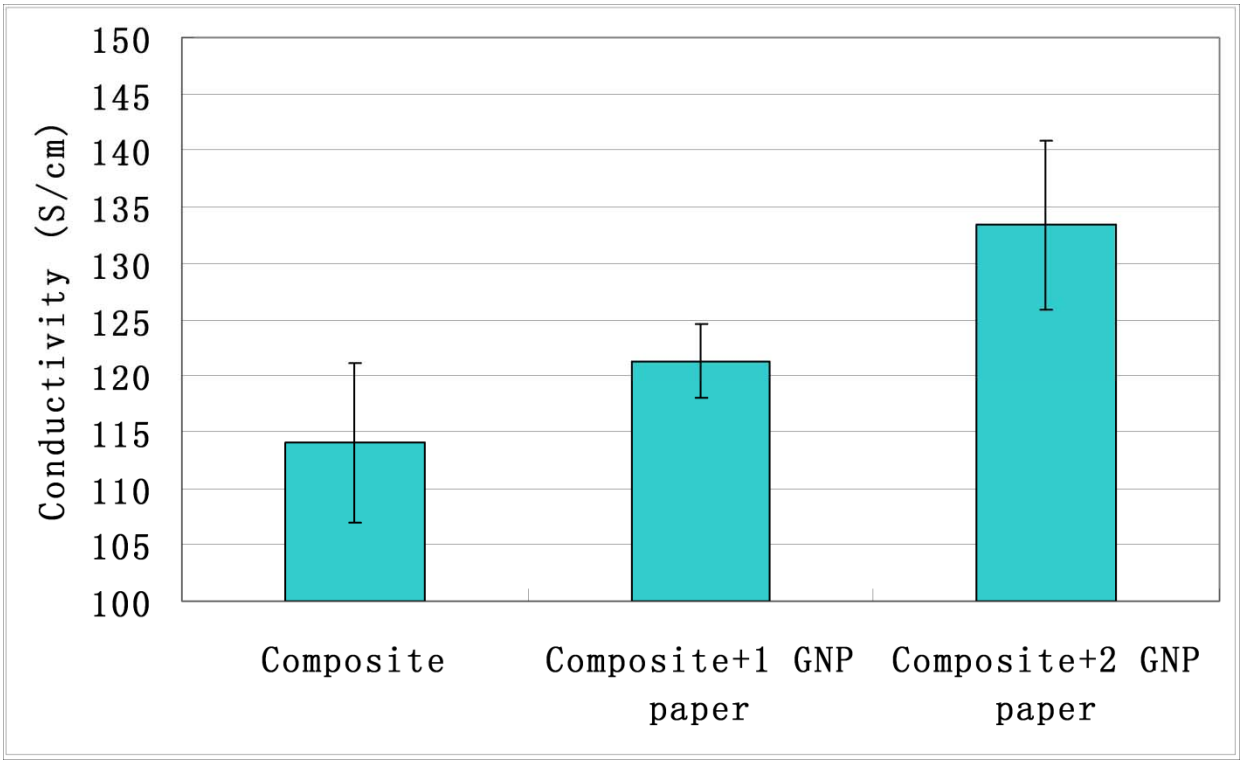

Figure 7.12. In-plane electrical conductivity of PPS/CB/GNP(s)/GNP(l) (40:20:10:30wt%) nanocomposites with zero, one, and two PPS impregnated GNP papers (PPS:50 wt%)

The in-plane electrical conductivity of the PPS/CB/GNP(s)/GNP(l) (40:20:10:30wt%) nanocomposites with zero, one, and two PPS impregnated GNP papers inside is shown in the Figure 7.12, from which it is clearly seen that the in-plane electrical conductivity is significantly enhanced by embedding GNP papers into the host nanocomposite. Moreover, the conductivity is

continuously improving as the number of GNP paper embedded increases. The enhancement in conductivity can be attributed to the high electrical conductivity of the PPS impregnated GNP paper (~700 S/cm).

A model is proposed here to predict the resulting in-plane electrical conductivity of the laminated PPS nanocomposites with GNP papers. That is, if the connection between the GNP paper and the host composite is perfect, they can be considered as two conductors connecting in parallel to each other. So the conductivity of the resulting laminated nanocomposite and the conductivity of each component should have this relationship:

$$S \times t = S_1 \times t_1 + S_2 \times t_2 \qquad [7.1]$$

Where S is the conductivity of the laminated nanocomposite; t is its thickness (~3.3 mm); S_1 is the conductivity of the PPS impregnated GNP paper (~700 S/cm), t_1 is its thickness (~80 μm for one GNP paper); S_2 is the conductivity of the host nanocomposite (~114 S/cm, as shown in the Figure 7.12), and $t_2 = t - t_1$.

The experimental data and the conductivity calculated by this model for the laminated nanocomposites with one and two PPS impregnated GNP papers are presented in the Figure 7.13. From this figure, it is noted that the experimental data is close to the theoretical value which suggests the connection between the GNP paper and the host composite is good although not perfect. Good connection and adhesion come from the fact that the GNP paper is firstly saturated with the host polymer, PPS, before it is embedded into the nanocomposite.

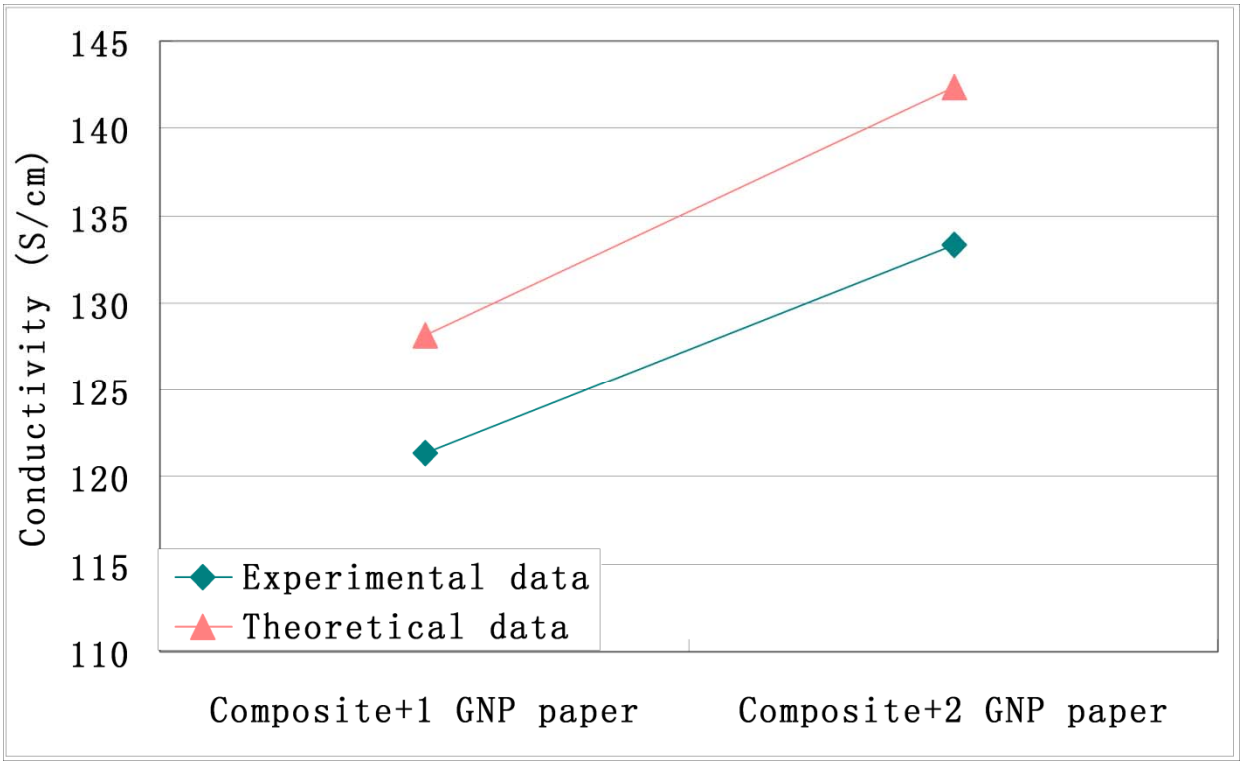

Figure 7.13. Experimental and theoretical electrical conductivity of PPS/CB/GNP(s)/GNP(l) (40:20:10:30wt%) nanocomposites with one and two PPS impregnated GNP papers (PPS:50 wt%)

The flexural properties of these laminated nanocomposites are shown in the Figure 7.14. It is noticed that the flexural strength is enhanced by 20% from 50 MPa to 60 MPa as two PPS impregnated GNP papers are embedded. Higher flexural strength in laminated PPS nanocomposites further confirms the adhesion between the GNP papers and the host nanocomposite is good. Delamination did not occur during the mechanical testing, which would otherwise be the major factor for the reduction of mechanical strength in the laminated composites [31]. In this case, these embedded GNP papers serve as better stress transfer media to resist the shearing and bending force because of their integrity and robustness, which consequently boost the flexural strength of the resulting laminated PPS nanocomposites.

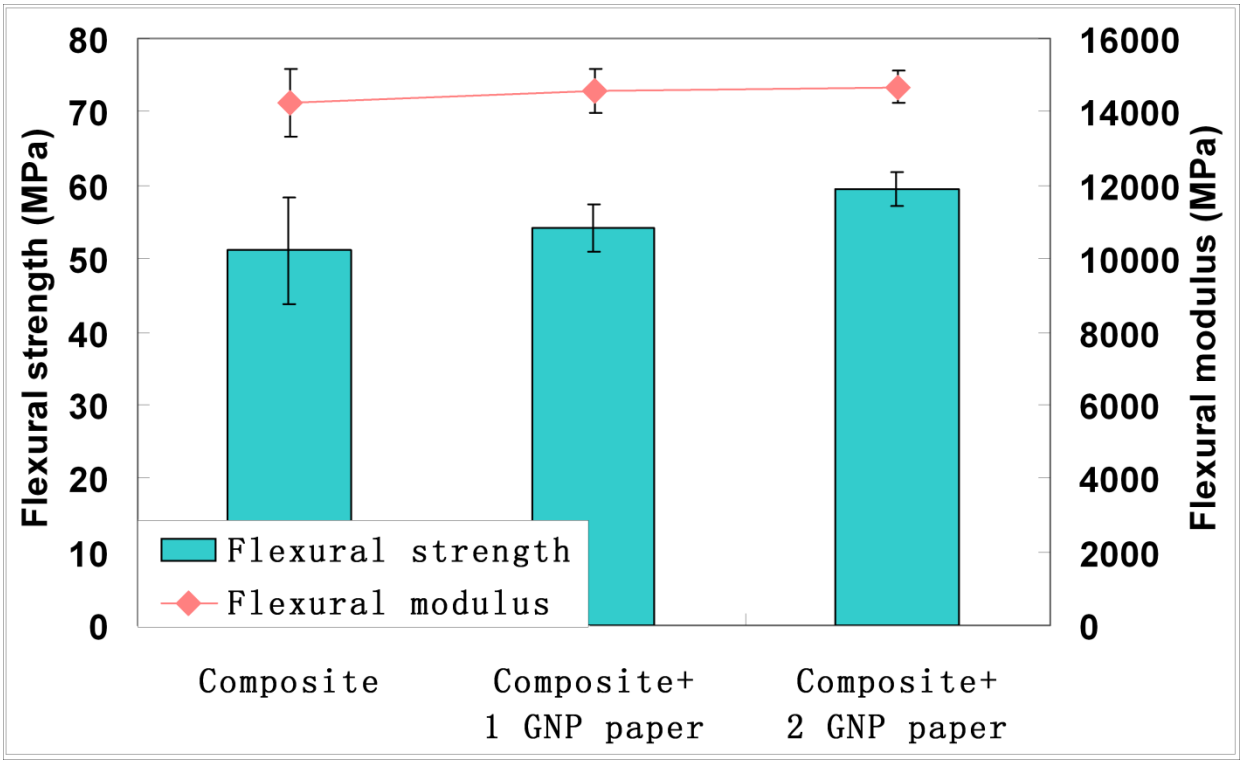

Figure 7.14. Flexural properties of PPS/CB/GNP(s)/GNP(l) (40:20:10:30wt%) nanocomposites with zero, one, and two PPS impregnated GNP papers (PPS:50 wt%)

The last but not least, Figure 7.15 illustrates the in-plane thermal conductivity of the PPS/CB/GNP(s)/GNP(l) (40:20:10:30wt%) nanocomposite with one PPS impregnated GNP paper. Because the thickness of the testing sample for thermal conductivity is 1.5 mm, which is half of the samples for the mechanical and electrical measurements. In this case, embedding one GNP paper into the thermal testing sample is equivalent to having two GNP papers in consideration of volume fraction. However, it is seen from this figure that the presence of the GNP paper does not enhance the thermal conductivity of the resulting nanocomposite. It suggests that the volume fraction of the GNP paper might be too low to improve the thermal conductivity. More PPS impregnated GNP papers are needed. And most importantly, it once again reveals the

difference in the principals of electron and phonon conduction. For electron transportation, once there is a conductive pathway, the resulting sample becomes electrical conductive. But for phonon conduction, the phonon scattering at the interface is the dominant factor in determining the thermal conductivity of the resulting nanocomposite. In this case, the induced large interfacial area between the GNP paper and the host nanocomposite may offset the positive effect of embedding highly conductive GNP papers.

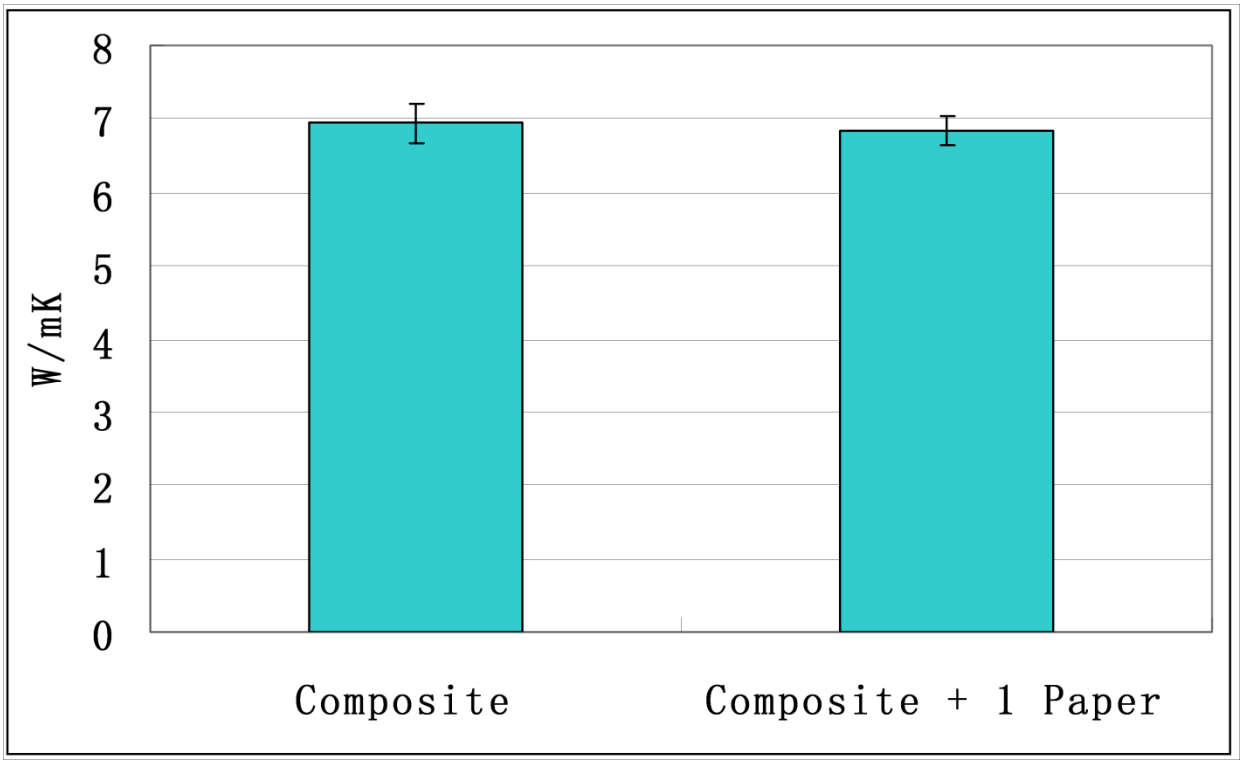

Figure 7.15. In-plane thermal conductivity of PPS/CB/GNP(s)/GNP(l) (40:20:10:30wt%) nanocomposites with zero and one PPS impregnated GNP papers (PPS:50 wt%)

Although the gas permeability of the PPS/CB/GNP hybrid nanocomposite with GNP papers has not been tested, the gas permeability of the PPS impregnated GNP paper is found to be as low as 2.1×10^{-10} $cm^3/(cm^2*s)$ due to the excellent gas barrier properties of GNP nanoplatelets and their

good alignment in the GNP paper. It is thus believed the gas barrier property of the resulting laminated nanocomposites should be further improved.

7.5 Conclusions

In this chapter, the impregnation of polymers into GNP papers has been successfully achieved by a solution incorporation method and a co-filtration technique. Results showed that the polymer impregnated GNP paper made by these two methods exhibits excellent electrical and thermal properties due to the presence of good GNP alignment and large conductive networks. However, the co-filtration technique has several advantages over the solution incorporation method such as: it is a time-saving and environmentally friendly method; it can concisely control the amount of polymer impregnated; and it is suitable to any thermoplastics especially for those there is no common solvent to dissolve them. Meanwhile, processes have been developed to embed these polymer impregnated GNP papers into polymeric nanocomposites, which lead to improved mechanical, electrical, thermal, and gas barrier properties in the resulting laminated nanocomposites.

REFERENCES

REFERENCES

[1] Geim AK. Graphene: Status and Prospects. Science. 2009;324(5934):1530-4.

[2] Lee C, Wei X, Kysar JW, Hone J. Measurement of the Elastic Properties and Intrinsic Strength of Monolayer Graphene. Science. 2008;321(5887):385-8.

[3] Zhao H, Min K, Aluru NR. Size and Chirality Dependent Elastic Properties of Graphene Nanoribbons under Uniaxial Tension. Nano Letters. 2009;9(8):3012-5.

[4] Li X, Zhang G, Bai X, Sun X, Wang X, Wang E, et al. Highly conducting graphene sheets and Langmuir-Blodgett films. Nat Nano. 2008;3(9):538-42.

[5] http://en.wikipedia.org/wiki/Graphene.

[6] Ghosh S, Calizo I, Teweldebrhan D, Pokatilov EP, Nika DL, Balandin AA, et al. Extremely high thermal conductivity of graphene: Prospects for thermal management applications in nanoelectronic circuits. Applied Physics Letters. 2008;92(15):151911-3.

[7] Balandin AA, Ghosh S, Bao W, Calizo I, Teweldebrhan D, Miao F, et al. Superior Thermal Conductivity of Single-Layer Graphene. Nano Letters. 2008;8(3):902-7.

[8] Kim H, Miura Y, Macosko CW. Graphene/Polyurethane Nanocomposites for Improved Gas Barrier and Electrical Conductivity. Chemistry of Materials. 2010;22(11):3441-50.

[9] Compton OC, Kim S, Pierre C, Torkelson JM, Nguyen ST. Crumpled Graphene Nanosheets as Highly Effective Barrier Property Enhancers. Advanced Materials.22(42):4759-63.

[10] Jiang X, Drzal LT. Multifunctional high density polyethylene nanocomposites produced by incorporation of exfoliated graphite nanoplatelets 1: Morphology and mechanical properties. Polymer Composites. 2010;31(6):1091-8.

[11] Jiang X, Drzal LT. Improving Electrical Conductivity and Mechanical Properties of High Density Polyethylene through Incorporation of Paraffin Wax Coated Exfoliated Graphene Nanoplatelets and Multi-wall Carbon Nano-tubes. Composites Part A: Applied Science and Manufacturing. 2011;42(11):1840-9

[12] Jiang X, Drzal LT. Reduction in Percolation Threshold of Injection Molded High Density Polyethylene/Exfoliated Graphene Nanoplatelets Composites by Solid State Ball Milling and Solid State Shear Pulverization. Journal of Applied Polymer Science 2011; In Press, Accepted Manuscript.

[13] Kalaitzidou K, Fukushima H, Drzal LT. Multifunctional polypropylene composites produced by incorporation of exfoliated graphite nanoplatelets. Carbon. 2007;45:1446–52.

[14] Kalaitzidou K, Fukushima H, Drzal LT. A new compounding method for exfoliated graphite/polypropylene nanocomposites with enhanced flexural properties and lower percolation threshold. Composites Science and Technology. 2007;67(10):2045-51.

[15] Endo M, Muramatsu H, Hayashi T, Kim YA, Terrones M, Dresselhaus MS. Nanotechnology: /`Buckypaper/' from coaxial nanotubes. Nature. 2005;433(7025):476

[16] Kim YA, Muramatsu H, Hayashi T, Endo M, Terrones M, Dresselhaus MS. Fabrication of High-Purity, Double-Walled Carbon Nanotube Buckypaper. Chemical Vapor Deposition. 2006;12(6):327-30.

[17] Gou J. Single-walled nanotube bucky paper and nanocomposite. Polymer International. 2006;55(11):1283-8.

[18] Yan X, Tai Z, Chen J, Xue Q. Fabrication of carbon nanofiber-polyaniline composite flexible paper for supercapacitor. Nanoscale.3(1):212-6.

[19] Lu H, Liu Y, Gou J, Leng J, Du S. Electroactive shape-memory polymer nanocomposites incorporating carbon nanofiber paper. International Journal of Smart and Nano Materials.1(1):2-12.

[20] Chen H, Müller MB, Gilmore KJ, Wallace GG, Li D. Mechanically Strong, Electrically Conductive, and Biocompatible Graphene Paper. Advanced Materials. 2008;20(18):3557-61.

[21] Compton OC, Dikin DA, Putz KW, Brinson LC, Nguyen ST. Electrically Conductive "Alkylated" Graphene Paper via Chemical Reduction of Amine-Functionalized Graphene Oxide Paper. Advanced Materials.22(8):892-6.

[22] http://www.buckypaper.com/.

[23] Compton OC, Nguyen ST. Graphene Oxide, Highly Reduced Graphene Oxide, and Graphene: Versatile Building Blocks for Carbon-Based Materials. Small.6(6):711-23.

[24] Vohrer U, Kolaric I, Haque MH, Roth S, Detlaff-Weglikowska U. Carbon nanotube sheets for the use as artificial muscles. Carbon. 2004;42(5-6):1159-64.

[25] Xiang J, Drzal LT. Thermal conductivity of exfoliated graphite nanoplatelet paper. Carbon.49(3):773-8.

[26] Wu H. Multifunctional Nanocomposite Reinforced by Graphite Nanoplatelets [PHD Dissertation]. East Lansing: Michigan State University; 2011.

[27] Dweiri R, Sahari J. Electrical properties of carbon-based polypropylene composites for bipolar plates in polymer electrolyte membrane fuel cell (PEMFC). Journal of Power Sources. 2007;171(2):424-32.

[28] Xia L-g, Li A-j, Wang W-q, Yin Q, Lin H, Zhao Y-b. Effects of resin content and preparing conditions on the properties of polyphenylene sulfide resin/graphite composite for bipolar plate. Journal of Power Sources. 2008;178(1):363-7.

[29] Song LN, Xiao M, Meng YZ. Electrically conductive nanocomposites of aromatic polydisulfide/expanded graphite. Composites Science and Technology. 2006;66(13):2156-62.

[30] Dhakate SR, Sharma S, Borah M, Mathur RB, Dhami TL. Development and Characterization of Expanded Graphite-Based Nanocomposite as Bipolar Plate for Polymer Electrolyte Membrane Fuel Cells (PEMFCs). Energy & Fuels. 2008;22(5):3329-34.

[31] Cantwell WJ, Morton J. The significance of damage and defects and their detection in composite materials: A review. The Journal of Strain Analysis for Engineering Design. 1992;27(1):29-42.

CHAPTER 8 SUMMARY AND FUTURE WORK

8.1 Summary

In summary, the potential of using exfoliated graphene nanoplatelets, GNP, as the multifunctional reinforcement in fabricating polymer/GNP nanocomposites and their prospective applications in bipolar plates for polymer electrolyte membrane (PEM) fuel cells have been investigated. The key idea of this research is to first reveal the relationship among the processing, morphology and the resulting performance of polymer/GNP nanocomposites and then use this relationship to find appropriate filler compositions and processing techniques to fabricate polymeric bipolar plates with tailored properties to meet the stringent requirements.

First of all, high density polyethylene was selected as the polymer matrix and the conventional compounding method of melt-extrusion and injection molding was applied to fabricate HDPE/GNP nanocomposites. The reason of choosing melt-extrusion and injection molding is because of its high design flexibility, low cost and labor, short cycle time and minimum scrap loss, which makes it as the most popular processing technique for manufacturing thermoplastics in industry. Then the mechanical properties, crystallization behaviors, thermal stability, thermal conductivity, and electrical conductivity of the resulting HDPE/GNP nanocomposites were evaluated as a function of GNP concentration. Results showed that HDPE/GNP nanocomposites exhibit equivalent flexural modulus and strength to HDPE composites filled with other commercial reinforcements such as CF, CB and GF but they have superior impact strength. The superior properties of HDPE/GNP nanocomposites reflect the good compatibility between the nano-reinforcement and the polymer matrix and also the exceptional mechanical properties of

GNP. Meanwhile, it was found that GNP size also plays a great role in determining various mechanical properties in the resulting GNP nanocomposites. HDPE nanocomposites filled with smaller GNP nanoplatelets always exhibit higher mechanical reinforcement which is attributed to the larger number of reinforcing particles per unit volume and the retention of platelet structure during the processing conditions.

Analysis of the crystallization behavior of HDPE/GNP nanocomposites showed that GNP is a good nucleating agent at low loading levels and as a result can significantly increase crystallization temperature and crystallinity of HDPE. At high GNP loadings, however, the close proximity of GNP particles retards the crystallization process by reducing the mobility of polymer chains.

Due to the high thermal stability and thermal conductivity of GNP nanoplatelets, enhanced thermal stability and thermal conductivity in HDPE were achieved by the addition of GNP. Evaluation of several thermal conductivity models to predict the thermal conductivity of HDPE/GNP nanocomposites as a function of GNP content indicates that the Maxwell-Eucken and Bruggeman models do not fit the experimental data well while the Agari model can successfully describe the thermal conductivity of HDPE/GNP nanocomposites.

By comparing the in-plane and through-plane thermal and electrical conductivity, it was found that HDPE/GNP nanocomposites fabricated by the conventional melt-extrusion and injection molding exhibit anisotropic conductive properties. Much higher in-plane conductivity is due to the preferential GNP alignment during the injection molding process and the anisotropic conductive properties of GNP. Meanwhile, results revealed that HDPE nanocomposites filled

with larger GNP tend to have higher thermal and electrical enhancement which is opposite to the results for mechanical properties. The superiority of large GNP platelets in conductivity is due to their much higher aspect ratio and much easier formation of conductive networks in the polymer matrix.

Based on the morphology investigation of these HDPE/GNP nanocomposites, it is concluded that the melt-extrusion conditions used in this study does not achieve a good GNP separation and dispersion which leads to severe aggregation of GNP in the polymer matrix. The presence of large GNP aggregates drastically reduces the number of GNP platelets available as 'effective' reinforcing particles and significantly decreases the electrical conductivity in the resulting nanocomposites. Therefore, the superb electrical properties of GNP cannot be as yet fully translated into good electrical conductivity of GNP nanocomposites.

In order to lower the percolation threshold and increase the electrical conductivity of GNP nanocomposites, two special processing methods named SSBM and SSSP were applied. These procedures have succeeded in lowering the percolation threshold by creating a continuous GNP coating on the surface of polymer which will selectively aggregate at HDPE-GNP interfaces in forming GNP-rich regions (conductive pathways) during the injection molding process. The electrical conductivity of the resulting nanocomposites is thus significantly enhanced. However, reduced mechanical strength and thermal conductivity were observed for these nanocomposites at high GNP loadings, which also result from the severe GNP aggregation in the GNP-rich regions. The disassociation between the electrical and thermal conductivity in this study has illustrated the different transportation mechanism between electrons and phonons.

If we want to lower the percolation threshold for HDPE/GNP nanocomposites but also enhance or at least maintain their good mechanical and thermal properties, the key factor is getting GNP dispersed uniformly throughout the polymer matrix, which ensures a good connectivity between GNP platelets in forming conductive networks and favors load transfer within nanocomposites. To enhance the dispersion of GNP in polymers, an easy but efficient non-covalent functionalization technique, wax coating, was thus developed and analyzed. The mechanism of the wax coating method in improving the dispersion of GNP nanoplatelets in HDPE is to prevent their re-aggregation during processing conditions based on a steric repulsion force between the wax coated nano-particles. In this case, the resulting wax coated GNP nanocomposites exhibit substantially higher mechanical and electrical properties due to a greatly improved GNP dispersion. In addition, the advantage of this wax coating technique over some covalent functionalization methods is that it can not only be applicable to the conventional compounding process of melt-extrusion and injection molding, but also maintain the graphene structure and the electronic properties of GNP platelets in their pristine state.

Then, the feasibility of using highly conductive GNP nanocomposites to substitute conventional metallic and graphite bipolar plates in fuel cells was fully investigated. Polymer/GNP nanocomposites were made by SSBM and compression molding on account of its processability and the resulted high electrical conductivity as described in this study. Research showed that HDPE/GNP and PPS/GNP nanocomposites at 60 wt% GNP loading exhibit good mechanical and gas barrier properties that can successfully meet the DOE target for bipolar plates. In order to enhance their electrical and thermal conductivity, synergistic effects between GNP and other

conductive fillers such as MWCNT and CB was analyzed. It was found that the binary blends of GNP with CB result in better enhancements in electrical and thermal properties. Meanwhile, the combination of small GNP platelets with larger ones was discovered to be another crucial parameter in determining various properties of the resulting nanocomposites. These synergistic effects have offered us a useful insight into the processing of polymeric bipolar plates with tailored properties to meet the stringent requirements.

The last but not least, in order to fully utilize the excellent properties of GNP, GNP papers were fabricated by a method of vacuum assisted self-assembly. The electrical conductivity of a GNP paper was found to be more than 1000 S/cm and the thermal conductivity is over 300 W/mK. GNP papers are thus considered as useful components to be embedded into polymeric GNP nanocomposites to enhance their electrical and thermal properties. To ensure a good adhesion between a GNP paper and a polymeric nanocomposite, the GNP paper should be firstly saturated with the host polymer before it is embedded into the composite. Two techniques named solution incorporation and co-filtration were applied for this purpose. Results showed that even with around 50 wt% polymer, the polymer impregnated GNP paper still exhibits excellent electrical and thermal conductivity due to the highly continuous GNP networks formed in the vacuum filtration process. Meanwhile, processes have been developed to embed these polymer impregnated GNP papers into polymeric nanocomposites, which lead to improved mechanical, electrical, thermal, and gas barrier properties in the resulting laminated nanocomposites.

8.2 Future Investigations and Opportunities

To improve the dispersion of GNP in polymers, the wax coating method has been applied which is based on a non-ionic surfactant coating on the surface of GNP. Results have shown that the dispersion of GNP is significantly improved which leads to greatly enhanced mechanical and electrical properties in the resulting nanocomposites. However, due to the high mobility of paraffin wax as a small molecule and its total compatibility with HDPE, it is believed that wax will easily diffuse into the polymer matrix during the melt-extrusion process rather than stay on the surface of GNP, which may eventually lower the efficiency of wax as the non-ionic surfactant to prevent the re-aggregation of GNP. Moreover, the interfacial adhesion between GNP and the polymer matrix is not improved by the wax coating method (the interaction between wax and GNP is still the Van der Waals force), which may explain the reason why there is no significant enhancement in thermal conductivity in the resulting wax coated GNP nanocomposites. To improve the interfacial adhesion and interaction between GNP nanoplatelets and a polymer matrix for a better compatibility and distribution, covalent modification of GNP is normally used which relies on the special surface treatment of GNP platelets to obtain functional groups or polymer chains that are compatible with the polymer matrix chemically anchored on the edge. However, covalent modification of GNP is relatively complicated due to involving chemical reactions and it always introduces sp^3 bonding and defects to the graphene basal plane which deteriorate the desirable mechanical, electrical and thermal properties of GNP platelets. In this case, a method that can not only enhance the interfacial interaction but also maintain the graphene structure and the electronic properties of GNP platelets in their pristine state is still of

high research interest. Here I propose another novel non-covalent modification technique by using a pi coupling agent. A pi coupling agent is a compatibilizer consisting of a chemical moiety (pyrene) that is capable of π-π bonding with the basal plane of GNP and it is also compatible with the polymer resin or matrix into which the GNP platelets are dispersed.

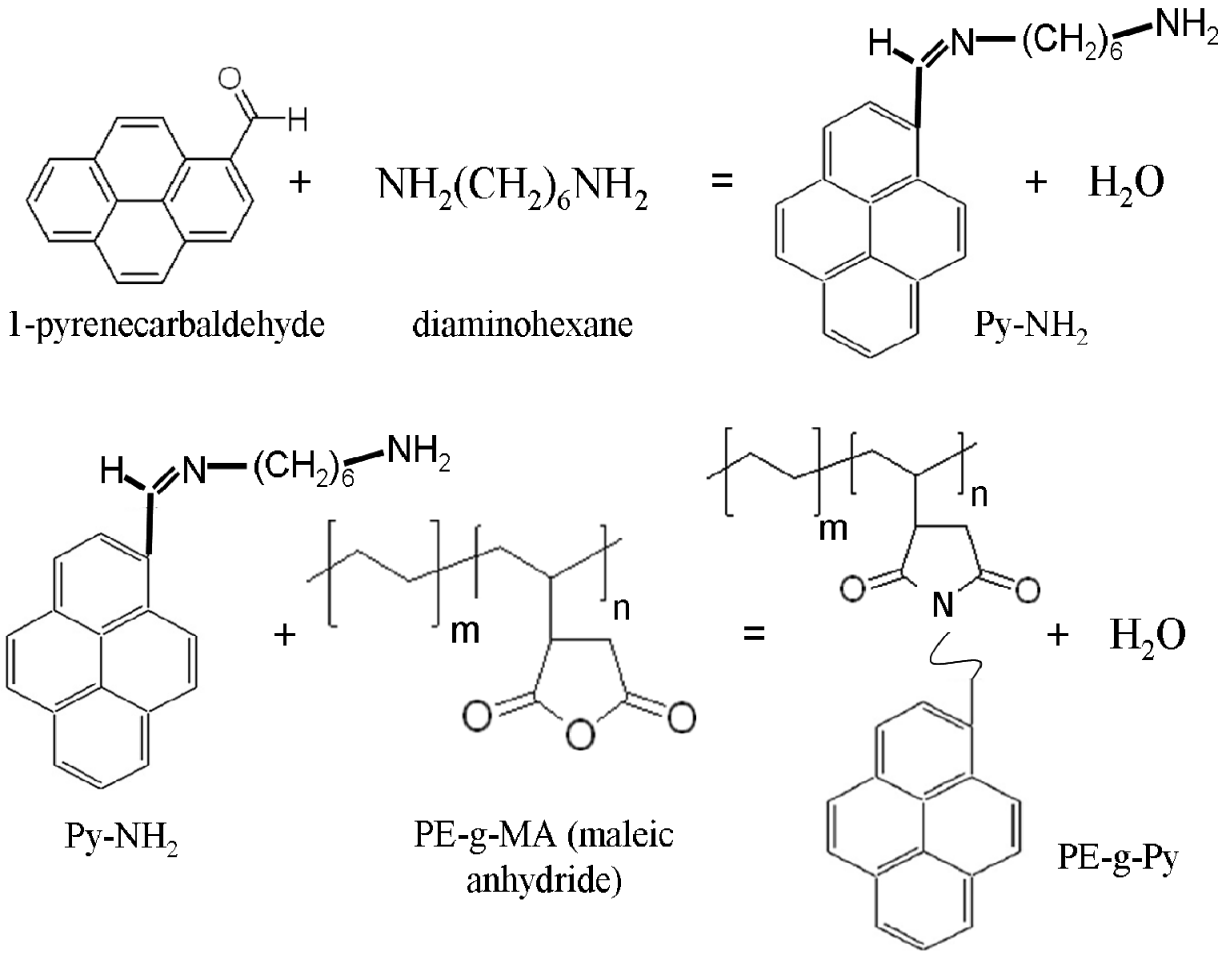

Figure 8.1. The basic procedures of producing pyrene functionalized polyethylene (PE-g-Py)

Take the dispersion of GNP in HDPE for example, pyrene functionalized polyethylene (PE-g-Py) can be synthesized as the pi coupling agent. The procedure of this synthesis is briefly presented in the Figure 8.1. It is believed that by using this pyrene functionalized polyethylene as the

compatibilizer, the interfacial interaction between GNP and HDPE will be greatly improved which will eventually leads to a better GNP dispersion and greatly enhanced mechanical, electrical and thermal properties in the resulting nanocomposites.

In the meantime, HDPE/GNP and PPS/GNP nanocomposites have been fabricated as the polymeric bipolar plates. The highest electrical and thermal conductivity got so far are 133 S/cm and 10.3 W/mK, which are just a little bit higher than the DOE target. However, it is known that the polymer impregnated GNP paper exhibit excellent electrical and thermal properties (electrical conductivity: ~ 700 S/cm; thermal conductivity: ~ 110 W/mK) even with 50 wt% polymer content. If we can stack several of these GNP papers together with the hope of retaining their superb electrical and thermal properties, the resulting stacked GNP paper composite will become a much better candidate for bipolar plates.

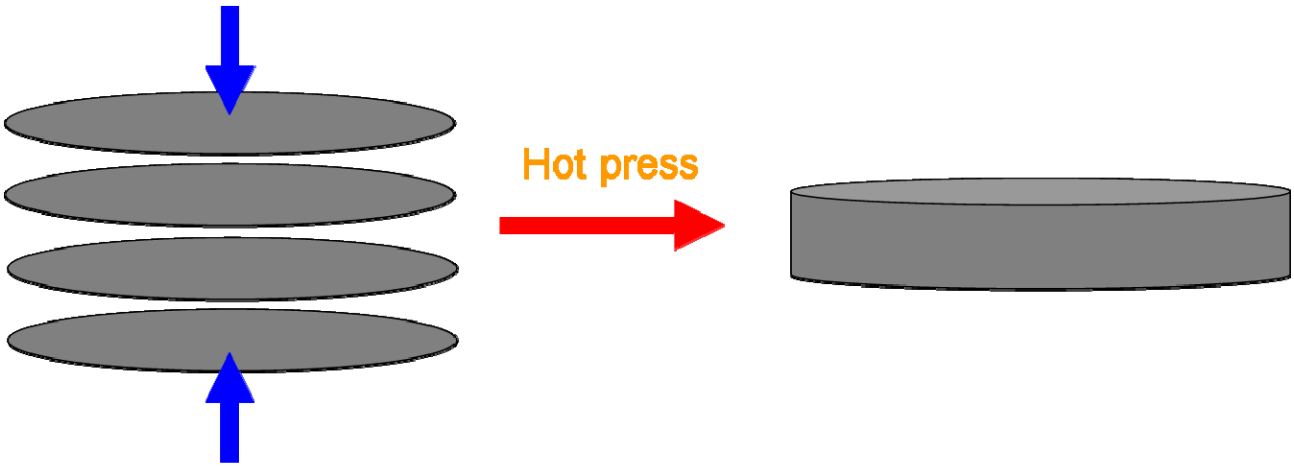

Figure 8.2. Stacking of polymer impregnated GNP papers to form GNP nanocomposites with desired thickness